Fracture Mechanics Fatigue Life Assessment of Welded Joints Under Ultrasonic Impact Treatment

Mehrdad Sarafrazi

A Thesis

in

The Department

of

Mechanical, Industrial and Aerospace Engineering (MIAE)

Presented in Partial Fulfillment of the Requirements

for the Degree of Master of Applied Science (Mechanical Engineering) at

Concordia University

Montréal, Québec, Canada

December 2020

CONCORDIA UNIVERSITY

SCHOOL OF GRADUATE STUDIES

This is to certify that the thesis prepared

By: Mehrdad Sarafrazi

Entitled: Fracture Mechanics Fatigue Life Assessment of Welded Joints Under Ultrasonic Impact Treatment

and submitted in partial fulfillment of the requirements for the degree of

Master of Applied Science (Mechanical Engineering)

compiles with the regulations of the University and meets the accepted standards with respect to originality and quality.

Signed by the final Examining Committee:

Dr. Behrooz Yousefzadeh	Chair
Dr. Biao Li	Examiner to Program
Dr. Ion Stiharu	Examiner
Dr. Ayhan Ince	Thesis Supervisor

Approved by Dr. Mamoun Medraj

Graduate Program Director

December 10 2020 Dr. Mourad Debbabi

Dean of Faculty

ABSTRACT

Fracture Mechanics Fatigue Life Assessment of Welded Joints Under Ultrasonic Impact Treatment

Mehrdad Sarafrazi

Welding joints are the most used joining method to fabricate engineering structures due to their low cost, structural strength, and geometric flexibility. Irregular geometries, micro cracks, defects, high stress concentration and tensile residual stresses are some of the results of a highly metallurgical process considered as welding. Thus, an important subject of growing concern in product design is to consider some of the critical factors caused from the weld process including high tensile residual stresses and stress concentrations to properly evaluate the fatigue life of the structures. Lightweight design of welded steel and aluminum structures in cyclic service requires the use of post-treatment approaches like Ultrasonic Impact Treatment (UIT). In this thesis, an evaluation of fatigue tests carried out recently on welded specimens exposed to UIT under the effect of the constant amplitude (CA) loading on the fatigue strength is described.

First, the effects of the various fatigue damage parameters on the as-welded (AW) condition and the impact treated welds are described in the literature review. Furthermore, fatigue test data have been taken from literature for both conditions under CA loading for several different stress ranges for each material. Following the tests, residual stress distributions below the weld toe surface have been specified by x-ray diffraction of untested specimens. More importantly, the test data obtained from the literature were analyzed through out the thesis and were used to define input parameter values for fracture mechanics analyses of the welded joint specimens. After that, the crack growth assessment of welded structures is provided. For comparison purposes, both Walker and Forman fatigue crack growth models are thoroughly reviewed and their advantages as invaluable tools for predicting the effects of UIT on fatigue performance for welded joints are examined. Subsequently, the benefit of the models in predicting fatigue crack growth behaviors

for nine distinct materials are examined and the effects of the various material strength parameters on the impact treatment performance are assessed. Then, fatigue crack propagation life of the materials is displayed. In the end, the crack shape evolution of the materials is depicted. In conclusion, the outcomes of this investigation accompanied by proposed future work are mentioned.

ACKNOWLEDGEMENTS

First, I wish to sincerely acknowledge my thesis supervisor Prof. Ayhan Ince, who has the substance of a genius: he unconditionally provided academic directions and firm supports during my graduate program. He was quite willing to share his great wisdoms and valuable experiences which gave me strong motivations even when the road got tough. He familiarized me with the world of fatigue and research. Literally, he showed endless patience throughout the entire program.

I wish to show my warm thanks to Prof. Ion Stiharu, who kindly offered helpful advices and generous supports throughout my graduate program. Without his co-funding, this thesis could not have reached its goal.

I would like to profusely thank Prof. Halid Can Yildirim. Without his cooperation and fatigue data, the numerical model validation of this work could hardly have been done and the writing in this thesis would have been challenging.

I would like to implicitly acknowledge the thesis committee for their constructive comments and encouraging questions.

I would like to express my real gratitude to fellow graduate student Farshid Hajializadeh. His assistance made plenty of things more straightforward. He helped to assure the completion of my master program by having joyful and informative conversations with me.

I would like to recognize my heartfelt appreciation to government of Canada, government du Québec and Canadian Red Cross etc. for their endless supports throughout COVID-19 pandemic.

Finally, I must express my deepest gratitude to my parents for their enormous helps and active encouragement for these years. I would not have this golden opportunity in Concordia without them. Further, the strong backing and great love of my family: my wife, Mona; my daughter, Melody. They kept me going on and this research would not have been possible without their input.

DEDICATION

To honour the memory of COVID-19 victims,

We will hold you in our hearts until we can hold you again in heaven.

Always on our minds, forever in our hearts.

TABLE OF CONTENTS

LIST OF TABLES

LIST OF FIGURES

SYMBOLS

S_{ap}	Applied stress
$\frac{a}{c}$	Aspect ratio
N_i	Crack initiation
N_p	Crack propagation
a	Crack size / Crack depth
$2c$	Crack length
c	Crack surface
X	Crack surface in X-direction
Y	Crack depth in Y-direction
$a-N$	Crack depth versus number of cycles curve
$c-N$	Crack surface versus number of cycles curve
$\Delta\varepsilon_e$	Elastic strain range
ε_{e-a}	Elastic strain amplitude
$\varepsilon_f{}'$	Fatigue ductility coefficient
c	Fatigue ductility exponent
$\sigma_f{}'$	Fatigue strength coefficient
b	Fatigue strength exponent
a_f	Final crack size
C	Fitting constant of $S-N$ model
m	Fitting constant of $S-N$ model
C_P	Fitting constants of Paris model
m_P	Fitting constants of Paris model
C_W	Fitting constants of Walker model
m_W	Fitting constants of Walker model
γ	Fitting constants of Walker model
C_F	Fitting constants of Forman model
m_F	Fitting constants of Forman model
ϕ	Flank angle

$\frac{da}{N} - \Delta K$	Fracture mechanics life curve
Y	Geometry factor
a_i	Initial crack size / Initial crack depth
c_i	Initial crack surface
S_{loc}	Local stress
S_{loc-ap}	Locally applied stress
S_{loc-a}	Local amplitude stress
S_{loc-m}	Local mean stress
S_{loc-y}	Local yield strength
N	Loading cycles
S_{max}	Maximum stress
S_{min}	Minimum stress
S_m	Mean stress
K_{max}	Maximum stress intensity
K_{max}	Minimum stress intensity
S_n	Nominal stress
T, t	Plate thickness
$\Delta\varepsilon_p$	Plastic strain range
ε_{p-a}	Plastic strain amplitude
S_{rs}	Residual stress
$S - N$	Stress-life curve
$\varepsilon - N$	Strain-life curve
R	Stress ratio
S	Stress / Load
S_a	Stress amplitude
$\sigma(x)$	Stress distribution
K	Stress intensity factor
K_t, K_w	Stress concentration
ΔK	Stress intensity range

K_{th}	Threshold stress intensity
ΔK_{th-ST}	Threshold stress intensity factor for steel
ΔK_{th-AL}	Threshold stress intensity factor for aluminum
N_f	Total life
ε_{t-a}	Total strain amplitude
S_u	Ultimate tensile strength
ρ, r	Weld toe radius
θ	Weld toe angle
$m(x, a)$	Weight function
S_y	Yield strength
E	Young's modulus
E_{ST}	Young's modulus of steel
E_{AL}	Young's modulus of aluminum

ABBREVIATIONS

ACDP	Alternating current potential drop
AL	Aluminum
AW	As-welded
$AWvsUIT - W - X$	Comparison between the AW and UIT conditions for Walker model for X MPa stress level
$AWvsUIT - F - X$	Comparison between the AW and UIT conditions for Walker model for X MPa stress level
CA	Constant amplitude
FCG	Fatigue crack growth
FEA	Finite element analysis
FE	Finite element
$AW - F - X$	Forman model under the AW condition for X stress level
$UIT - F - X$	Forman model under the UIT condition for X stress level
FT	Fracture toughness
HAZ	Heat-affected zone
HCF	High-cycle fatigue
HDM	Hole drilling method
IIW	International Institute of Welding
LEFM	Linear elastic fracture mechanics
LCF	Low-cycle fatigue
PWT	Post-weld treatment
SEM	Scanning electronic microscopic
S / ST	Steel
SCF	Stress concentration factor
SIF	Stress intensity factor
THSIF	Threshold stress intensity factor
2D	Two-dimensional
UIT	Ultrasonic impact treatment
$AW - W - X$	Walker model under the AW condition for X stress level

$UIT - W - X$	Walker model under the UIT condition for X stress level
WF	Weight Function
XRD	X-ray diffraction

CHAPTER 1: INTRODUCTION

1.1) Statement of Need

Automobile, aerospace and marine etc. industries are facing a growing demand for lighter structures. Presently, engineers are actively seeking for cost-effective solutions to reduce their products weight. Environmentally, greenhouse gas emissions can be dramatically reduced by weight reduction. Then, it will lead to rising payload and through this saving fuel consumption in the above-mentioned industries. Optimizing the weight can be safely accomplished by welding the joint components from high strength steels etc. The principal purpose for selecting high strength steels is gaining benefit of higher strength steels regarding the yield criterion, decreased dimensions and allowable higher stresses etc. (Gresnigt & Steenhuis, 1997; Svensson et al., 2015).

Welding joints are the most used joining method to fabricate engineering structures due to their low cost, structural strength and geometric flexibility etc. Several engineering segments encounter fatigue loading throughout all or part of their lifetime. Some of the results of a highly metallurgical process considered as welding are irregular geometries, micro-cracks, defects, high stress concentration and tensile residual stresses etc. The main location of fatigue failures is mostly welded joints since the welded joints pose much lower fatigue strength than non-welded components. Raising the yield or tensile strength does not even increase the fatigue strength of steel in the as-welded (AW) condition (Gurney & Saunders, 1981).

Thus, cracks can appear and expand to a risky length in the presence of a flaw. Remember that flaws are natural in all materials. Cracks that may appear from these flaws should be considered when engineers design and analyze such structures. If a crack is detected by frequent inspections, then the component can be changed or repaired or overhauled, as needed. The fatigue fracture life of the structures can assist us determining the inspections intervals. The number of cycles took to expand a crack from a least measurable size to a risky size can lead us to calculate fatigue fracture life. In the literature, analytical fatigue crack growth (FCG) models are accessible for plentiful generalized geometries such as a centre crack and an edge crack etc. simply to mention a few (Tada et al., 2000).

Hence, an important subject of growing concern in product design is to consider some of the critical factors caused from the weld process including high tensile residual stresses and stress concentrations to properly evaluate the fatigue life of the structures. Lightweight design of welded steel and aluminum structures in cyclic service requires the use of post-treatment approaches like Ultrasonic Impact Treatment (UIT). In this thesis, an evaluation of fatigue tests carried out recently on welded specimens exposed to UIT under the effect of the constant amplitude (CA) loading on the fatigue strength is described.

1.2) Objectives

Note that there is an important gap that has been derived from the literature review. The gap had to be further investigated to improve fracture mechanics crack growth methodologies. First, a proper comprehension of the crack growth models is required to evolve future approaches. Presently, Walker and Forman models have been employed to express the crack growth propagation. Yet, the aforesaid models are slightly different from each other when calculating the fatigue strength.

Second, a good comprehension of fatigue mechanics life of the structures is required. Numerous studies have shown the fatigue strength of different welded materials by utilizing either Walker or Forman model. These studies have only employed one of the models to predict the fatigue strength of such materials with respect to limited range of experimental data and the most common specific sort of loads – assumptions – geometries – conditions etc. However, there is limited knowledge of determining the fatigue crack propagation life phase accompanied by predicting the evolution shape of fatigue cracks. On top of that, there is limited analogy of the foresaid implications.

Ultimately, crack growth assessment of the structures must be analysed in depth so that will clearly expose the fundamental shortcomings and essential differences in the gap.

1.3) Scientific Approach

First, the effects of the various fatigue damage parameters on the AW condition and impact treated welds are described in the literature review. Furthermore, fatigue test data have been taken from literature for both conditions under CA loading for several different stress ranges for each

material. Following the tests, residual stress distributions below the weld toe surface have been specified by x-ray diffraction of untested specimens. More importantly, test data obtained from the literature were analyzed through out the thesis and were used to define input parameter values for fracture mechanics analyses of the welded joint specimens.

After that, the crack growth assessments of the welded structures are provided. For comparison purposes, both Walker and Forman fatigue crack growth models are thoroughly reviewed and their advantages as invaluable tools for predicting the effects of UIT on fatigue performance for welded joints are examined. Subsequently, the benefit of the models in predicting fatigue crack growth behaviors for nine different materials are examined and the effects of the various material strength parameters on the impact treatment performance are assessed. Then, fatigue crack propagation life of the materials is displayed. In the end, the crack shape evolution of the materials is depicted. In conclusion, the outcomes of this investigation accompanied by proposed future work are mentioned.

1.4) Assumptions

The following assumptions were applied in this study for the whole materials:

- Stress ratio equivalent to 0.1 was utilized for all materials.
- Load spectrum was constant amplitude fatigue cyclic loading.
- Residual stress was employed in depth direction from weld toe.
- An initial crack already existed at weld toe.
- The crack type was toe crack.
- The crack size was less than $0.5\ mm$ which simply means in microscopic scale.
- The crack shape was semi-elliptical.
- The crack was 2D which simply means in depth and on surface dimensions.
- The final crack size was half of the thickness.
- The fatigue failure of the weld joints occurred at weld toe.
- The fracture happened when the crack was reached its critical size.

1.5) Limitations

The following aspects were considered and applied in this investigation:

- The stimulations focused on assessing the fatigue strength of the welded structures were derived from chosen limited number of experimental data available for the most common loads like CA.
- The resemblances concentrated on an elected composition of residual stresses, geometry and material characteristics developed on limited available statistics from the literature.
- Work accomplished in this thesis was limited to a 2D semi-elliptical crack at weld toe.
- The crack growth of the welded joints was analysed through fatigue analysis program FALPR (V6.9).

1.6) Thesis Outline

The achievement of the stated objectives accompanied by the outcomes of the conducted research are explained in five chapters formed and outlined as follows:

Chapter 1 performs an overall review of the statement of the problem. Then, the primary justification of this research is defined based on the present state-of-art in reference to fracture mechanics crack growth. In a nutshell, the substantial affiliation of this study is to improve fracture mechanics crack growth methodologies by thoroughly scrutinizing the pros and the cons of both models. In brief, this chapter reveals an important gap in the knowledge concerning an evaluation of fatigue tests carried out recently on welded specimens exposed to UIT under the effect of the CA loading.

Chapter 2 looks into a lack of comprehension in fracture mechanics analyses in two-dimensional domains by going through an in-detail overview of the core concepts related to fatigue. A literature review with respecting to these domains as well as defining the concepts of various fatigue damage parameters are described to present the special purposes of this work. To summarize, a detailed investigation of the essential gap is carried out through this chapter.

Chapter 3 describes the two-dimensional crack growth using Walker's and Forman's equations to accomplish the evaluation of recent fatigue tests. After implementing the fatigue crack

propagation life of the materials, the crack shape evolution of the materials is carried out. In essence, the solutions of the derived nonlinear equations are numerically performed.

Chapter 4 introduces the predictions of Walker and Forman models by providing the input fatigue parameters. To experimentally validate the numerical results of the models, the experimental derived data from the literature are employed. The fatigue crack propagation life of the materials is presented. The crack shape evolution of the materials is represented. In closing, a meaningful comparison between the models and the derived experimental data are presented.

Chapter 5 explains the outcomes of this investigation accompanied by proposed future work. In the first part, the overall outcomes of this research are mentioned. Further, the first part outlined the substantial affiliation of the pursued study as well. The second part introduced proposed future work.

CHAPTER 2: REVIEW OF LITERATURE

2.1) Fatigue

The bulk of engineering failures are often induced by fatigue. A microscopic crack may form under the impact of arising stresses caused by fatigue cyclic loadings. Fatigue happens when engineering structures are subjected to such frequent loading and unloading cycles. The degraded material eventually fractures at some point. Generally, fractures occur in high-cyclic fatigue domain which represents lower loads. Usually, fractures take place in a shorter period than typically predicated (Dowling et al., 2013). In accordance with American Society for Testing and Materials Standard E. (ASTM, 1823), an alternative signification of fatigue is: "Fatigue is the process of progressive localized permanent structural change occurring in a material subjected to conditions that produce fluctuating stresses and strains at some point or point and that may culminate in cracks or complete fracture after a sufficient number of fluctuations".

The fatigue procedure is mainly categorized into three phases:

1: Crack initiation

2: Slow, stable crack growth

3: Rapid fracturing

Crack growth regime is consisted of two phases. The two phases are under the name of "STAGE I" [Shear Mode] and "STAGE II" [Tensile Mode], respectively. Figure 1 depicts schematically stage I and stage II of the FCG. A crack begins from the surface and expands about a few grains predominately governed by shear stresses and strains amid the first stage of crack growth. After reaching over multiple grains, it carries on extending in an orientation perpendicular to the greatest tensile principal stress. In rapid fracturing regime, the crack size is larger than the remaining cross section. Eventually, the component does not endure the fatigue load and following that absolute fracture occurs (Dowling et al., 2013; Suresh, 1998; Lampman & DiMatteo, 1996; Stephens et al., 2001; Lassen & Recho, 2006).

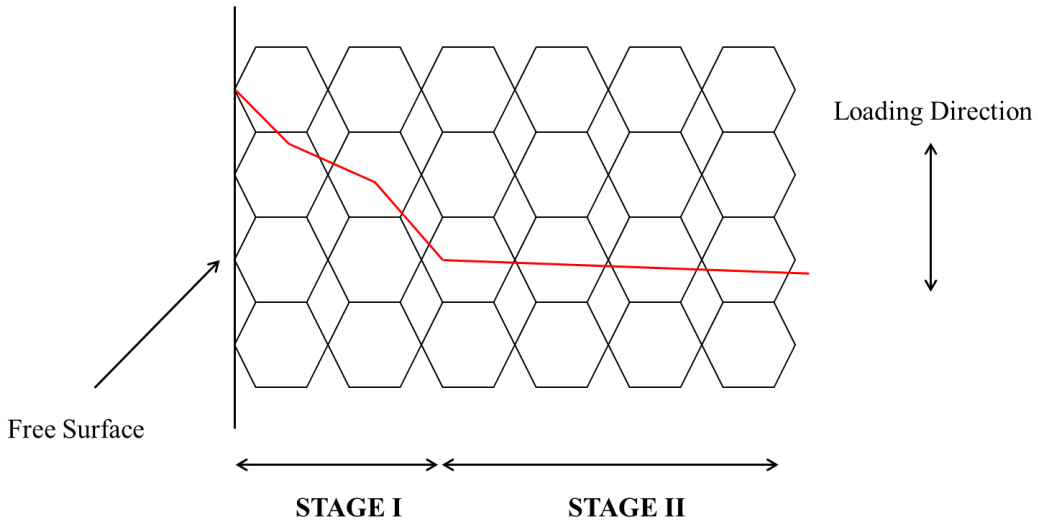

Figure 1: Schematic portrait of stage I and stage II of fatigue crack growth (Harati, 2015)

Cracks usually originate along slip lines aligned in the planes of maximum shear stress in crack formation regime. Cracks may originate as well as at or close material discontinuities like imperfections, grains boundaries, holes and voids.

2.2) Recent Fatigue Incidents

Metal fatigue crack is the root cause of the horrifying incident that has recently occurred in aerospace industry back in August 2016 as broadcasted by American National Transportation Safety Board (NTSB). In Figure 2, a blade of the engine had microscopic cracks that splintered open under the type of stress positioned on the engine.

Figure 2: Schematic illustration of a recent metal fatigue incident in aerospace industry reported by American National Transportation Safety Board (NTSB) back in August 2016 – Courtesy: NTSB NEWS AND EVENTS

Metal fatigue is the principal reason of the tragic event that has recently arisen in aerospace industry back in October 2016 as announced by American National Transportation Safety Board (NTSB). In Figure 3, a microscopic crack initiated between the left main landing gear. Unfortunately, the crack went undetected and slowly advanced till the gear crashed.

Figure 3: Schematic image of a recent metal incident in aerospace industry reported by American National Transportation Safety Board (NTSB) back in October 2016 – Courtesy: NTSB NEWS AND EVENTS

Fatigue is the prime cause of the striking cases that have recently happened in marine industry as shown in Figure 4. Microscopic cracks, already existed in hull structure due to the welding, propagated through depth and surface of hull girder.

Figure 4: Schematic picture of a recent propagation of cracks incident in marine industry – Courtesy: FIVEOCEANSALVAGE / Hasan Saad

In Figure 5, the crack engendered either in machining or casting. This figure indicates schematically the fatigue crack initiation and propagation phases for an edge crack (Bhaumik et al., 2008).

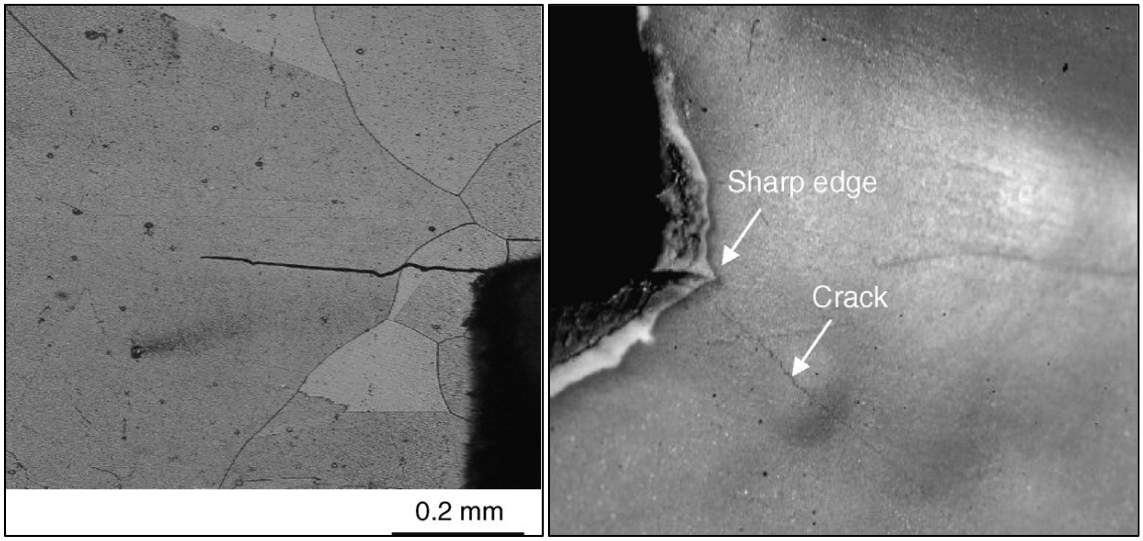

Figure 5: Schematic image of optical microstructure demonstrating an edge fatigue crack initiated from sharp edges due to stress raisers (Bhaumik et al., 2008).

In Figure 6, the cracks were progressed at the rivet holes for a second stage compressor rotor drum. Because of stress concentration at this spot, the cracks were established at the surface of the rivet hole which is unexpected (Bhaumik et al., 2008).

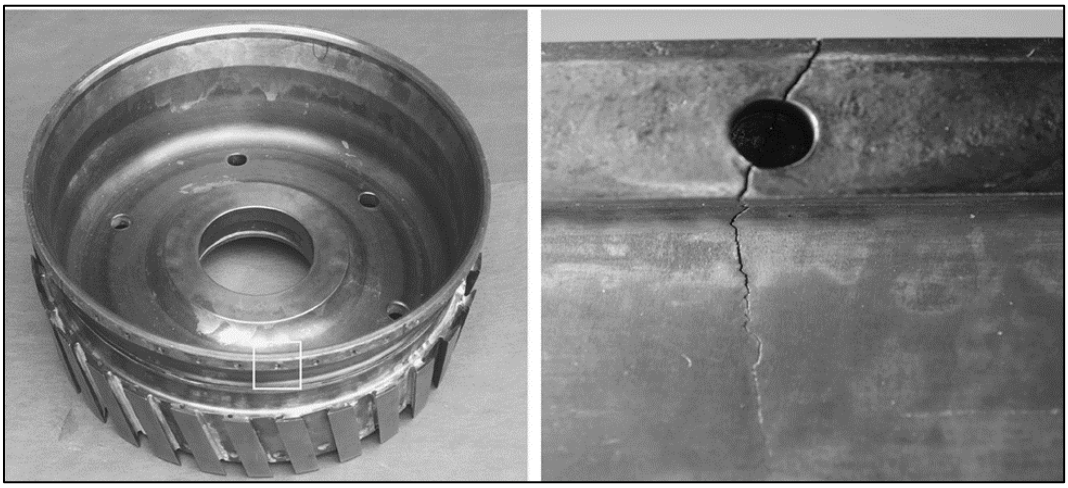

Figure 6: Schematic picture of a second stage compressor rotor drum and a progressed crack at the rivet hole surface (Bhaumik et al., 2008).

2.3) Fatigue Methods

Generally, there are different modeling methods to predict the fatigue life of a material:

1: Stress-life method $[S-N]$

2: Strain-life method $[\varepsilon-N]$

3: Linear elastic fracture mechanics (LEFM) method $[\frac{da}{N}-\Delta K]$

Stress-life and Strain-life methods are used for performance and simulation of fatigue crack initiation life. On the other hand, LEFM method is utilized for implementation and simulation of fatigue crack propagation life.

2.4) Stress-Life and Strain-life Methods

To use either the stress-life or the strain-life method, it depends on whether it is the stress or the strain dominating the cycling among maximum and minimum stress / strain levels. Thus, the core conceptions of the stress-life and the strain-life methods are debated for a better understanding.

Stress-life method was introduced by A. Wöhler who carried out rotating bend tests on different alloys during the mid-1800s (Lampman & DiMatteo, 1996). An effective traditional approach to assess the life of the components because of frequent fatigue loads. He also conducted several fatigue tests on railway axles, then he reported that stress range is more critical than maximum stress.

Figure 7 displays graphically a common stress cycle in which the key concepts are displayed. ΔS is stress range. In other words, the difference between maximum, S_{max}, and minimum, S_{min}, stresses:

$$\Delta S = S_{max} - S_{min} \tag{2.1}$$

S_a is stress amplitude which is the stress range divided by two:

$$S_a = \frac{\Delta S}{2} \tag{2.2}$$

S_m is mean stress which is averaging the maximum and the minimum amounts:

$$S_m = \frac{S_{max} + S_{min}}{2} \quad (2.3)$$

R is stress ratio:

$$R = \frac{S_{min}}{S_{max}} \quad (2.4)$$

Note that the feasible range for the R-ratio is: $-1 \leq R \leq 1$.

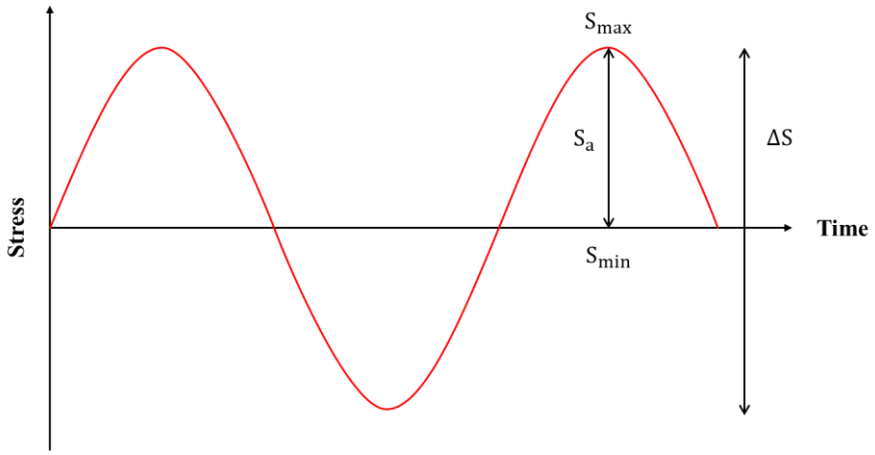

Figure 7: Schematic sketch of alternating stress

To acquire a stress-life curve, a great deal of different stress levels needs to be depicted. The stress-life curve is also named $S-N$ curve or nominal stress technique where S refers to the stress and N stands for the number of cycles. The stress range, ΔS, or the stress amplitude, S_a, is usually displayed against the number of cycles. It should be noted that %50 fatigue failures are anticipated via median life which simply means %50 of the probability of that variation is the confidence level.

To acquire a mathematical demonstration of the $S-N$ curve, equation (2.5) can be fitted.

$$S_a = C(N)^m \quad (2.5)$$

C and m are fitting constants of $S-N$ model.

Manson-Coffin in the mid-1950s represented equation (2.6) to correlate the relationship among plastic strain and fatigue life in low-cycle high-strain fatigue region:

$$\frac{\Delta\epsilon_p}{2} = \epsilon_f'(2N_f)^c \quad (2.6)$$

$\frac{\Delta\varepsilon_p}{2}$ is plastic strain amplitude, $2N_f$ is reversals to failure, ϵ_f' is fatigue ductility coefficient and c fatigue ductility exponent. Parameters ϵ_f' and c are fatigue properties of the material which ϵ_f' is roughly equivalent to true fracture ductility and c ranges from -0.5 and -0.7.

Basquin in the early-1900s presented equation (2. 7) to correspond the relationship among plastic strain and fatigue life in high-cycle low-strain fatigue region:

$$\frac{\Delta\epsilon_e}{2} = \frac{\sigma_f'}{E}(2N_f)^b \quad (2.7)$$

$\frac{\Delta\epsilon_e}{2}$ is elastic strain amplitude, $2N_f$ is reversals to failure, σ_f' is fatigue strength coefficient, E is Young's modulus and b fatigue strength exponent. Parameters σ_f' and b are fatigue properties of the material which σ_f' is roughly equivalent to monotonic true fracture stress and b ranges from -0.12 and -0.05.

Eventually, strain-life method then was proposed by the combination of equations (2. 6) and (2. 7) (Nieslony et al., 2008):

$$\varepsilon_{t-a} = \varepsilon_{e-a} + \varepsilon_{p-a} = \frac{\sigma_f'}{E}(2N_f)^b + \epsilon_f'(2N_f)^c \quad (2.8)$$

ε_{t-a} is total strain amplitude, ε_{e-a} is elastic strain amplitude and ε_{p-a} is plastic strain amplitude.

In this investigation, all fatigue tests obtained from literature have been executed with a stress control method.

2.5) Fatigue Strength

The fatigue limit is the maximum stress amplitude level under which the material has an unlimited life. The endurance limit and the fatigue strength are its alternative names. It is generally noted after 2 to 5 million cycles (Gurney & Saunders, 1981; Dowling et al., 2013; BANNANTINE et al., 1990). Figure 8 illustrates a common $S-N$ curve:

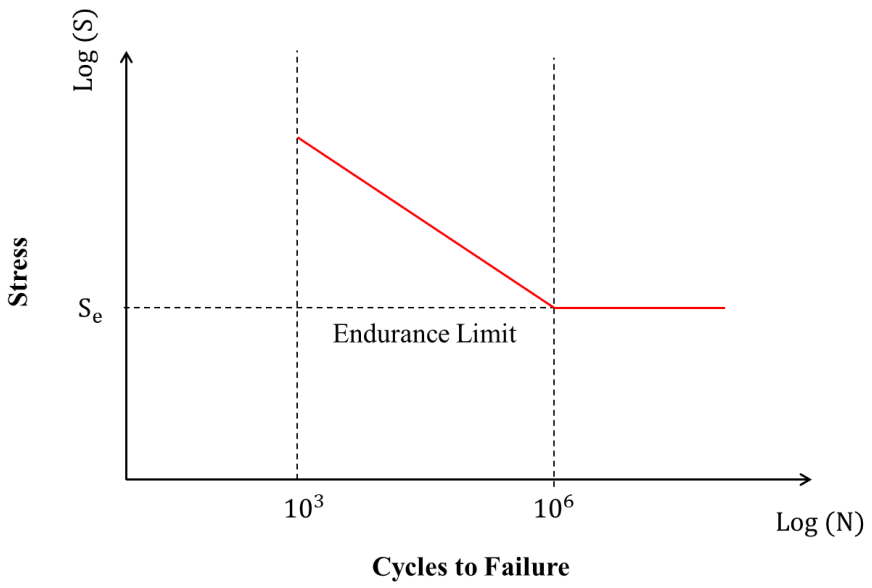

Figure 8: Schematic portrait of S — N curve

2.6) Transition Life

Low-cycle fatigue (LCF) region is distinguished by high cyclic stress levels exceeding the fatigue strength of the material. The endurance limit is generally admitted being around between 10^3 and 10^4 cycles. Further, the LCF is recognized by frequent plastic deformation in each cycle. In contrast, high-cycle fatigue (HCF) region is marked by elastic deformation. In other words, the number of cycles to fracture is high for the HCF and is low for the LCF. Figure 9 shows illustratively the overall concept of transition life between the LCF and the HCF for fatigue mechanics crack growth. In this research, the value (10^4) was employed as the transition line from LCF to HCF by setting frequency increment of the number of the cycles to 1000 for LCF and 10000 for HCF.

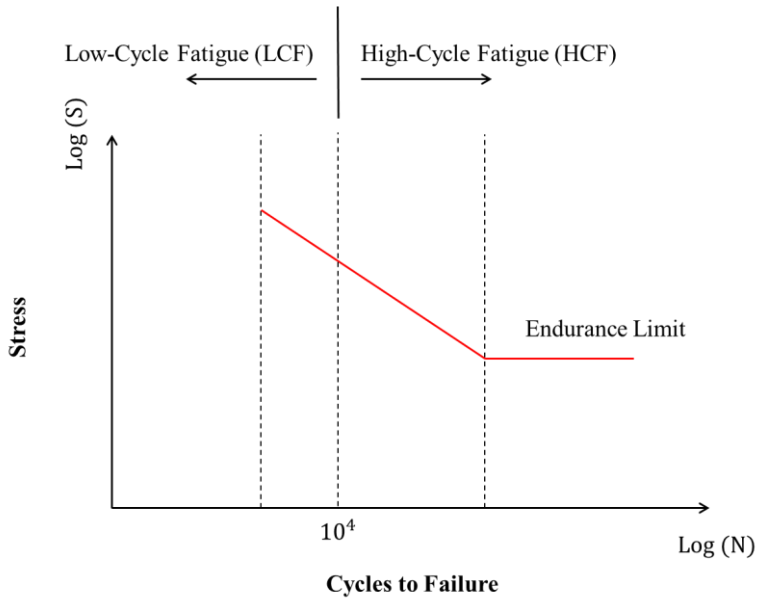

Figure 9: Schematic perspective of low-cycle fatigue and high-cycle fatigue

2.7) Welded Joints

Welding is a manufacturing process of joining components by which two or more pieces are merged together by the use of heat, pressure and or both of them. Welding is typically employed on metals, but weldability is an important factor in order to select appropriate materials to weld together so that high weld quality can be achieved.

To join components together, welding techniques are built processes because a great ratio of engineering structures are fabricated by welding. Generally, welding techniques can be classified into fusion welding and pressure welding. Fusion welding operations embrace localised melting and strengthening which can be processed with or without extra filler metal. Arc welding is the topmost generally utilized technique among fusion welding processes. In contradiction to fusion welding operations, pressure welding processes do not embrace melted material (Weman, 2003).

Main factors impacting on fatigue strength of welds are presence of weld imperfections, residual stresses and stress concentration at weld toe etc. which have strong negative influences on the fatigue life of the welded joints.

Welded joints pose much lower fatigue strength than non-welded components. Figure 10 demonstrates comparatively the endurance limit of a smooth plate, a plate with a hole and a fillet welded joint, respectively (Maddox, 2002; Kirkhope et al., 1999a).

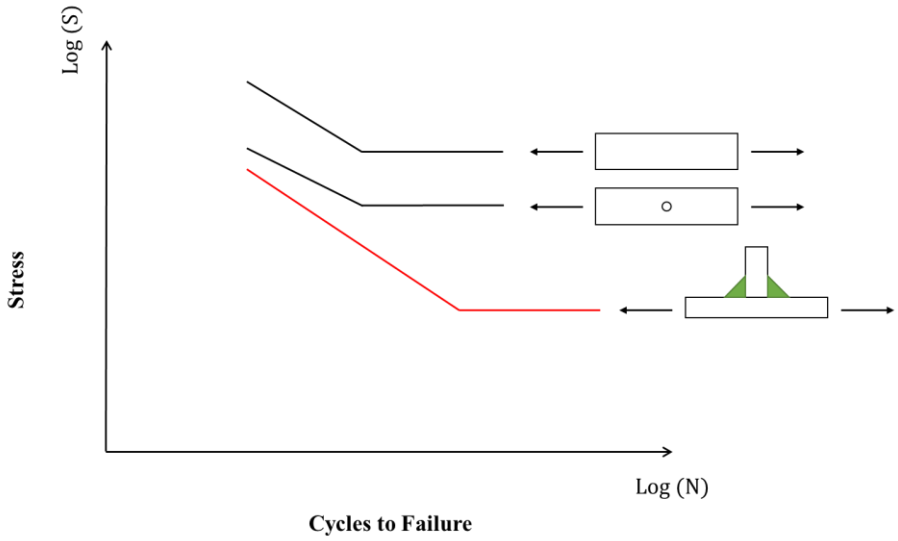

Figure 10: Endurance limit comparison of three different types of components (Harati, 2015)

2.8) Weld Imperfections

Various weld imperfections emerge at different zones of the weld segments which these defects perform as local stress raisers, a spot from where a fatigue crack may form. Unfortunately, the weld imperfections are problematic to detect due to their small sizes and troublesome locations. Figure 11 depicts schematically an overall perspective of some potential weld defects at a welding zone (AL-Emarani & Åkesson, 2013).

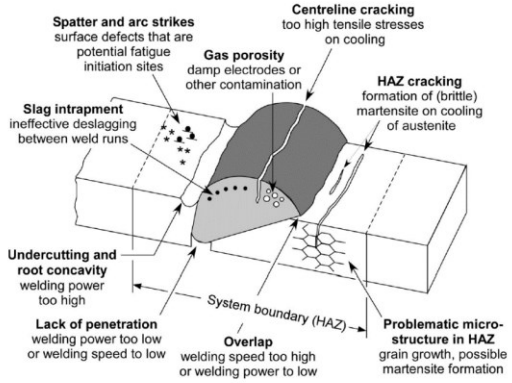

Figure 11: Schematic perspective of some potential weld defects at a welding zone (Zerbst et al., 2014)

In Figure 11, some of the typical appearing weld imperfections with disastrous effects on the fatigue strength of a welding structure are demonstrated.

The crack initiation stage is the utmost essential phase for smooth structures. The bulk of the life is put on the initiation of the small cracks. Conversely, it is widely acknowledged that the small imperfections already exist at the weld areas. Generally speaking, the crack initiation stage is comparatively negligible. The bulk of the life is put on the propagation of the cracks in the welded structures (Lassen & Recho, 2006). Nowadays, Commission XIII of the International Institute of Welding (IIW) has been actively boosting extensive detailed research to advance weld quality guidelines which significantly correlates weld recognition principles to the fatigue life of the welds (Fricke, 2013). The devastating impacts of the weld imperfections on the fatigue life have been investigated broadly (Seto et al., 2000; Jonsson et al., 2011; Schaumann & Collmann, 2013; Shirahata et al., 2014). These studies have demonstrated that the defects have diminished the fatigue strength of the welded structures.

Figure 12 displays graphically some of the weld imperfections in a welded joint such as root, transverse, toe and underbed cracks. In this study, toe cracks have been investigated. In a nutshell, material imperfections act as crack initiation sites of paramount significance for fatigue strength assessments of the welded structures.

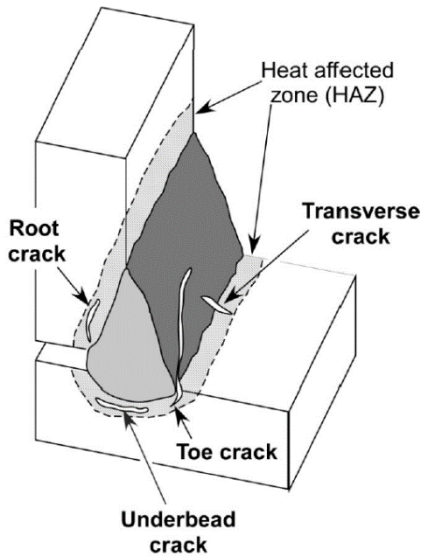

Figure 12: Schematic sketch of some diverse types of cracks in a welded joint (Zerbst et al., 2014)

2.9) Residual Stresses

Residual stresses are known as stress distributions that exist within a body without any external forces. In fatigue assessment, residual stresses can be categorized into two groups: undesirable [+] and desirable [−]. Undesirable residual stresses are based on tensile stresses induced by manufacturing procedures like the welding and in-service repair like replacing the components etc. In fact, the welding operations induce high amounts of tensile residual stresses inside and near the weld along with compressive ones further away from the centre of the plate. Potentially, the welded connections may experience premature fracture (Sharpe, 2008). On the other hand, desirable residual stresses are as a consequence of eliminating undesirable residual stresses from the crack initiation zone by Post-Weld Treatment (PWT) techniques like Ultrasonic Impact Treatment (UIT) to induce beneficial compressive residual stresses. UIT imparts beneficial compressive residual stresses into the welded attachments.

Figure 13 shows illustratively penalizing tensile residual stresses leading to a risk of premature failure. On the contrary, Figure 14 presents compressive residual stresses raising resilience to fatigue cracking.

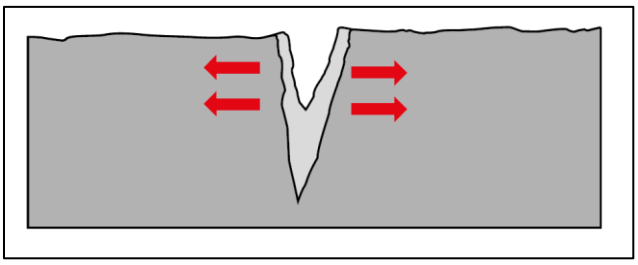

Figure 13: Schematic portrait of undesirable residual stresses leading to a risk of premature failure (EUROPE TECHNOLOGIES SONATS, 2020)

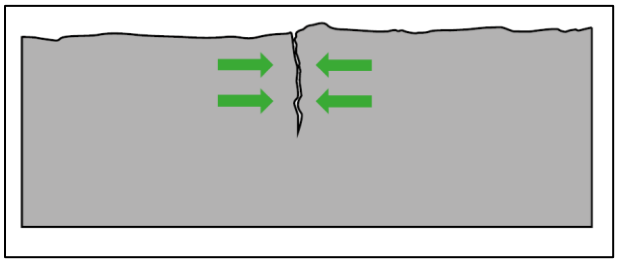

Figure 14: Schematic illustration of desirable residual stresses endurance of fatigue cracking (EUROPE TECHNOLOGIES SONATS, 2020)

During the welding processes, heating and cooling cycles occurs in the welded areas. Some of the devastating consequences of this phenomena are uneven heat distributions, plastic deformations, residual stress field and phase alternations etc. (Rossini et al., 2012). In practice, heat-affected zones (HAZ) point to diverse compositions of residual stresses further to the welded section.

Figure 15 represents an instance of the residual stresses' distributions within a butt weld. As shown in this figure, a butt joint is utilized for a better visualization of the residual stresses concept.

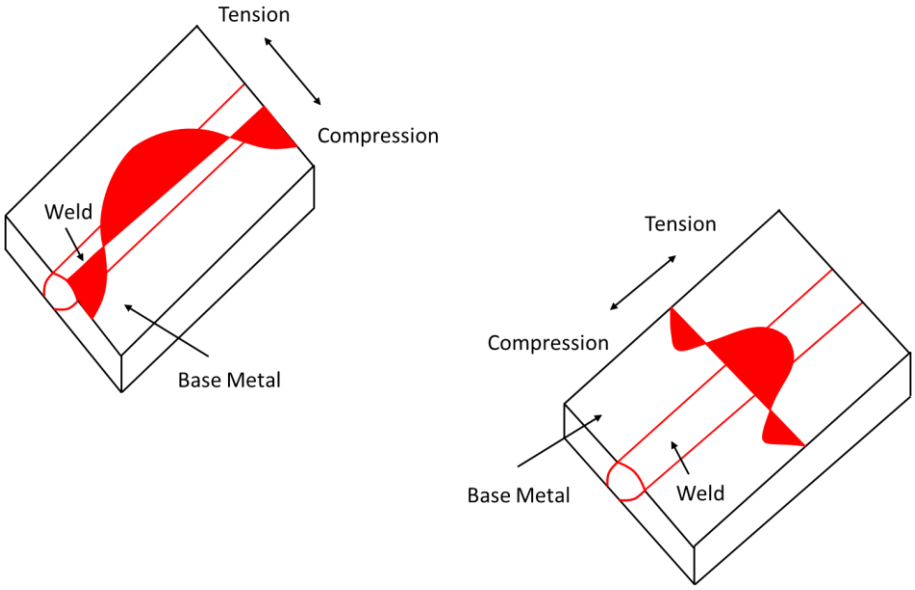

Figure 15: Common distributions of residual stresses in a butt joint for longitudinal and transverse directions

When the tensile residual stresses advance the yield strength of the base metal, fatigue strength of the welded components deteriorates dramatically. The impacts of the tensile residual stresses are similar that of comparable mean stresses. Figure 16 depicts schematically the ramifications of such principal effect in fracture mechanics.

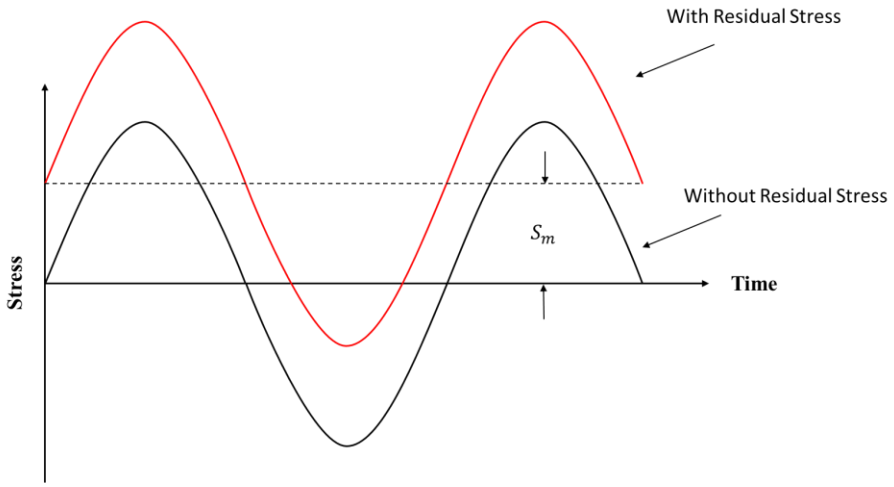

Figure 16: Impact of tensile RS on stress cycles.

In the figure, the mean stress is increased remarkably. For this reason, the structure is excessively less fatigue resistant (Stephens et al., 2001; Lassen & Recho, 2006; Withers & Bhadeshia, 2001a, 2001b; Webster & Ezeilo, 2001; James et al., 2007).

Figure 17 displays graphically the benefit of such techniques to capture the spirit of the concept.

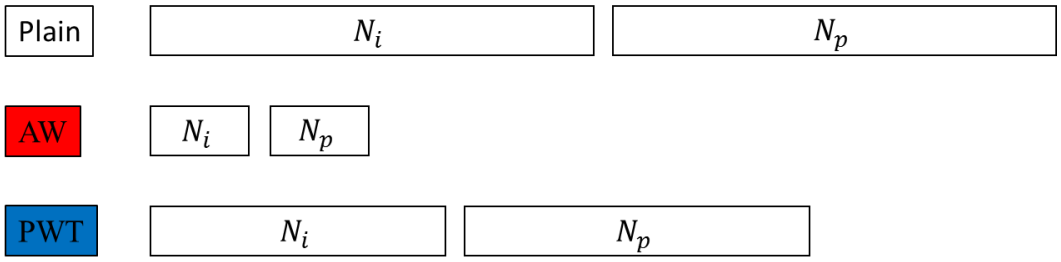

Figure 17: Advantage of PWT techniques in recovering crack initiation and propagation life of a welded specimen (Mosiello & Kostakakis, 2013)

From the figure, N_i is crack initiation life and N_p is crack propagation life. As illustrated, the PWT techniques can extensively restore crack propagation life as well as crack initiation life of a welded component. The formation of undetected cracks in the slip bands lead to marked rise of stress concentration in the zone (Schijve, 2008).

The residual stresses are usually measured non-destructively by x-ray techniques or mechanical ones. The residual stresses are determined based on strain measurements which the strains are computed through the strain in metal's atomic crystal lattice (Paul, 1986). All techniques of stress specification need evaluation of some inherent feature such as area and strain or force accompanied by the computation of the correlated stress (Paul, 1986). Note that the residual stresses are also named "self-equilibrium stresses". In contrast to the tensile residual stresses, the beneficial compressive residual stresses can enhance substantially fatigue strength of such components. Hence, a deep understanding of the residual stresses is necessary for the precise evaluation of fatigue strength of the welds (Stephens et al., 2001). Figure 18 shows illustratively a portable system for in-lab and in-field services to correctly identify critical zones with the tensile residual stresses and to accurately measure the compressive residual stresses etc.

Figure 18: Schematic image of a residual stress analysis device by x-ray diffraction - Stresstech Xstress 3000 G2R (EUROPE TECHNOLOGIES SONATS, 2020)

The scientific approach of such device is the x-ray beam is collimated to the surface of the part. After that, the evolution of the diffraction angle in reference to the variation of the incident beam angle is gauged as shown in Figure 19 using the current conventional methods like $\sin^2\psi$ (Mishchenko et al., 2018; ASTM E2860, 2012; BS EN 15305, 2008) [Bragg's Law].

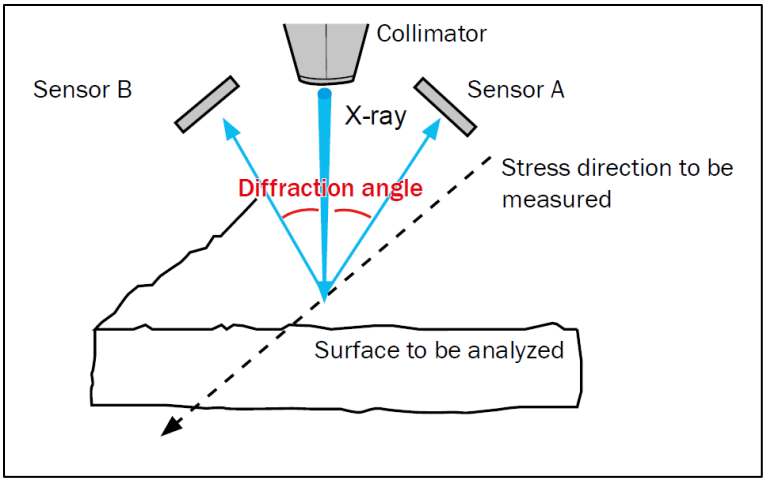

Figure 19: Schematic sketch of an x-ray diffraction measurement layout (EUROPE TECHNOLOGIES SONATS, 2020)

In this thesis, residual stresses were employed in depth below weld toe,

2.10) Ultrasonic Impact Treatment

Ultrasonic Impact Treatment (UIT) is a lately advanced Post-Weld Treatment (PWT) method by Statnikov et al. in former Soviet Union (2000). UIT has attracted increased attention from researchers around the world in recent years due to its efficiency and ease of application. Figure 20 introduces some applications of UIT such as treatment of circumferential welding on heavy plant front loaders, railway track repairs, peening of road infrastructures, strengthening defence vehicles and repair of marine structures etc. from left to right in the picture, respectively.

Figure 20: Introduction of some applications of UIT (EUROPE TECHNOLOGIES SONATS, 2020)

UIT operates at a high ultrasonic frequency of approximately 18000-27000 Hz and treats the welding surface with needles or hammer-like rods. Figure 21 represents schematic view of a portable UIT system. In short, it is composed of a central unit that has an ultrasonic generator inside it, a handheld peening head with an end-piece that can be changed depending on the application. The handheld peening head is an acoustic set which has a piezo-electrical convertor, a booster and a sonotrode. An electrical signal will be created by the generator, then will be converted into a mechanical vibration by the convertor. This mechanical energy will be amplified by the combination of the booster and the sonotrode. Through a needle or a rod, the waves will be transmitted to the part for treatment as shown in Figure 21.

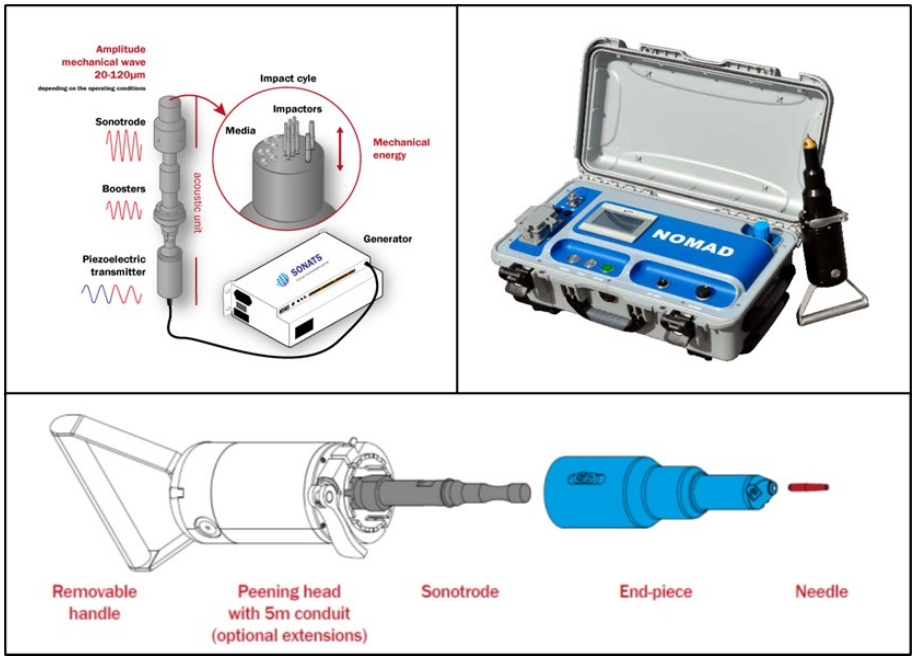

Figure 21: Schematic view of a portable UIT system accompanied with a breakdown of its component and its principal – NOMAD (EUROPE TECHNOLOGIES SONATS, 2020)

UIT method seems to be so efficient and multiple studies reported that the advantageous impression of these approaches is based on the high compressive residual stresses which are induced in the treated region. In fact, the principal aim for the enhancement of fatigue strength is UIT creates ultrasonic vibration to impact and plastically deform the weld toe, resultantly introducing compressive residual stresses by eliminating tensile residual stresses (Deng & Murakawa, 2006). Other determining features for the constructive influence of UIT are declining of stress concentration in weld toe areas and enhancement of mechanical properties of the superficial layers (Roy, 2003; Roy & Fisher, 2005; Y. Kudryavtsev et al., 1995). Over the past several decades, numerous PWT techniques, including traditional techniques such as hammer peening, shot peening, grinding and TIG dressing showed that UIT is the most effective enhancement treatment of weld joints in comparison to the previous methods (E. S. Statnikov et al., 2002; Fisher et al., 2001; Yuri Kudryavtsev & Kleiman, 2013; Lotsberg et al., 2014). Geometry enhancement methods such as TIG dressing and grinding concentrate on eradicating flaws and declining stress concentration of welded constituents. While residual stress modification methods like hammer peening and shot peening tend to emphasize on introducing favorable compressive residual stresses and adjusting residual stresses distributions of welded joints (Marquis et al.,

2013). Figure 22 depicts schematically the significant influences of UIT process by modifying the weld toe geometry and inducing compressive residual stresses as shown in the figure.

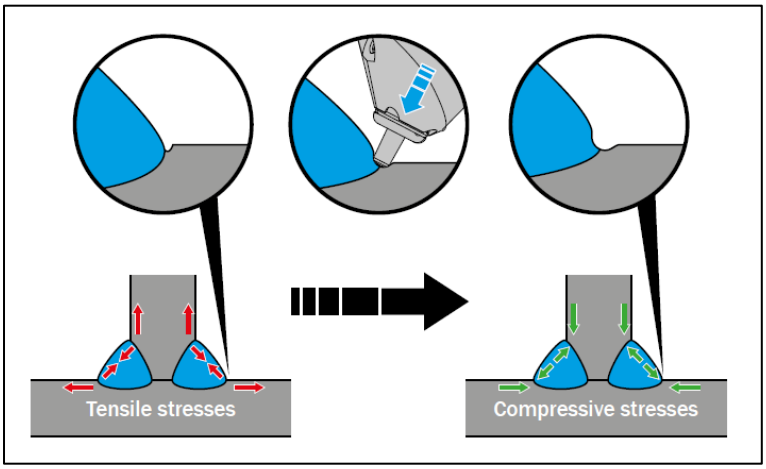

Figure 22: Schematic portrait of profound principal of UIT (EUROPE TECHNOLOGIES SONATS, 2020)

Note that UIT is a cold mechanical treatment that engage hitting the weld toe by a needle or a rode. Figure 23 displays graphically some applications of UIT such as weld toe peening, radius peening and heat affected zone peening etc. to match for different cracks and various geometries.

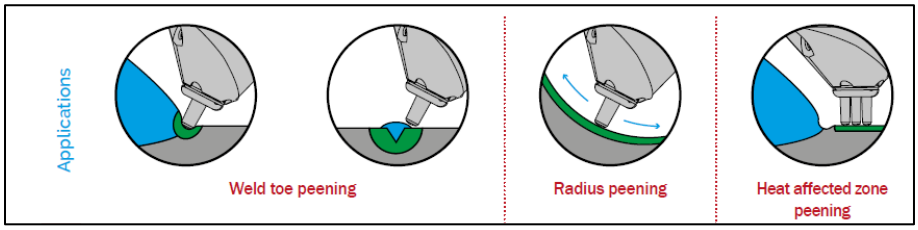

Figure 23: Schematic illustration of some UIT applications and its accessories for reaching difficult locations of welded joints (EUROPE TECHNOLOGIES SONATS, 2020)

Figure 24 shows illustratively how an actual preventive treatment is done after the welding. Figure 24 demonstrate visually how much UIT is more user and environmentally friendly than other traditional methods. In summary, UIT process is fully controlled and automated. It is a clean process with low energy and material consumptions. No risk of damage to customer parts, no danger to operators and less risk of musculoskeletal disorders for operators are some remarkable features of UIT technique as well.

Figure 24: Detecting of a fatigue crack initiation followed by preventive treatment

Numerous studies have shown fatigue strength of different materials for either welded or un-welded components. To simply mention a few:

The authors (Cui et al., 2018) investigated the impact of UIT on fatigue resistance of T-shape welded attachments by utilizing nominal stress, effective notch stress and peak stress methods. It has been observed that fatigue cracks initiated at weld toe between flange and gusset plates. Test specimens were symmetrical cruciform welded samples. It was shown that fatigue resistance of the welded attachments raised by approximately 35% due to reducing stress concentration and weld residual stresses by utilizing UIT technique. It has been compared to other methods as well which proved that UIT is a robust technique.

The authors (Roy, 2003) studied the effect of UIT on fatigue crack initiation and propagation of welded transverse stiffeners. UIT highlighted that fatigue performance of all treated details increased significantly. This increase was more profound at lower minimum stress and lower stress range for the UIT condition. UIT enhanced weld toe geometry and diminished macro-discontinuities at weld toe region via surface erosion, plastic deformation and transformation in micro-structure. Beneficial residual stresses were induced by UIT to the order of that material's yield stress at treated surface.

The authors (Yuan & Sumi, 2015; Tang et al., 2020) used FEA to simulate distribution of residual stresses in welded joints before and after treatment as well as fatigue resistance assessments and FCG behaviors of a cruciform joint (Yuan & Sumi, 2015), a butt joint and a T-joint (Tang et al., 2020), respectively. Yuan and Sumi (2015) employed commercial codes

SYSWELD and LS-DYNA for the simulations. While Tang et al. (2020) used ABAQUS software for forecasting residual stresses and utilized double-ellipsoidal heat source model described as a function of a heat flux (Goldak et al., 1984) along with using eight-node Hex (C3D8T) meshed elements. Tang et al. (2020) also employed conceptions of SC and SIF accompanied by WF already described through Chapter 2 for both conditions (Chattopadhyay et al., 2011). The authors (Yuan & Sumi, 2015; Tang et al., 2020) demonstrated that by comparing experimental outcomes versus Finite Element (FE) models and FEA simulations, it still highlighted that UIT is a highly impressive method for improving fatigue life of the welded joints. The authors (Tang et al., 2020) also investigated the influence of R- ratio on the Aw and the UIT conditions. It has been demonstrated that the greatest improvement of fatigue life happened at the R-ratio equal to 0.1 which stress amplitude was about $150\ MPa$ whereas the lowest enhancement of fatigue life took place at the R-ratio equivalent to 0.5 which stress amplitude was approximately $150\ MPa$ as well. Further, it was proven through the simulation outcomes that UIT retarded crack shape evolution as well.

The affect of UIT in aluminum alloys has been also studied (Castillo-Morales & Salas-Zamarripa, 2010) since aluminum alloys are quite popular in aerospace industries. Apart from introducing beneficial residual stresses described above, UIT also showed a significant raise in roughness and hardness of the material which led to enhancing fatigue life of the material. Specimen was an un-welded component, UIT was used to treat surface of the material in order to cover up porosity of the material. Due to fact that pores and cracks can collide at some point which will increase the cracks length (Hellan, 1984; Ritchie, 1999; Vaidya, 1985).

Forecasting of UIT treatment benefit has been limited to assessment using either nominal stress $S-N$ curvatures (Marquis et al., 2013) or local stress methods (Ghahremani, 2015). Just insufficient investigations have used fracture mechanics models to assess the fatigue life enhancement due to UIT treatment either alone or in two stage models (initiation and propagation) (K. Ghahremani, 2015; Tehrani Yekta et al., 2013; Lihavainen, 2006; Josi & Grondin, 2010).

The aforementioned literatures have demonstrated that UIT can also be efficient in improving the fatigue life of the welded constructions which had experienced a period of service. Figure 25 demonstrates comparatively how UIT can improve the fatigue life by eliminating the appearance of the cracks. In a nutshell, UIT acts on weld imperfections to delay crack initiation as

well as to slow down crack propagation as shown in the figure. Crack initiation phase experienced a substantial delay because of inversing the internal residual stresses which led to modifying the fatigue life of the welded component. Crack propagation phase encountered a considerable retardation because of inducing compressive residual stresses and plastically deforming the weld toe. In the end, schematic perspective of fatigue life improvement is vividly presented in Figure 25.

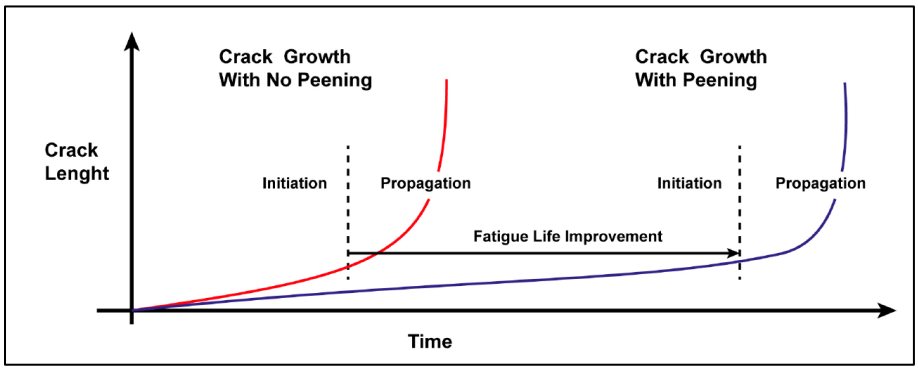

Figure 25: Schematic perspective of lifetime of a component after UIT

2.11) Stress Concentration

Stress Concentration Factor (SCF) plays a profound role in fatigue failure of the welded structures. However, the significance of various factors which control the fatigue strength of these structures is not well known due to its complexity when the effect of SCF combines with different contributed factors (Maddox, 2002). The SCF is one of the key factors that has a strong influence on the fatigue failure of such structures.

After the welding, the impact of stress concentrations – due to variations in the geometry at the weld toe, merged with increased local mean stresses – because of the undesirable residual stresses, requires a better understanding of such phenomena towards better fatigue design standards and safer structures of the welded components. On top of that, when the influence of the stress concentrations is added to the tensile residual stresses, its contribution is extremely destructive. The relationship of local stress concentrations and local yield strength are also studied here (Farajian-Sohi et al., 2010). Figure 26 represents schematically prone locations of the stress concentrations and its concept in short.

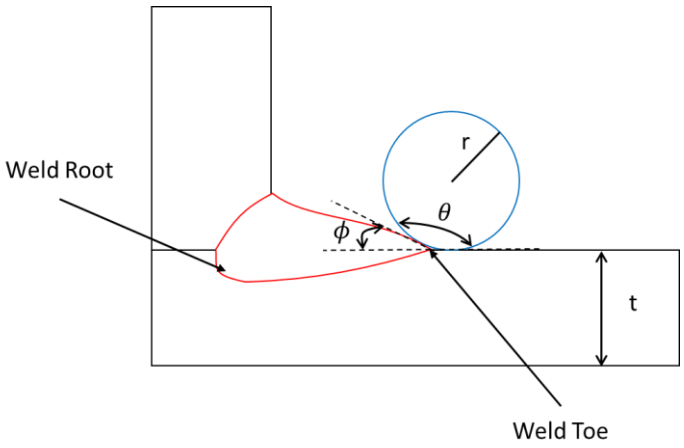

Figure 26: Schematic sketch of stress concentration sites at weld toe and weld root

As already stated, the weld toe is the most expected crack initiation areas where potential existence of crack-like defects causes the weld toe a crucial site for cracking (Kirkhope et al., 1999a, 1999b). Sites with the large stress concentrations are prone to fatigue cracks (Fricke, 2013). In general, the main geometrical aspects that govern the fatigue life are the weld toe radius and the angle. To enhance the fatigue strength, the stress concentrations can be decreased by raising either the weld toe radius or the angle (Caccese et al., 2006; Niu & Glinka, 1987; Martinsferreira &

Mourabranco, 1989; Pang, 1993; Teng et al., 2002; Lee et al., 2009; Williams et al., 1970; Radhi & Barrans, 2010; Barsoum & Jonsson, 2011).

Welding operations creates stress flow discontinuity inside the welded region as a result of that local high stress peaks are generated as described in (Dürr, 2007) and also due to changes in cross section of the welded structures like different joint types such as T-joint, cruciform-joint and longitudinal joint etc. In summary, the SCF, K_t, in unitless form is ratio between local peak stress, S_{loc}, at the welded area and nominal stress of a remote load, S_n, at the uniform segment of the specimen:

$$K_t = \frac{S_{loc}}{S_n} \qquad (2.9)$$

One of the practical approaches to determine the SCF is through equation (2. 9). Figure 27 presents visually stress distributions through the thickness as well the weld toe line and statically linearized equivalent stress profiles (Chattopadhyay et al., 2011).

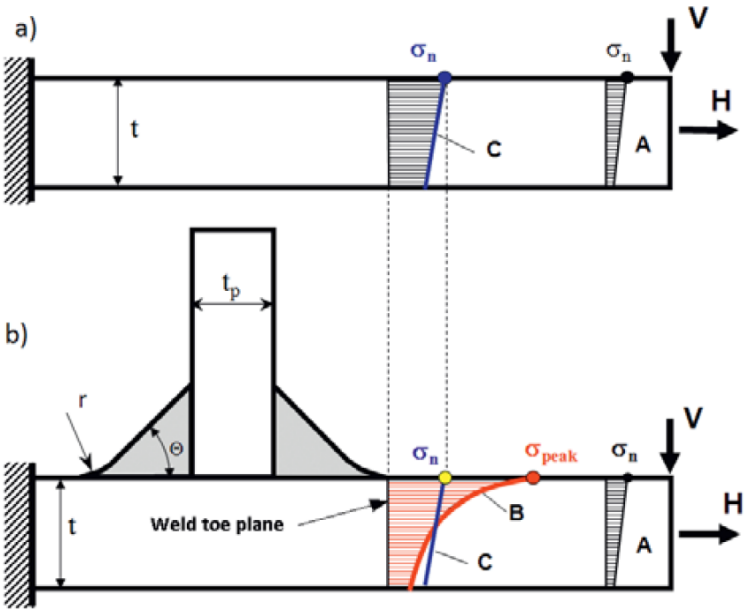

Figure 27: Schematic picture of stress fields in an unwelded plate versus stress fields in a plate with non-load carrying one-sided attachment with fillet welds (Chattopadhyay et al., 2011)

Niu and Glinka (1987) introduced another robust approach towards determining the SCF. In brief, equation (2. 10) was proposed for the SCF, K_w, at a weld toe derived from the weld profile as shown in Figure 27:

$$K_w = 1 + 0.5121(\Phi)^{0.572}(\frac{T}{\rho})^{0.469} \quad (2.\ 10)$$

ρ is weld toe radius (r), ϕ is flank angle for a fillet weld, T is plate thickness (t) and θ is weld toe angle which is equal to $180 - \phi$, respectively. Note that to calculate various parameters of equation (2. 10), it is necessary to have high tech sophisticated laboratory equipment. After implementing the geometry measurements by taking high quality pictures at micro scale, the necessary info needs to be extracted from the images by using either AutoCAD or ImageJ to for example fit an ellipse by extracting the dimensions of it via the digital image of the final crack shape. Note that the cracks are at micro scale in this thesis since there are micro-cracks.

In another investigations, weld toe fields were modeled using Finite Element Analysis (FEA) to establish the elastic stress distribution and the SCF for fillet welded attachments (Niu & Glinka, 1987; Pang, 1993). Figure 28 depicts schematically the stress distributions through the thickness as well the weld toe line and statically linearized equivalent stress profiles.

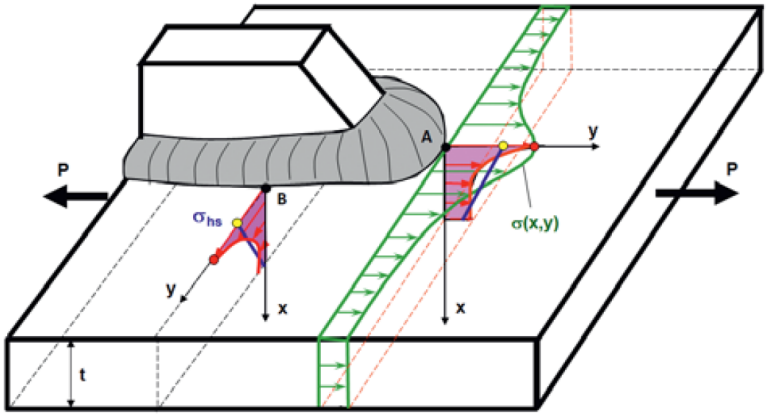

Figure 28: Actual stress distributions through thickness as well weld toe line and statically linearized equivalent stress profiles (Chattopadhyay et al., 2011)

Pang (1993) stated that increasing weld toe radius from 1 to 2.5 mm will carry out roughly 14% decline in the SCF. Alam et al. (2010) indicated that the weld toe radius is not constantly the main aspect in fatigue crack initiation. Weld ripples cause local micro geometry impacts can be noteworthy as well by correlating the geometrical aspects to the stress concentrations. The authors (Niu & Glinka, 1987; Chattopadhyay et al., 2011) determined that through the thickness stress distributions and weight function technique can be employed for simulating the FCG as well as computing the SCF and stress intensity factor etc.

Figure 29 displays graphically the dependency of fatigue limit on component type as stated by (P. J. Haagensen, 2011).

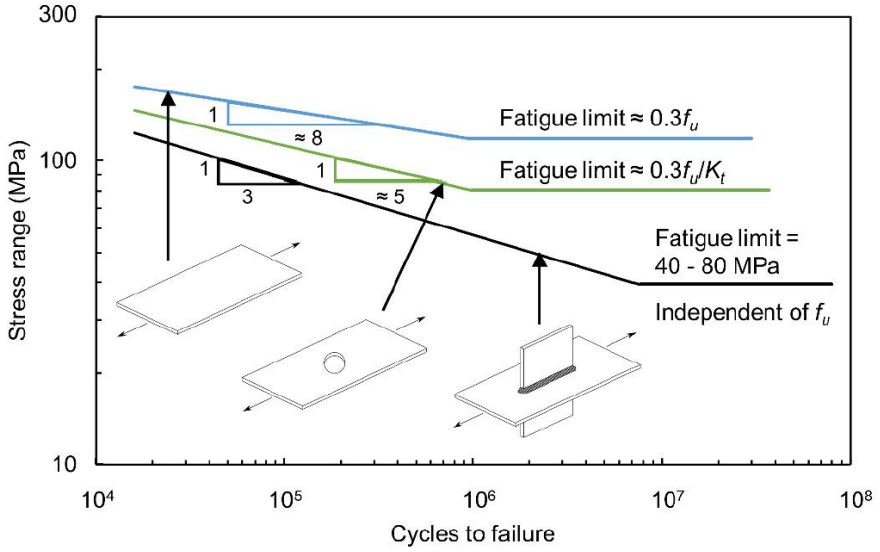

Figure 29: Association of fatigue limit on component type as stated by (P. J. Haagensen, 2011)

There is a proven fact for the traditional $S - N$ technique that the author (P. J. Haagensen, 2011) demonstrated the SCF is independent of ultimate tensile strength, S_u, for the welded components due to some unknown phenomena at micro scale such as high local stress concentrations accompanied by high local mean stresses in the welded region.

Figure 30 shows illustratively the total lifespan of a welded component exposed to cycling loading. It can be interpreted that the first state indicates the adequate number of cycles requires for a specimen copes under the applied loading. It can be also specified that the first state illustrates the sufficient number of cycles expects towards the formation of a fatigue crack. Peeker (1997) demonstrated that the local stresses are extremely greater than the nominal stresses in neighboring regimes. Schijve (2001) also stated that the stress concentrations are comparatively immense engendering micro-cracks surrounding notches under cyclic loading. Numerous studies have shown such phenomena in material science like the fundamental concepts of dislocations and slip bands plastic deformations etc. as well as in fracture mechanics (Al-Emrani & Åkesson, 2013; NDT Eduation Resource Center, 2014; Bhat & Patibandla, 2011; Fong & J., 1979).

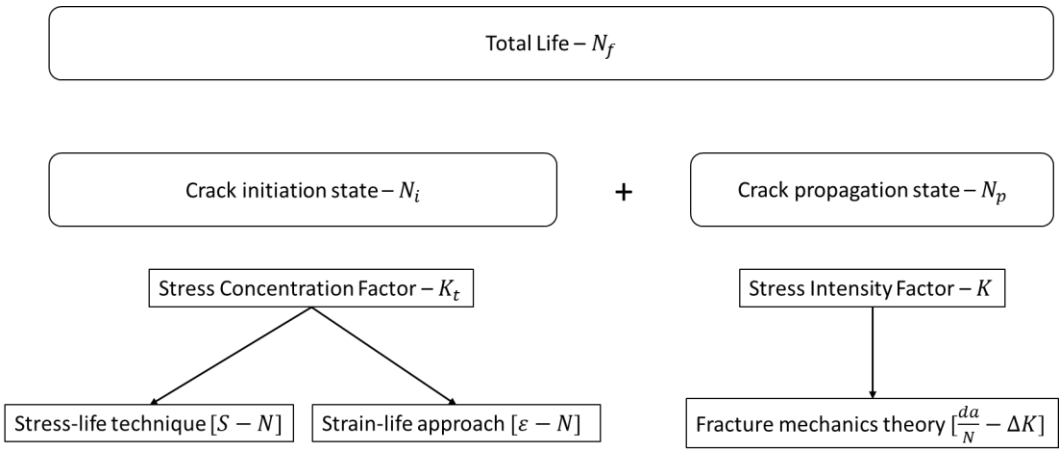

Figure 30: Schematic image of different states of fatigue life and relevant factors

To express the extremity of fatigue loading of the crack initiation state, the SCF is employed. The first state is based on the number of cycling loading demanded to active a fatigue crack in this regime as shown in Figure 30.

2.12) Linear Elastic Fracture Mechanics Approach

In a nutshell, traditional strength-of-materials methods are not accurate enough for the crack propagation state as shown in Figure 30. The prediction and the diagnosis of such failure due to existence of a crack or an imperfection leading to magnifying the stress in the proximity of that crack within a welded component is utilized by fracture mechanics theory.

The traditional methods apply strength-of-materials concepts to the design and the analysis of such parts. Applied loading creates the stresses within the welded regime. Failure is established to happen when the applied stress surpasses the material's strength either the yield strength, S_y, or the ultimate strength bounds by the principal for that failure.

Stress Intensity Factor (SIF) is a handy concept for describing the stress field near the crack tip. Hence, the SIF is another key parameter in fracture mechanics crack growth as shown in Figure 30. Stress density changing around the crack tip is meant as an assessment of finding fatigue crack propagation rate.

The SIF is computed as a function of applied stress, crack size and component geometry. Fracture takes place when the SIF exceeds the material's facture toughness, K_c. In this situation, the crack will advance in an accelerated and instable manner till failure.

In brief, stress distribution around the crack tip determines the crack behaviour and how fast crack grow in that direction. The SIF is given in equation (2. 11) as the simplest formulation:

$$K = S_n\sqrt{\pi a}.Y \qquad (2.\ 11)$$

Where K is stress intensity factor, S_n is nominal stress of a remote load, a is crack length and Y is geometry factor which is function of geometry itself and loading of the detail. The SCF is dimensionless, since it simply describes the geometry of the specimen, while the SIF has units of $MPa\sqrt{m}$. Equation (2. 11) was also evolved from the stress field near a sharp notch on in regard to a concept of elasticity solution (Broek, 1986).

Figure 31 represents schematically a typical fracture mechanics fatigue crack initiation and propagation behaviour. It is plotted under log-log scales and it consists of three different regions:

- Region I is called as Threshold region → Crack Threshold Stage
- Region II is named as Paris Law region → Crack Propagation Stage
- Region III is entitled as Fracture region → Crack Failure Stage

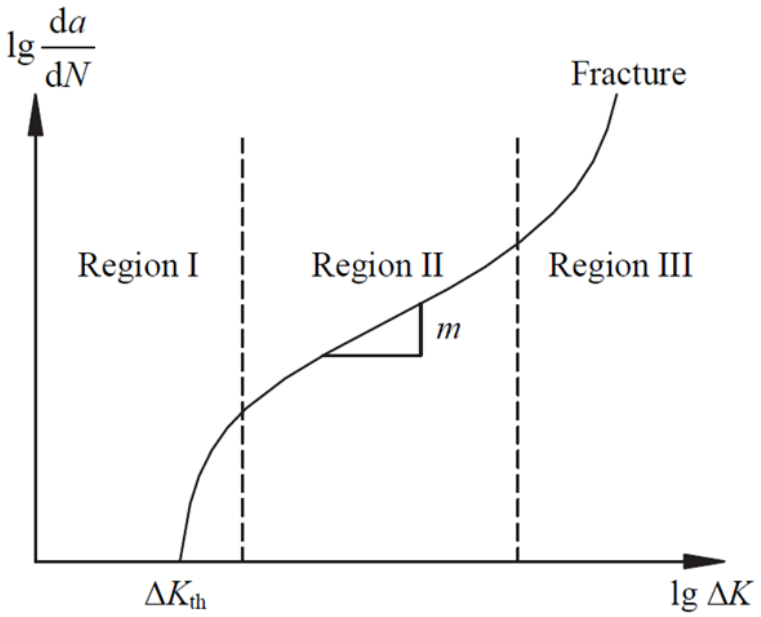

Figure 31: Schematic sketch of typical fracture mechanics fatigue crack initiation and propagation behaviour

Figure 32 demonstrates comparatively three different modes of failure in fracture mechanics. MODE I is treated as opening mode which is interpreted as opening of the crack due to the tensile loading. MODE II is considered as sliding mode which is understood as

displacements perpendicular to the crack tip edge from in-plane shear stresses. MODE III is acknowledged as tearing mode which is deciphered as displacements parallel to the crack tip edge from out-of-plane shear stresses. Note that MODE I is generally the most critical case among them.

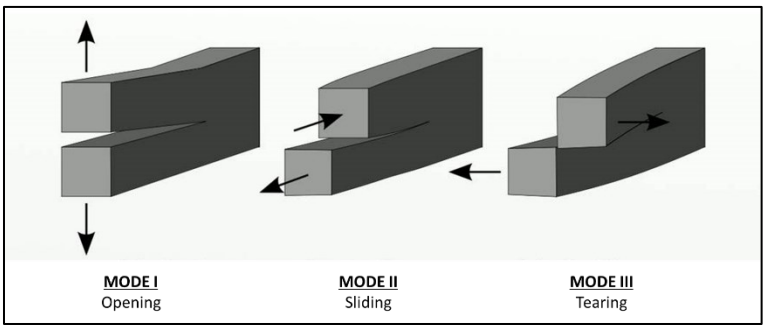

Figure 32: Different modes of failure in fracture mechanics

Region I and II are described in the following next sections while Region III is explained in Chapter 3. To explicit the extremity of fatigue loading of the crack propagation state, the concept of the SIF is utilized. The second state is based on the propagation of the fatigue cracks in cycling loading duration as shown in Figure 31 (AL-Emarani & Åkesson, 2013).

A material can withstand the applied stress severity up to a critical amount above which the crack will develop in a rapid and unstable manner until fracture happens. In other words, Fracture Toughness (FT) of a material is the critical stress severity and it is denoted by K_c. The FT of the material is relying on lots of different aspects including environmental temperature, environmental composition such as air, saltwater, fresh water etc., material thickness and loading rate simply to mention a few.

As already mentioned, fracture is expected to happen when K overtakes the critical SIF, K_C, which is revolved around the material and specimen geometry. K_c will reach a minimum amount named the plain strain critical SIF, or FT if the specimen is massive enough that a state of plain strain exists (Broek, 1986). The FT belongs to REGION III of the FCG curve as illustrated in Figure 31. REGION III depicts rapid unstable crack growth in fracture mechanics. The factor K_c is proposed to specify the FT of different materials in REGION III as shown in Figure 31. This parameter considers three distinct modes as show in Figure 32. To show the extremity of fatigue loading of the cack propagation state, the FT is used.

Threshold stress intensity factor (THSIF) is a stress intensity below which cracks will not progress and is denoted by K_{th}. In traditional fatigue analyses, this is comparable to the fatigue strength. The cracks will not expand unless the initial crack size and the stress range are immense enough to exceed the THSIF. Note that the THSIF stays relatively constant as a function of stress since ΔK_{th} reduces with raising the R-ratio or vise versa.

The THSIF belongs to REGION I of the FCG curve as presented in Figure 31. REGION I depicts slow crack growth in fracture mechanics. To show the extremity of fatigue loading of the crack initiation state, the THSIF is applied.

Fracture fatigue is a time-consuming process which materializes under cyclic fatigue loading in the welded structures. The load spectrum including CA fatigue loading is indicated in Figure 33. The final fatigue load is typically lower than unpredictable design and analysis load. Hence, the destructive impression of such loading should be considered during the design process of such structures that are intended to resist the applied cyclic fatigue loading (Ashcroft, 2011).

In Figure 33, CA load is known as the frequent stress cycle that does not fluctuate in time. Further, CA load is the greatest popular sort of applied loading to conduct laboratory tests. As illustrated in Figure 33, the structures exposed to the tensile cyclic loading encounter the maximum and the minimum stresses. Still, the amounts of theses stresses may not be the same for these peaks (Al-Emrani & Åkesson, 2013).

CA cyclic fatigue loading is in scheme of sine wave to express a smooth repetitive oscillation of the fatigue load. The conversion of the waved load spectrum into an equivalent CA stress histogram is usually acquired through cyclic counting methods as stated here (Al-Emrani & Åkesson, 2013).

It is worth noting that there are other components of loads as well like shear loading which is perpendicular to the tensile loading. In this thesis, tensile loading is the dominant force and is perpendicular to the crack. In other words, it is the deriving fatigue force.

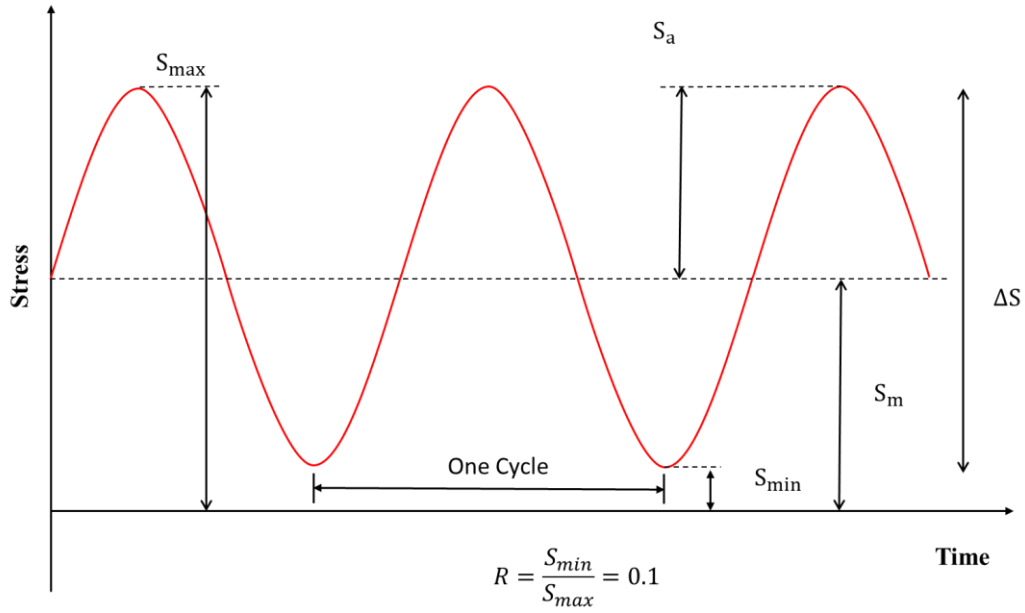

Figure 33: Typical Constant Amplitude Cyclic Fatigue Loading with a R-ratio equal to 0.1

To investigate the impact of loading spectrum in the fatigue analyses, CA cyclic fatigue loading with a R-ratio equivalent to 0.1 was applied for the whole materials in this thesis, obtained and derived from the literature.

CHAPTER 3: RESEARCH METHODOLOGY

3.1) Fatigue Analyses

Several crack growths models have been evolved to explain the relationship among fatigue crack growth, $\frac{da}{dN}$, and stress intensity range, ΔK, within the three mentioned regions as shown in Figure 31. Two models employed extensively in this thesis are Walker and Forman crack growth models to predict fracture mechanics fatigue crack propagation behaviour of nine distinct materials.

The crack propagation period of the fatigue life of the welded structures is often regarded to represent the bulk of total fatigue life since the fatigue crack initiation period in welded structures is considered to be significantly shorter in comparison to the crack propagation period (Fricke, 2003) . Therefore, the crack propagation period plays a decisive role for accurate fatigue life assessment of the welded joints under fatigue cyclic loading. Due to the pre-existing crack, the crack propagation can be generally computed depending on the simple power law as follows:

3.2) Paris Crack Growth Model

In LEFM, the crack growth is concerned with the local stress intensity (Griffith, 1921; Irwin, 1948, 1957). Paris and Erdogan (1963) estimated the intermediate crack growth region with a power law relationship recognized nowadays as Paris equation (3. 1), where a is crack size, N is loading cycles, ΔK is stress intensity range obtained by $\Delta K = K_{max} - K_{min}$, C_P and m_P are fitting constants of Paris model depending on the material.

Given initial crack size a_i and failure crack size a_f , the life of the component can be forecasted through equation (3. 1):

$$\frac{da}{dN} = C_P(\Delta K)^{m_P} \qquad (3.\ 1)$$

By integrating equation (3. 1) with the appropriate SIF, the cycles needed to grow a crack from its initial size to final size can be computed as follows depending on the applied criteria and the engineering assumptions that are used:

$$N_f = \int_{a_i}^{a_f} \frac{da}{C_P(\Delta K)^{m_P}} \qquad (3.2)$$

Note that K_{min} is served as zero because the tensile loading performs the main interaction with the crack growth while the compressive residual stresses lessen the crack growth. In case of the compressive stresses, K_{min} is zero.

Equation (3. 1) displays mathematically Region II (the central region) of the crack growth rate curve as shown in Figure 31. To calculate the development of the crack size and the analogous life cycles, Paris equation can be applied to Region II for specific amounts of the R-ratio. This equation is formed to describe first order estimation of life behavior when particularly insufficient data are available.

In brief, Paris equation indicates that the fatigue life of the joint leans directly on the stress range that the component is exposed to. The stress range illustrates the amplitude among the lowest and the highest stresses influencing the material. In other words, the shorter the fatigue life is the wider the stress range is.

3.3) Walker Crack Growth Model

To account for the residual stresses, the mean stress and the R-ratio effects on the FCG, Walker and Forman models in equations (3. 3) and (3. 4) are employed. Walker (1970) examined the impacts of the R-ratio on the crack propagation for aluminum alloys, achieving that rising R-ratio caused in an increase growth rate as expressed in equation (3. 3):

$$\frac{da}{dN} = \frac{C_W(\Delta K)^{m_W}}{(1-R)^{\gamma}} \qquad (3.3)$$

Where C_W, m_W and γ are fitting constants which are empirically determined from experimental data.

Paris and Walker equations operate well in region II of the crack growth rate curve as illustrated in Figure 31; however, do not address the asymptotic behavior in the unstable region. To tackle this behavior, Forman equation was applied next to address such behaviour.

3.4) Forman Crack Growth Model

Forman, Kearney and Engle (1967) suggested equation (3. 4), which is broadly employed to account for the asymptotic behavior at the end of crack propagation as well as the R-ratio and the mean stress effect similar to Walker equation:

$$\frac{da}{dN} = \frac{C_F(\Delta K)^{m_F}}{(1-R)K_c - \Delta K} \tag{3. 4}$$

Equation (3. 4) can be simplified as:

$$\frac{da}{dN} = \frac{C_F(\Delta K)^{m_F}}{(1-R)(K_c - K_{max})} \tag{3. 5}$$

Note that C_F and m_F are material constants which are empirically specified from experimental data.

When K_{max} reaches K_c, the asymptotic behavior increases in the unstable region as shown in Figure 31 which simply means $\frac{da}{dN}$ turns towards infinity. This model is capable of depicting both Region II and Region III of the crack growth rate curve as presented in Figure 31. Note that ΔK is characterized as the equivalent stress intensity range at $R = 0.1$ in this research for Walker and Forman models.

3.5) Weight Function Approach

To reveal stress intensity factors for the cracks in the welded structures, the weight function technique is used (Bueckner, 1970; Glinka & Shen, 1991). The weight function (WF) method is used to calculate the SIF, K, influenced by the straightforward load configuration as shown in Chapter 4 – experimental fatigue data (Chattopadhyay et al., 2011). The SIF, K, can also be calculated on the basis of the WF method in equation (3. 5). The knowledge of stress distribution and the WF is necessary to compute the stress intensity factor K by means of integrating the product of the stress distribution, $\sigma(x)$, and the WF, $m(x, a)$, in the perspective crack plane in equation (3. 5):

$$K = \int_0^a \sigma(x).m(x,a).dx \qquad (3.5)$$

The overall concept is for the stress distribution, a weld toe radius is assumed, and it is already estimated within the local stress analysis.

The stress distribution is obtained to calculate the SIF. As for an applied tension loading, S, as shown in Chapter 4, the through-thickness stress distribution is calculated by accounting the local applied stress and the residual stress induced by the welding and UIT processes for each material.

3.6) Road Map of Numerical Models

To indicate the fatigue enhancement induced by UIT, fatigue analysis program FALPR (V6.9) is employed to perform FCG analyses for Walker and Forman models under the AW and the UIT conditions. Several distinct key concepts and plenty various fatigue parameters are generally engaged during the FCG analyses. To easily grasp the core concepts and the fundamental parameters, accompanying graph gives a roadmap of numerical implementations in this research done through FALPR (V6.9). Figure 34 displays a schematic perspective of the FCG analyses in this study. Analysis options and input parameters in terms of component, crack geometry, loadings, residual stress and material data etc. for FALPR (V6.9) are shown in Figure 34.

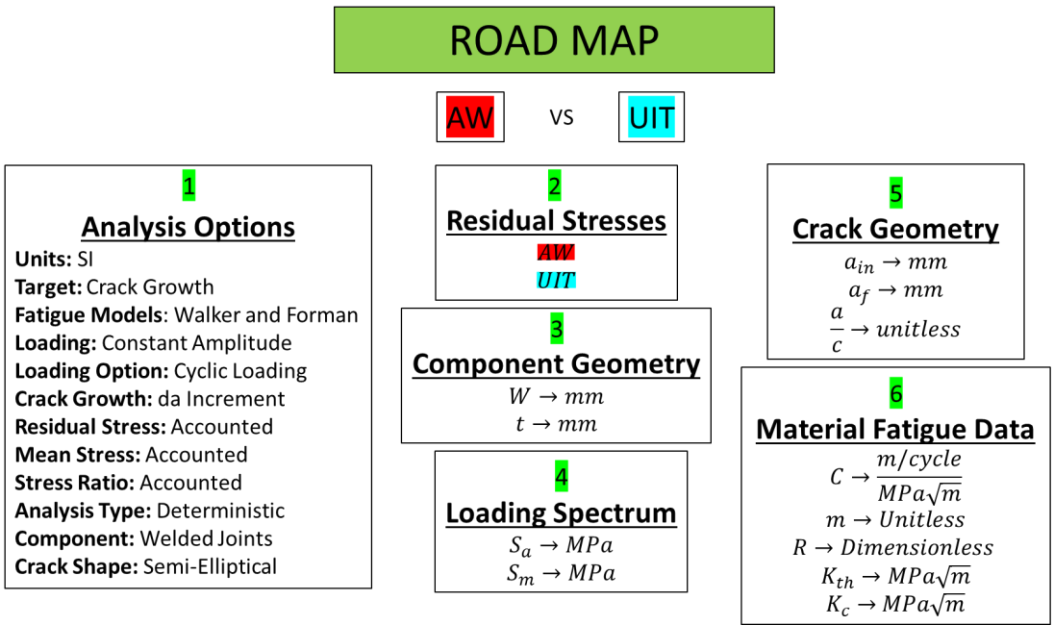

Figure 34: Schematic perspective of fatigue crack growth analyses of AW and UIT conditions

In this thesis, the fundamental assumption is that the crack already exists at weld toe and the crack is toe crack. It should be emphasized that the crack size is less than 0.5 mm which simply means in microscopic scale. Note that the crack shape is semi-elliptical and also the crack is 2D which simply means in depth and on surface dimensions. It should be indicated that the fatigue fracture of the welded joint occurs at the weld toe. The final crack size is considered to be half of the thickness. The fracture happens when the crack is reached its critical size.

Figure 35 depicts schematically geometry of a crack at weld toe where BB' indicates crack length and A demonstrates crack depth.

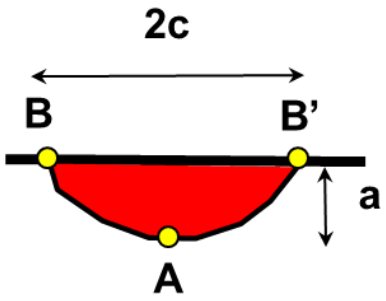

Figure 35: Schematic portrait of geometry of a semi-elliptical crack at weld toe

Hence, this research mainly copes with the crack propagation phase. Figure 36 demonstrate comparatively Walker versus Forman models for in depth and on surface dimensions. The below equations are employed for a two-dimensional crack case as follows:

Walker Model

$$K^A = \int_0^a [\sigma(y) m_A(y,a)]\, dy$$

$$\frac{da}{dN} = \frac{C_W \left(\Delta K_i^A\right)^m}{(1-R)^\gamma}$$

$$K^B = \int_0^a [\sigma(y) m_B(y,a)]\, dy$$

$$\frac{da}{dN} = \frac{C_W \left(\Delta K_i^B\right)^m}{(1-R)^\gamma}$$

Forman Model

$$K^A = \int_0^a [\sigma(y) m_A(y,a)]\, dy$$

$$\frac{da}{dN} = \frac{C_F \left(\Delta K_i^A\right)^m}{(1-R)K_c - \Delta K}$$

$$K^B = \int_0^a [\sigma(y) m_B(y,a)]\, dy$$

$$\frac{da}{dN} = \frac{C_F \left(\Delta K_i^B\right)^m}{(1-R)K_c - \Delta K}$$

Figure 36: Schematic illustration of Walker and Forman models for in depth and on surface dimensions

Figure 37 represents a schematic image of FALPR (V6.9) which is a fracture mechanics-based fatigue analysis program.

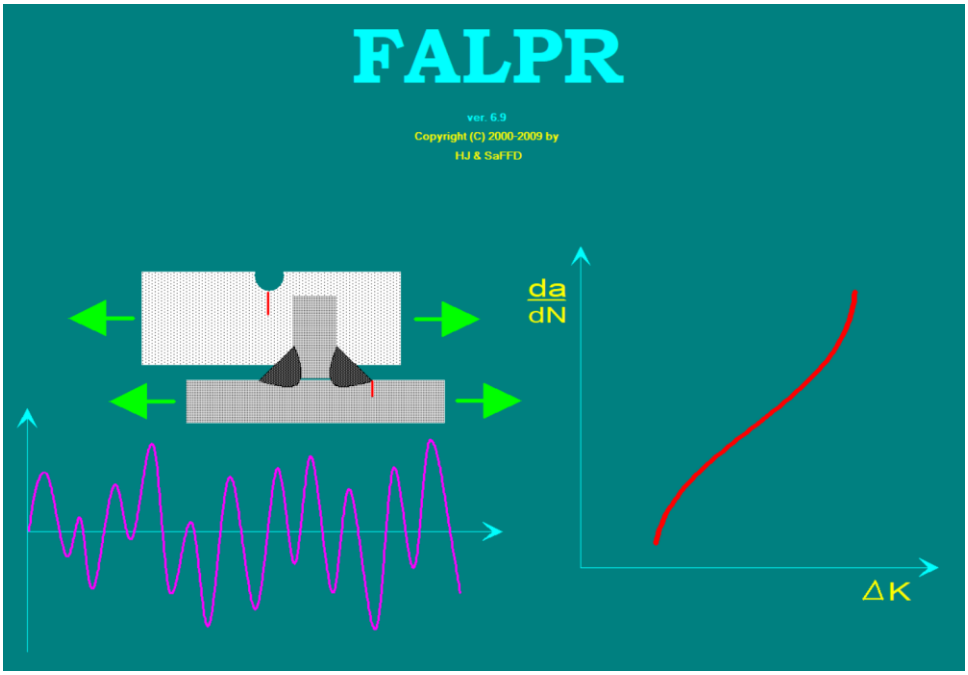

Figure 37: Schematic image of FALPR (V6.9)

Accordingly, FALPR (V6.9) is utilized to obtain FCG predictions for Walker and Forman models. The numerical results obtained from FALPR (V6.9) are then sorted, examined and imported into EXCEL for the further verifications and expansions. In the end, MATLAB and EXCEL are used to plot the numerical results.

3.7) Numerical Execution of Local Stress

On average, 10 stress range levels are defined for each material for the AW as well as the UIT conditions depending on the experimental data from the literature. To compute the maximum and the minimum nominal stresses, equations (2. 1), (2. 2), (2. 3) and (2. 4) are used:

$$S_{max} = \frac{\Delta S}{1 - R} \tag{3. 6}$$

$$S_{min} = \frac{\Delta S. R}{1 - R} \tag{3. 7}$$

To calculate the nominal stress amplitudes and the nominal mean stresses, (2. 1), (2. 2), (2. 3) and (2. 4) are utilized to extract the following ones:

$$S_a = \frac{S_{min}(1-R)}{2R} \quad (3.8)$$

$$S_m = \frac{S_{min}(1+R)}{2R} \quad (3.9)$$

To determine the local nominal stress amplitudes, S_{loc_a}, and the local mean stresses, S_{loc_m}, equations (2. 2), (2. 3), (2. 9), (3. 8) and (3. 9) are employed to acquire the following ones:

$$S_{loc\_a} = K_t . S_a \quad (3.10)$$

$$S_{loc\_m} = K_t . S_m \quad (3.11)$$

The welding tensile residual stresses and the stress concentrations due to the local geometry tend to make joints the weakest location in terms of fatigue failure. Accordingly, the core concept of notch stress method explains this important matter by introducing the SCF (Fricke, 2012).

Figure 38 displays numerically the concept of the local stress amplitude and the local mean stress at the weld toe utilizing the stress concentrations conception.

Stress Ratio (R)	0.1
K_t (AW)	2.2
K_t (UIT)	1.8

Number of Points: 9 / Condition: AW						
Nominal					Local	
ΔS	S_Max	S_Min	S_a	S_m	S_a	S_m
190	211.1111111	21.11111111	95	116.1111111	209	255.4444444
170	188.8888889	18.88888889	85	103.8888889	187	228.5555556
150	166.6666667	16.66666667	75	91.66666667	165	201.6666667
130	144.4444444	14.44444444	65	79.44444444	143	174.7777778
110	122.2222222	12.22222222	55	67.22222222	121	147.8888889
90	100	10	45	55	99	121
70	77.77777778	7.777777778	35	42.77777778	77	94.11111111
50	55.55555556	5.555555556	25	30.55555556	55	67.22222222
30	33.33333333	3.333333333	15	18.33333333	33	40.33333333

Number of Points: 9 / Condition: UIT						
Nominal					Local	
ΔS	S_Max	S_Min	S_a	S_m	S_a	S_m
290	322.2222222	32.22222222	145	177.2222222	261	319
260	288.8888889	28.88888889	130	158.8888889	234	286
230	255.5555556	25.55555556	115	140.5555556	207	253
200	222.2222222	22.22222222	100	122.2222222	180	220
170	188.8888889	18.88888889	85	103.8888889	153	187
140	155.5555556	15.55555556	70	85.55555556	126	154
110	122.2222222	12.22222222	55	67.22222222	99	121
90	100	10	45	55	81	99
70	77.77777778	7.777777778	35	42.77777778	63	77

Figure 38: Schematic illustration of computing local stress amplitude and local mean stress using stress concentration conception for AW and UIT conditions for each stress level [Material: Aluminum]

After obtaining the necessary load data of the material for both conditions by using the stress concentrations, the local stress amplitude and the local mean stress conceptions following

the same procedure as described above, the data sets are individually used as the input parameter values of loading spectrum for that material in the models.

3.8) Analytical Performance of Fatigue Strength

FCG results obtained from Walker and Forman models are utilized to generate the $S-N$ curves for these models which these curves represent crack growth life of the welded joints. Figure 39 shows numerically the concept of calculating fatigue strength of both conditions for both models using the derived fatigue parameters from the literature, the estimated factors based on the recommendations criteria and or the common engineering assumptions etc.

Walker

Model: Walker			
C	2.52E-12	RS	AW
m	3.96	a/c	0.47
ai	0.2		
ΔS	N_f		
190	6.92E+03		
170	9.99E+03		
150	1.50E+04		
130	2.38E+04		
110	4.01E+04		
90	7.39E+04		
70	1.55E+05		
50	4.01E+05		
30	1.56E+06		

Model: Walker			
C	2.52E-12	RS	UIT
m	3.96	a/c	0.71
ai	0.2		
ΔS	N_f		
290	1.05E+04		
260	1.66E+04		
230	2.78E+04		
200	5.06E+04		
170	1.02E+05		
140	2.41E+05		
110	7.23E+05		
90	1.88E+06		
70	6.71E+06		
60	2.65E+07		

Forman

Model: Forman			
C	5.42E-10	RS	AW
m	3.96	a/c	0.47
ai	0.2		
ΔS	N_f		
190	4.03E+03		
170	6.18E+03		
150	9.92E+03		
130	1.69E+04		
110	3.12E+04		
90	6.42E+04		
70	1.55E+05		
50	4.93E+05		
30	2.69E+06		

Model: Forman			
C	5.42E-10	RS	UIT
m	3.96	a/c	0.71
ai	0.2		
ΔS	N_f		
290	3.11E+03		
260	5.19E+03		
230	9.25E+03		
200	1.80E+04		
170	3.96E+04		
140	1.04E+05		
110	3.69E+05		
90	1.15E+06		
70	5.58E+06		

Figure 39: Schematic perspective of calculating fatigue strength of AW and UIT conditions for each stress level by Walker and Forman models using fatigue parameters [Material: Aluminum]

To plot $S-N$ curves of fatigue strength of both conditions and both models, the calculated number of cycles, N_f, versus the stress ranges, ΔS, can be depicted on a log-log scale for the FCG analysis. In the end, the curves can be validated by the derived experimental data from the literature as shown in Figure 40.

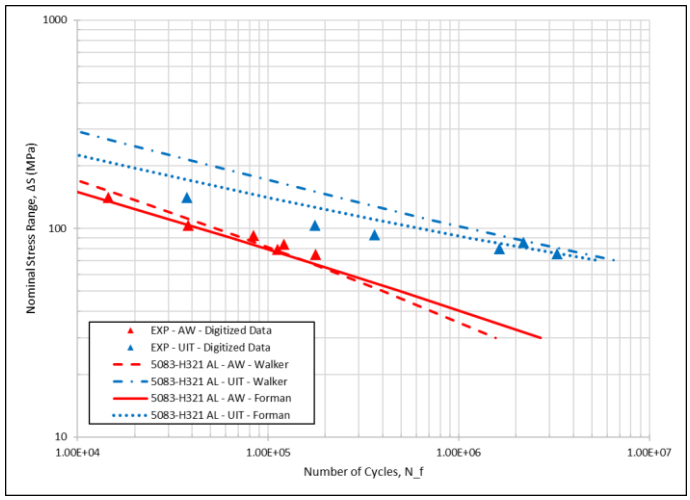

Figure 40: Schematic aspect of fatigue strength of a welded joint subjected to CA fatigue loadings using Walker and Forman models for AW and UIT conditions [Material: Aluminum]

Figure 40 depicts graphically fatigue strength of a welded joint for the AW and the UIT conditions for both models. It is anticipated that UIT enhances the fatigue life of the welded joint as demonstrated in Figure 40.

3.9) Numerical Implementation of Fatigue Crack Growth

To further establish the crack propagation as well as the final fracture states of the FCG, the extracted crack growth data from the models can be numerically educed through interpolation of the data via the crack depth, the crack surface and the aspect ratio, $\frac{a}{c}$, as well as by iterating, i, the following formula and using the calculated rate from interpolation of the data:

$$c_{(i)} = \frac{a_{(i)}}{(\frac{a}{c})_{(i)}} \qquad (3.12)$$

Where c is crack surface and a is crack depth.

Eventually, $a - N$ curves can be outlined which are the crack depths versus the number of cycles also $c - N$ curves can be laid out which are the crack surfaces versus the number of cycles. Figure 41 and Figure 42 show graphically schematic sketches of $a - N$ and $c - N$ curves under $70\ MPa$ fatigue cyclic loading using the extracted data through interpolation perception.

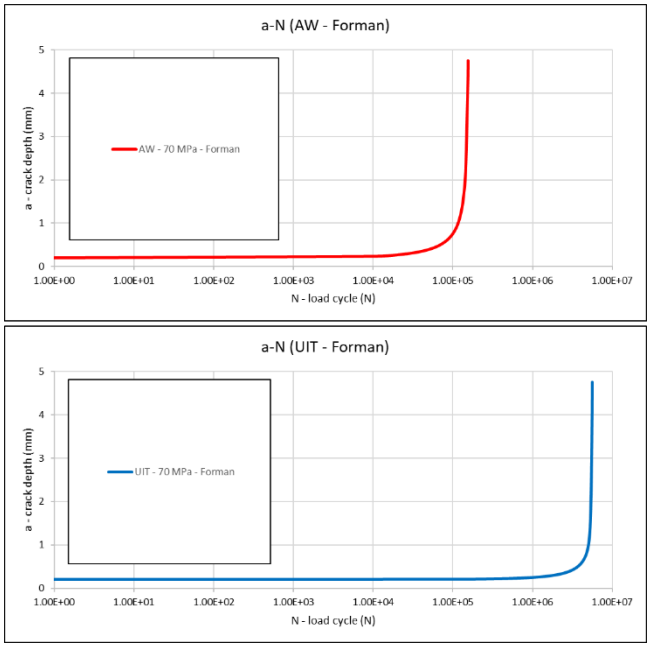

Figure 41: Schematic sketch of a-N curves of a welded joint under 70 MPa CA fatigue cyclic loading using extracted data through interpolation for AW and UIT conditions for Forman model [Material: Aluminum]

In Figure 41, it is predicted that UIT can dramatically improve the fatigue life by significantly delaying crack initiation state as already marked in Figure 25 as well. It is also anticipated to slow down crack propagation phase in depth direction which will lead to enhancing the fatigue life as already illustrated in Figure 25.

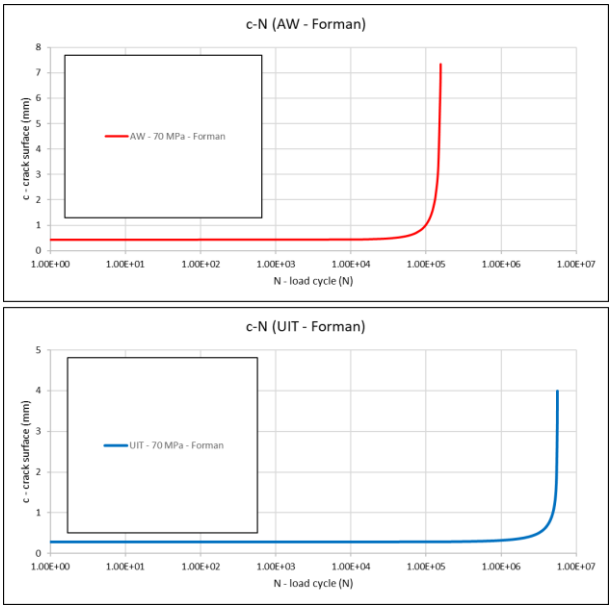

Figure 42: Schematic sketch of c-N curves of a welded joint under 70 MPa CA fatigue cyclic loading using extracted data through interpolation for AW and UIT conditions for Forman model [Material: Aluminum]

In Figure 42, it is expected that UIT can considerably enlarge the fatigue life by significantly delaying crack initiation state as already revealed in Figure 25 as well. It is forecasted that UIT holds back crack propagation phase on surface direction which will result in enhancing the fatigue life as well. It is worth noting that UIT can slightly close the surface of the crack.

3.10) Analytical Accomplishment of Crack Shape Evolution

Since the crack is semi-elliptical and 2D, the concept of the ellipse can be utilized to determine crack shape evolution. The shape evolution of that crack can be forecasted as:

$$\frac{c^2}{{c_i}^2} + \frac{a^2}{{a_i}^2} = 1 \qquad (3.\ 13)$$

It can be also simplified as follows:

$$c = c_i \times \sqrt{1 - (\frac{a}{a_i})^2} \qquad (3.\ 14)$$

Eventually, the crack surface indicates X-direction and also the crack depth implies Y-direction as exhibited in Figure 43. Then, it can be rewritten in following way:

$$X = c_i \times \sqrt{1 - (\frac{Y}{a_i})^2} \qquad (3.\ 15)$$

Given crack depth, $a = Y$, initial crack surface, c_i, and initial crack depth, a_i, the crack shape evolution can be predicated.

To plot $a - c$ curves of the crack for both conditions and both models, the computed crack surfaces and the determined crack depths under each fatigue cyclic loading can be graphing as for example Figure 43.

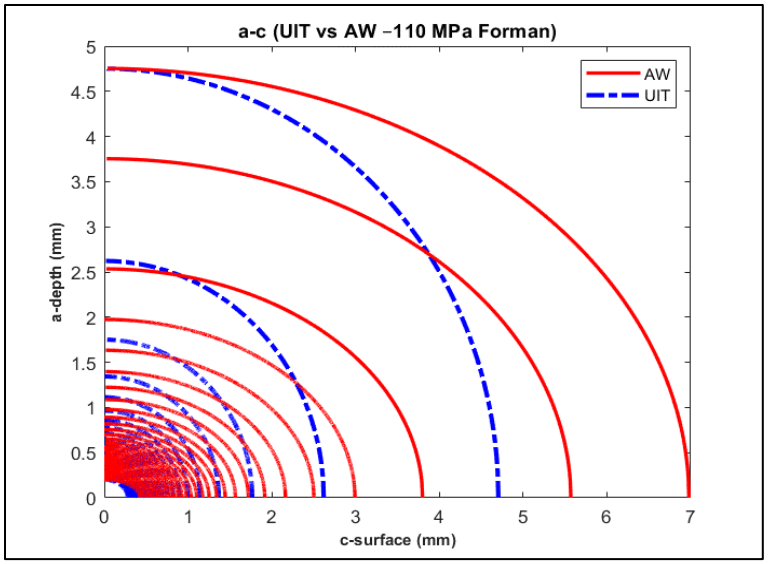

Figure 43: Schematic picture of crack shape evolution of a weld joint under 110 MPa CA fatigue cyclic loading using both derived and computed data from Forman model for AW and UIT conditions [Material: Aluminum]

In Figure 43, it is anticipated to see how effective UIT can close the surface of the crack to further retarding crack propagation phase. On top of that, the crack behaviour and how fast the crack grows in depth and on surface can be properly comprehended.

3.11) Recap

Following the similar manner as expressed above for each stress level range for nine different materials considering the key concepts and the different derived fatigue parameters from the literature, the estimated factors based on the recommendations criteria and or the common engineering assumptions etc., the outcomes of the numerical implementations are prominently represented in Chapter 5.

CHAPTER 4: EXPERIMENTAL FATIGUE DATA

Loading spectrum has been set up as CA cyclic fatigue loading. The R-ratio has been set to 0.1 for all materials, and the abort criterion is burst fracture. In this thesis, aluminum is abbreviated to AL and steel is simplified in S or ST which are embedded into the materials names.

The type of weld specimens, schematic geometry of the examined specimens, chemical composition of the materials, the type of initial cracks as well as the shape of final cracks are presented under each material section in this chapter.

The residual stresses followed by their distribution across the plate thickness are required to be determined in order to perform accurate fatigue life predictions on the basis of the crack propagation methodologies. The conception of the residual stresses is already expressed in Chapter 2. From literature, measurements of depth stresses were performed using X-ray diffraction (XRD) method like on Philips Pro XRD or mechanical ones like using hole drilling method (HDM) which their results are represented under each material section in this chapter.

To validate fatigue strength predictions of the models, fatigue life experimental data of the materials are shown under each material section in this chapter. Apart from the plots, the outcomes of the fatigue tests are also summarized in Appendix (A): Table 10, Table 11, Table 12, Table 13, Table 14, Table 15, Table 16, Table 17 and Table 18 which are for H083-H321 AL, CSA 350W ST, A514 ST, S355, S460, S690, S960, 5083-H11 AL and 2024-T351 AL, respectively.

4.1) H083-H321 Aluminum Alloy

The welded specimen of this material was cruciform-joint and was made-up from 9.5 mm (3/8") thick aluminum plate (H083-H321 AL). The aforesaid specimen was welded to the plate at room temperature and the welded plate has been examined to meet the quality of the welds and no weld quality problems were detected. The stiffener welds were carried out by Metal Inter Gas (MIG) welding. The welds were executed in a single pass. Figure 44 depicts schematically geometry of the investigated specimen for the above-mentioned material (Kasra Ghahremani, Ranjan, et al., 2015; Ranjan et al., 2016).

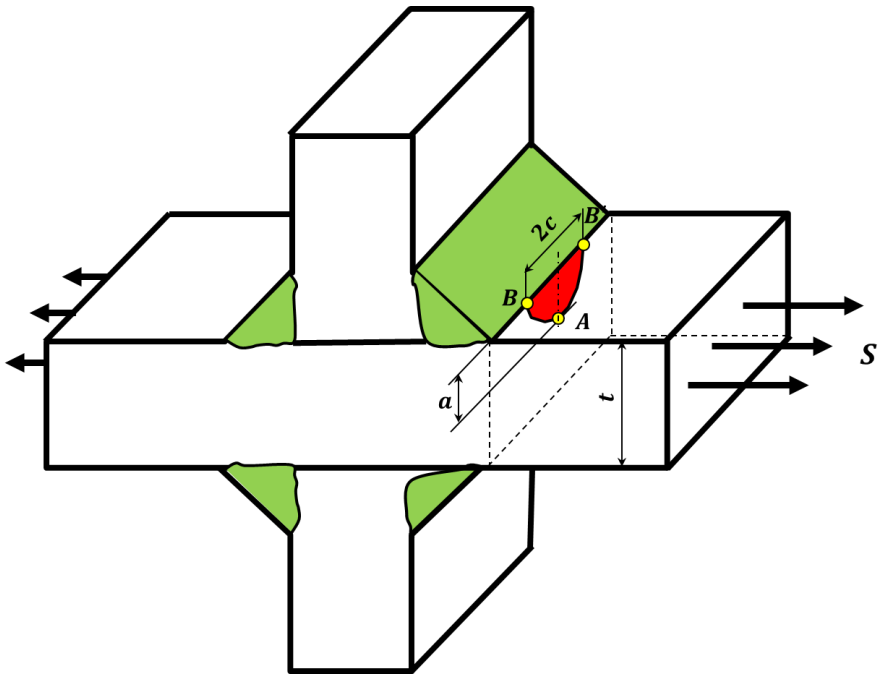

Figure 44: Schematic portrait of the specimen for H083-H321 AL material cruciform-joint (Kasra Ghahremani, Ranjan, et al., 2015; Ranjan et al., 2016)

5083-H321 AL is a popular alloy for structural sheet usages and its chemical designation is ($A1\ Mg4.5Mn0.7$). The abbreviation of H321 demonstrates its temper which means it became strain-hardened and partly annealed during its forming process. Nominally, it consisted of $4-4.9\ wt\%\ Mg$, $0.05-0.25\ wt\%\ Cr$, and $0.4-1\ wt\%\ Mn$ (Kasra Ghahremani, Ranjan, et al., 2015; Ranjan et al., 2016). To determine the final crack shape, it was photographed in advance of fracture. The crack shape was similar to that of ellipse as shown in Figure 44 and the crack type was toe crack (Kasra Ghahremani, Ranjan, et al., 2015; Ranjan et al., 2016).

Figure 45 shows illustratively its residual stresses measurements for the AW and the UIT conditions.

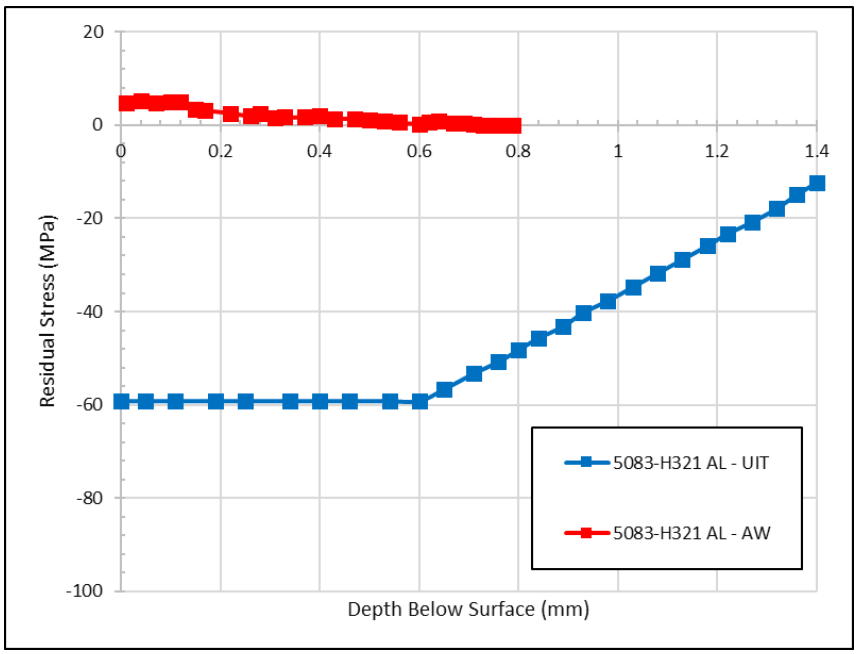

Figure 45: Residual stress measurement results of 5083-H321 AL cruciform-joint specimen under AW and UIT conditions (Tehrani Yekta et al., 2013; Kasra Ghahremani, Ranjan, et al., 2015; Ranjan et al., 2016)

Figure 46 presents its fatigue life experimental data for both conditions.

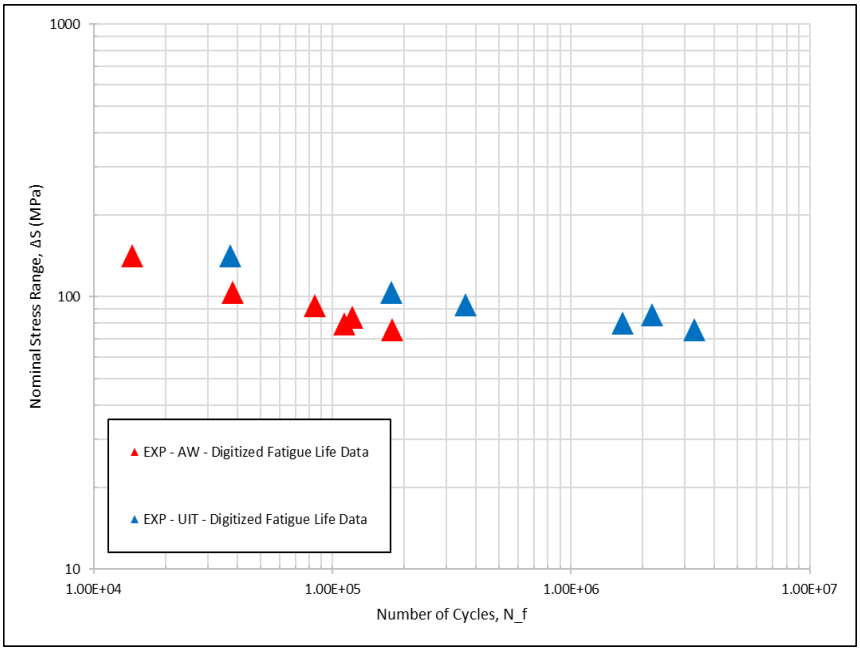

Figure 46: Fatigue life experimental data for 5083-H321 AL cruciform-joint specimen under AW and UIT conditions (Tehrani Yekta et al., 2013; Kasra Ghahremani, Ranjan, et al., 2015; Ranjan et al., 2016)

4.2) CSA 350W Steel Alloy

The welded specimen of this material was cruciform-joint and was fabricated from 9.5 mm (3/8") mild steel plate (CSA 350W ST). The forenamed specimen was welded to the plate at room temperature and the welded plate has been inspected to comply with the quality of the welds and no weld quality problems were observed. The transverse stiffeners were performed by flux-cored arc (FCAW) welding. Figure 47 displays graphically geometry of the studied specimen for the mentioned material (Tehrani Yekta et al., 2013).

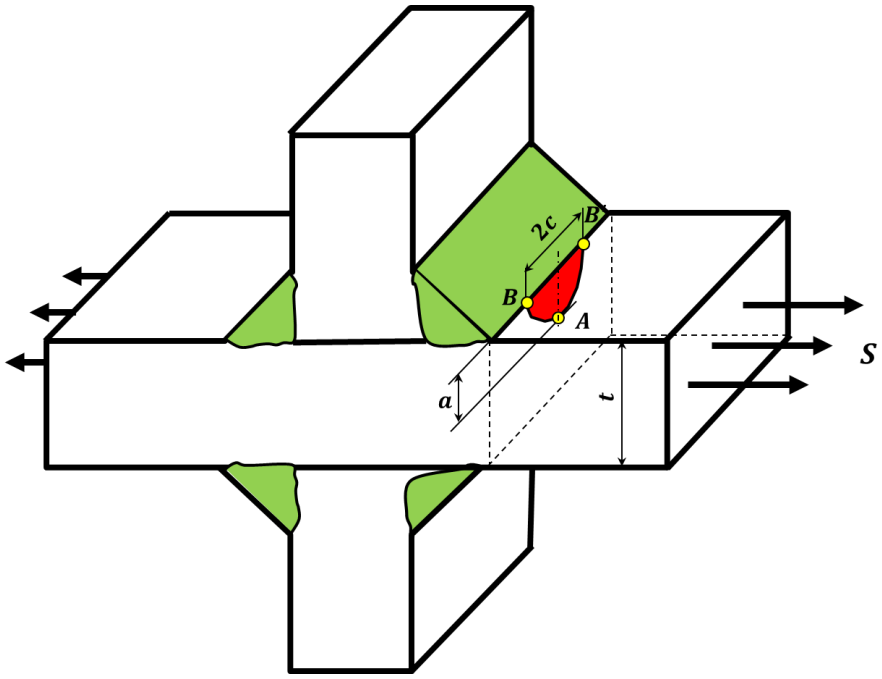

Figure 47: Schematic illustration of the specimen for CSA 350W ST material cruciform-joint (Tehrani Yekta et al., 2013)

CSA 350W ST is a mild, weldable strutcural steel grade. It contained $C < 0.23\%$, Mn $(0.5 - 1.5\%)$, P $(< 0.04\%)$, S $(< 0.05\%)$, Si $(< 0.4\%)$ and other alloying elements or impurities $(< 0.1\%)$ (Tehrani Yekta et al., 2013).

It was pressumed that the initial defect was crack-like in order to implement fracture mechanics analyses. The Alternating Current Potential Drop (ACDP) approach was utilized to obtain the necessary info related to the crack dimensions. So, the critical crack depth of 0.5 mm was noticed. The crack shape was toe crack (Tehrani Yekta et al., 2013). Then, the crack shape was considered to be similar to that of ellipse as depicted in Figure 47 (Kasra Ghahremani, Ranjan, et al., 2015; Ranjan et al., 2016).

Figure 48 demonstrates comparatively its residual stresses measurements for the AW and the UIT conditions.

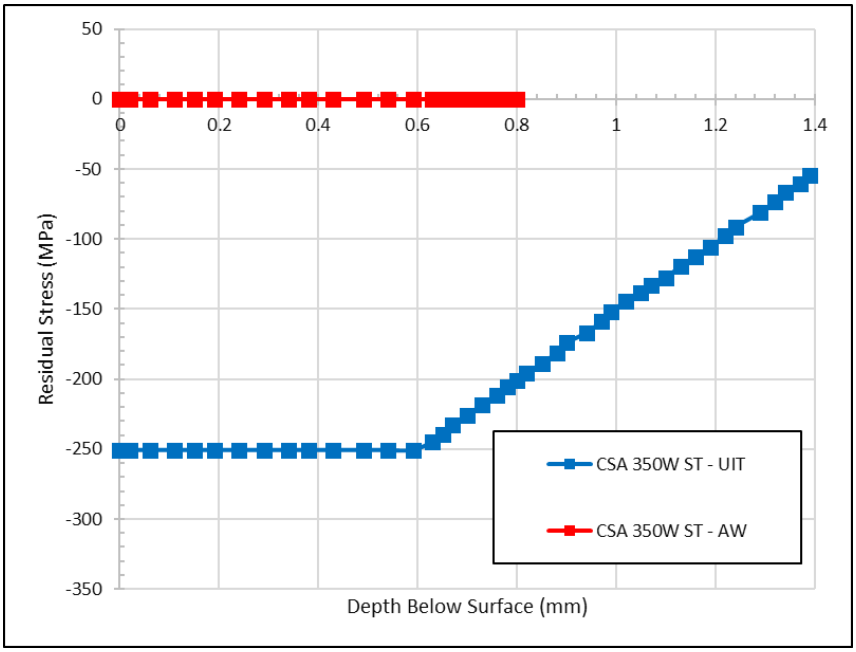

Figure 48: Residual stress measurement results of CSA 350W ST cruciform-joint specimen under AW and UIT conditions (Tehrani Yekta et al., 2013; Kasra Ghahremani, Ranjan, et al., 2015; Ranjan et al., 2016)

Figure 49 represents its fatigue life experimental data for both conditions.

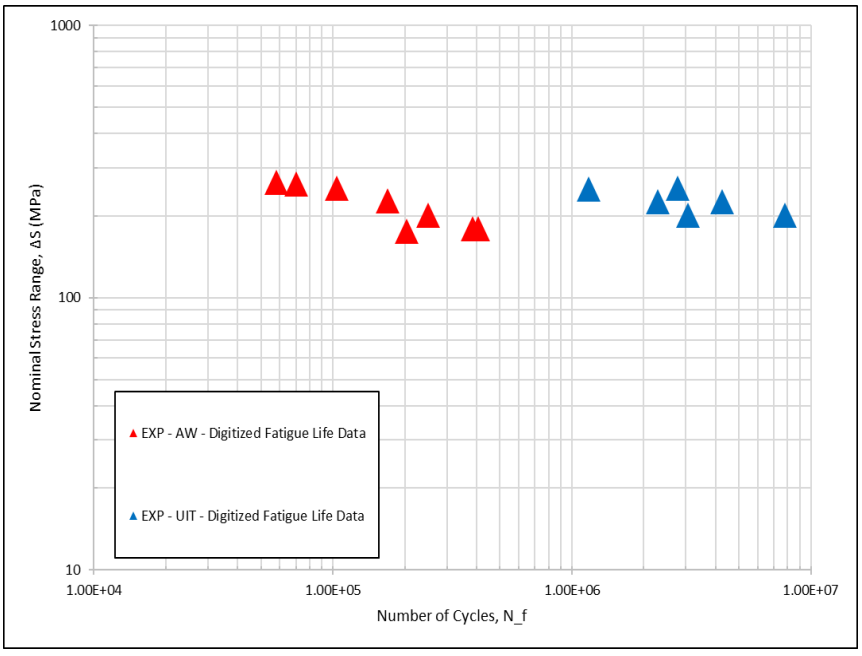

Figure 49: Fatigue life experimental data for CSA 350W ST cruciform-joint specimen under AW and UIT conditions (Tehrani Yekta et al., 2013; Kasra Ghahremani, Ranjan, et al., 2015; Ranjan et al., 2016)

4.3) ASTM A514 Steel Alloy

The welded specimen of this material was cruciform-joint and was manufactured from 9.5 mm (3/8") high strength steel plate (ASTM A514 ST). The foresaid specimen was welded to the plate at room temperature and the welded plate has been checked out to satisfy the quality of the welds and no weld quality problems were distinguished. The stiffener welds were done by Metal Inter Gas (MIG) welding. The welds were executed in a single pass. Figure 50 shows illustratively geometry of the researched specimen for the above-mentioned material (Kasra Ghahremani, Ranjan, et al., 2015; Ranjan et al., 2016).

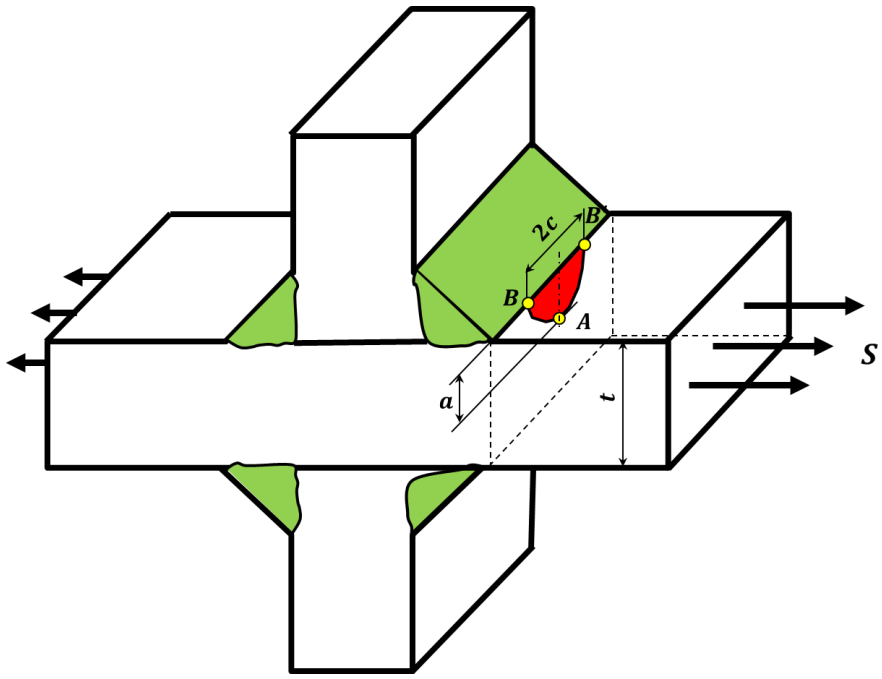

Figure 50: Schematic sketch of the specimen for A514 ST material cruciform-joint (Kasra Ghahremani, Ranjan, et al., 2015; Ranjan et al., 2016)

A514 ST is a weldable, high-yield strength, quenched and tempered alloy steel. It compromised of $0.18\,wt\%\,C$, $1.2\,wt\%\,Mn$, $0.014\,wt\%\,P$, $0.004\,wt\%\,S$, $0.24\,wt\%\,Si$, $0.02\,wt\%\,Ni$, $0.12\,wt\%\,Cr$, $0.14\,wt\%\,Mo$ and $0.02\,wt\%\,Cu$ (Kasra Ghahremani, Ranjan, et al., 2015; Ranjan et al., 2016).

To verify the final crack shape, it was photoed in advance of fracture. The crack shape was similar to that of ellipse as displayed in Figure 50 and the crack type was toe crack (Kasra Ghahremani, Ranjan, et al., 2015; Ranjan et al., 2016).

Figure 51 shows illustratively its residual stresses measurements for the AW and the UIT conditions.

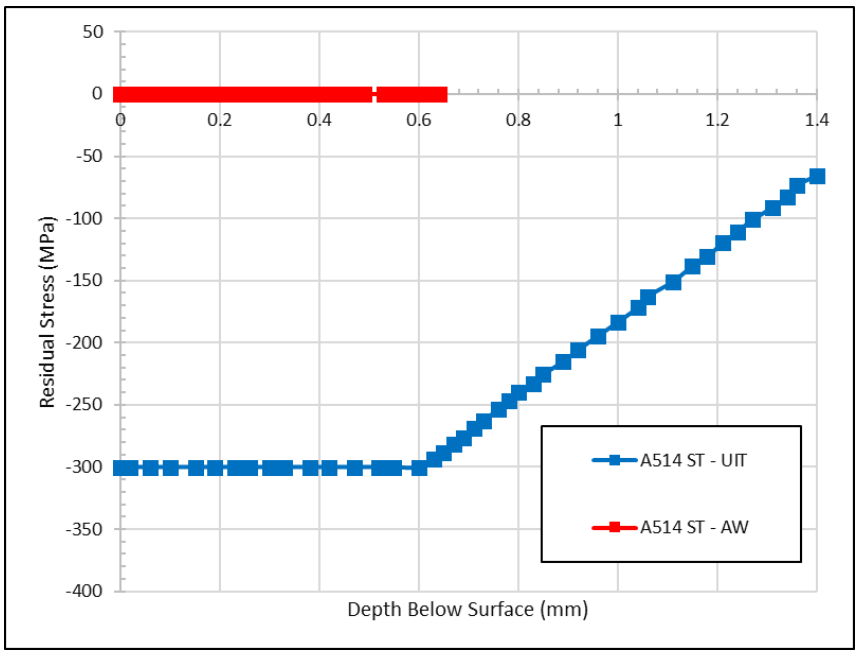

Figure 51: Residual stress measurement results of A514 ST cruciform-joint specimen under AW and UIT conditions (Kasra Ghahremani, Ranjan, et al., 2015; Tehrani Yekta et al., 2013; Ranjan et al., 2016)

Figure 52 displays its fatigue life experimental data for both conditions.

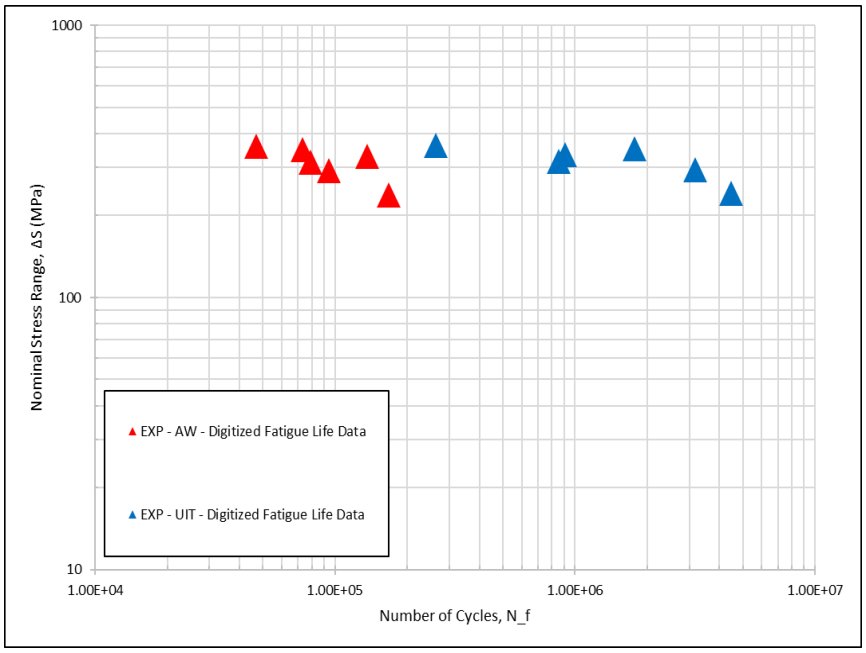

Figure 52: Fatigue life experimental data for A514 ST cruciform-joint specimen under AW and UIT conditions (Tehrani Yekta et al., 2013; Kasra Ghahremani, Ranjan, et al., 2015; Ranjan et al., 2016)

4.4) S355 Steel Alloy

The welded specimen of this material was cruciform-joint and was made-up from 12 mm (15/32") mild steel plate (S355). The aforesaid specimen was welded to the plate at room temperature and the welded plate has been examined to meet the quality of the welds and no weld quality problems were detected. The stiffener welds were carried out by Gas Metal Arc (MAG) welding. Figure 53 depicts schematically geometry of the investigated specimen for the above-mentioned material (Ulrike Kuhlmann et al., 2005; U. Kuhlmann et al., 2006).

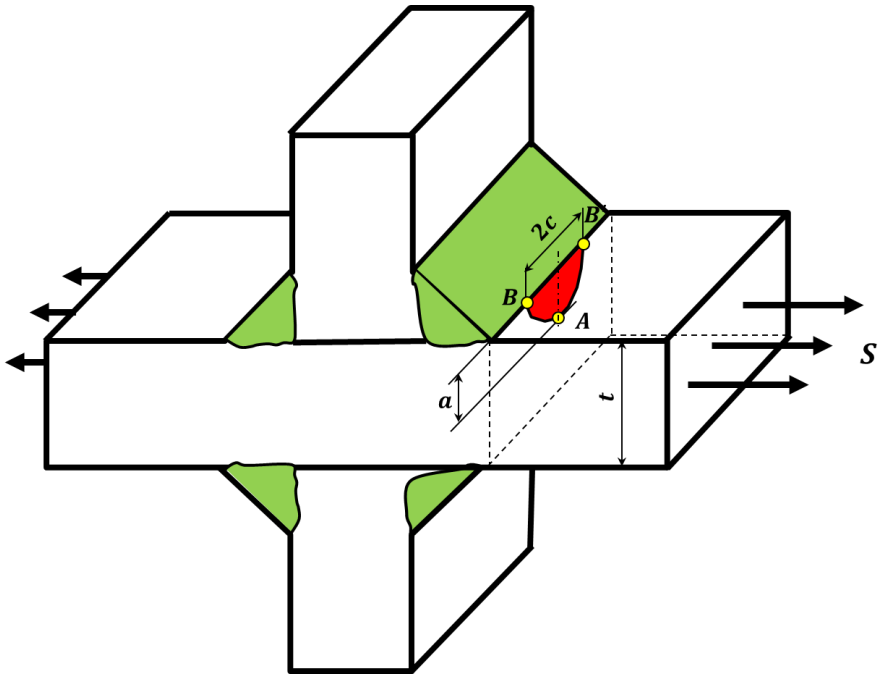

Figure 53: Schematic portrait of the specimen for S355 ST material cruciform-joint (Kasra Ghahremani, Ranjan, et al., 2015; Ranjan et al., 2016)

It consisted of 0.139 $wt\%\ C$, 0.504 $wt\%\ Si$, 1.56 $wt\%\ Mn$, 0.017 $wt\%\ P$, 0.0014 $wt\%\ S$ and 0.045 $wt\%\ AL$. There is no information about the crack shape, but the crack type was toe crack (Ulrike Kuhlmann et al., 2005; U. Kuhlmann et al., 2006). It has been reported by several studies that the fatigue crack in the weld joint areas were observed to be semi-elliptical in shape (Kasra Ghahremani, Ranjan, et al., 2015; Leitner et al., 2015; Ranjan et al., 2016). For this material, the crack was considered to be similar to that of ellipse as sketched in Figure 53.

Figure 54 shows illustratively its residual stresses measurements for the AW and the UIT conditions.

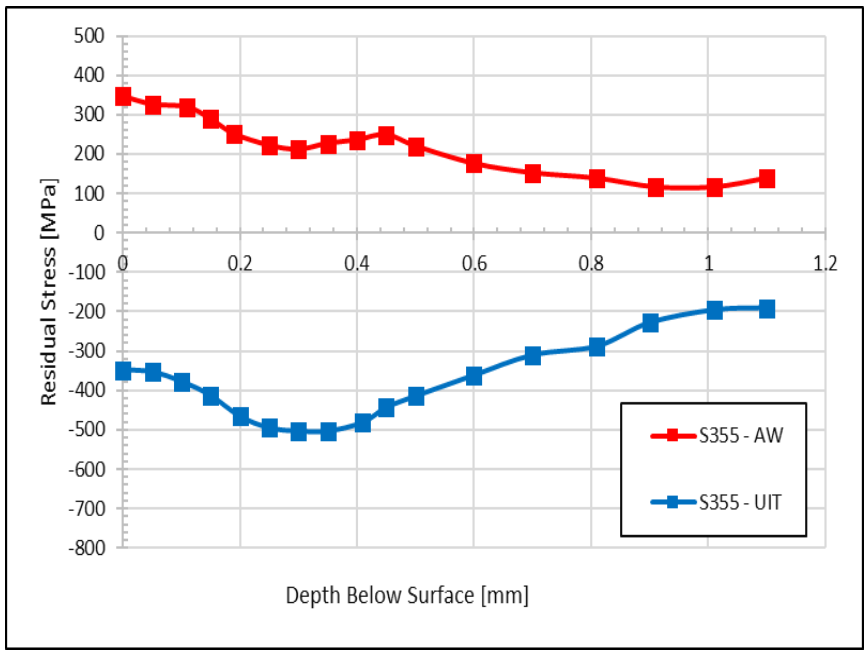

Figure 54: Residual stress measurement results of S355 cruciform-joint specimen under AW and UIT conditions (Ulrike Kuhlmann et al., 2005; U. Kuhlmann et al., 2006)

Figure 55 presents its fatigue life experimental data for both conditions.

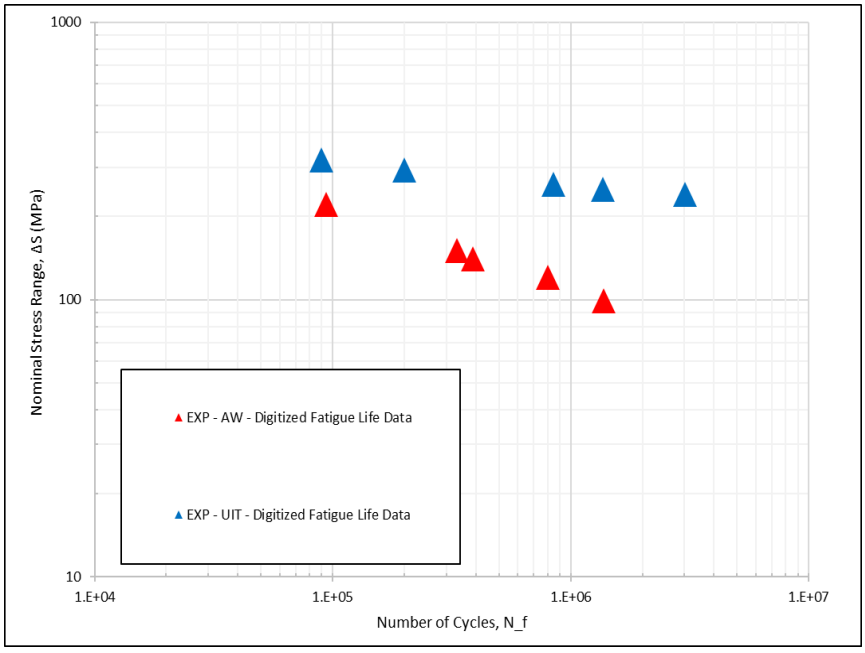

Figure 55: Fatigue life experimental data for S355 cruciform-joint specimen under AW and UIT conditions (Ulrike Kuhlmann et al., 2005; U. Kuhlmann et al., 2006)

4.5) S460 Steel Alloy

The welded specimen of this material was cruciform-joint and was fabricated from 12 mm (15/32") high strength steel plate (S460).The forenamed specimen was welded to the plate at room temperature and the welded plate has been inspected to comply with the quality of the welds and no weld quality problems were observed. The stiffener welds were performed by Gas Metal Arc (MAG) welding. Figure 56 displays graphically geometry of the studied specimen for the mentioned material (U. Kuhlmann et al., 2006; Ulrike Kuhlmann et al., 2005).

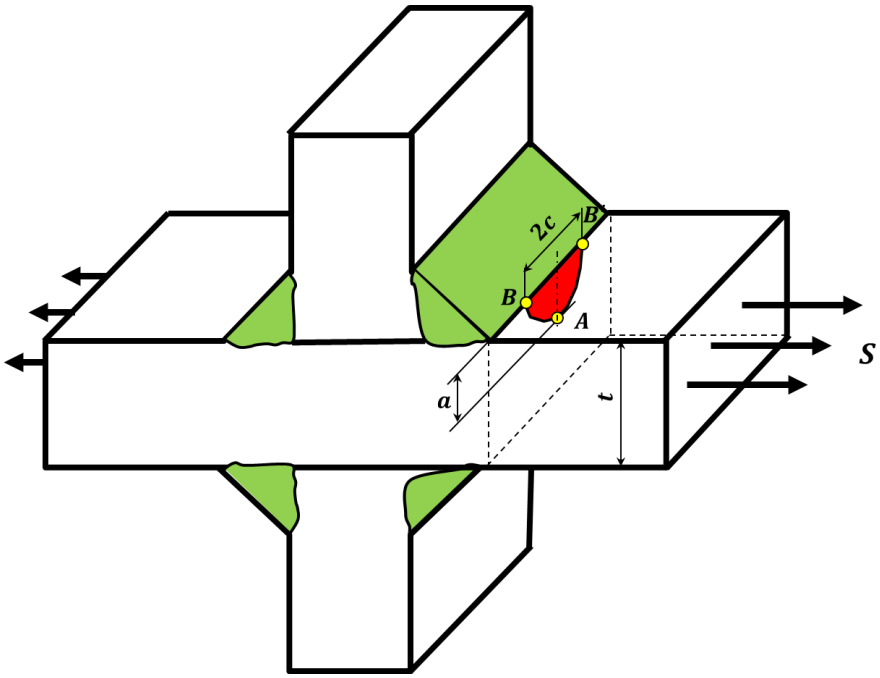

Figure 56: Schematic illustration of the specimen for S460 ST material cruciform-joint (Ulrike Kuhlmann et al., 2005; U. Kuhlmann et al., 2006)

It contained 0.037 $wt\%\ C$, 0.320 $wt\%\ Si$, 1.50 $wt\%\ Mn$, 0.004 $wt\%\ P$, 0.0010 $wt\%\ S$ and 0.037 $wt\%\ AL$, 0.180 $wt\%\ Cr$, 0.020 $wt\%\ Ni$, 0.002 $wt\%\ Mo$, 0.025 $Cu\ wt\%$, 0.008 $wt\%\ V$, 0.014 $wt\%\ Ti$, 0.045 $wt\%\ Nb$ and 0.0045 $wt\%\ N$. There is no information about the crack shape, but the crack type was toe crack (Ulrike Kuhlmann et al., 2005; U. Kuhlmann et al., 2006). It has been stated by numerous investigations that the fatigue crack in the weld joint areas were seen to be semi-elliptical in shape (Kasra Ghahremani, Ranjan, et al., 2015; Leitner et al., 2015; Ranjan et al., 2016). The crack was assumed to be similar to that of ellipse as illustrated in Figure 56 for this material also.

Figure 57 demonstrates comparatively its residual stresses measurements for the AW and the UIT conditions.

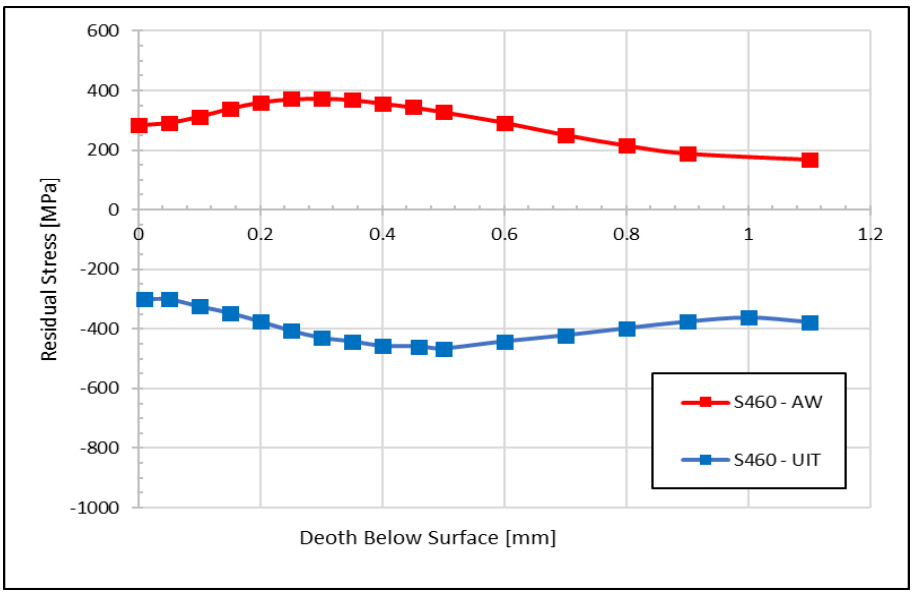

Figure 57: Residual stress measurement results of S460 cruciform-joint specimen under AW and UIT conditions (Ulrike Kuhlmann et al., 2005; U. Kuhlmann et al., 2006)

Figure 58 represents its fatigue life experimental data for both conditions.

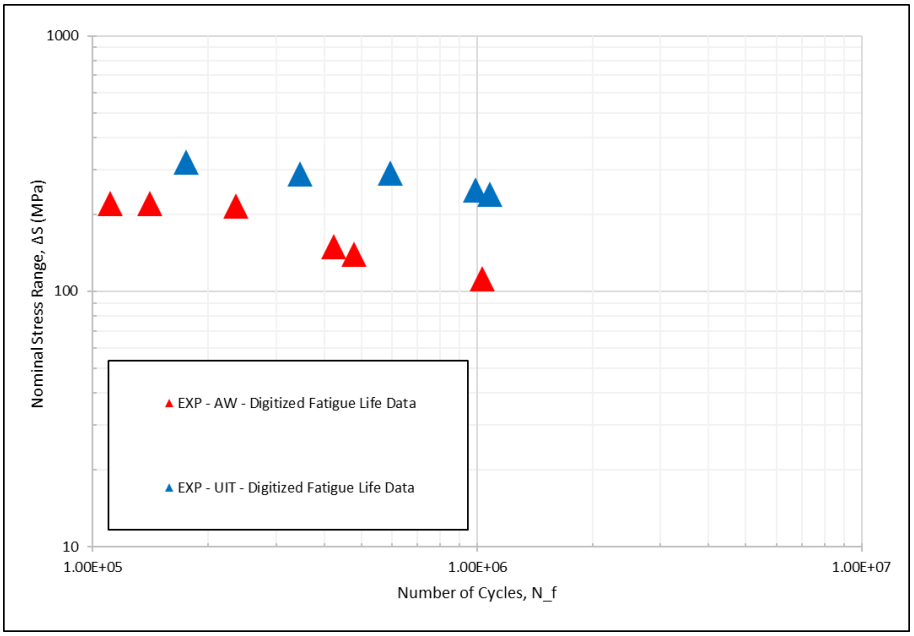

Figure 58: Fatigue life experimental data for S460 cruciform-joint specimen under AW and UIT conditions (Ulrike Kuhlmann et al., 2005; U. Kuhlmann et al., 2006)

4.6) S690 Steel Alloy

The welded specimen of this material was cruciform-joint and was fabricated from 12 mm (15/32") high strength steel plate (S460). The foresaid specimen was welded to the plate at room temperature and the welded plate has been checked out to satisfy the quality of the welds and no weld quality problems were distinguished. The stiffener welds were done by Gas Metal Arc (MAG) welding. Figure 59 shows illustratively geometry of the researched specimen for the above-mentioned material (U. Kuhlmann et al., 2006; Ulrike Kuhlmann et al., 2005).

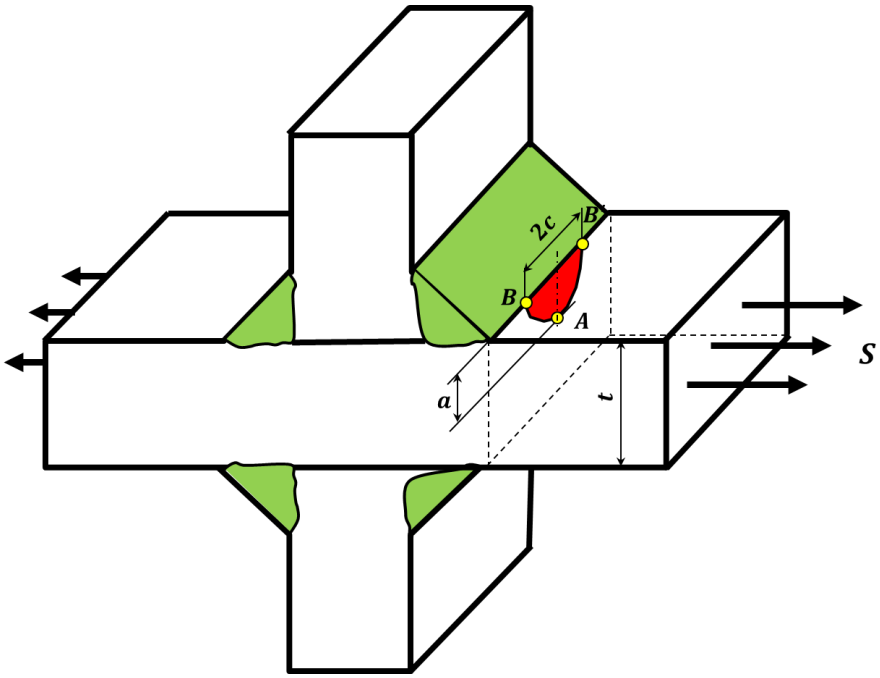

Figure 59: Schematic sketch of the specimen for S690 material cruciform-joint (Ulrike Kuhlmann et al., 2005; U. Kuhlmann et al., 2006)

It compromised of 0.074 $wt\%\ C$, 0.3380 $wt\%\ Si$, 1.61 $wt\%\ Mn$, 0.010 $wt\%\ P$, 0.0010 $wt\%\ S$ and 0.036 $wt\%\ AL$, 0.0.20 $wt\%\ Cr$, 0.020 $wt\%\ Ni$, 0.550 $wt\%\ Mo$, 0.021 $Cu\ wt\%$, 0.055 $wt\%\ V$, 0.003 $wt\%\ Ti$, 0.017 $wt\%\ Nb$ and 0.0049 $wt\%\ N$ and other alloying elements. There is no information about the crack shape, but the crack type was toe crack (Ulrike Kuhlmann et al., 2005; U. Kuhlmann et al., 2006). It has been incidated by number of researches that the fatigue crack in the weld joint areas were observed to be semi-elliptical in shape (Kasra Ghahremani, Ranjan, et al., 2015; Leitner et al., 2015; Ranjan et al., 2016). The crack was deemed to be similar to that of ellipse as indicated in Figure 59.

Figure 60 shows illustratively its residual stresses measurements for the AW and the UIT conditions.

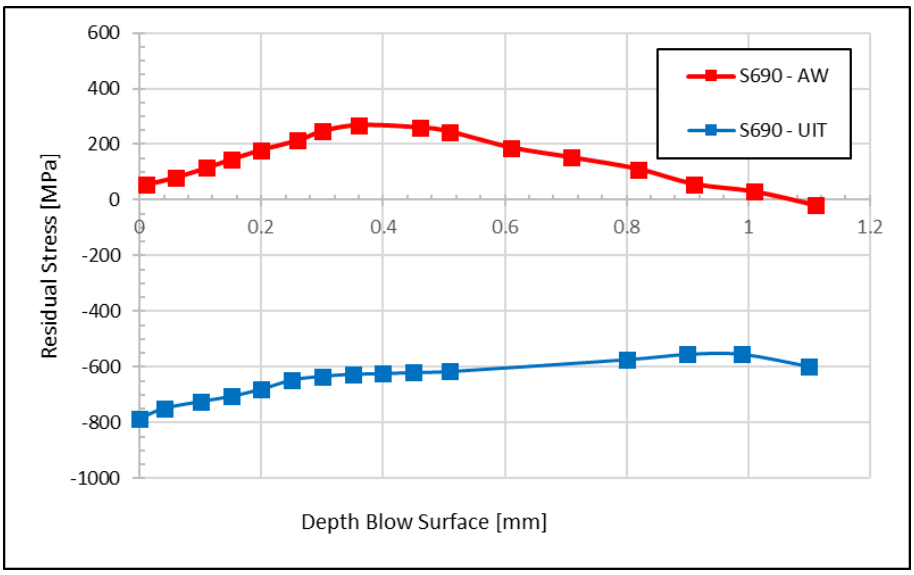

Figure 60: Residual stress measurement results of S690 cruciform-joint specimen under AW and UIT conditions (Ulrike Kuhlmann et al., 2005; U. Kuhlmann et al., 2006)

Figure 61 displays its fatigue life experimental data for both conditions.

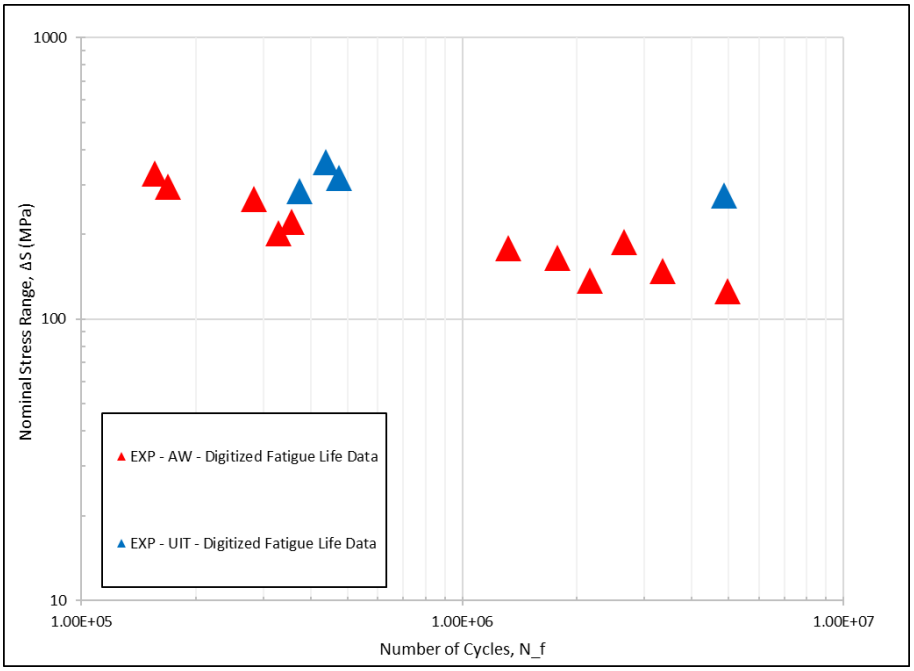

Figure 61: Fatigue life experimental data for S690 cruciform-joint specimen under AW and UIT conditions (Ulrike Kuhlmann et al., 2005; U. Kuhlmann et al., 2006)

4.7) S960 Steel Alloy

The welded specimen of this material was longitudinal stiffener joint and was made-up from 5 mm (13/64″) high strength steel plate (S960). The aforesaid specimen was welded to the plate at room temperature and the welded plate has been examined to meet the quality of the welds and no weld quality problems were detected. However, previous studies higlighted that because of an optimized calibration of the welding process (Michael Stoschka et al., 2012; M. Stoschka et al., 2013), a bare minimum angular distortion in the span of one-tenth degrees was eventually seen. The stiffener welds were carried out by Gas Metal Arc (MAG) welding. Figure 62 depicts schematically geometry of the investigated specimen for the above-mentioned material (Leitner et al., 2017).

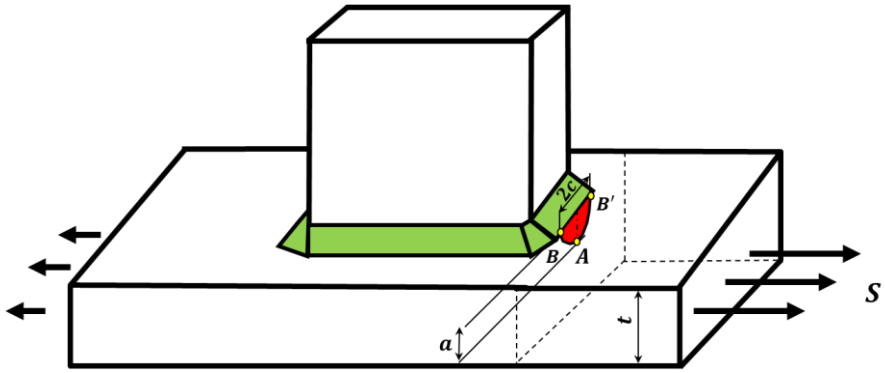

Figure 62: Schematic portrait of the specimen for S960 material longitudinal stiffener joint (Leitner et al., 2017)

There are no information about its composition and the crack shape. The crack type was toe crack (Leitner et al., 2017). It has been declared by many studies that the fatigue crack in the weld joint areas were discovered to be semi-elliptical in shape (Kasra Ghahremani, Ranjan, et al., 2015; Leitner et al., 2015; Ranjan et al., 2016). For this material, the crack was presumed to be similar to that of ellipse as highlighted in Figure 62.

Figure 63 shows illustratively its residual stresses measurements for the AW and the UIT conditions.

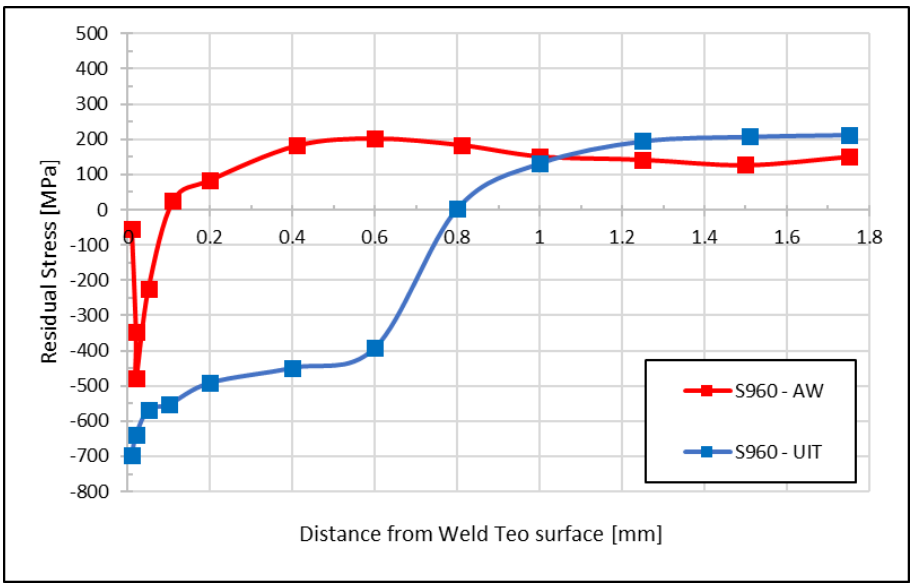

Figure 63: Residual stress measurement results of S960 longitudinal stiffener joint specimen under AW and UIT conditions (Leitner et al., 2017)

Figure 64 presents its fatigue life experimental data for both conditions.

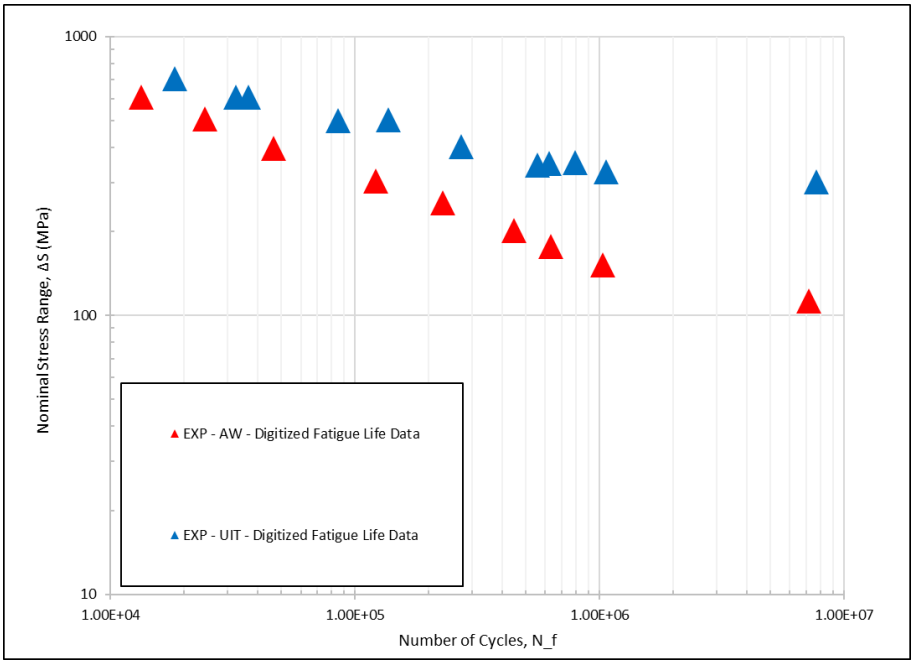

Figure 64: Fatigue life experimental data for S960 longitudinal stiffener joint specimen under AW and UIT conditions (Leitner et al., 2017)

4.8) 5083-H11 Aluminum Alloy

The welded specimen of this material was T-joint and was fabricated from $10\ mm$ $(25/64")$ aluminum plate (5083-H11 AL). The forenamed specimen was welded to the plate at room temperature and the welded plate has been inspected to comply with the quality of the welds and no weld quality problems were observed. The transverse stiffeners were performed by Metal Intert Gas (MIG) welding. Figure 65 displays graphically geometry of the studied specimen for the mentioned material (Sidhom et al., 2005).

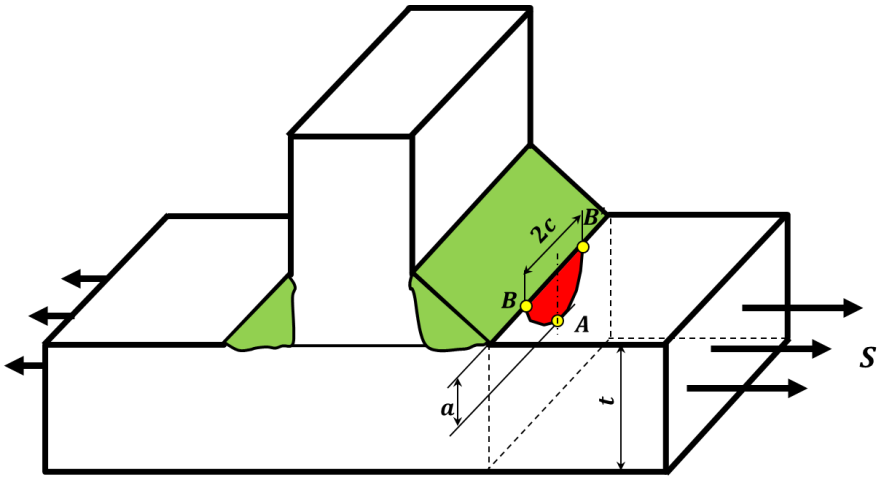

Figure 65: Schematic illustration of the specimen for CSA 5083-H11 AL T-joint (Sidhom et al., 2005)

5083-H11 AL is a popular alloy for structural sheet applications. The abbreviation of H321 demonstrates its temper which means it became work hardened $(1/4\ hard)$ and annealed at $350^{\circ}\ C$ for $2h$. It contained $0.14\ wt\%\ Si$, $0.25\ wt\%\ Fe$, $0.06\%\ wt\ Cu$, $0.53\ wt\%\ Mn$, $4.54\ wt\%\ Mg$, $0.11\ wt\%\ Cr$, $2.7\ wt\%\ Ni$, $0.08\ wt\%\ Zn$, $0.02\ wt\%\ Ti$, $1.4\ wt\%\ Zr$ and $4\ wt\%\ Pb$ (Sidhom et al., 2005).

There is no information about the crack shape. The surface accuracy was investigated employing a scanning electronic microscope (SEM) and the crack was toe crack (Sidhom et al., 2005). According to the mentioned researches, for this material likewise the crack was determined to be similar that of ellipse as demonstrated in Figure 65.

Figure 66 shows illustratively its residual stresses measurements for the AW and the UIT conditions.

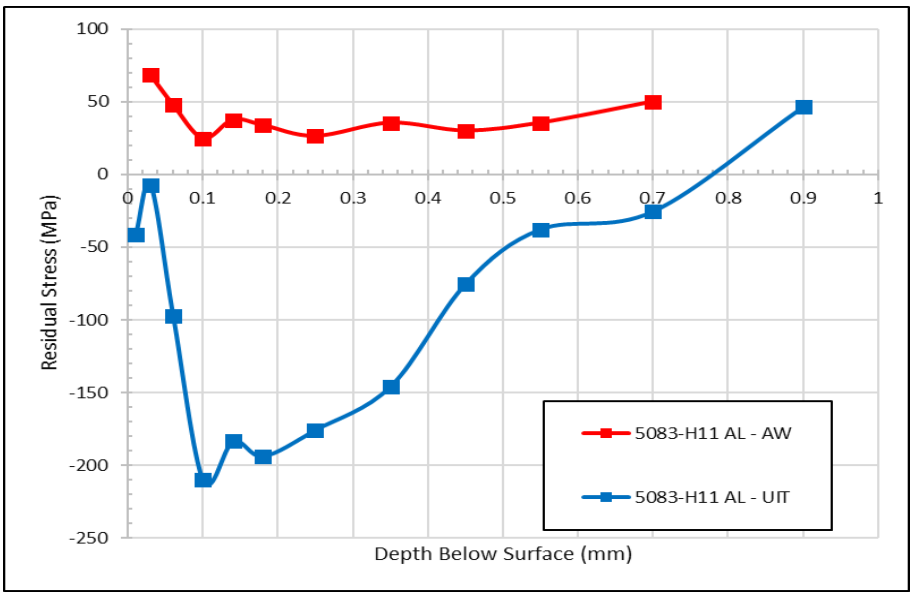

Figure 66: Residual stress measurement results of 5083-H11 AL T- joint specimen under AW and UIT conditions (Sidhom et al., 2005)

Figure 67 presents its fatigue life experimental data for both conditions.

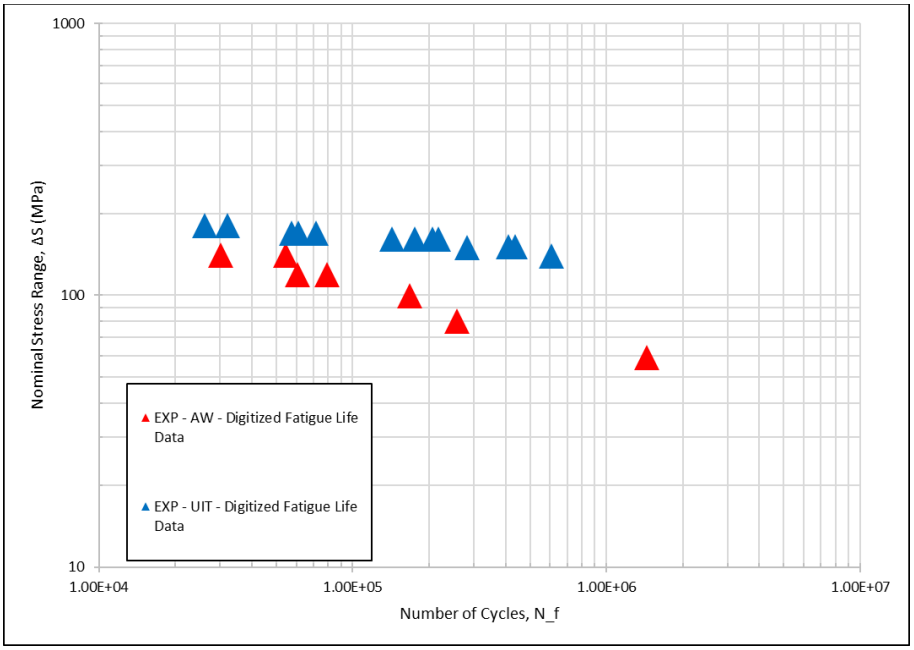

Figure 67: Fatigue life experimental data for 5083-H11 AL T- joint specimen under AW and UIT (Sidhom et al., 2005)

4.9) 2024-T351 Aluminum Alloy

The specimen of this material was plate and was manufactured from $4.5\,mm$ $(11/64")$ aluminum plate (2024-T351 AL). The foresaid specimen was examined at room temperature and the plate has been checked out to satisfy the quality of the research and no quality problems were distinguished. Figure 68 shows illustratively geometry of the researched specimen for the above-mentioned material (Kasra Ghahremani, Ranjan, et al., 2015; Ranjan et al., 2016).

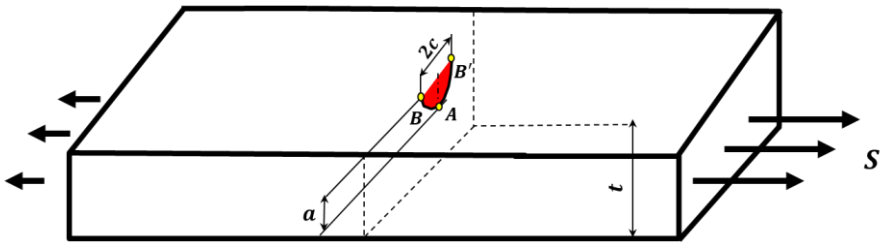

Figure 68: Schematic illustration of the specimen for 2024-T351 material plate (Rodopoulos et al., 2007)

There is no information about the crack shape. However, the propagation of the crack was taken using an optical microscope and a dedicated image-capturing card with the help of a high-end computer. It should be note that the crack was surface crack (Sidhom et al., 2005). Based on the above-mentioned studies, the crack was also considered to be similar that of ellipse for this material too as presented in Figure 68.

Figure 69 shows illustratively its residual stresses measurements for the AW and the UIT conditions.

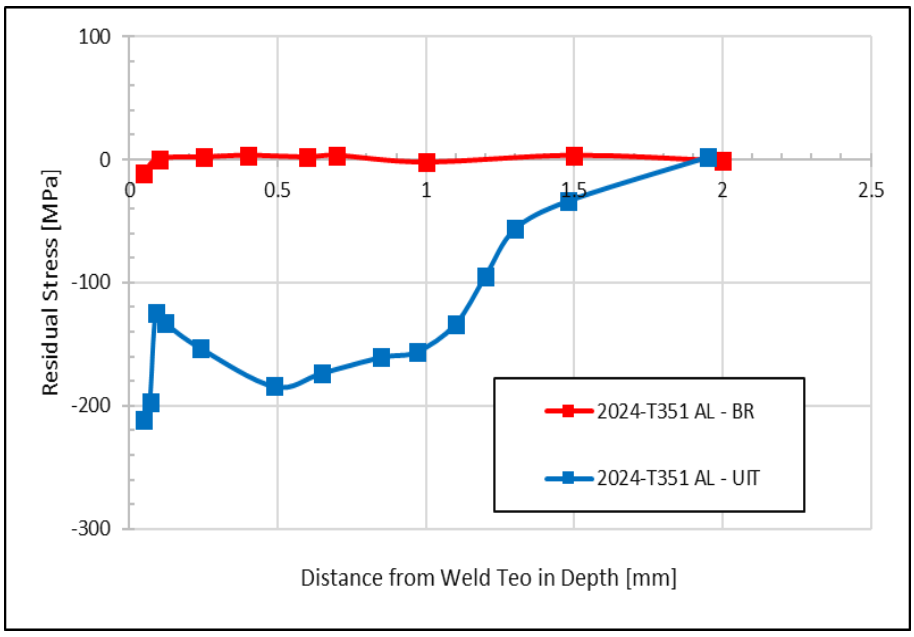

Figure 69: Residual stress measurement results of 2024-T351 AL plate specimen under AW and UIT conditions (Rodopoulos et al., 2007)

Figure 70 displays its fatigue life experimental data for both conditions.

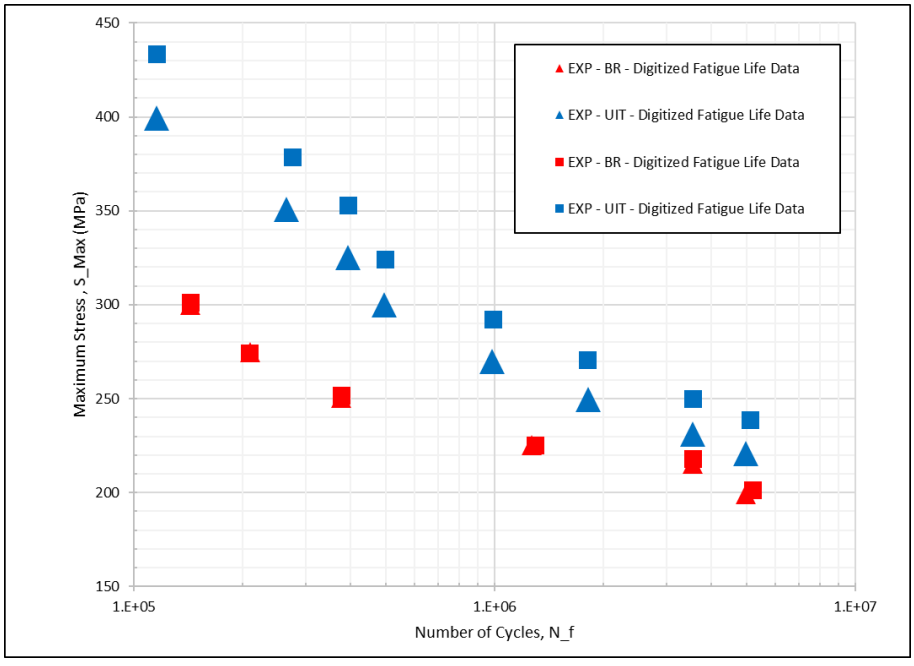

Figure 70: Fatigue life experimental data for 2024-T351 AL plate specimen under AW and UIT (Rodopoulos et al., 2007)

Table 1 gives a summerized information about the yield strengths and the ultimate tensile strengths as well as corresponding geometry types of all materials. From the literature, the values are either obtained through the tables or dervied from the stress-strain diagrams.

Table 1: Table of properties and corresponding geometry types for all materials (Sidhom et al., 2005; U. Kuhlmann et al., 2006; Rodopoulos et al., 2007; Tehrani Yekta et al., 2013; Ranjan et al., 2016; Leitner et al., 2017)

Material	**Properties**		**Geometry Type**
	S_y	S_u	
H083-H321 AL	240.7 MPa	368.2MPa	Cruciform-Joint
CSA 350W ST	396.3 MPa	574.3 MPa	Cruciform-Joint
ASTM A514 ST	792.5 MPa	903.9 MPa	Cruciform-Joint
S355	398.3 MPa	537.2 MPa	Cruciform-Joint
S460	503.5 MPa	553.4 MPa	Cruciform-Joint
S690	812.8 MPa	870.8 MPa	Cruciform-Joint
S960	960 MPa	1050 MPa	Longitudinal Stiffener Joint
5083-H11 AL	140 MPa	314 MPa	T-Joint
2024-T351 AL	347.4 MPa	504.6 MPa	Plate

Related supplementary information about the welding procedures of the materials are in the corresponding cited literature. The perception of the welding processes is arleady described in Chapter 2.

4.10) Residual Stresses Measurement

From Figure 45, Figure 48 and Figure 51, by evaluating the residual stresses results of 5083-H321 AL, CSA 350W ST and A514 ST for both conditions, respectively; it can be understood that even or multi-linear residual stress distributions were used for UIT based on a trial and error process (Ranjan et al., 2016). Further, uniform stress distributions closed to zero were assumed for the AW specimens for the mentioned materials (K. Ghahremani, 2015). Actually, it was explored that the residual stresses were very low, with similar scatter on average around $0\ MPa$ (Ranjan et al., 2016).

However, The authors (Kasra Ghahremani, Ranjan, et al., 2015; Ranjan et al., 2016) states that UIT imparts a compressive residual stress neighboring the area of the treated weld toe in the span of $75 - 200\ MPa$ for 5083-H311 AL and $300 - 600\ MPa$ for A514 ST specimens due to some scatter in the residual stresses. In fact, measured residual stresses outcomes are very sensitive to the exact position of the site, so obtaining measurements are really problematic for the exact same site for distinct specimens. Given the substantial fatigue life enhancement that was witnessed in the test outcomes, it was speculated that the residual stresses abnormality happens over tiny gaps throughout the weld. Eventually, even if a crack commences in a regime of low compressive residual stresses, it is caught in the neighbouring regimes were the residual stresses magnitude are higher. This assumption was proposed by (Kasra Ghahremani, Ranjan, et al., 2015; Ranjan et al., 2016) and further evaluations would be required.

Comparing the outcomes, it can be note that the residual stresses for A514 ST are at the upper extremity of the limit that of CSA 350W ST. It was expected to be larger, but CSA 350W ST was treated in a completely different time / setting / operator / tool etc. (Ranjan et al., 2016). It is noteworthy that the maximum values of the desirable residual stresses are at a depth of almost $0.6\ mm$ for the said materials.

The desirable residual stresses were imparted deep by the UIT method into 5083-H311 AL and CSA 350W ST test specimens inside and near the weld over a depth of up to roughly $1.4\ mm$. On the contrary, the undesirable residual stresses were induced by the welding operation inside and near the weld over a depth of up to approximately $0.8\ mm$.

The beneficial compressive residual stresses were propagated deep by the UIT method into A514 ST test specimen within and close the weld over a depth of up to roughly $1.4\ mm$. In contrast, the tensile residual stresses were induced by the welding operation within and close the weld over a depth of up to roughly less than $0.7\ mm$.

From Figure 54, Figure 57 and Figure 60, by assessing the residual stresses results of S355, S460 and S690 for both conditions, respectively; it can be comprehended that the desirable residual stresses were imparted deep by the UIT method into S355, S460 and S690 test specimens inside and near the weld over a depth of up to roughly $1.1\ mm$. By contrast, the undesirable residual stresses were induced by the welding operation within and close the weld over a depth of up to almost $1.1\ mm$ as well. It should be noted that the maximum values of the desirable residual stresses are at a depth of approximately $0.3\ mm$ to $0.4\ mm$ for the materials except S690 seems to be a little below the surface.

From Figure 63, the residual stresses results of S960 for both conditions, it should be pointed out that the compressive beneficial residual stresses were propagated deep by the UIT method into S960 test specimen inside and near the weld over a depth of up to roughly $1.75\ mm$. Conversely, the tensile residual stresses were induced by the welding operation within and close the weld over a depth of up to roughly $1.75\ mm$ as well.

In the first $0.1\ mm$, the post-welded treatment accomplishes a desirable residual stress of about $550\ to\ 700\ MPa$ as shown in Figure 63. Moving forward, the impact of UIT treatment is distinguishable up to a depth of almost $1\ mm$. In the first $0.1\ mm$, the residual stress for the AW condition does not reflect properly the true values for some unknown reasons like measurement errors etc.

From Figure 66, the residual stresses effects of 5083-H11 AL for both conditions, by comparison to the initial portion of the graph, Figure 66 demonstrates that there is no significant relaxation of the undesirable residual stresses up to a depth of roughly $0.075\ mm$. The desirable residual stresses were imparted deep by the UIT method into 5083-H11 AL test specimen inside and near the weld over a depth of up to approximately $0.9\ mm$. On the contrary, the undesirable residual stresses were induced by the welding operation within and close the weld over a depth of up to roughly $0.7\ mm$.

Figure 69 represents illustratively the residual stresses measurements of 2024-T351 AL which is plate provided by Airbus UK and fabricated by Alcoa (Rodopoulos et al., 2007) for both conditions. UIT dominates the regime among 0.4 and $1.1\ mm$ and UIT exposes penetration depth of almost $1.8\ mm$ considering some errors during the UIT process as well. Whereas the tensile residual stresses were induced by the welding operation inside and near the weld over a depth of up to approximately $2\ mm$.

Recent modeling and experimental works have also indicated that UIT results insignificant effects on residual stresses of the weld joints (Tang et al., 2018; Zheng et al., 2018). UIT is particularly more effective on steels with high strength considering the yield strength of the materials. In a nutshell, it is vital to bring down the tensile residual stresses at or just below the surface to a depth about approximately $0.5\ mm$ in order to increase fatigue strength of the materials (Radaj, 1995). In this research, the derived data – from the cited literature – of the plotted graphs are employed in the models.

CHAPTER 5: RESULTS AND DISCUSSION

5.1) Input Fatigue and Geometry Parameters

The entire applied and the residual stresses followed by their distribution across the plate thickness are required to be determined in order to perform accurate fatigue life predictions on the basis of the crack propagation methodologies as already stated. Hence, the effect of the residual stresses condition must be considered to calculate the fatigue life more precisely for the AW and the UIT conditions for each material. As already clarified, the welding tensile residual stresses and the stress concentrations due to the local geometry tend to make joints the weakest location in terms of fatigue failure. Accordingly, the core concept of notch stress method explains this important matter by introducing a SCF (Fricke, 2012). From Chapter 3, equations (3. 10) and (3. 11) have already described such phenomena so that local stress load can be calculated for each stress level.

Through measuring the geometry feature, K_t can be obtained which is so critical for fracture analyses. Table 2, Table 3 and Table 4 provide the stress concentrations values for both AW and UIT conditions.

Table 2: Stress concentration for the first three materials

Parameter	**5083 − H311 AL** [a]	**CSA 350W ST** [a]	**A514 ST** [a]
$K_t - AW$	2.2	2	2
$K_t - UIT$	1.8	1.3	1.3

[a] (Estimated – assumed)

Table 3: Stress concentration for the second three materials

Parameter	**S355** [a]	**S460** [a]	**S690** [a]
$K_t - AW$	2.54	2.51	2.24
$K_t - UIT$	2.11	2.07	1.96

[a] (U. Kuhlmann et al., 2006)

Table 4: Stress concentration for the third three materials

Parameter	**S960** [a]	**5083 − H11 AL** [a]	**2024 − T351 AL** [b]
$K_t - AW$	2.1	2.5	1.11

$K_t - UIT$	1.8	1.9	1.2

[a] (Estimated – assumed)

[b] (Rodopoulos et al., 2007)

When the local yield strength of the material is smaller than the locally applied stress ($S_{loc-ap} \geq S_{loc-y}$), the constancy of these stresses is extremely essential, and relaxation takes place (Sonsino, 2009; Farajian, Nitschke-Pagel, et al., 2012; Yildirim & Marquis, 2013). As a matter of fact, the compressive residual stresses up to a depth of $1.6 - 2\ mm$ have been generated as:

$$S_{ap} = K_t S_n + S_{rs} \qquad (4.1)$$

S_{ap} is applied stress, K_t is stress concentration, S_n is nominal stress and S_{rs} is residual stress.

These differences are related to the load of the fatigue tests. Comparable circumstances have been found in the following studies (Weich et al., 2009; Farajian, Barsoum, et al., 2012; Yildirim & Marquis, 2012, 2013; Khurshid et al., 2014).

Another dominant element that restricts the reachable degree of fatigue enhancement meant for impact treated welds is the possibility of alternative modes of failure other than weld toe failure (Kasra Ghahremani, Walbridge, et al., 2015). Another significant factor is that for the crack shape, the aspect ratio $\frac{a}{c}$ must be considered in a proper range (A. Hobbacher, 2012).

The quantity of γ depends on the R-ratio in equation (3.3) for Walker model. It illustrates how strongly the R-ratio influence the crack growth rate in that material. It is important to bear in mind that Walker model is a generalization of Paris model to deem the impression of the R-ratio on crack growth rate as already mentioned in Chapter 3. Since the R-ratio equal to 0.1 does not establish such high liability on fatigue crack growth analyses unlike the R-ratio higher than 0.5. Thus, γ was considered based on probabilistic fracture mechanics. It was set to the default value of approximately 0.5 ± 0.1 by considering several similar various material databases. As stated by (Dowling, 2013), 0.5 is a typical amount γ for many materials.

There are two failure criteria. One is the maximum SIF should be compared to the critical SIF from the material databases to determined failure. Other is checking yielding across the uncrack section is usual. In this matter, the maximum applied stress is usually compared to the follow stress which is the average of the yield strength and the ultimate strength.

The fatigue crack propagation and crack increments resulted from subsequent cyclic loadings are calculated by Walker and Forman models with the fatigue parameters given in Table 5, Table 6 and Table 7. The input parameters are obtained from the recent publications, estimated from the engineering assumptions and or assumed based on the recommendations predicated on average values (Pearson, 1966; Harrison, 1970; Tada et al., 1973; Frost et al., 1974; Ulrike Kuhlmann et al., 2005; U. Kuhlmann et al., 2006; Wallbrink et al., 2006; A. Hobbacher, 2012; Kasra Ghahremani, Ranjan, et al., 2015; Ranjan et al., 2016; A. F. Hobbacher, 2016; Marquis & Barsoum, 2016; Richard & Sander, 2016; Leitner et al., 2016; Hadley, 2018). These parameters are summarized in the below tables:

Table 5: Input fatigue and geometry parameters employed in fracture mechanics analyses for the first three materials

Parameter	5083-H311 AL	CSA 350W ST	A514 ST
$w\ (mm)$[a]	30	30	30
$t\ (mm)$[a]	9.5	9.5	9.5
$E\ (GPa)$[a]	71.4	201.5	209.9
R [a]	0.1	0.1	0.1
$C_W - Walker$ $(MPa, \sqrt{m})$[a, b, c1]	2.521^{e-12}	3.50^{e-12}	5.38^{e-12}
$C_F - Forman$ $(MPa, \sqrt{m})$[b, c1/2]	5.42^{e-10}	7.53^{e-10}	1.15^{e-9}
m[a]	3.96	3	2.64
$\Delta K_{th}\ (MPa, \sqrt{m})$[a]	0.796	2.529	3.604
$a_i\ (mm)$[a]	0.2	0.15	0.15
$a_f\ (mm)$[a, d]	4.75	4.75	4.75
$\frac{a}{c} - AW\ (mm)$[a]	0.47	0.4	0.29
$\frac{a}{c} - UIT\ (mm)$[a]	0.71	0.6	0.15

[a] (Kasra Ghahremani, Ranjan, et al., 2015; Ranjan et al., 2016)

[b] (A. F. Hobbacher, 2016; Marquis & Barsoum, 2016; Richard & Sander, 2016; Hadley, 2018)

[c] (Estimated / Assumed (1) - Derived from similar that of the material crack growth data and Walker based on (Joshua, 2014) average value considering the recommendations (2))

[d] (Half of the thickness $- a_f = \frac{t}{2}$)

It should be underlined that C_W is computed in accordance with $LN(C)$ values here (Ranjan et al., 2016) and it is also converted from mm to m as well, as follows:

$$C_W = \frac{2.71828^{LN(C)}}{\sqrt{10^{-3}}} \qquad (4.2)$$

ΔK_{th} was also converted from mm to m. Note that the initial defect depth, a_i, was assumed 0.2 for 5083-H321 AL. The aspect ratio was considered 0.4 and 0.6 for the AW and the UIT conditions, respectively for CSA 350W ST.

The logical assumed range of aspect ratio for the AW condition is generally within $0.2 \leq \frac{a}{c_{AW}} \leq 0.6$ whereas the good presumed range of aspect ratio for the UIT condition is usually into the interior of $0.6 \leq \frac{a}{c_{UIT}} \leq 0.8$ proportional to quality of the weld, joint type, geometry of the weld attachment etc. It is generally expected that the aspect ratio of a crack will contribute to converge on an ideal "equilibrium" condition, irrespective of the initial value (Wallbrink et al., 2006). The initial aspect ratio as well as the initial crack depth were opting in compliance with comparisons to the corresponding experimental results, considering the above-mentioned description and based on the common engineering assumptions. The aspect ratio estimated also based on the chosen initial crack size as stated by (P. Shams-Hakimi, 2017; Poja Shams-Hakimi et al., 2018).

Table 6: Input fatigue and geometry parameters applied in fracture mechanics analyses for the second three materials

Parameter	S355	S460	S690
$w\ (mm)$[a]	160	160	160
$t\ (mm)$[a]	12	12	12
$E\ (GPa)$[a]	207.4	206.5	212.5
R [a]	0.1	0.1	0.1
$C_W - Walker$ $(MPa, \sqrt{m})$[b, c1]	2.6^{e-13}	6.77^{e-13}	6.83^{e-13}

$C_F - Forman$ $(MPa, \sqrt{m})$[c1/2, b]	5.59^{e-11}	1.45^{e-10}	1.47^{e-10}
m[b, c1]	3.5	2.88	2.88
$\Delta K_{th}\ (MPa, \sqrt{m})$[d]	0.61	0.61	0.61
$a_i\ (mm)$[c1]	0.2	0.25	0.1
$a_f\ (mm)$[a, e]	6	6	6
$\frac{a}{c} - AW\ (mm)$[c1]	0.4	0.3	0.4
$\frac{a}{c} - UIT\ (mm)$[c1]	0.65	0.65	0.7

[a] (U. Kuhlmann et al., 2006)

[b] (A. F. Hobbacher, 2016; Marquis & Barsoum, 2016; Richard & Sander, 2016; Hadley, 2018)

[c] (Estimated / Assumed (1) - Derived from similar that of the material crack growth data and Walker based on (Joshua, 2014) average value considering the recommendations (2))

[d] (A. Hobbacher, 2012; Leitner et al., 2016)

[e] (Half of the thickness $- a_f = \frac{t}{2}$)

For the R-ratio equal to 0.1 which is within the following range $0 \leq R \leq 0.5$, ΔK_{th} can be approximated for steel as follows (A. Hobbacher, 2012; Leitner et al., 2016):

$$\Delta K_{th} = 5.4\ to\ 6.8\ \times R \qquad (4.3)$$

It is important to note that Walker model is a generalization of Paris model to consider the impact of the R-ratio on crack growth rate as already mentioned in Chapter 3. Since the R-ratio equivalent to 0.1 does not impose such great burden on fatigue crack growth analyses unlike the R-ratio higher than 0.5. Hence, cracks with depth of less than 1 mm can be treated in this manner as both models are quite identical when the R-ratio value is close to zero.

The initial crack depth was assumed 0.2, 0.25, 0.1 for S355, S460 and S690, respectively. The aspect ratio was considered 0.4, 0.3 and 0.4 for AW condition, respectively for S355, S460 and S690 while the aspect ratio was presumed 0.65, 0.65 and 0.7 for UIT condition, respectively for S355, S460 and S690.

Table 7: Input fatigue and geometry parameters applied in fracture mechanics analyses for the third three materials

Parameter	S960	5083-H11 AL	2024-T351 AL
$w\ (mm)$[a]	50	60	5.5
$t\ (mm)$[a]	5	10	4.5
$E\ (GPa)$[a]	200	72	70
R [a]	0.1	0.1	0.1
$C_W - Walker$ $(MPa, \sqrt{m})$[b, c1]	1.85^{e-12}	1.56^{e-12}	2.38^{e-12}
$C_F - Forman$ $(MPa, \sqrt{m})$[c1/2, b]	3.95^{e-10}	3.35^{e-10}	2.48^{e-9}
m[b, c1]	3	3.96	3.2
$\Delta K_{th}\ (MPa, \sqrt{m})$[d]	0.61	0.205	0.205
$a_i\ (mm)$[c1]	0.1	0.2	0.2
$a_f\ (mm)$[a, e]	2.5	5	2.25
$\frac{a}{c} - AW\ (mm)$[c1]	0.4	0.45	0.46
$\frac{a}{c} - UIT\ (mm)$[c1]	0.7	0.61	0.66

[a] (Sidhom et al., 2005; Rodopoulos et al., 2007; Leitner et al., 2017)

[b] (A. F. Hobbacher, 2016; Marquis & Barsoum, 2016; Richard & Sander, 2016; Hadley, 2018)

[c] (Estimated / Assumed (1) - Derived from similar that of the material crack growth data and Walker based on (Joshua, 2014) average value considering the recommendations (2))

[d] (A. Hobbacher, 2012; Hadley, 2018)

[e] (Half of the thickness $- a_f = \frac{t}{2}$)

It should be emphasized that Young's modulus of steel, E, is typically around 190 GPa to 215 GPa at room temperature. When the exact value is not presented, the current practice is to presume it to be about 200 GPa depending of course on the grade of steel and thickness etc.

The initial crack depth was considered 0.1, 0.2, 0.2 for S960, 5083-H11 AL and 2024-T351 AL, respectively. The aspect ratio was presumed 0.4, 0.45 and 0.46 for AW condition,

respectively for S960, 5083-H11 AL and 2024-T351 AL whereas the aspect ratio was assumed 0.7, 0.61 and 0.66 for UIT condition, respectively for S960, 5083-H11 AL and 2024-T351 AL.

For the R-ratio equivalent to 0.1 which is in the following range $0 \leq R \leq 0.5$, ΔK_{th} can be approximated for aluminum as follows (A. Hobbacher, 2012; Leitner et al., 2016):

$$\Delta K_{th} = 1.8\ to\ 2.3 \times R \tag{4.4}$$

The recommended crack growth constants for steels could be employed to other materials with Young's modulus E by utilizing the following value (Pearson, 1966; Harrison, 1970; Frost et al., 1974; Tada et al., 1973):

$$C = 5.21^{3-13} \times (\frac{E_{ST}}{E_{AL}})^3 \tag{4.5}$$

Similarly, the THSIF can be derived as follows (Pearson, 1966; Harrison, 1970; Frost et al., 1974; Tada et al., 1973):

$$\Delta K_{th-AL} = \Delta K_{th-ST}(\frac{E}{E_{ST}}) \tag{4.6}$$

Equations (4.4), (4.5) and (4.6) were applied to H5083-H11 to determine C_W as well as ΔK_{th}. Further, equations (4.4) and (4.6) were used for 2024-T351 AL to compute ΔK_{th}.

5.2) Fatigue Strength Analysis

The fatigue life on the basis of fatigue crack propagation of the welded joints under the AW and the UIT conditions are computed by Walker and Forman crack growth models for nine different materials. To evaluate the effects of UIT on the fatigue performance of the welded attachments, the stress concentrations and the residual stresses adjustments were considered for the prediction of the fatigue life under the CA cyclic fatigue loading with the R-ratio equivalent to 0.1 as explained in the previous sections. The overall aim of this section is to clarify which model not only predicted the life better but also depicted the fatigue strength of that material with more reliability and accuracy for both conditions.

Figure 71, Figure 72, Figure 73, Figure 74, Figure 75, Figure 76, Figure 77, Figure 78 and Figure 79 demonstrate comparatively the fracture mechanics results in order to evaluate fatigue strength of 5083-H311 AL, CSA 350W ST, A514 ST, S355, S460, S690, S960, 5083-H11 AL and 2024-T351 AL, respectively.

The figures show illustratively the nominal stress-life, $S-N$ curves, of the weld joints under the AW and the UIT treated conditions. In these charts, the AW specimens are shown with red symbols and the UIT treated specimens are shown in blue ones. In all cases, the blue symbols are shifted to the right, representing that a rise in the fatigue life has led to the successful UIT treatment.

As a general rule, the fatigue life rise is further conspicuous for the mild steel and the high-strength steel specimens rather than the aluminum weld specimens as an example with an observation of the first three materials, 5083-H311 AL, CSA 350W ST and A514 ST, respectively. Figure 71, Figure 72 and Figure 73 display graphically such description for both conditions and models.

The aim of the CA cyclic fatigue loading tests was to study the impact of the UIT treatment subjected to a loading history that is acknowledged to be surprisingly harsh for impact-treated welds (Ranjan et al., 2016). Looking at the first three materials, it is clear that substantial fatigue life raises still occurred because of the UIT treatment, subjected to this loading history. In more general terms, the fatigue efficiency development because of the UIT treatment proliferates as the nominal stress range diminishes, because of the sophomoric slope of the UIT curves.

Figure 71 shows that both models overpredicted the life a bit more for the UIT condition between 1×10^4 cycles to 3×10^5cycles . On the contrary, after 3×10^5 cycles the estimated life demonstrates a good agreement with the test results in HCF region. Note that Forman model appears to be more reliable in comparison to Walker model for the UIT post-weld treatment. In addition, the AW condition looks fine for both models. Still, Forman model performed an iota better prediction over Walker model for this material.

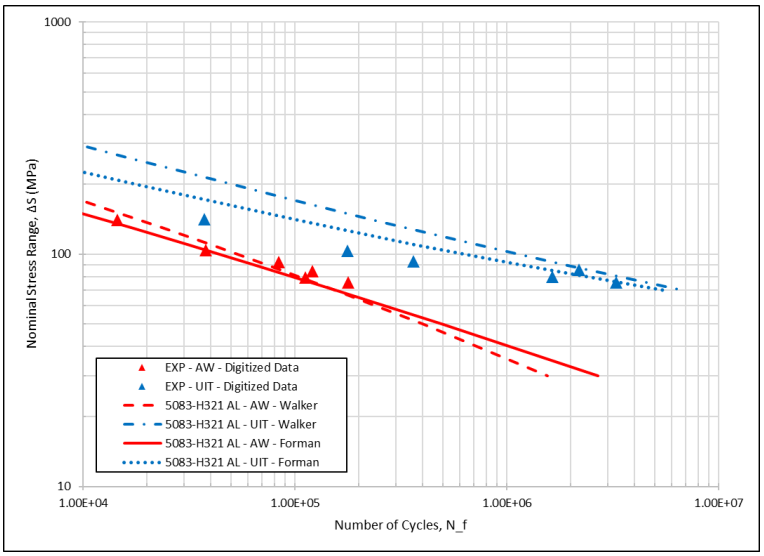

Figure 71: Fracture mechanics analysis results for 5083-H321 AL subjected to CA cyclic fatigue loading with R-ratio equal to 0.1 for AW and UIT conditions for Walker and Forman models (Kasra Ghahremani, Ranjan, et al., 2015; Ranjan et al., 2016)

According to Figure 72, the experimental data are positioned in the high cycle region for the UIT condition, both models estimated the life still quite well. Due to lack of the experimental data before 1×10^6 cycles, it seems difficult to evaluate the models in that domain. Despite the fact that the AW condition seems to illustrate an acceptable compliance with the experimental results for both models.

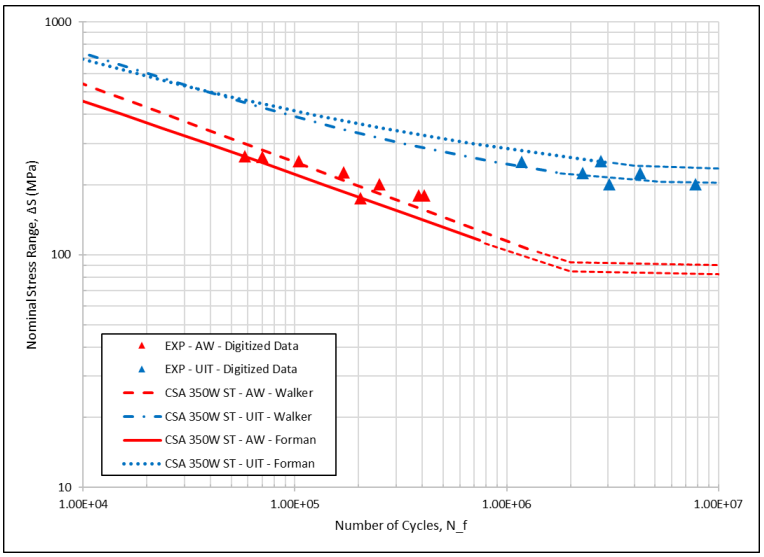

Figure 72: Fracture mechanics analysis results for CSA 350W ST subjected to CA cyclic fatigue loading with R-ratio equal to 0.1 for AW and UIT conditions for Walker and Forman models (Kasra Ghahremani, Ranjan, et al., 2015; Ranjan et al., 2016)

Further, Figure 73 indicates that both models predicted the life quite satisfactory for the AW condition. Figure 73 also represents that both models assessed the life under the UIT condition in a good promise. It is worth noting that Forman model estimated the life better than even Walker model for the UIT condition before 2×10^5 cycles.

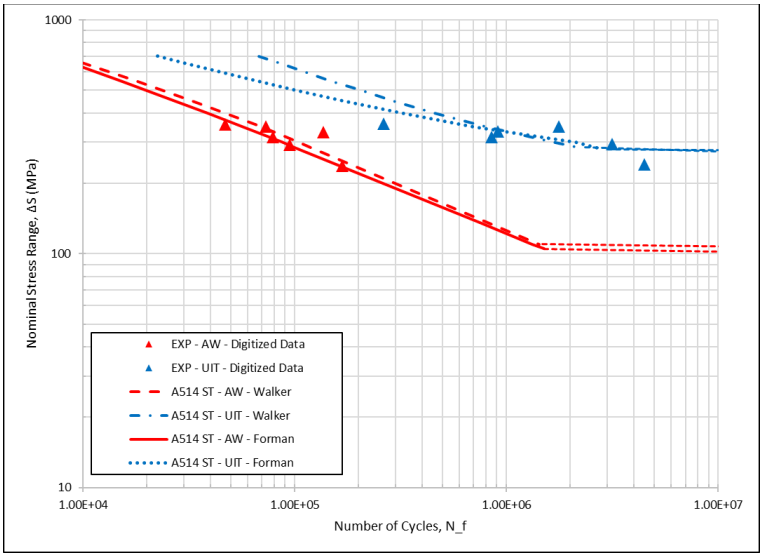

Figure 73: Fracture mechanics analysis results A514 ST subjected to CA cyclic fatigue loading with R-ratio equal to 0.1 for AW and UIT conditions for Walker and Forman models (Kasra Ghahremani, Ranjan, et al., 2015; Ranjan et al., 2016)

Figure 74, Figure 75 and Figure 76 depict diagrammatically the impact of UIT on the fatigue proficiency of S355, S460 and S690, respectively, under both conditions as well as models.

As reflected in Figure 74, both models forecasted the life quite agreeable for both conditions. However, Walker and Forman models overestimated the life slightly for the UIT condition as shown in Figure 75 before 3×10^5 cycles. It should be noted that both models are still fairly satisfactory for that condition.

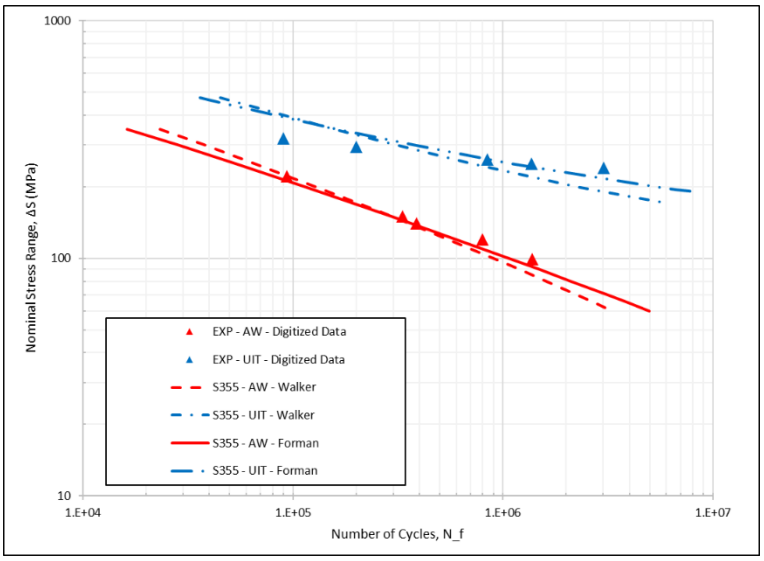

Figure 74: Fracture mechanics analysis results S355 subjected to CA cyclic fatigue loading with R-ratio equal to 0.1 for AW and UIT conditions for Walker and Forman models

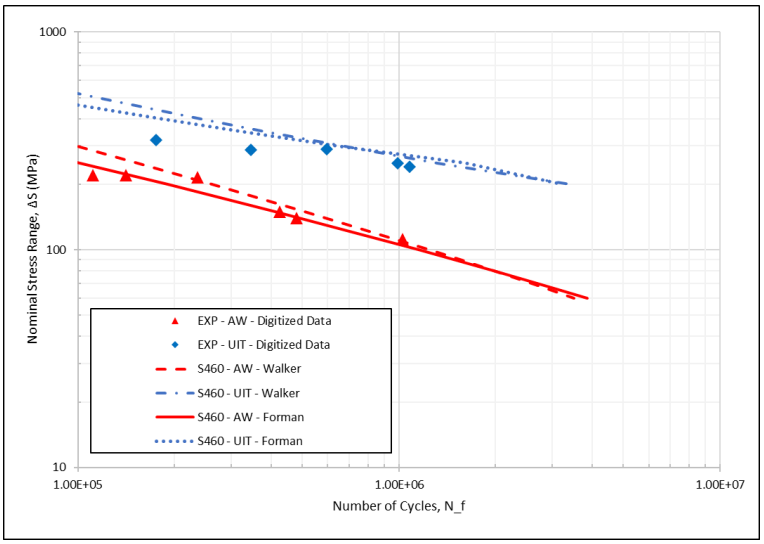

Figure 75: Fracture mechanics analysis results S460 subjected to CA cyclic fatigue loading with R-ratio equal to 0.1 for AW and UIT conditions for Walker and Forman models

As illustrated in Figure 76, Walker and Forman models performed completely good predictions for the life under the AW condition. It should be pointed out that Forman model estimated the life superior to Walker Model for both conditions. The experimental data are adjacent

to each other for the AW and the UIT conditions which is around 3×10^5 cycles to 6×10^5 cycles. It is apparent that Walker model still is not as good as Forman model in this material for the UIT condition as shown in the figure.

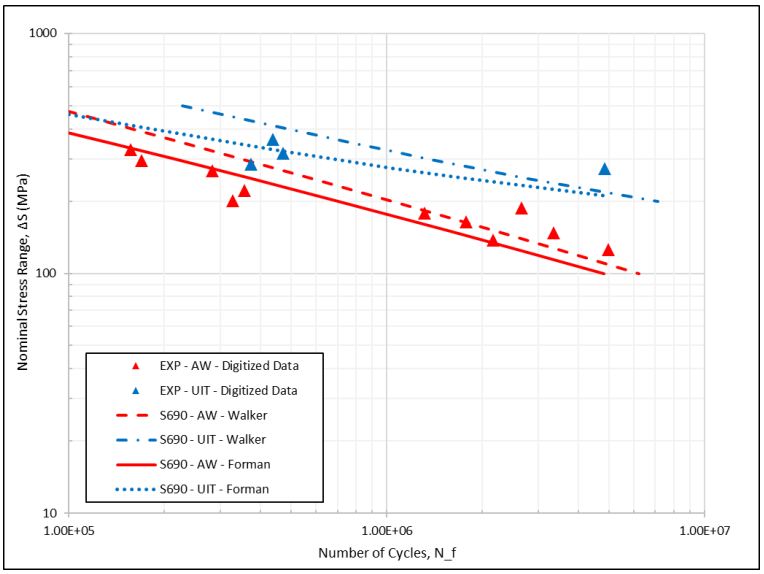

Figure 76: Fracture mechanics analysis results S690 subjected to CA cyclic fatigue loading with R-ratio equal to 0.1 for AW and UIT conditions for Walker and Forman models

As can be seen from Figure 77, the HCF strength of the AW condition illustrates a hike by approximately 39% in comparison to the mild steel performance. The authors (Michael Stoschka et al., 2012; M. Stoschka et al., 2013) stated that these experimental discoveries demonstrate that through employing optimized weld operation parameters, it can be accomplished. It can be inferred that an enhancement of the weld toe mapping, residual stress and hardness status; a usage of high-strength steels can be useful also without any subsequent PWT (Michael Stoschka et al., 2012; M. Stoschka et al., 2013). In the event of the UIT treated condition, the assessed results disclose an improvement by roughly 34% of the high-strength steel compared to the mid steel as base material. The advantage of the PWT including UIT can be proved by comparing the AW and the UIT conditions for high-strength steel. An enhancement by a factor of roughly three in HCF region is the proof. As indicated in Figure 77, The prediction of the calculated life through Walker and Forman models is done entirely well under both conditions.

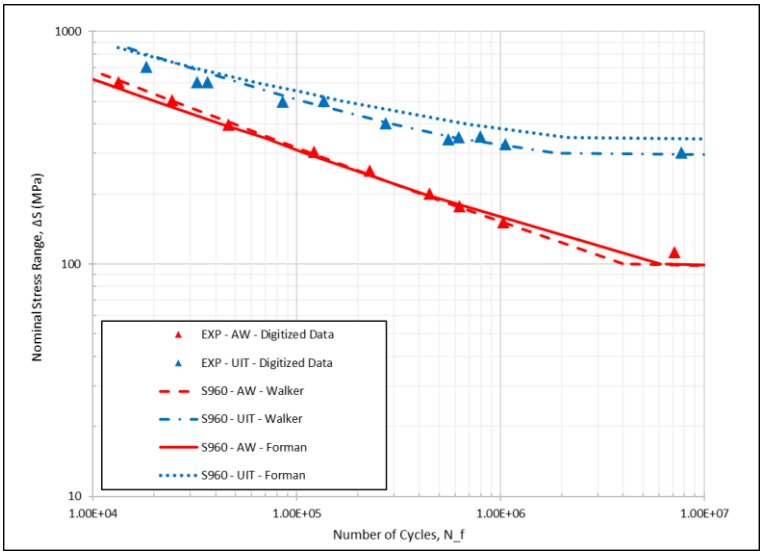

Figure 77: Fracture mechanics analysis results S960 subjected to CA cyclic fatigue loading with R-ratio equal to 0.1 for AW and UIT conditions for Walker and Forman models

Percentage of decreasing of fatigue strength as compared to the base material is about 55% to 58% for the AW condition whereas percentage of enhancing of fatigue strength to the weld joint is about 135% (Sidhom et al., 2005). 5083-H11 AL behaviour was assumed to be isotropic and linearly elastic (Sidhom et al., 2005). Figure 78 depicts comparatively the evaluated fatigue strength of 5083-H11 AL under both conditions.

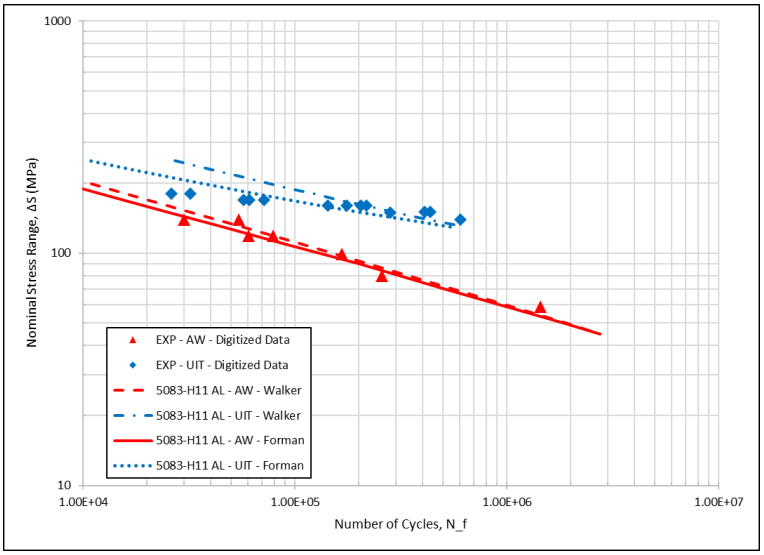

Figure 78: Fracture mechanics analysis results 5083-H11 AL subjected to CA cyclic fatigue loading with R-ratio equal to 0.1 for AW and UIT conditions for Walker and Forman models

Both models estimated the life quite fine for both conditions. It is important to mention that Forman model still performed better prediction versus Walker model for the UIT condition. As a matter of principle, comparing the aluminum against the mild steel and the high-strength steel, it can be concluded that the fatigue life increase of the steels is better than the fatigue life of the aluminums as indicated in Figure 78 and Figure 79 which simply means the impact of UIT is glaringly apparent.

Figure 79 displays the assessed fatigue strength of 2024-T351 AL for both conditions. It should be note that BR stands for bare material. In spite of the fact that 2024-T351 AL was a plate, then it should be recognized in its fracture mechanics analysis results as detailed in Figure 79.

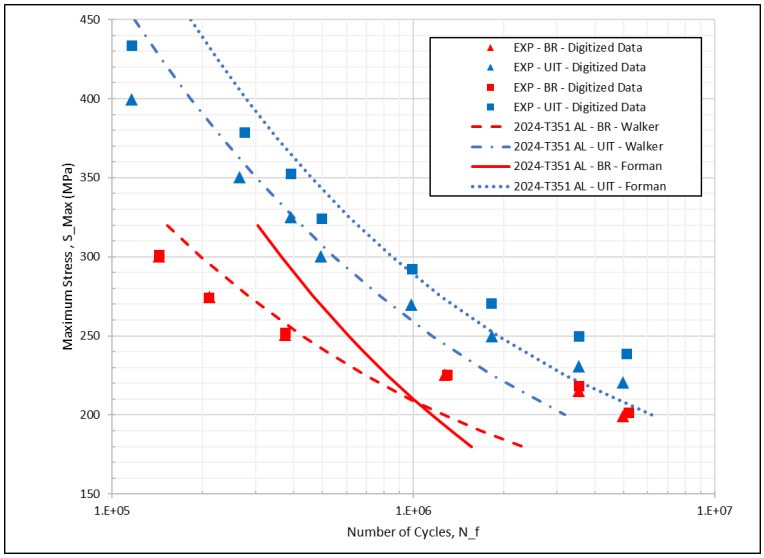

Figure 79: Fracture mechanics analysis results 2024-T351 AL subjected to CA cyclic fatigue loading with R-ratio equal to 0.1 for AW and UIT conditions for Walker and Forman models

In Figure 79, the computed life through the models for the BR and UIT conditions are represented. It is crucial to mention that the maximum stress versus the number of cycles is not in log scale so that a better comparison and a good understanding versus the source here (Rodopoulos et al., 2007) could be done. Walker and Forman models proved that the calculated life under the UIT condition seem to be in a really good correlation along with the experimental results.

On the other side, the estimated life for the BR conditions look to be somehow fine in a conservative point of view. However, it is imperative to note that the test specimen was a plate, and the crack was a surface crack (Rodopoulos et al., 2007). As already clarified, various weld imperfections emerge at different zones of the weld segments which these defects perform as local

stress raisers, a spot from where a fatigue crack may form as shown in Figure 11. Unfortunately, these weld imperfections have disastrous significance on the fatigue strength of the welded joints which this material is not the case because it is a plate not a welded joint. Besides, the author (Rodopoulos et al., 2007) stated that the SIF has not been utilized. In fact, it has been avoided. In addition to that the fitting constants of Forman model as well as the undesirable residual stresses result for the BR condition could be also other contributing causes on the prediction of the fatigue strength for the BR condition for Forman model.

Based on the results, nonlinear fracture mechanics models, Walker and Forman highlighted that both are valuable engineering tools. The output results lead to a good agreement along with the experimental tests data. Ultimately, it can be concluded that the fatigue life improvement resulted from UIT treatment was observed to rise with higher material strength. For example, S960 versus S355 can easily prove it as the real growth relies on level of the stress. The most suitable model for predicting the life under the mentioned conditions appears to be Forman model.

After UIT, the fatigue strength enhancement of welded joint generally improves by 50% to 200% at 2×10^6 cycles (Wright, 1996; E.Sh. Statnikov, 1997b; P. Haagensen et al., 1998; Roy & Fisher, 2005). However, it can be less or even more than the mentioned proportion depending on numerous factors like environmental impacts etc.

Table 8 gives an insight of how much fatigue life improved for all materials for the specified stress levels in HCF region for both models. Further, it provides the perception of the determined fatigue life are approximately in the same bulk range for both models with respect to the experimental data. Yet, Forman demonstrated a bit better correlation with the experimental data in general.

Table 8: Fatigue Life Improvement factor

Material	Experimental Data	HCF - Walker	HCF - Forman	Stress Level (MPa)
$5083-H311\ AL$	4	5	5	70
$CSA\ 350W\ ST$	5	3	5	250
$A514\ ST$	5	4	4	290
$S355$	5	3	5	240
$S460$	3	3	3	240
$S690$	4	3	3	270
$S960$	3	4	5	325
$5083-H11\ AL$	3	3	3	140
$2024-T351\ AL$	3	3	3	250

5.3) Fatigue Crack Growth Analysis

It can be demonstrated through $a - N$ and $c - N$ curves how UIT can improve the fatigue life by eliminating the appearance of the cracks. In a nutshell, UIT acts on weld imperfections to delay crack initiation state as shown in Figure 25. Crack initiation phase expected to experience a substantial delay because of inversing the internal residual stresses which led to modifying the fatigue life of the weld joints. It is expected that UIT can also considerably enlarge the fatigue life by significantly slowing crack propagation state either in depth or on surface depending on various stated concepts as already revealed throughout chapter 2 and 3 as well. The general purpose of this section is to analyze which model anticipated better the fatigue crack growth in depth and on surface of that material for both conditions under each fatigue cyclic loading.

Further, it can be understood how much the crack propagated from its initial size up to its final size for that number of specified cycles. It should be emphasized that one material is selected to be presented in this section out of nine materials. For the rest materials, the results and the conclusions are described in Appendix (B).

5.3.1) A514 ST

Figure 80 and Figure 81 depict graphically fatigue crack growth analysis results of A514 ST under the AW and the UIT conditions for Walker and Forman models. Crack depth and crack surface versus the number of cycles are displayed in these figures.

Both models predicted crack propagation state quite well as it can be observed that the fatigue life has been shifted to the right and the surface of the crack has been either slightly or significantly diminished which means it has led to the successful UIT treatment.

As reflected in Figure 81, Forman performed a better forecasting of fatigue crack growth of the material in depth as well as on surface for the AW condition. From approximately $700\ MPa$ to $400\ MPa$ stress levels, Walker could not properly depict the fatigue crack growth on the surface of the crack unlike Forman model.

As illustrated in Figure 81, Forman anticipated the fatigue crack growth of the material in depth as well as on surface quite satisfactory in comparison to Walker model under the UIT condition due to the fact that the surface of the crack is substantially decreased throughout the life as indicated in Figure 81.

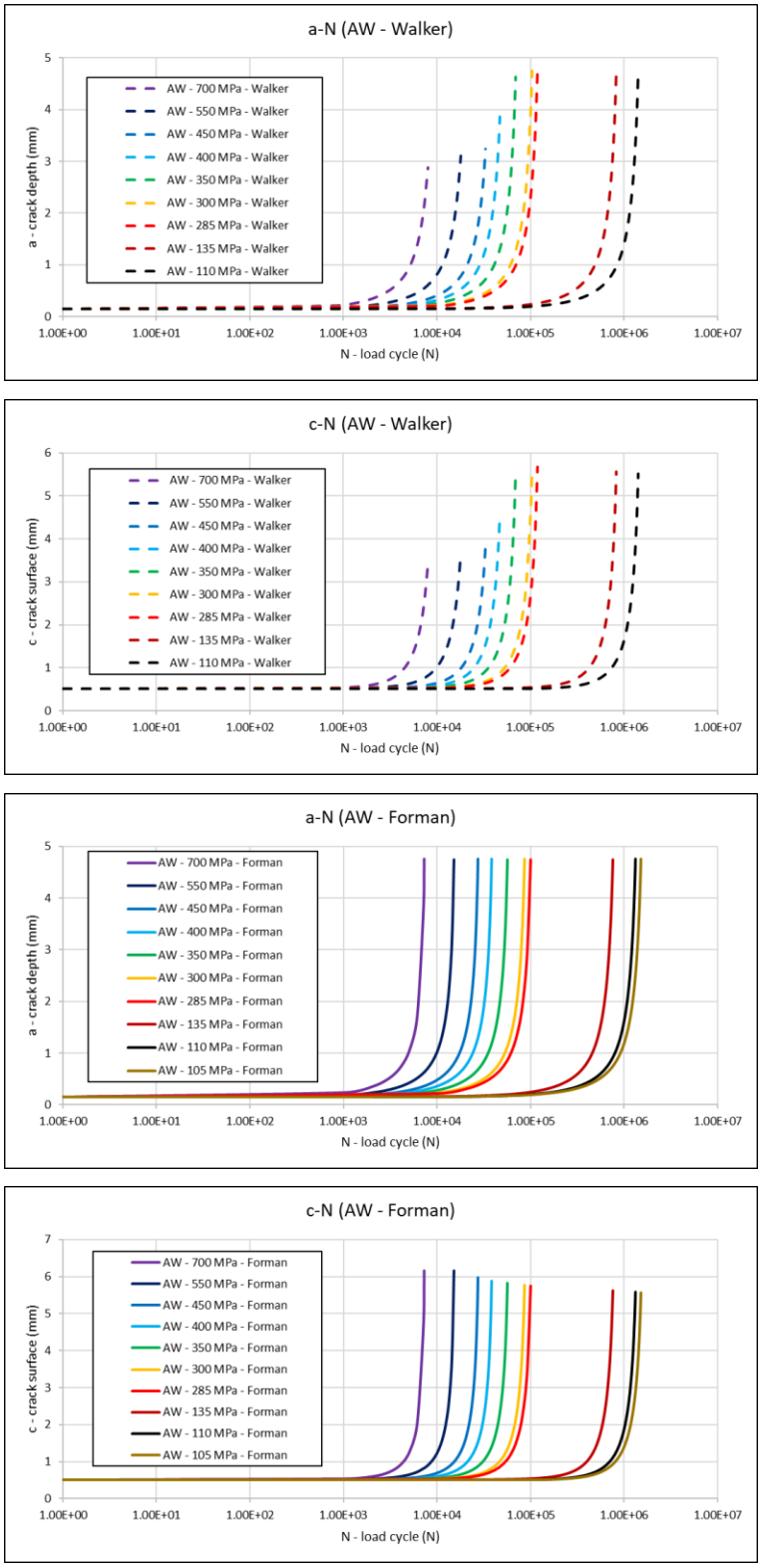

Figure 80: Fatigue crack growth analysis results of A514 ST under AW condition for Walker vs Forman, crack depth and crack surface against the number of cycles for the whole stress level ranges

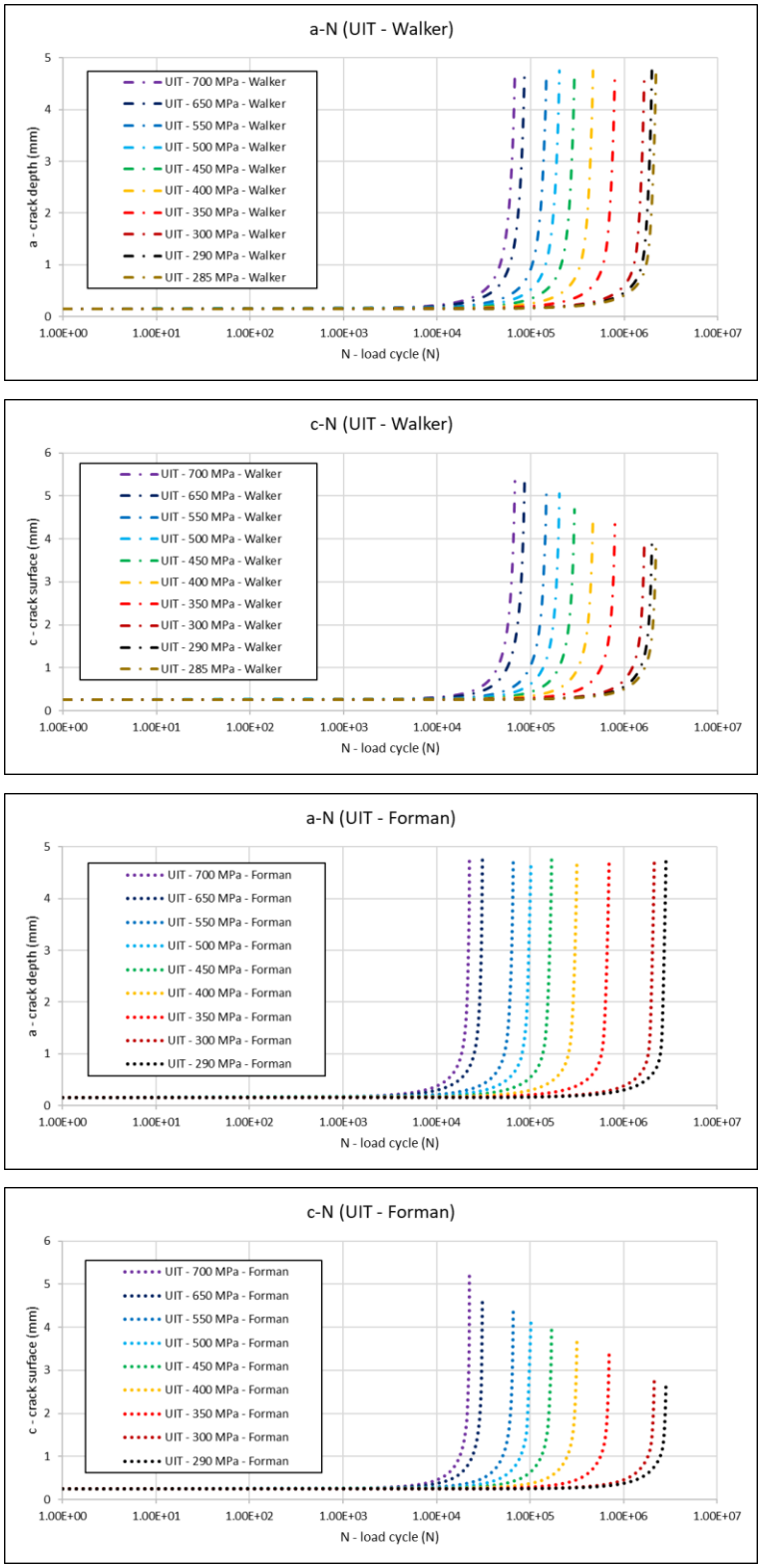

Figure 81: Fatigue crack growth analysis results of A514 ST under UIT condition for Walker vs Forman, crack depth and crack surface against the number of cycles for the whole stress level ranges

5.4) Crack Shape Evolution Analysis

It can be demonstrated through $a - c$ curves how effective UIT can close the surface of the crack to further delay crack initiation state as well as retarding crack propagation phase. On top of that, the crack behaviour and how fast the crack grows in depth and on surface can be properly comprehended. The key objective of this section is to investigate which model forecasted better the crack growth along with the evolution of the crack shape in depth and on surface of that material for both conditions under each fatigue cyclic loading.

The fatigue crack growth analysis requires to be conducted to resemble the evolution of the crack shape throughout the life of the weld. Further, there were various parameters that were engaged in this methodology including the initial crack size, the final crack size, the aspect ratio, the stress distribution, the SIF etc.

Table 9 shows the corresponding abbreviated terms that is used throughout this section as well as Appendix (C). For the sake of simplifications, the above-mentioned terms are used for a better understanding.

Table 9: Related abbreviated terms for Walker and Forman models under AW and UIT conditions as well as AW versus UIT for relevant stress levels

$\boldsymbol{AW - W - X}$	Walker model under the AW condition for X stress level
$\boldsymbol{AW - F - X}$	Forman model under the AW condition for X stress level
$\boldsymbol{UIT - W - X}$	Walker model under the UIT condition for X stress level
$\boldsymbol{UIT - F - X}$	Forman model under the UIT condition for X stress level
$\boldsymbol{AWvsUIT - W - X}$	Comparison between the AW and UIT conditions for Walker model for X stress level
$\boldsymbol{AWvsUIT - F - X}$	Comparison between the AW and UIT conditions for Walker model for X stress level

In the figures, there may be a stress level that has more curves than its higher stress level that is due to the number of written $a - N$ data for that stress level. By setting upper limit of frequency increment of the number of cycles to an acceptable amount, the number of $a - N$ results could be less so that it became possible to embed all results in one text file for the sake of avoiding misunderstandings. It is one of the difficulties of fracture mechanics analyses which is dealing with tons of data.

It should be mentioned that one material is chosen to be represented in this section out of nine materials. For the rest materials, the results and the conclusions are described in Appendix (C).

5.4.1) A514 ST

Figure 82, Figure 83 and the figures in Appendix (C.3) depict graphically crack shape evolution analysis results of A514 ST under the AW and the UIT conditions for Walker and Forman models as well as their comparisons under both conditions for that model. Crack depth versus crack surface is displayed in these figures.

From $AW-W-135$, $AW-F-350$, $AW-F-135$ and $UIT-F-350$ which are the figures in Appendix (C.3), it should be pointed out that the last two curves are the way that Walker and Forman models tried to determine the final crack size for that condition.

For example, from $UIT-W-300$ and $UIT-F-300$ which are the figures in Appendix (C.3), it should be noted that UIT incredibly retarded crack initiation phase as well as remarkably slowed down crack propagation phase in depth and on surface so that the fatigue life was noticeably improved .

For instance, comparing $AWvsUIT-W-300$ and $AWvsUIT-F-300$ together, it demonstrates that Forman model projected the crack growth and the crack shape evolution completely satisfactory. It is quite fascinating to note that the crack was at first advancing quicker into depth and on surface after reducing the stress it is a little bit slowed down for the AW condition. However, it is noteworthy that after achieving a certain depth, it still commenced expanding significantly for the AW condition. After impact treatment, the crack is extremely slowed down which indicates that UIT considerably enlarge the fatigue life.

From $AWvsUIT-F-300$, such phenomena can be interpreted as how effective UIT can close the surface of the crack to further delay crack initiation state as well as retarding crack propagation phase. Additionally, the crack behaviour and how fast the crack grows in depth and on surface can be properly comprehended.

Even though Walker model is overall an effective method to assess fatigue life of the welded structures for the AW and the UIT conditions, when it comes to predicting crack shape evolution and anticipating fatigue crack growth, its consistency and its reliability is not perfect that of Forman model. From $AwvsUIT-W-700, 550\ and\ 450$, it can be understood.

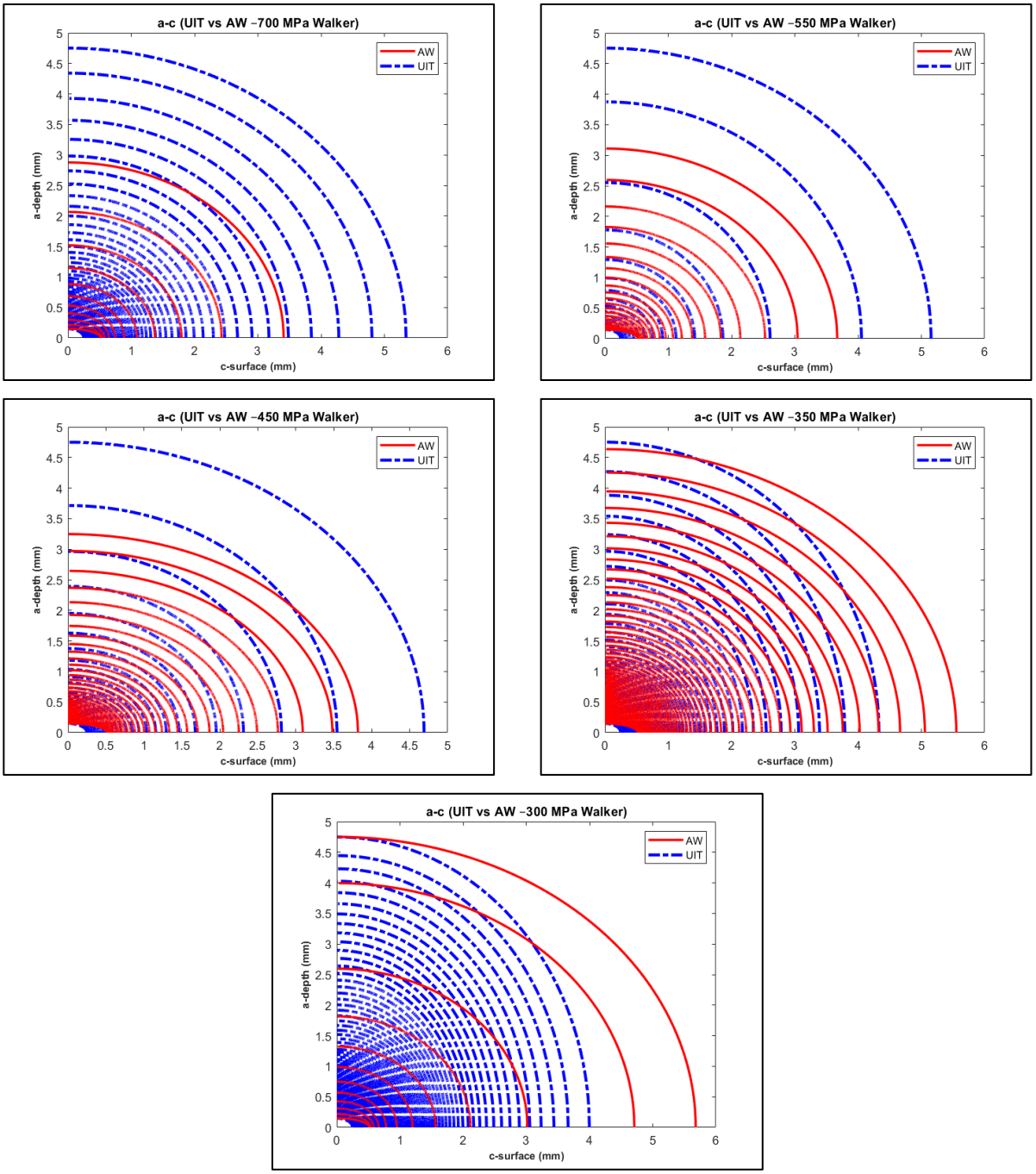

Figure 82: Crack shape evolution analysis results of A514 ST for AW vs UIT conditions for Walker, crack depth against crack surface for covering stress level ranges

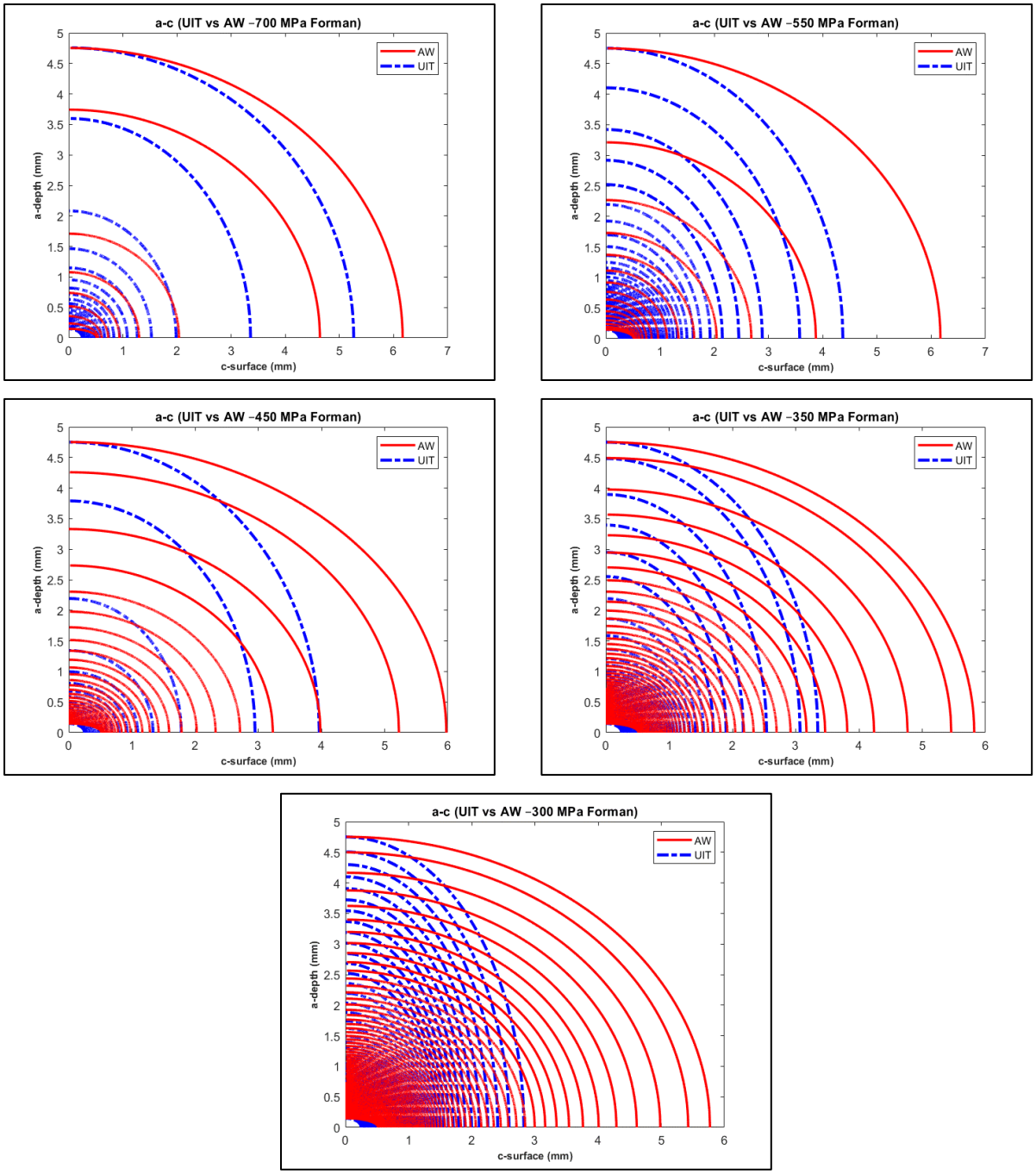

Figure 83: Crack shape evolution analysis results of A514 ST for AW vs UIT conditions for Forman, crack depth against crack surface for covering stress level ranges

CHAPTER 6: FINDINGS AND CONCLUSIONS

A brief summary of all the research as well as the outcomes of this investigation accompanied by proposed future work are explained in this chapter. In brief, the overall outcomes of this research are mentioned in the first part of this chapter. The second part outlines the substantial affiliation of the pursued study. In the end, the third part introduces proposed future work.

5.1) Summarization of Research

A lack of comprehension in fracture mechanics analyses in two-dimensional domains by going through an in-detail overview of the core concepts related to fatigue were explained. A literature review with respecting to these domains as well as defining the concepts of various fatigue damage parameters were described to present the special purposes of this work. To summarize, a detailed investigation of the essential gap was carried out through the early chapters.

There is adequate literature on fatigue fracture mechanics analyses on predicting fatigue strength $(S-N)$ curves of materials, yet very few contain fatigue crack growth analyses $(a-N)$ and $(c-N)$ curves as well as crack front geometry analyses $(a-c)$ curves of materials.

The two-dimensional crack growth analysis using Walker's and Forman's equations to accomplish the evaluation of recent fatigue tests were expressed. After implementing the fatigue crack propagation life of the materials, the crack shape evolution of the materials was carried out. In essence, the solutions of the derived nonlinear equations were numerically performed.

The predictions of Walker and Forman models by going through the key concepts and predicting the input fatigue parameters were introduced. To experimentally validate the numerical results of the models, the experimental derived data from the literature were employed. The fatigue crack propagation life of the materials was presented. The crack shape evolutions of the materials were represented. In closing, a meaningful comparison between the models and the derived experimental data were represented.

In a nutshell, the effects of the various fatigue damage parameters on the as-welded (AW) condition and the impact treated welds were described in the literature review. Furthermore,

fatigue test data has been taken from literature on both conditions under constant amplitude (CA) cyclic fatigue loading conditions for several different stress ranges for each material. Following the tests, residual stress distributions below the weld toe surface were specified by x-ray diffraction of untested specimens. More importantly, the test data obtained from literature were analyzed through out the thesis and were used to define input parameter values for fracture mechanics analyses of the welded joint specimens.

After that, the crack growth assessment of the welded structures was provided. For comparison purposes, both Walker and Forman fatigue crack growth models were thoroughly reviewed and their advantages as invaluable tools for predicting the effects of Ultrasonic Impact Treatment (UIT) on fatigue performance for the welded joints were examined. Subsequently, the benefit of the models in predicting fatigue crack growth behavior for nine different materials were investigated and the effects of the various material strength parameters on the impact treatment performance were assessed. Then, fatigue crack propagation life of the materials was displayed. In the end, the crack shape evolution of the materials was depicted. In conclusion, the outcomes of this investigation accompanied by proposed future work are as follows.

5.2) Conclusions

The fatigue life on the basis of fatigue crack propagation of the welded joints under the AW and the UIT conditions were computed by Walker and Forman crack growth models for nine different materials. To evaluate the impacts of UIT on the fatigue performance of the welded attachments, the stress concentrations and the residual stresses adjustments as well as other core concepts and key parameters were considered for the predictions of the fatigue life under the CA cyclic fatigue loading with the R-ratio equal to 0.1 as already described throughout the thesis.

It was demonstrated through $a - N$ and $c - N$ curves how UIT improved the fatigue life by eliminating the appearance of the cracks. UIT noticeably improved the fatigue life by incredibly retarding crack initiation state. UIT enormously enhanced the fatigue life by remarkably slowing down crack propagation state in depth and on surface directions. Ultimately, the combination of crack initiation state and crack propagation state consisted the total life which eventually led to dramatically increasing the fatigue life which means the life shifted to the right in the figures. Ultimately, UIT demonstrated to be the most effective enhancement treatment of weld joints in comparison to the previous methods. UIT imparts ultrasonic vibration deep into the material to impact and plastically deform the weld toe, resultantly introducing compressive residual stresses by eliminating tensile residual stresses. Other determining features for the constructive influence of UIT are declining of stress concentration in weld toe areas and enhancement of mechanical properties of the superficial layers.

The fatigue life rise is further conspicuous for the mild steel and the high-strength steel specimens rather than the aluminum weld specimens under UIT condition as observed from Chapter 5. As seen from Chapter 5, the fatigue strength of the AW condition in HCF regime illustrated a hike by approximately 25% to 45% in comparison to the mild steel performance. In the event of the UIT treated condition, the assessed results disclose an improvement by roughly 20% to 40% of the high-strength steel compared to the mid steel as base material. The advantage of the PWT including UIT can be proved by comparing the AW and the UIT conditions for high-strength steel. An enhancement by a factor of roughly three in HCF region is the proof.

In summary, as shown in the figures, the fatigue strength $(S - N)$ curves of the welded attachments were shifted to the right. The fatigue crack growth $(a - N)$ and $(c - N)$ curves of the

weld joints were shifted to the right as well. The fatigue crack growth analysis requires to be conducted to resemble the evolution of the crack shape throughout the life of the weld. The crack shape evolution $(a - c)$ curves of the welded components indicated that how effective UIT could close the surface of the crack to further delay crack initiation state as well as retarding crack propagation phase. On top of that, the crack behaviour and how fast the crack grows in depth and on surface were seen.

Walker model which is one of the fracture mechanics approaches toward evaluating the fatigue crack growth rates. Unlike Paris model, Walker model tackles the impacts of the R-ratio. It is important to bear in mind that Walker model is an extension of Paris model to deem the impression of the R-ratio on crack growth rate. Since the R-ratio equivalent to 0.1 does not impose such great burden on fatigue crack growth analyses unlike the R-ratio higher than 0.5. Then, Forman model has the cutting edge of the fatigue crack growth analysis in this regime.

Since the R-ratio 0.1 is close to zero, it does not have a strong influence on fitting constants of the models in comparison to the R-ratio higher than 0.5. Crack growth fitting constants were all discovered to be well correlated for these materials.

Overall, Forman and Walker models determined the fatigue strength $(S - N)$ curves of the materials still quite well. However, Forman model generally had the upper hand versus Walker model since it accounted the mean stress effect and addressed the asymptotic behavior in the unstable region of fatigue crack growth as well as the R-ratio similar to Walker model.

Forman model appears to be more reliable in comparison to Walker model for the AW and the UIT conditions. Due to the fact that Forman model performed way better predictions over Walker model for these materials considering the fatigue crack growth analyses $(a - N)$ and $(c - N)$ curves and the crack shape evolution $(a - c)$ curves as reflected in the figures in Chapter 5.

Ultimately, Forman model simulation has demonstrated to be a viable approach for investigating fluctuation in fatigue fracture mechanics for a 2D semi-elliptical crack. Given the fact that the lack of the experimental data still exists in the literature like fatigue crack growth data under specified conditions like temperature and environmental conditions etc. and the absence of the crack images to observe experimentally the crack growth behavior as well as some fatigue parameter damages.

5.3) Future Work

Work accomplished in this thesis was bounded to a 2D semi-elliptical crack at weld toe. It is recommended that more experimental work should be conducted including high quality pictures at micro scale to be captured. Then, crack growth behavior as well as crack geometry can be both experimentally observed and numerically compared from an initial crack size to a final crack size. Further, it is suggested to consider different types of crack as well as various kinds of crack geometry so that a better understanding of crack growth behavior and crack geometry can be evaluated.

Worked performed in this thesis was limited to Walker and Forman models. It is advised to further implement different sorts of fatigue fracture mechanics model like UniGrow (Noroozi et al., 2007), AFGROW and NASGRO etc. so that pros and cons of each model versus Walker and Forman can be understood in depth and in details.

In this thesis, stress ratio was considered 0.1 for all materials. It is recommended to examine the impact of various stress ratio on crack growth behaviour and crack shape evolution as well as fatigue strength of materials for the models. Load spectrum was constant amplitude fatigue cyclic loading. It is advised to investigate the impact of variable fatigue cyclic loading or any other types of fatigue load spectrum on crack growth behaviour and crack shape evolution as well as fatigue strength of materials for the models.

Residual stress was employed in Y-direction. It is suggested to study the impact of residual stresses in X-direction or in Z-direction on crack growth behaviour and crack shape evolution as well as fatigue strength of materials for the models.

Eventually, numerical analysis can be performed on different joint types as well as materials other than steel and aluminum. Different methods like A Monte Carlo simulation can be employed to conduct research on random numbers from distributions of random variables representing constants of the models.

LIST OF REFERENCES

[1] Alam, M. M., Barsoum, Z., Jonsén, P., Kaplan, A. F. H., & Häggblad, H. Å. (2010). The influence of surface geometry and topography on the fatigue cracking behaviour of laser hybrid welded eccentric fillet joints. *Applied Surface Science*, *256*(6), 1936–1945. https://doi.org/10.1016/j.apsusc.2009.10.041

[2] AL-Emarani, M., & Åkesson, B. (2013). *Steel Structures* [Thesis]. Chalmers University of Technology.

[3] Al-Emrani, M., & Åkesson, B. (2013). *Steel structures: Course literature–VSM 191* [Course Literature].

[4] Ashcroft, I. A. (2011). Fatigue Load Conditions. In L. F. M. da Silva, A. Öchsner, & R. D. Adams (Eds.), *Handbook of Adhesion Technology* (pp. 845–874). Springer Berlin Heidelberg. https://doi.org/10.1007/978-3-642-01169-6_33

[5] ASTM E2860. (2012). *Test Method for Residual Stress Measurement by X-Ray Diffraction for Bearing Steels*. ASTM International. https://doi.org/10.1520/E2860-12

[6] ASTM, S. E. (1823). *Standard terminology relating to fatigue and fracture testing-Annual Book of ASTM Standards.* (Vol. 1–96). American Society for Testing and Materials, West Conshohocken.

[7] BANNANTINE, J., COMER, J., & Handrock, J. (1990). *Fundamentals of metal fatigue analysis* (Vol. 1–286). Englewood Cliffs, NJ, Prentice Hall.

[8] Barsoum, Z., & Jonsson, B. (2011). Influence of weld quality on the fatigue strength in seam welds. *Engineering Failure Analysis*, *18*(3), 971–979. https://doi.org/10.1016/j.engfailanal.2010.12.001

[9] Bhat, S., & Patibandla, R. (2011). Metal Fatigue and Basic Theoretical Models: A Review. In Alloy Steel-Properties and Use. *IntechOpen*.

[10] Bhaumik, S. K., Sujata, M., & Venkataswamy, M. A. (2008). Fatigue failure of aircraft components. *Engineering Failure Analysis*, *15*(6), 675–694. https://doi.org/10.1016/j.engfailanal.2007.10.001

[11] Broek, D. (1986). *Elementary engineering fracture mechanics*. Springer Netherlands. https://doi.org/10.1007/978-94-009-4333-9

[12] BS EN 15305. (2008). *Non-destructive Testing—Test Method for Residual Stress analysis by X-ray Diffraction*. British Standards Institution.

[13] Bueckner, H. F. (1970). NOVEL PRINCIPLE FOR THE COMPUTATION OF STRESS INTENSITY FACTORS. *Zeitschrift Fuer Angewandte Mathematik & Mechanik*, *50*(9), 529–546.

[14] Caccese, V., Blomquist, P. A., Berube, K. A., Webber, S. R., & Orozco, N. J. (2006). Effect of weld geometric profile on fatigue life of cruciform welds made by laser/GMAW processes. *Marine Structures*, *19*(1), 1–22. https://doi.org/10.1016/j.marstruc.2006.07.002

[15] Castillo-Morales, M., & Salas-Zamarripa, A. (2010). The Effects of UIT in the Fatigue Life of Al 2024-T3. *Key Engineering Materials*, *449*, 15–22. https://doi.org/10.4028/www.scientific.net/KEM.449.15

[16] Chattopadhyay, A., Glinka, G., El-Zein, M., Qian, J., & Formas, R. (2011). Stress Analysis and Fatigue of welded structures. *Welding in the World*, *55*(7–8), 2–21. https://doi.org/10.1007/BF03321303

[17] Cui, C., Zhang, Q., Bao, Y., Kang, J., & Bu, Y. (2018). Fatigue performance and evaluation of welded joints in steel truss bridges. *Journal of Constructional Steel Research*, *148*, 450–456. https://doi.org/10.1016/j.jcsr.2018.06.014

[18] Deng, D., & Murakawa, H. (2006). Numerical simulation of temperature field and residual stress in multi-pass welds in stainless steel pipe and comparison with experimental measurements. *Computational Materials Science*, *37*(3), 269–277. https://doi.org/10.1016/j.commatsci.2005.07.007

[19] Dowling, N. E. (2013). *Mechanical behavior of materials: Engineering methods for deformation, fracture, and fatigue* (4th ed). Pearson.

[20] Dowling, N. E., Siva Prasad, K., & Narayanasamy, R. (2013). *Mechanical behavior of materials: Engineering methods for deformation, fracture, and fatigue* (4. ed., internat. ed). Pearson.

[21] Dürr, A. (2007). *Zur Ermüdungsfestigkeit von Schweißkonstruktionen aus höherfesten Baustählen bei Anwendung von UIT-Nachbehandlung*. https://doi.org/10.18419/OPUS-265

[22] EUROPE TECHNOLOGIES SONATS. (2020). *Innovative Impact Surface Treatment Solutions*. SONATS. https://sonats-et.com/en/

[23] Farajian, M., Barsoum, Z., Weich, I., & Nitschke-Pagel, T. (2012). *A literature survey on residual stress related fatigue strength improvement techniques for welded components and structures.* (IIW Doc XIII-WG6-008-12). International Institute of Welding. https://www.researchgate.net/publication/293756150_A_Literature_Survey_on_Residual

_Stress_Related_Fatigue_Strength_Improvement_Techniques_for_Welded_Components_and_Structures

[24] Farajian, M., Nitschke-Pagel, T., & Lieurade, H. P. (2012). *Farajian, M., Nitschke-Pagel, T., & Lieurade, H. P. (2012). Shot peening as a tool for fatigue strength improvement of welds: A review.* (IIW Doc XIII-WG6-009-12). International Institute of Welding. https://www.researchgate.net/publication/293756131_Shot_Peening_as_a_tool_for_fatigue_strength_improvement_of_welds_a_review

[25] Farajian-Sohi, M., Nitschke-Pagel, T., & Dilger, K. (2010). Residual Stress Relaxation of Quasi-Statically and Cyclically-Loaded Steel Welds. *Welding in the World*, *54*(1–2), R49–R60. https://doi.org/10.1007/BF03263484

[26] Fisher, J. W., Statnikov, E. S., & Tehini, L. (2001). Fatigue strength enhancement by means of weld design change and the application of ultrasonic impact treatment. *In Proc. of Intl. Symp. on Steel Bridges, Chicago*.

[27] Fong, & J., T. (1979). *Fatigue mechanisms*. ASTM International.

[28] Forman, R. G., Kearney, V. E., & Engle, R. M. (1967). Numerical Analysis of Crack Propagation in Cyclic-Loaded Structures. *Journal of Basic Engineering*, *89*(3), 459–463. https://doi.org/10.1115/1.3609637

[29] Fricke, W. (2012). *IIW recommendations for the fatigue assessment of welded structures by notch stress analysis*. WP, Woodhead Publ.

[30] Fricke, W. (2013). IIW guideline for the assessment of weld root fatigue. *Welding in the World*, *57*(6), 753–791. https://doi.org/10.1007/s40194-013-0066-y

[31] Frost, N. E., Marsh, K. J., & Pook, L. P. (1974). *Metal fatigue*. Clarendon Press.

[32] Ghahremani, K. (2015). *Fatigue assessment of repaired highway bridge welds using local approaches. Doctoral Thesis* [Doctoral Thesis]. University of Waterloo.

[33] Ghahremani, Kasra, Ranjan, R., Walbridge, S., & Ince, A. (2015). Fatigue Strength Improvement of Aluminum and High Strength Steel Welded Structures using High Frequency Mechanical Impact Treatment. *Procedia Engineering*, *133*, 465–476. https://doi.org/10.1016/j.proeng.2015.12.616

[34] Ghahremani, Kasra, Walbridge, S., & Topper, T. (2015). High cycle fatigue behaviour of impact treated welds under variable amplitude loading conditions. *International Journal of Fatigue*, *81*, 128–142. https://doi.org/10.1016/j.ijfatigue.2015.07.022

[35] Glinka, G., & Shen, G. (1991). Universal features of weight functions for cracks in mode I. *Engineering Fracture Mechanics*, *40*(6), 1135–1146. https://doi.org/10.1016/0013-7944(91)90177-3

[36] Goldak, J., Chakravarti, A., & Bibby, M. (1984). A new finite element model for welding heat sources. *Metallurgical Transactions B*, *15*(2), 299–305. https://doi.org/10.1007/BF02667333

[37] Griffith, A. A. (1921). *Philosophical transactions of the royal society of london. Series A, containing papers of a mathematical or physical character*. *221*, 163–198.

[38] Gurney, T. R., & Saunders, H. (1981). Fatigue of Welded Structures (2nd Edition). *Journal of Engineering Materials and Technology*, *103*(2), 185–185. https://doi.org/10.1115/1.3224993

[39] Haagensen, P. J. (2011). Fatigue strength improvement methods. In *Fracture and Fatigue of Welded Joints and Structures* (pp. 297–329). Elsevier. https://doi.org/10.1533/9780857092502.2.297

[40] Haagensen, P., Statnikov, E. S., & López-Martínez, L. (1998). Introductory fatigue tests on welded joints in high strength steel and aluminium improved by various methods including ultrasonic impact treatment (UIT). *IIW*, *13*, 1748–1798.

[41] Hadley, I. (2018). BS 7910:2013 in brief. *International Journal of Pressure Vessels and Piping*, *165*, 263–269. https://doi.org/10.1016/j.ijpvp.2018.07.010

[42] Harati, E. (2015). *Fatigue strength of welds in 800 MPa yield strength steels: Effects of weld toe geometry and residual stress*. University West.

[43] Harrison, J. D. (1970). ANALYSIS OF DATA ON NON-PROPAGATING FATIGUE CRACKS ON A FRACTURE MECHANICS BASIS. *Metal Constr. Brit. Weld. J. 2: 93-8(Mar 1970)*, *2*(3), 24–26.

[44] Hellan, K. (1984). *Introduction to fracture mechanics*. McGraw-Hill.

[45] Hobbacher, A. (2012). *Update of the fracture mechanics chapters of the IIW fatigue design recommendations*. International Institute of Welding; IIW-document XIII-2370r1-11/XV-1376r1-11.

[46] Hobbacher, A. F. (2016). *Recommendations for Fatigue Design of Welded Joints and Components* (2nd ed. 2016). Springer International Publishing : Imprint: Springer. https://doi.org/10.1007/978-3-319-23757-2

[47] Irwin, G. R. (1948). Fracturing of metals. *ASM, Cleveland*, *147*(19–9).

[48] Irwin, G. R. (1957). Analysis of stresses and strains near the end of a crack transversing a plate. *Trans. ASME, Ser. E, J. Appl. Mech.*, *24*, 361–364.

[49] James, M. N., Hughes, D. J., Chen, Z., Lombard, H., Hattingh, D. G., Asquith, D., Yates, J. R., & Webster, P. J. (2007). Residual stresses and fatigue performance. *Engineering Failure Analysis*, *14*(2), 384–395. https://doi.org/10.1016/j.engfailanal.2006.02.011

[50] Jonsson, B., Samuelsson, J., & Marquis, G. B. (2011). Development of Weld Quality Criteria Based on Fatigue Performance. *Welding in the World*, *55*(11–12), 79–88. https://doi.org/10.1007/BF03321545

[51] Joshua, H. M. (2014). *Fatigue Crack Growth Analysis with Finite Element Methods and a Monte Carlo Simulation* [Virginia Polytechnic Institute and State University]. https://vtechworks.lib.vt.edu/bitstream/handle/10919/48432/Melson_JH_T_2014.pdf?sequence=1&isAllowed=y

[52] Josi, G., & Grondin, G. Y. (2010). *Reliability-based management of fatigue failures* [Doctoral Thesis]. University of Alberta.

[53] Khurshid, M., Barsoum, Z., & Marquis, G. (2014). Behavior of Compressive Residual Stresses in High Strength Steel Welds Induced by High Frequency Mechanical Impact Treatment. *Journal of Pressure Vessel Technology*, *136*(4), 041404. https://doi.org/10.1115/1.4026651

[54] Kirkhope, K. J., Bell, R., Caron, L., Basu, R. I., & Ma, K.-T. (1999a). Weld detail fatigue life improvement techniques. Part 1: Review. *Marine Structures*, *12*(6), 447–474. https://doi.org/10.1016/S0951-8339(99)00013-1

[55] Kirkhope, K. J., Bell, R., Caron, L., Basu, R. I., & Ma, K.-T. (1999b). Weld detail fatigue life improvement techniques. Part 2: Application to ship structures. *Marine Structures*, *12*(7–8), 477–496. https://doi.org/10.1016/S0951-8339(99)00031-3

[56] Kudryavtsev, Y., Mikheev, P., & Korshun, V. (1995). Influence of plastic deformation and residual stresses, created by ultrasonic impact treatment, on the fatigue strength of welded joints. *Paton Welding Journal*, *12*, 3–7.

[57] Kudryavtsev, Yuri, & Kleiman, J. (2013). Fatigue Improvement of Welded Elements and Structures by Ultrasonic Peening. *Volume 6A: Materials and Fabrication*, V06AT06A060. https://doi.org/10.1115/PVP2013-97185

[58] Kuhlmann, U., Dürr, A., Bergmann, J., Thumser, R., & Forschungsvereinigung Stahlanwendung (Eds.). (2006). *Effizienter Stahlbau aus höherfesten Stählen unter Ermüdungsbeanspruchung =: Fatigue strength improvement for welded high strength steel connections due to the application of post-weld treatment methods*. Verl.- und Vertriebsges.

[59] Kuhlmann, Ulrike, Bergmann, J., Dürr, A., Thumser, R., Günther, H.-P., & Gerth, U. (2005). Erhöhung der Ermüdungsfestigkeit von geschweißten höherfesten Baustählen durch Anwendung von Nachbehandlungsverfahren. *Stahlbau*, *74*(5), 358–365. https://doi.org/10.1002/stab.200590066

[60] Lampman, S. R., & DiMatteo, N. D. (1996). *ASM handbook: Volume 19, fatigue and fracture.* (Vol. 1–19). ASM International.

[61] Lassen, T., & Recho, N. (2006). *Fatigue life analyses of welded structures*. http://www.books24x7.com/marc.asp?bookid=13832

[62] Lee, C.-H., Chang, K.-H., Jang, G.-C., & Lee, C.-Y. (2009). Effect of weld geometry on the fatigue life of non-load-carrying fillet welded cruciform joints. *Engineering Failure Analysis*, *16*(3), 849–855. https://doi.org/10.1016/j.engfailanal.2008.07.004

[63] Leitner, M., Barsoum, Z., & Schäfers, F. (2016). Crack propagation analysis and rehabilitation by HFMI of pre-fatigued welded structures. *Welding in the World*, *60*(3), 581–592. https://doi.org/10.1007/s40194-016-0316-x

[64] Leitner, M., Gerstbrein, S., Ottersböck, M. J., & Stoschka, M. (2015). Fatigue Strength of HFMI-treated High-strength Steel Joints under Constant and Variable Amplitude Block Loading. *Procedia Engineering*, *101*, 251–258. https://doi.org/10.1016/j.proeng.2015.02.036

[65] Leitner, M., Khurshid, M., & Barsoum, Z. (2017). Stability of high frequency mechanical impact (HFMI) post-treatment induced residual stress states under cyclic loading of welded steel joints. *Engineering Structures*, *143*, 589–602. https://doi.org/10.1016/j.engstruct.2017.04.046

[66] Lihavainen, V.-M. (2006). *A novel approach for assessing the fatigue strenght of ultrasonic impact treated welded structures*. Lappeenrannan Teknillinen Yliopisto.

[67] Lotsberg, I., Fjeldstad, A., Helsem, M. R., & Oma, N. (2014). Fatigue life improvement of welded doubling plates by grinding and ultrasonic peening. *Welding in the World*, *58*(6), 819–830. https://doi.org/10.1007/s40194-014-0161-8

[68] Maddox, S. J. (2002). *Fatigue Strength of Welded Structures*. Elsevier. https://doi.org/10.1016/C2013-0-17455-7

[69] Marquis, G. B., & Barsoum, Z. (2016). *IIW Recommendations for the HFMI Treatment*. Springer Singapore. https://doi.org/10.1007/978-981-10-2504-4

[70] Marquis, G. B., Mikkola, E., Yildirim, H. C., & Barsoum, Z. (2013). Fatigue strength improvement of steel structures by high-frequency mechanical impact: Proposed

fatigue assessment guidelines. *Welding in the World*, *57*(6), 803–822. https://doi.org/10.1007/s40194-013-0075-x

[71] Martinsferreira, J., & Mourabranco, C. (1989). Influence of the radius of curvature at the weld toe in the fatigue strength of fillet welded joints. *International Journal of Fatigue*, *11*(1), 29–36. https://doi.org/10.1016/0142-1123(89)90044-3

[72] Mishchenko, A., Wu, L., da Silva, V. K., & Scotti, A. (2018). Analysis of residual stresses resulting from the surface preparation for X-ray diffraction measurement. *Journal of the Brazilian Society of Mechanical Sciences and Engineering*, *40*(2), 94. https://doi.org/10.1007/s40430-018-1036-5

[73] Mosiello, A., & Kostakakis, K. (2013). *The benefits of Post Weld Treatment for cost efficient and sustainable bridge design*. Chalmers University of Technology.

[74] NDT Eduation Resource Center. (2014). *NDT Eduation Resource Center*. https://www.nde-ed.org/index_flash.htm

[75] Nieslony, A., Dsoki, C., Kaufmann, H., & Krug, P. (2008). New method for evaluation of the Manson–Coffin–Basquin and Ramberg–Osgood equations with respect to compatibility. *International Journal of Fatigue*, *30*(10–11), 1967–1977. https://doi.org/10.1016/j.ijfatigue.2008.01.012

[76] Niu, X., & Glinka, G. (1987). The weld profile effect on stress intensity factors in weldments. *International Journal of Fracture*, *35*(3), 20.

[77] Noroozi, A., Glinka, G., & Lambert, S. (2007). A study of the stress ratio effects on fatigue crack growth using the unified two-parameter fatigue crack growth driving force. *International Journal of Fatigue*, *29*(9–11), 1616–1633. https://doi.org/10.1016/j.ijfatigue.2006.12.008

[78] Pang, H. (1993). Analysis of weld toe profiles and weld toe cracks. *International Journal of Fatigue*, *15*(1), 31–36. https://doi.org/10.1016/0142-1123(93)90074-Z

[79] Paris, P., & Erdogan, F. (1963). A Critical Analysis of Crack Propagation Laws. *Journal of Basic Engineering*, *85*(4), 528–533. https://doi.org/10.1115/1.3656900

[80] Paul, S. P. (1986). X-Ray Diffraction Residual Stress Techniques. In R. E. Whan (Ed.), *Materials Characterization* (pp. 380–392). ASM International. https://doi.org/10.31399/asm.hb.v10.a0001761

[81] Pearson, S. (1966). Fatigue Crack Propagation in Metals. *Nature*, *211*(5053), 1077–1078. https://doi.org/10.1038/2111077a0

[82] Peeker, E. (1997). *Extended numerical modeling of fatigue behavior*. https://doi.org/10.5075/EPFL-THESIS-1617

[83] Radaj, D. (1995). Ermüdungsfestigkeit: Grundlagen für Leichtbau. Maschinen-und Stahlbau. *SpringerVerlag*.

[84] Radhi, H. E., & Barrans, S. (2010). *FINITE ELEMENT ANALYSIS OF EFFECT OF WELD TOE RADIUS AND PLATE THICKNESS ON FATIGUE LIFE OF BUTT WELDED JOINT*. 60–64. http://eprints.hud.ac.uk/id/eprint/9316

[85] Ranjan, R., Ghahremani, K., Walbridge, S., & Ince, A. (2016). Testing and fracture mechanics analysis of strength effects on the fatigue behavior of HFMI-treated welds. *Welding in the World*, *60*(5), 987–999. https://doi.org/10.1007/s40194-016-0354-4

[86] Richard, H. A., & Sander, M. (2016). *Fatigue Crack Growth* (Vol. 227). Springer International Publishing. https://doi.org/10.1007/978-3-319-32534-7

[87] Ritchie, R. O. (1999). [No title found]. *International Journal of Fracture*, *100*(1), 55–83. https://doi.org/10.1023/A:1018655917051

[88] Rodopoulos, C. A., Kermanidis, A. Th., Statnikov, E., Vityazev, V., & Korolkov, O. (2007). The Effect of Surface Engineering Treatments on the Fatigue Behavior of 2024-T351 Aluminum Alloy. *Journal of Materials Engineering and Performance*, *16*(1), 30–34. https://doi.org/10.1007/s11665-006-9004-0

[89] Rossini, N. S., Dassisti, M., Benyounis, K. Y., & Olabi, A. G. (2012). Methods of measuring residual stresses in components. *Materials & Design*, *35*, 572–588. https://doi.org/10.1016/j.matdes.2011.08.022

[90] Roy, S. (2003). Fatigue resistance of welded details enhanced by ultrasonic impact treatment (UIT). *International Journal of Fatigue*, *25*(9–11), 1239–1247. https://doi.org/10.1016/S0142-1123(03)00151-8

[91] Roy, S., & Fisher, J. W. (2005). Enhancing fatigue strength by ultrasonic impact treatment. International Journal of Steel Structures. *International Journal of Steel Structures*, *5*(3), 241–252.

[92] Schaumann, P., & Collmann, M. (2013). Influence of Weld Defects on the Fatigue Resistance of Thick Steel Plates. *Procedia Engineering*, *66*, 62–72. https://doi.org/10.1016/j.proeng.2013.12.062

[93] Schijve, J. (2001). *Fatigue of structures and materials*. Kluwer Academic.

[94] Schijve, J. (2008). *Fatigue of Structures and Materials*. Springer Science & Business Media. https://doi.org/10.1007/0-306-48396-3

[95] Seto, A., Masuda, T., Machida, S., & Miki, C. (2000). Very low cycle fatigue properties of butt welded joints containing weld defects. Study of acceptable size of defects in girth welds of gas pipelines. *Welding International*, *14*(1), 26–34. https://doi.org/10.1080/09507110009549134

[96] Shams-Hakimi, P. (2017). *Performance of high-frequency mechanical impact treatment for bridge application* [Doctoral dissertation, Department of Architecture and Civil Engineering, Chalmers University of Technology]. https://core.ac.uk/download/pdf/84870083.pdf

[97] Shams-Hakimi, Poja, Zamiri, F., Al-Emrani, M., & Barsoum, Z. (2018). Experimental study of transverse attachment joints with 40 and 60 mm thick main plates, improved by high-frequency mechanical impact treatment (HFMI). *Engineering Structures*, *155*, 251–266. https://doi.org/10.1016/j.engstruct.2017.11.035

[98] Sharpe, W. N. (2008). *Springer handbook of experimental solid mechanics*. Springer.

[99] Shirahata, H., Miki, C., Yamaguchi, R., Kinoshita, K., & Yaginuma, Y. (2014). Fatigue crack detection by the use of ultrasonic echo height change with crack tip opening. *Welding in the World*, *58*(5), 681–690. https://doi.org/10.1007/s40194-014-0149-4

[100] Sidhom, N., Laamouri, A., Fathallah, R., Braham, C., & Lieurade, H. (2005). Fatigue strength improvement of 5083 H11 Al-alloy T-welded joints by shot peening: Experimental characterization and predictive approach. *International Journal of Fatigue*, *27*(7), 729–745. https://doi.org/10.1016/j.ijfatigue.2005.02.001

[101] Sonsino, C. (2009). Effect of residual stresses on the fatigue behaviour of welded joints depending on loading conditions and weld geometry. *International Journal of Fatigue*, *31*(1), 88–101. https://doi.org/10.1016/j.ijfatigue.2008.02.015

[102] Statnikov, A. S. (2000). Applications of operational ultrasonic impact treatment (UIT) technologies in production of welded joints. *WELDING IN THE WORLD-LONDON*, *44*(3), 11–21.

[103] Statnikov, E. S., Muktepavel, V. O., & Blomqvist, A. (2002). Comparison of Ultrasonic Impact Treatment (UIT) and Other Fatigue Life Improvement Methods. *Welding in the World*, *46*(3–4), 20–32. https://doi.org/10.1007/BF03266368

[104] Statnikov, E.Sh. (1997b). Comparison of post-weld deformation methods for increase in fatigue strength of welded joints. *IIW*. Doc. XIII-1668-97.

[105] Stephens, R. I., Fatemi, A., Stephens, R. R., & Fuchs, H. O. (2001). *Metal Fatigue in Engineering*. John Wiley and Sons. Inc., New York.

[106] Stoschka, M., Leitner, M., Posch, G., & Eichlseder, W. (2013). Effect of high-strength filler metals on the fatigue behaviour of butt joints. *Welding in the World*, *57*(1), 85–96. https://doi.org/10.1007/s40194-012-0010-6

[107] Stoschka, Michael, Di Leitner, M., Fössl, T., & Posch, G. (2012). Effect of High-Strength Filler Metals on Fatigue. *Welding in the World*, *56*(3–4), 20–29. https://doi.org/10.1007/BF03321332

[108] Suresh, S. (1998). *Fatigue of materials* (2nd ed). Cambridge University Press.

[109] Tada, H., Paris, P. C., & Irwin, G. R. (1973). *The stress analysis of cracks handbook, Del Research Corp.*

[110] Tang, L., Ince, A., & Zheng, J. (2018). Numerical Simulation of Residual Stresses in Welding and Ultrasonic Impact Treatment Process. In P. Ferro & F. Berto (Eds.), *Residual Stress Analysis on Welded Joints by Means of Numerical Simulation and Experiments*. InTech. https://doi.org/10.5772/intechopen.72394

[111] Tang, L., Ince, A., & Zheng, J. (2020). Numerical modeling of residual stresses and fatigue damage assessment of ultrasonic impact treated 304L stainless steel welded joints.

Engineering Failure Analysis, *108*, 104277. https://doi.org/10.1016/j.engfailanal.2019.104277

[112] Tehrani Yekta, R., Ghahremani, K., & Walbridge, S. (2013). Effect of quality control parameter variations on the fatigue performance of ultrasonic impact treated welds. *International Journal of Fatigue*, *55*, 245–256. https://doi.org/10.1016/j.ijfatigue.2013.06.023

[113] Teng, T.-L., Fung, C.-P., & Chang, P.-H. (2002). Effect of weld geometry and residual stresses on fatigue in butt-welded joints. *International Journal of Pressure Vessels and Piping*, *79*(7), 467–482. https://doi.org/10.1016/S0308-0161(02)00060-1

[114] Vaidya, W. V. (1985). Fatigue crack propagation under a microstructural gradient in a plain carbon steel. *Scripta Metallurgica*, *19*(5), 597–602. https://doi.org/10.1016/0036-9748(85)90344-8

[115] Walker, K. (1970). The Effect of Stress Ratio During Crack Propagation and Fatigue for 2024-T3 and 7075-T6 Aluminum. In M. Rosenfeld (Ed.), *Effects of Environment and Complex Load History on Fatigue Life* (pp. 1-1–14). ASTM International. https://doi.org/10.1520/STP32032S

[116] Wallbrink, C., Peng, D., Jones, R., & Dayawansa, P. H. (2006). Predicting the fatigue life and crack aspect ratio evolution in complex structures. *Theoretical and Applied Fracture Mechanics*, *46*(2), 128–139. https://doi.org/10.1016/j.tafmec.2006.07.004

[117] Webster, G. A., & Ezeilo, A. N. (2001). Residual stress distributions and their influence on fatigue lifetimes. *International Journal of Fatigue*, *23*, 375–383. https://doi.org/10.1016/S0142-1123(01)00133-5

[118] Weich, I., Ummenhofer, T., Nitschke-Pagel, T., Dilger, K., & Eslami Chalandar, H. (2009). Fatigue Behaviour of Welded High-Strength Steels after High Frequency Mechanical Post-Weld Treatments. *Welding in the World*, *53*(11–12), R322–R332. https://doi.org/10.1007/BF03263475

[119] Weman, K. (2003). *Welding processes handbook*. CRC Press.

[120] Williams, H. E., Ottsen, H., Lawence, F. V., & Munse, W. H. (1970). The Effects Of Weld Geometry On The Fatigue Behavior Of Welded Connrctions. *University of Illinois Engineering Experiment Station. College of Engineering. University of Illinois at Urbana-Champaign.* http://hdl.handle.net/2142/14783

[121] Withers, P. J., & Bhadeshia, H. K. D. H. (2001a). Residual stress. Part 1 – Measurement techniques. *Materials Science and Technology*, *17*(4), 355–365. https://doi.org/10.1179/026708301101509980

[122] Withers, P. J., & Bhadeshia, H. K. D. H. (2001b). Residual stress. Part 2 – Nature and origins. *Materials Science and Technology*, *17*(4), 366–375. https://doi.org/10.1179/026708301101510087

[123] Wright, W. (1996). *Post-weld Treatment of A Welded Bridge Girder by Ultrasonic Hammer Peening* (p. 6).

[124] Yildirim, H. C., & Marquis, G. B. (2012). Fatigue strength improvement factors for high strength steel welded joints treated by high frequency mechanical impact. *International Journal of Fatigue*, *44*, 168–176. https://doi.org/10.1016/j.ijfatigue.2012.05.002

[125] Yildirim, H. C., & Marquis, G. B. (2013). A round robin study of high-frequency mechanical impact (HFMI)-treated welded joints subjected to variable amplitude loading. *Welding in the World*. https://doi.org/10.1007/s40194-013-0045-3

[126] Yuan, K. L., & Sumi, Y. (2015). Modelling of ultrasonic impact treatment (UIT) of welded joints and its effect on fatigue. *Frattura Ed Integrità Strutturale*, *9*, 34.

[127] Zerbst, U., Ainsworth, R. A., Beier, H. Th., Pisarski, H., Zhang, Z. L., Nikbin, K., Nitschke-Pagel, T., Münstermann, S., Kucharczyk, P., & Klingbeil, D. (2014). Review on fracture and crack propagation in weldments – A fracture mechanics perspective. *Engineering Fracture Mechanics*, *132*, 200–276. https://doi.org/10.1016/j.engfracmech.2014.05.012

[128] Zheng, J., Ince, A., & Tang, L. (2018). Modeling and simulation of weld residual stresses and ultrasonic impact treatment of welded joints. *Procedia Engineering*, *213*, 36–47. https://doi.org/10.1016/j.proeng.2018.02.005

APPENDIXES

(A) Fatigue Test Results

The outcomes of the fatigue tests are summarized in Table 10 for 5083-H321 AL, Table 11 for CSA 350W ST, Table 12 for A514 ST, Table 13 for S355, Table 14 for S460, Table 15 for S690, Table 16 for S960, Table 17 for 5083-H11 AL and Table 18 for 2024-T51, respectively. In general, this fatigue life increase is more pronounced for the mild and high strength steel welded specimens than for the aluminum welded specimens.

ΔS is simply represented by equation (2. 1) which is nominal stress range. Further, ΔS data is put on Y-axis of the $S - N$ curve of the fatigue strength. Whereas N_f is simply presented by equations (3. 1), (3. 3) and (3. 4) which is the number of cycles. Besides, N_f data is put on X-axis of the $S - N$ curve of the fatigue strength. Other than that, the nominal stress, or the load divided by the cross-section area, is just the stress.

Table 10, Table 11 and Table 12 gives a breakdown of fatigue test results for 5083-H321 AL, CSA 350W ST and A514 ST test specimens, respectively. In this thesis, the AW specimens are marked by red colour while the UIT specimens are pointed out by blue colour. In these tables, the dramatic impact of the UIT treatment on the fatigue life of the welded specimens are readily comprehensible. For example, when the ΔS is $92.5642\ MPa$, the corresponding N_f is $8.42E + 4\ cycles$ for the AW condition for 5083-H311 AL cruciform joint. Whereas the ΔS is $93.435\ MPa$, the comparable N_f is $3.63E + 05\ cycles$ for the UIT condition for 5083-H311 AL cruciform joint. It can be understood that the effective impact of the UIT treatment on the fatigue life of the welded specimens is expected to be shifted to the right in the $S - N$ curve of the fatigue strength as represented in Chapter 5 as well as in Appendix (B).

Table 10: Fatigue test results for 5083-H321 AL cruciform-joint test specimen for AW and UIT conditions (Kasra Ghahremani, Ranjan, et al., 2015; Ranjan et al., 2016)

AW	
Number of Cycles, N_f	Nominal Stress Range (MPa), ΔS
1.45E+04	140.927
3.81E+04	104.1
8.42E+04	92.5642
1.12E+05	79.3102
1.21E+05	84.3674
1.78E+05	75.4836

UIT	
Number of Cycles, N_f	Nominal Stress Range (MPa), ΔS
3.74E+04	141.297
1.77E+05	103.773
3.63E+05	93.435
1.64E+06	80.0728
2.19E+06	85.699
3.28E+06	75.7455

Table 11: Fatigue test results for CSA 350W ST cruciform-joint test specimen for AW and UIT conditions (Kasra Ghahremani, Ranjan, et al., 2015; Ranjan et al., 2016)

AW	
Number of Cycles, N_f	Nominal Stress Range (MPa), ΔS
5.81E+04	265.32
7.00E+04	262.402
1.04E+05	252.442
1.69E+05	226.017
2.04E+05	175.266
2.50E+05	201.243
3.84E+05	179.185
4.07E+05	179.185

UIT	
Number of Cycles, N_f	Nominal Stress Range (MPa), ΔS
1.18E+06	251.05
2.29E+06	224.771
2.78E+06	252.442
3.06E+06	200.134
4.27E+06	224.771
7.78E+06	201.243

Table 12: Fatigue test results for A514 ST cruciform-joint test specimen for AW and UIT conditions (Kasra Ghahremani, Ranjan, et al., 2015; Ranjan et al., 2016)

AW	
Number of Cycles, N_f	Nominal Stress Range (MPa), ΔS
4.68E+04	358.399
7.30E+04	349.773
7.89E+04	314.86
9.44E+04	292.368
1.36E+05	331.007
1.68E+05	238.475

UIT	
Number of Cycles, N_f	Nominal Stress Range (MPa), ΔS
2.64E+05	361.183
8.52E+05	315.532
9.12E+05	333.629
1.76E+06	350.773
3.16E+06	295.11
4.49E+06	240.664

Table 13, Table 14 and Table 15 show the related amounts of the fatigue test results for S355, S460 and S690 test specimens, respectively. Following the same procedure as interpreted above, it can be predicated that the fatigue life of the weld specimens for high-strength steels tend to be

shifted dramatically to the right in the $S-N$ curve of the fatigue strength in comparison to mild-strength steels and aluminums as presented in Appendix (B).

Table 13: Fatigue test results for S355 cruciform-joint test specimen for AW and UIT conditions (Ulrike Kuhlmann et al., 2005; U. Kuhlmann et al., 2006)

AW	
Number of Cycles, N_f	**Nominal Stress Range (MPa), ΔS**
9.38E+04	221
3.88E+05	140
3.32E+05	150
8.00E+05	120
1.38E+06	99

UIT	
Number of Cycles, N_f	**Nominal Stress Range (MPa), ΔS**
8.45E+05	260
8.99E+04	320
1.37E+06	250
3.02E+06	240
2.01E+05	294

Table 14: Fatigue tests results for S460 cruciform-joint test specimen for AW and UIT conditions (Ulrike Kuhlmann et al., 2005; U. Kuhlmann et al., 2006)

AW	
Number of Cycles, N_f	**Nominal Stress Range (MPa), ΔS**
2.36E+05	216
1.11E+05	220
4.79E+05	140
1.41E+05	220
4.24E+05	150
1.03E+06	112

UIT	
Number of Cycles, N_f	**Nominal Stress Range (MPa), ΔS**
5.95E+05	290
1.75E+05	320
3.46E+05	287
9.93E+05	250
1.08E+06	240

Table 15: Fatigue tests results for S690 cruciform-joint test specimen for AW and UIT conditions (Ulrike Kuhlmann et al., 2005; U. Kuhlmann et al., 2006)

AW	
Number of Cycles, N_f	**Nominal Stress Range (MPa), ΔS**
1.56E+05	328.1
1.69E+05	295.834
2.83E+05	267.234
3.28E+05	200.97
3.57E+05	221.599
1.32E+06	178.7
1.78E+06	164.448
2.16E+06	137.23
2.66E+06	187.562
3.36E+06	147.662
4.97E+06	125.753

UIT	
Number of Cycles, N_f	**Nominal Stress Range (MPa), ΔS**
3.75E+05	284.721
4.38E+05	360.92
4.73E+05	317.497
4.86E+06	273.979

Table 16 identifies the dependant amounts of the fatigue test results for S960 test specimen. Following the similar procedure as detailed above, it is noteworthy that the fatigue life of the weld specimens for high-strength steel lean to be shifted markedly to the right in the $S - N$ curve of the fatigue strength as shown in Appendix (B).

Table 16: Fatigue test results for S960 Longitudinal stiffener joint test specimen for AW and UIT conditions (Leitner et al., 2017)

AW	
Number of Cycles, N_f	Nominal Stress Range (MPa), ΔS
1.33E+04	606.874
2.44E+04	506.087
4.62E+04	398.107
1.21E+05	303.173
2.28E+05	252.823
4.47E+05	201.477
6.30E+05	176.965
1.03E+06	151.454
7.17E+06	112.384

UIT	
Number of Cycles, N_f	Nominal Stress Range (MPa), ΔS
1.83E+04	704.51
3.25E+04	606.874
3.66E+04	606.874
8.53E+04	499.564
1.36E+05	502.815
2.73E+05	403.305
5.55E+05	345.166
6.24E+05	351.948
7.96E+05	354.239
1.06E+06	327.712
7.70E+06	301.213

Table 17 and Table 18 indicates the fatigue test results for 5083-H11 AL test specimen and 2024-T351 AL test plate. The authors (Sidhom et al., 2005) discovered that the AW condition reduced the nominal fatigue limit of 5083-H11 AL test specimen for approximately 55% to 60 % versus that of the base material while the UIT condition improved the fatigue limit roughly 135% in comparison to the welded joints. It should be emphasized that the authors (Sidhom et al., 2005; Rodopoulos et al., 2007) reported that UIT proved significant enhancement against other methods. The results are illustrated in Appendix (B).

Table 17: Fatigue test results for 5083-H11 AL T-joint test specimen for AW and UIT conditions (Sidhom et al., 2005)

AW	
Number of Cycles, N_f	**Nominal Stress Range (MPa), ΔS**
3.01E+04	140
5.42E+04	140
6.05E+04	119.25
7.92E+04	119.25
1.67E+05	99.5
2.57E+05	80
1.44E+06	59

UIT	
Number of Cycles, N_f	**Nominal Stress Range (MPa), ΔS**
2.61E+04	180.025
3.21E+04	180.025
5.74E+04	169.288
6.10E+04	169.288
7.15E+04	169.288
1.43E+05	160.3
1.76E+05	160.549
2.06E+05	160.3
2.18E+05	160.3
2.82E+05	149.563
4.11E+05	150.562
4.36E+05	150.562
6.05E+05	139.825

Table 18: Fatigue test results for 2024-T351 AL plate test specimen for AW and UIT conditions (Rodopoulos et al., 2007)

BR	
Number of Cycles, N_f	**Nominal Stress Range (MPa), ΔS**
3.67E+04	400.72
8.29E+04	349.14
8.66E+04	325.22
9.86E+04	300.14
1.43E+05	300.14
2.10E+05	274.78
3.76E+05	250.58
1.27E+06	225.50
3.55E+06	215.42
4.96E+06	199.28

UIT	OR
Number of Cycles, N_f	**Nominal Stress Range (MPa), ΔS**
1.16E+05	399.57
2.65E+05	350.58
3.92E+05	325.22
4.94E+05	300.14
9.86E+05	269.88
1.82E+06	249.71
3.55E+06	230.98
4.96E+06	220.61

(B) Fatigue Crack Growth Curves

(B.1) 5083-H11 AL

Figure 84 and Figure 85 depict graphically fatigue crack growth analysis results of 5083-H311 AL under the AW and the UIT conditions for Walker and Forman models. Crack depth and crack surface versus the number of cycles are displayed in these figures.

Both models predicted crack propagation state quite well as it can be observed that the fatigue life has been shifted to the right and the surface of the crack has been either slightly or significantly diminished which means it has led to the successful UIT treatment.

As reflected in Figure 84, Forman performed an iota better forecasting of fatigue crack growth of the material in depth as well as on surface for the AW condition. From approximately 190 MPa to 90 MPa stress levels, Walker could not properly depict the fatigue crack growth on the surface of the crack unlike Forman model.

As illustrated in Figure 85, Forman anticipated the fatigue crack growth of the material in depth as well as on surface quite satisfactory in comparison to Walker model under the UIT condition because of the fact that the surface of the crack is reduced throughout the life as indicated in Figure 85.

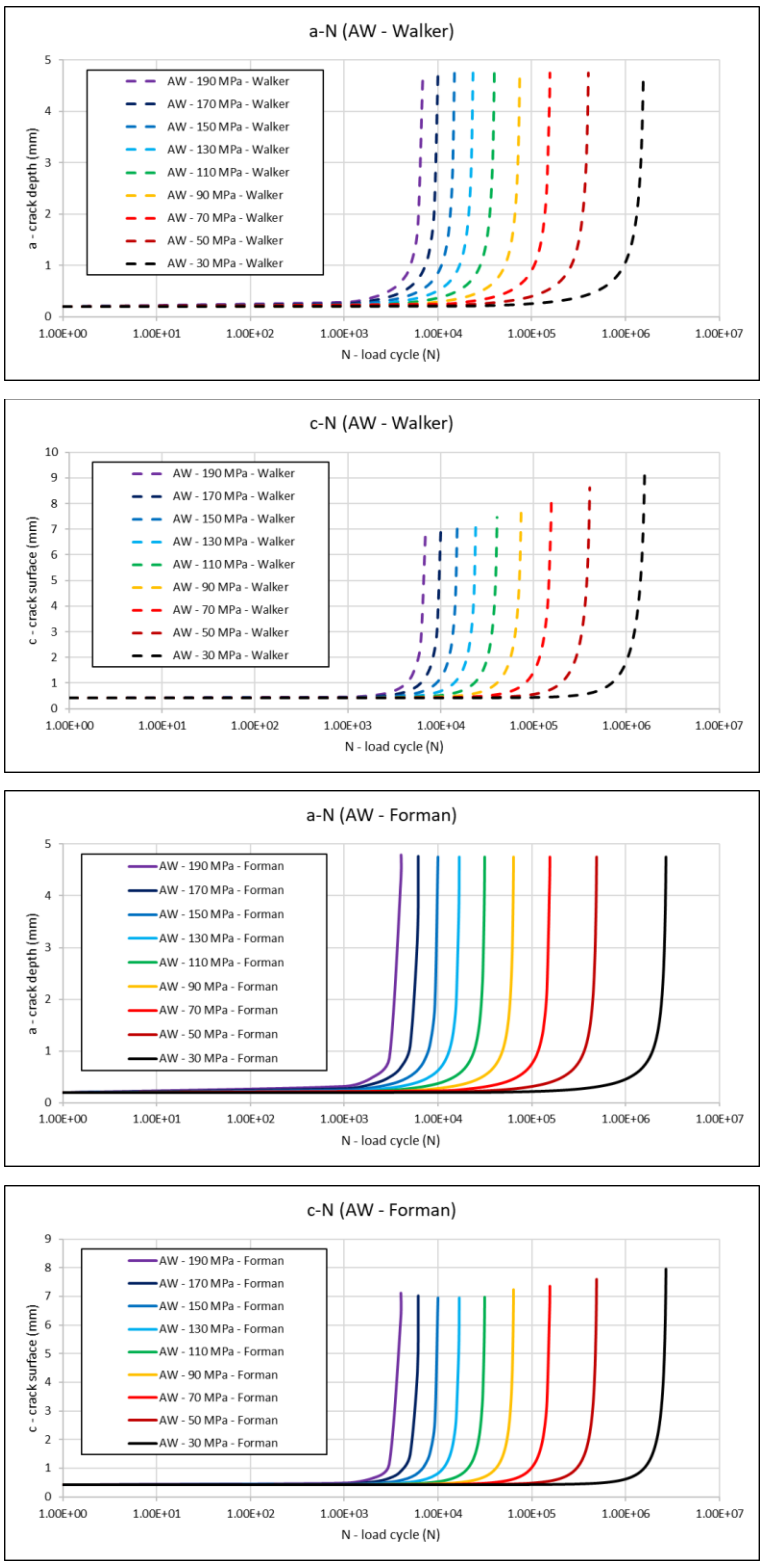

Figure 84: Fatigue crack growth analysis results of 5083-H311 AL under AW condition for Walker vs Forman, crack depth and crack surface against the number of cycles for the whole stress level ranges

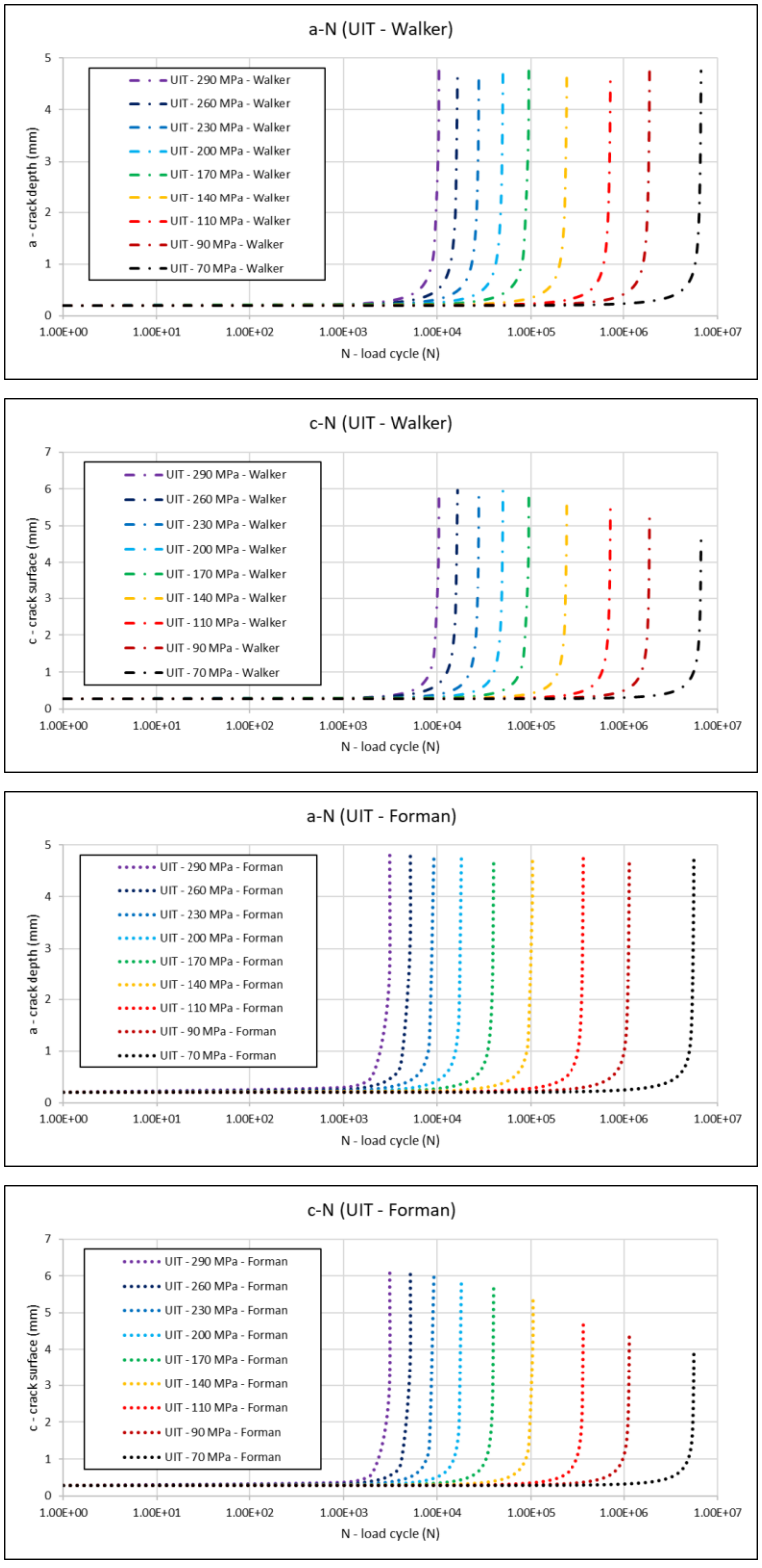

Figure 85: Fatigue crack growth analysis results of 5083-H311 AL under UIT condition for Walker vs Forman, crack depth and crack surface against the number of cycles for the whole stress level ranges

(B.2) CSA 350 W ST

Figure 86 and Figure 87 display diagrammatically fatigue crack growth analysis results of CSA 350W ST under the AW and the UIT conditions for Walker and Forman models. Crack depth and crack surface versus the number of cycles are displayed in these figures.

Both models predicted crack propagation state quite well as it can be observed that the fatigue life has been shifted to the right and the surface of the crack has been either slightly or significantly diminished which means it has led to the successful UIT treatment.

As reflected in Figure 86, Forman performed a bit better forecasting of fatigue crack growth of the material in depth as well as on surface for the AW condition. Forman model demonstrated a great consistency all over the life.

As illustrated in Figure 87, Forman anticipated the fatigue crack growth of the material in depth as well as on surface quite satisfying in comparison to Walker model under the UIT condition due to the fact that the surface of the crack is remarkedly reduced through the life as indicated in Figure 87. Even though Walker model showed some semi-good prediction for this material for the UIT condition, Forman model still is more decent compared to Walker model.

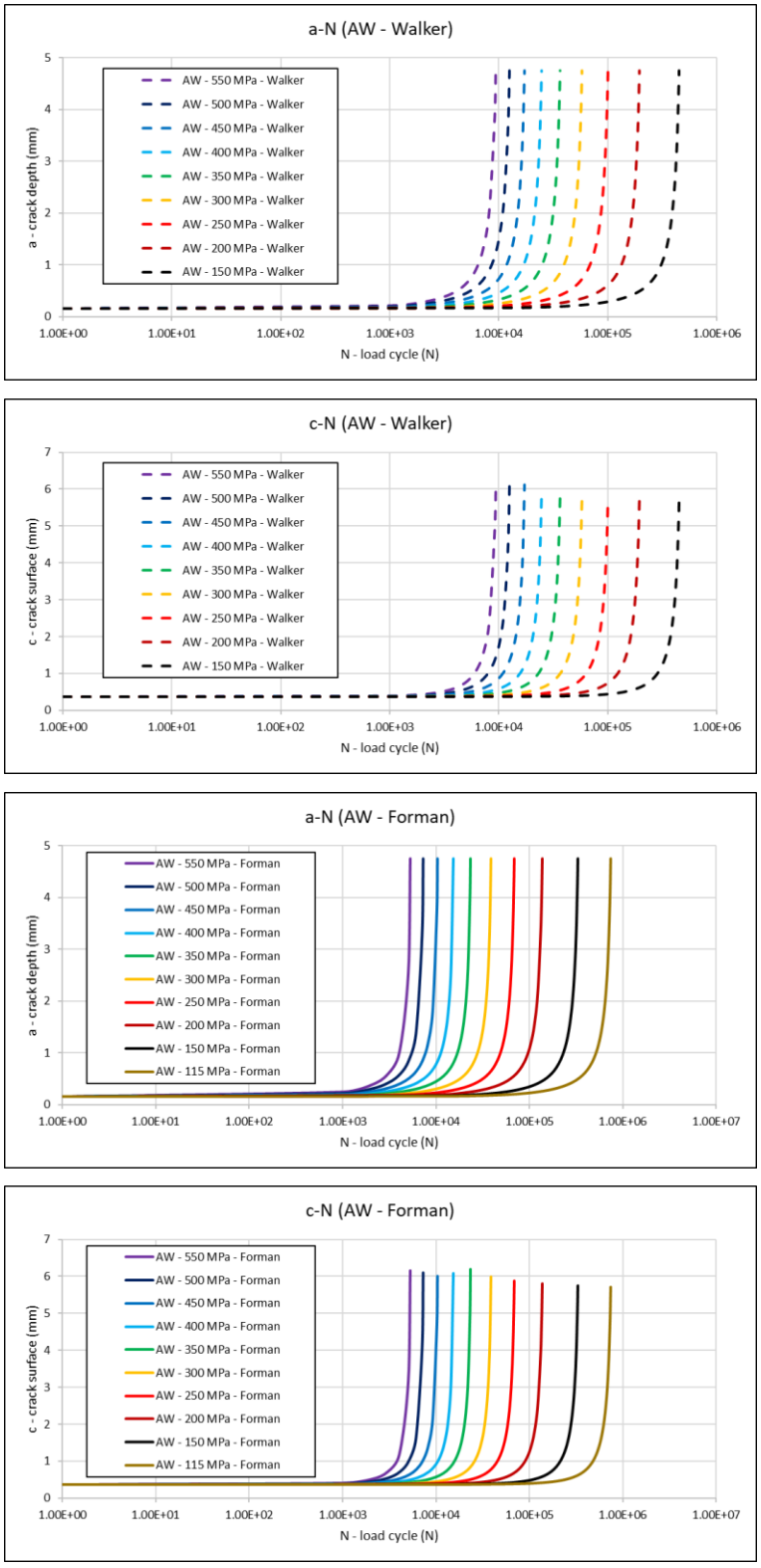

Figure 86: Fatigue crack growth analysis results of CSA 350W ST under AW condition for Walker vs Forman, crack depth and crack surface against the number of cycles for the whole stress level ranges

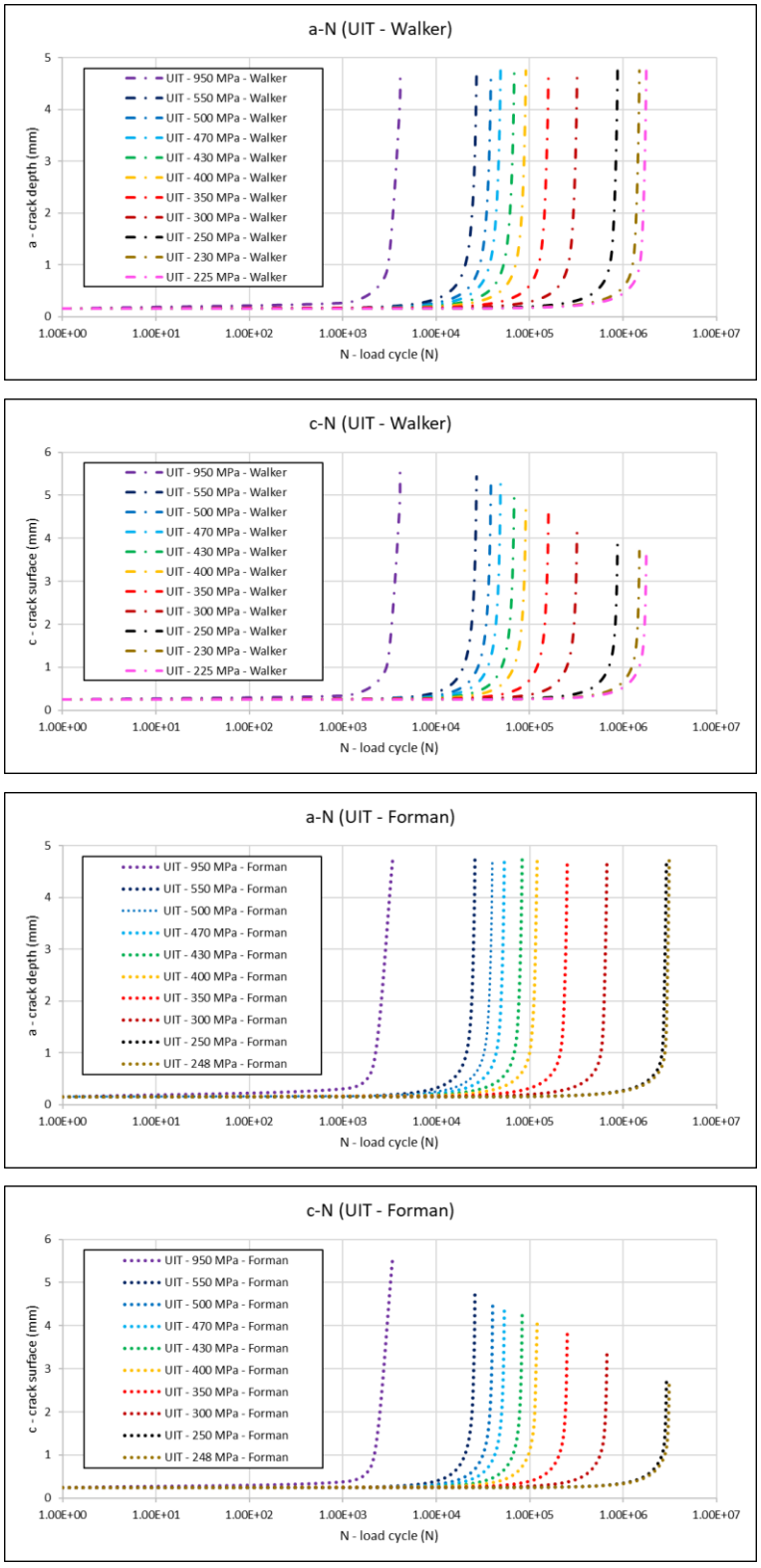

Figure 87: Fatigue crack growth analysis results of CSA 350W ST under UIT condition for Walker vs Forman, crack depth and crack surface against the number of cycles for the whole stress level ranges

(B.3) S355

Figure 88 and Figure 89 display diagrammatically fatigue crack growth analysis results of S355 under the AW and the UIT conditions for Walker and Forman models. Crack depth and crack surface versus the number of cycles are displayed in these figures.

Both models predicted crack propagation state quite well as it can be observed that the fatigue life has been shifted to the right and the surface of the crack has been either slightly or significantly diminished which means it has led to the successful UIT treatment.

As reflected in Figure 88, Forman performed a bit better forecasting of fatigue crack growth of the material in depth as well as on surface for the AW condition. Forman model demonstrated a great consistency all over the life. However, from roughly $150\ MPa$ to $60\ MPa$, Walker could not properly determine the crack growth on the surface direction unlike Forman model due to the fact that the crack diminished almost $0.5\ mm$.

As illustrated in Figure 89, Forman anticipated the fatigue crack growth of the material in depth as well as on surface quite satisfying in comparison to Walker model under the UIT condition due to the fact that the surface of the crack is considerably reduced through the life as indicated in Figure 89. Even though Walker model showed some semi-good prediction for this material for the UIT condition, Forman model still is more trustworthy compared to Walker model.

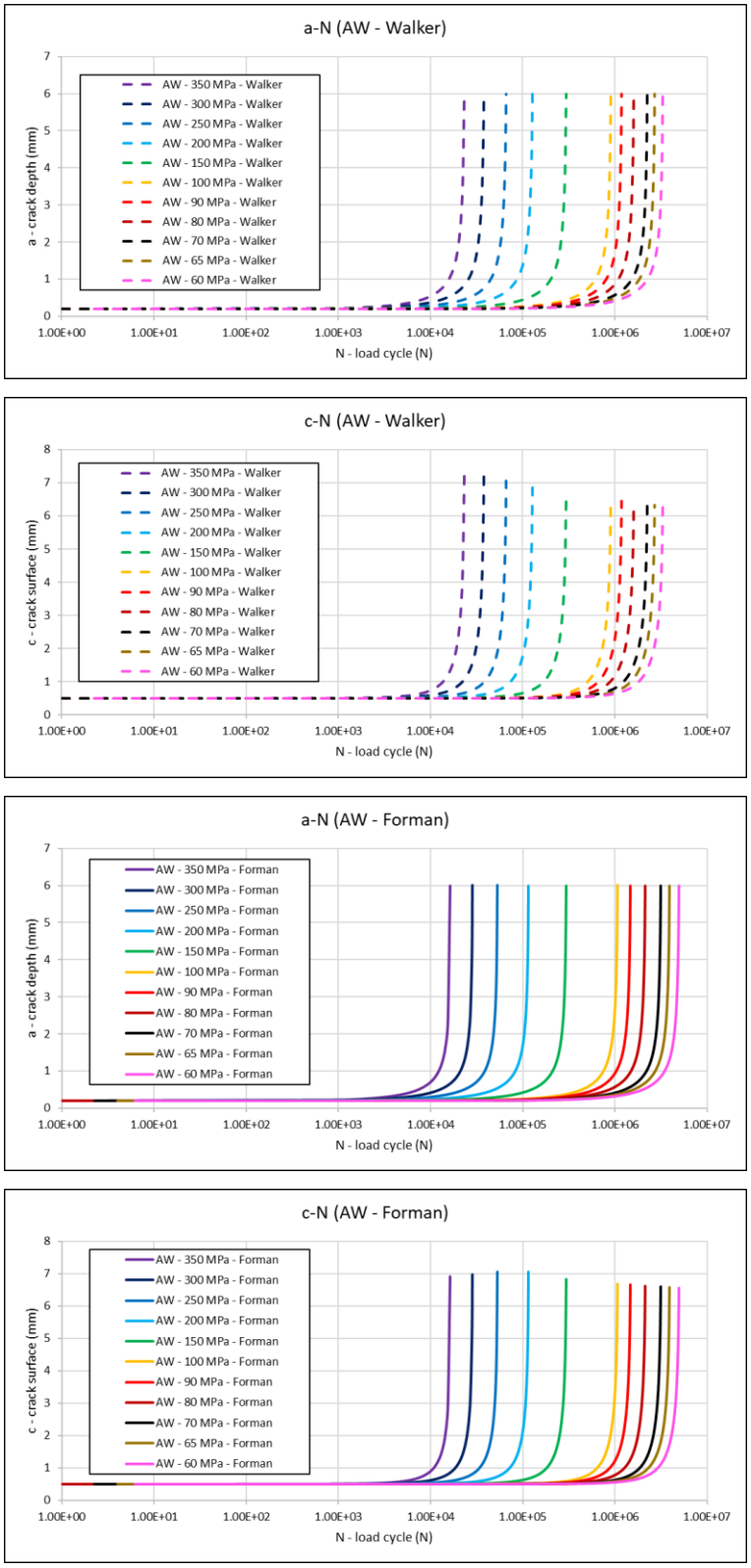

Figure 88: Fatigue crack growth analysis results of S355 under AW condition for Walker vs Forman, crack depth and crack surface against the number of cycles for the whole stress level ranges

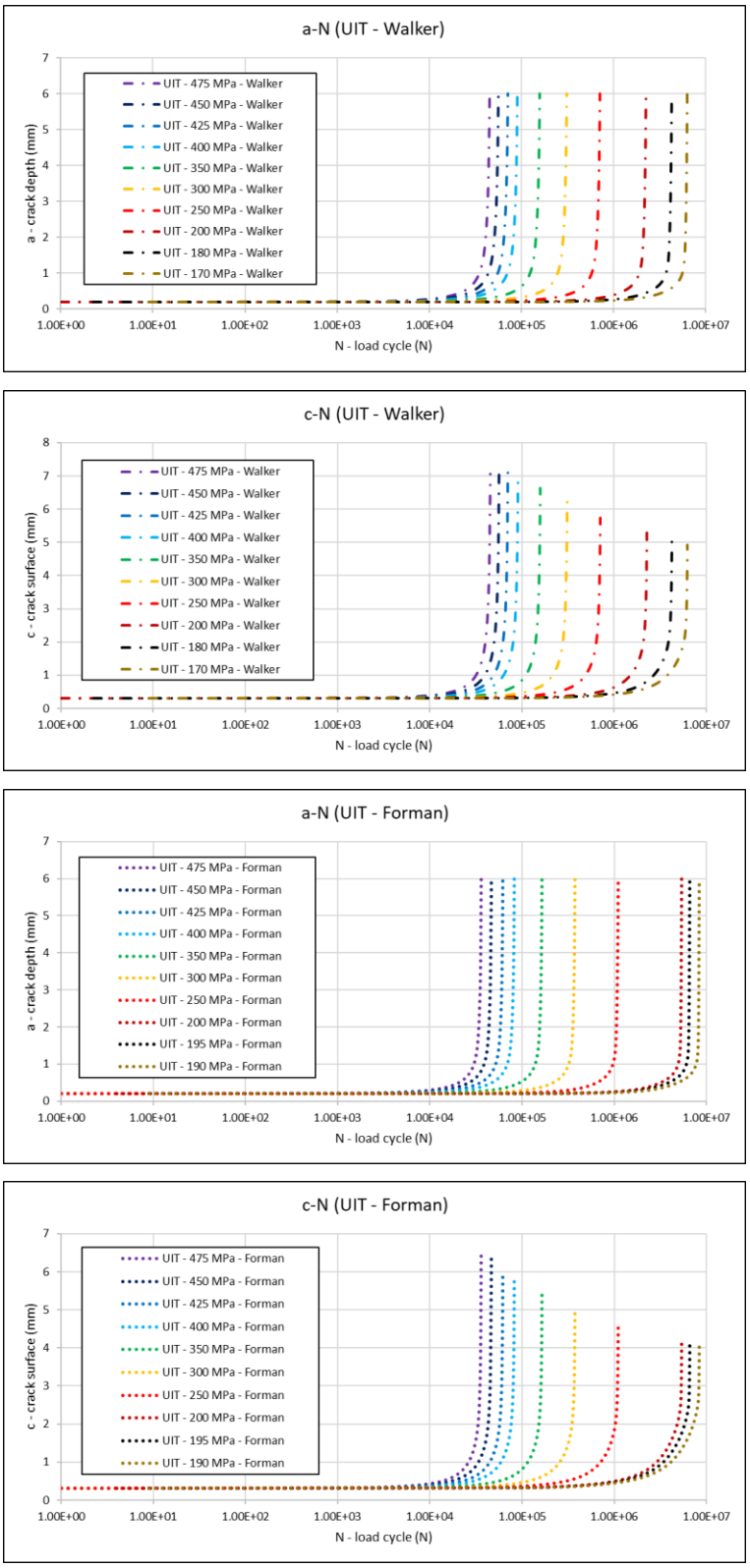

Figure 89: Fatigue crack growth analysis results of S355 under UIT condition for Walker vs Forman, crack depth and crack surface against the number of cycles for the whole stress level ranges

(B.4) S460

Figure 90 and Figure 91 depict graphically fatigue crack growth analysis results of S460 under the AW and the UIT conditions for Walker and Forman models. Crack depth and crack surface versus the number of cycles are displayed in these figures.

Both models predicted crack propagation state quite well as it can be observed that the fatigue life has been shifted to the right and the surface of the crack has been either slightly or significantly diminished which means it has led to the successful UIT treatment.

As reflected in Figure 90, both models assessed fatigue crack growth of the material in depth as well as on surface for the AW condition in a good promise.

As illustrated in Figure 91, Forman anticipated the fatigue crack growth of the material in depth as well as on surface quite satisfactory in comparison to Walker model under the UIT condition due to the fact that the surface of the crack is substantially diminished throughout the life as indicated in Figure 91.

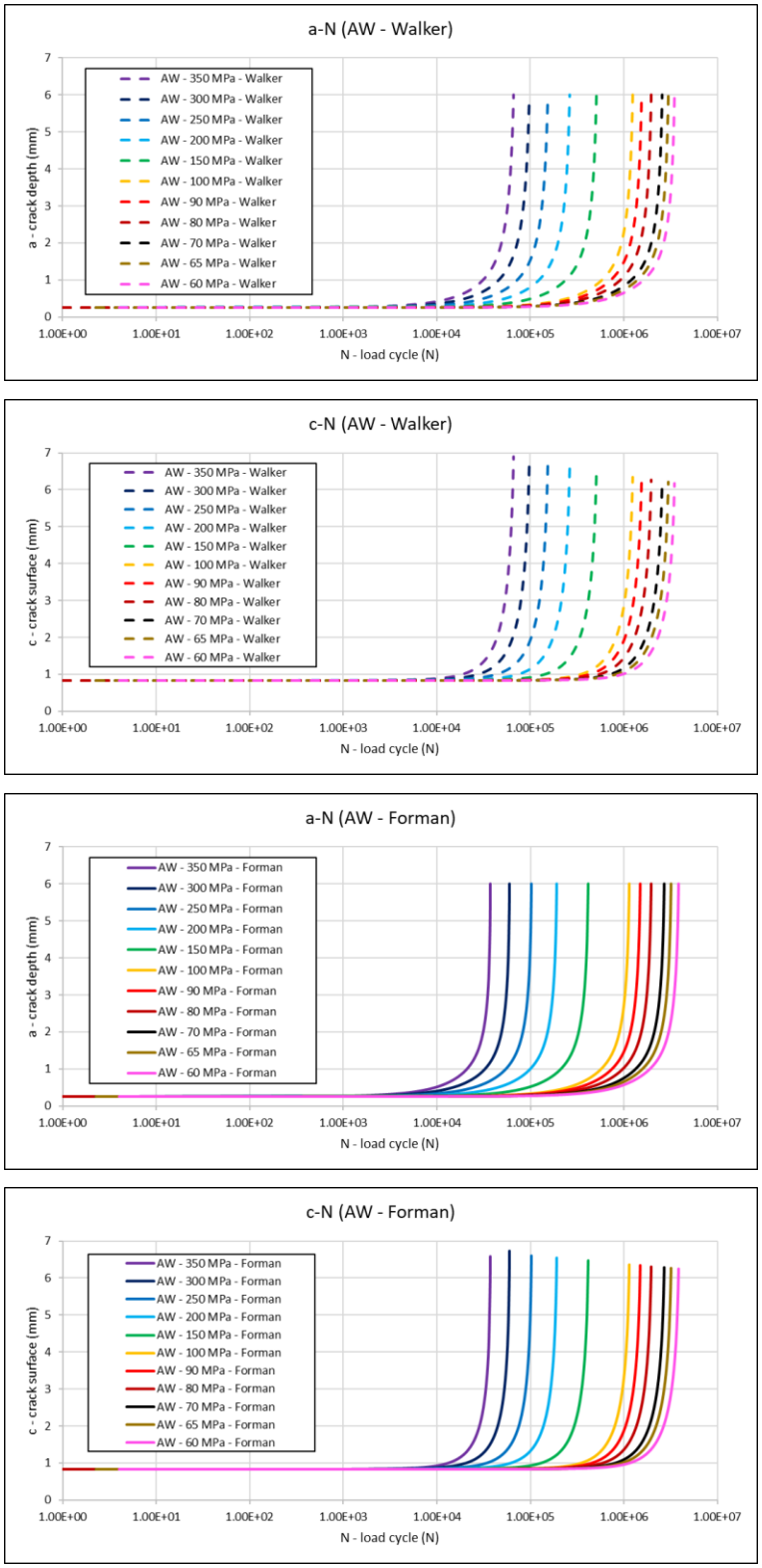

Figure 90: Fatigue crack growth analysis results of S460 under AW condition for Walker vs Forman, crack depth and crack surface against the number of cycles for the whole stress level ranges

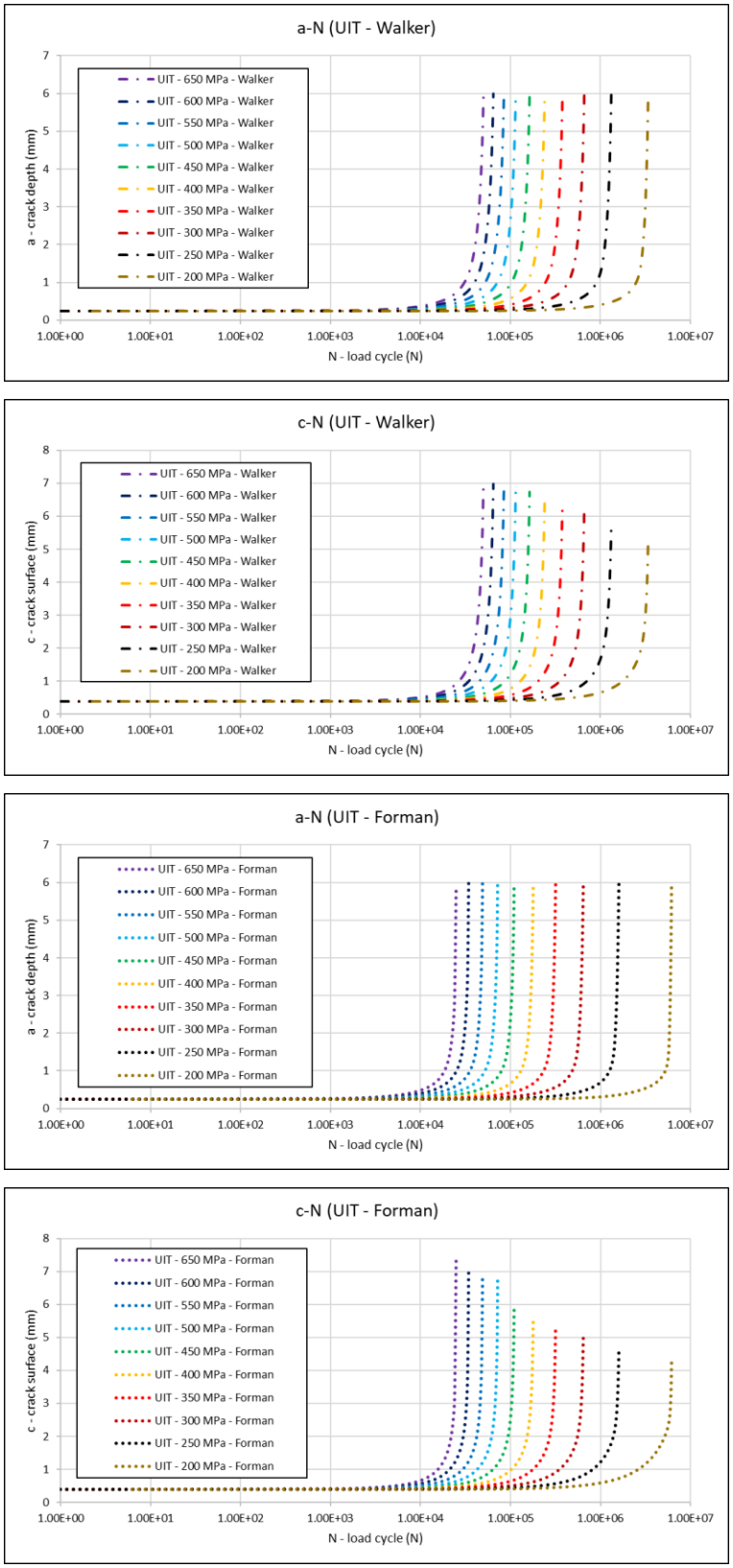

Figure 91: Fatigue crack growth analysis results of S460 under UIT condition for Walker vs Forman, crack depth and crack surface against the number of cycles for the whole stress level ranges

(B.5) S690

Figure 92 and Figure 93 display diagrammatically fatigue crack growth analysis results of S690 under the AW and the UIT conditions for Walker and Forman models. Crack depth and crack surface versus the number of cycles are displayed in these figures.

Both models predicted crack propagation state quite well as it can be observed that the fatigue life has been shifted to the right and the surface of the crack has been either slightly or significantly diminished which means it has led to the successful UIT treatment.

As reflected in Figure 92, Forman performed overall a better forecasting of fatigue crack growth of the material in depth as well as on surface for the AW condition, still both models represent some up and down on surface through out the life.

As illustrated in Figure 93, Forman anticipated the fatigue crack growth of the material in depth as well as on surface quite satisfactory in comparison to Walker model under the UIT condition due to the fact that the surface of the crack is gently reduced throughout the life as indicated in Figure 93. Overall, Forman has the upper hand in estimating the fatigue crack growth versus Walker in this material.

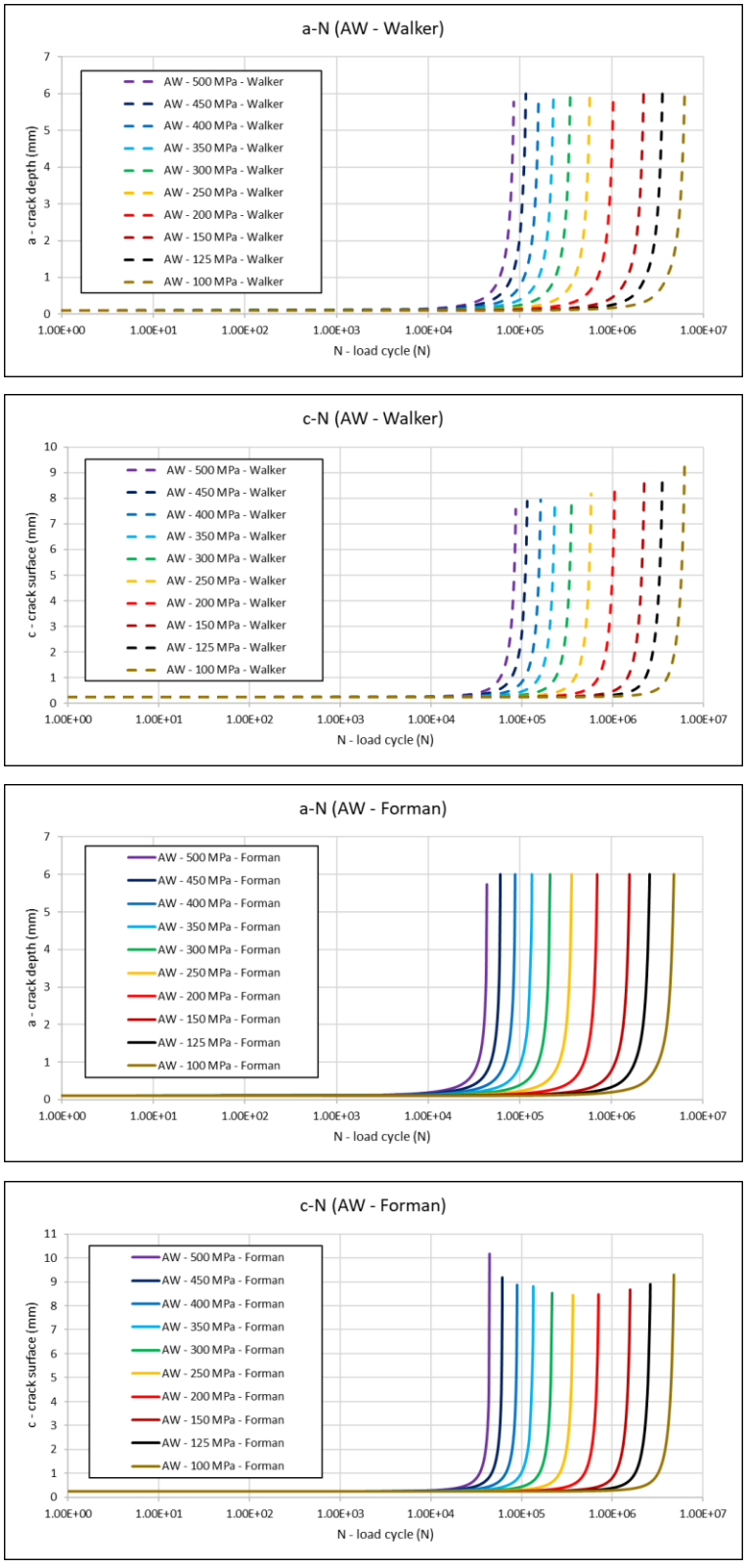

Figure 92: Fatigue crack growth analysis results of S690 under AW condition for Walker vs Forman, crack depth and crack surface against the number of cycles for the whole stress level ranges

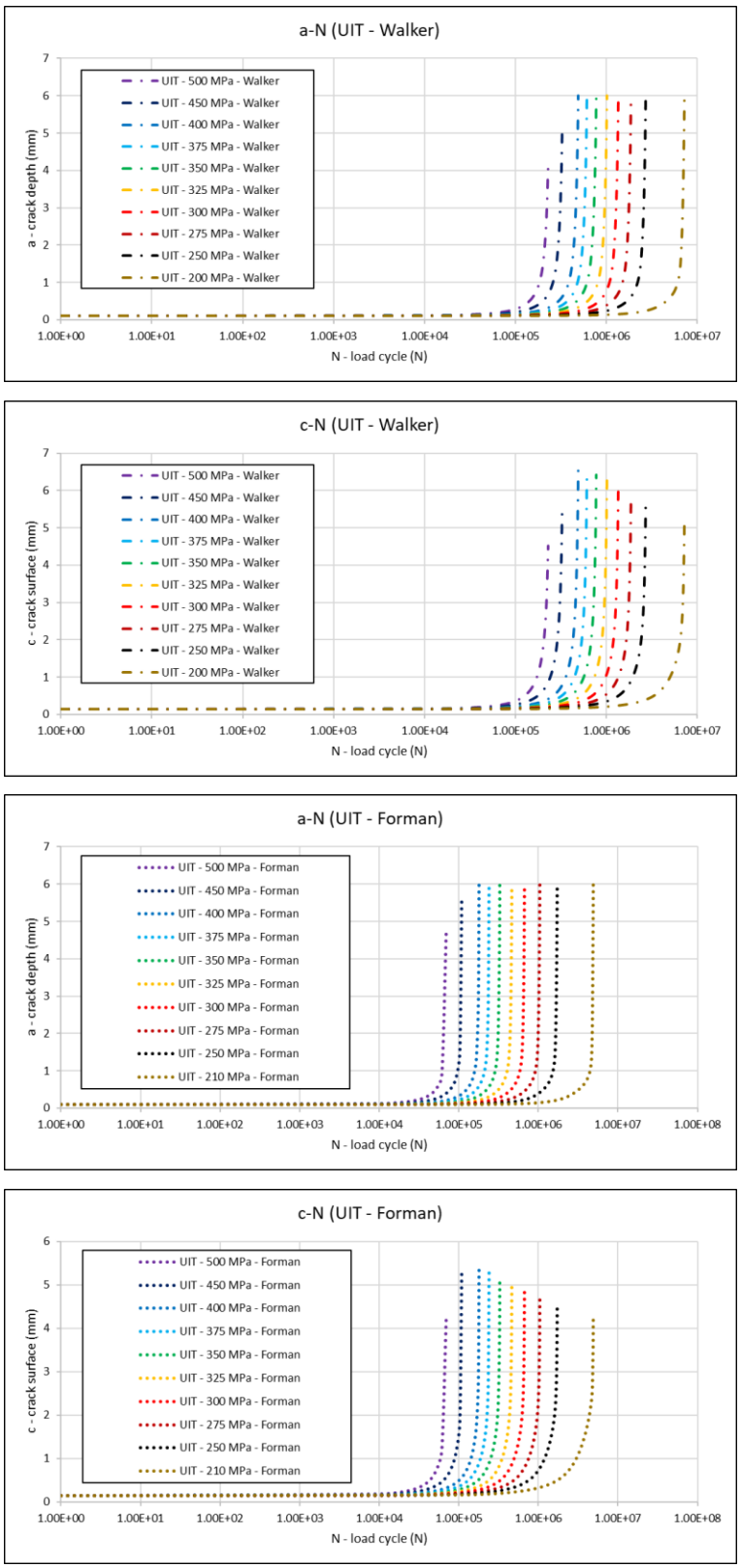

Figure 93: Fatigue crack growth analysis results of S690 under UIT condition for Walker vs Forman, crack depth and crack surface against the number of cycles for the whole stress level ranges

(B.6) S960

Figure 94 and Figure 95 depict graphically fatigue crack growth analysis results of S960 under the AW and the UIT conditions for Walker and Forman models. Crack depth and crack surface versus the number of cycles are displayed in these figures.

Both models predicted crack propagation state quite well as it can be observed that the fatigue life has been shifted to the right and the surface of the crack has been either slightly or significantly diminished which means it has led to the successful UIT treatment.

As reflected in Figure 94, Forman performed a better forecasting of fatigue crack growth of the material in depth for the AW condition. Walker could not properly depict the fatigue crack growth of the material for AW condition in HCF region. Forman model demonstrated a little more consistency on surface all over the life.

As illustrated in Figure 95, both models performed completely good predictions for the fatigue crack growth under the UIT condition.

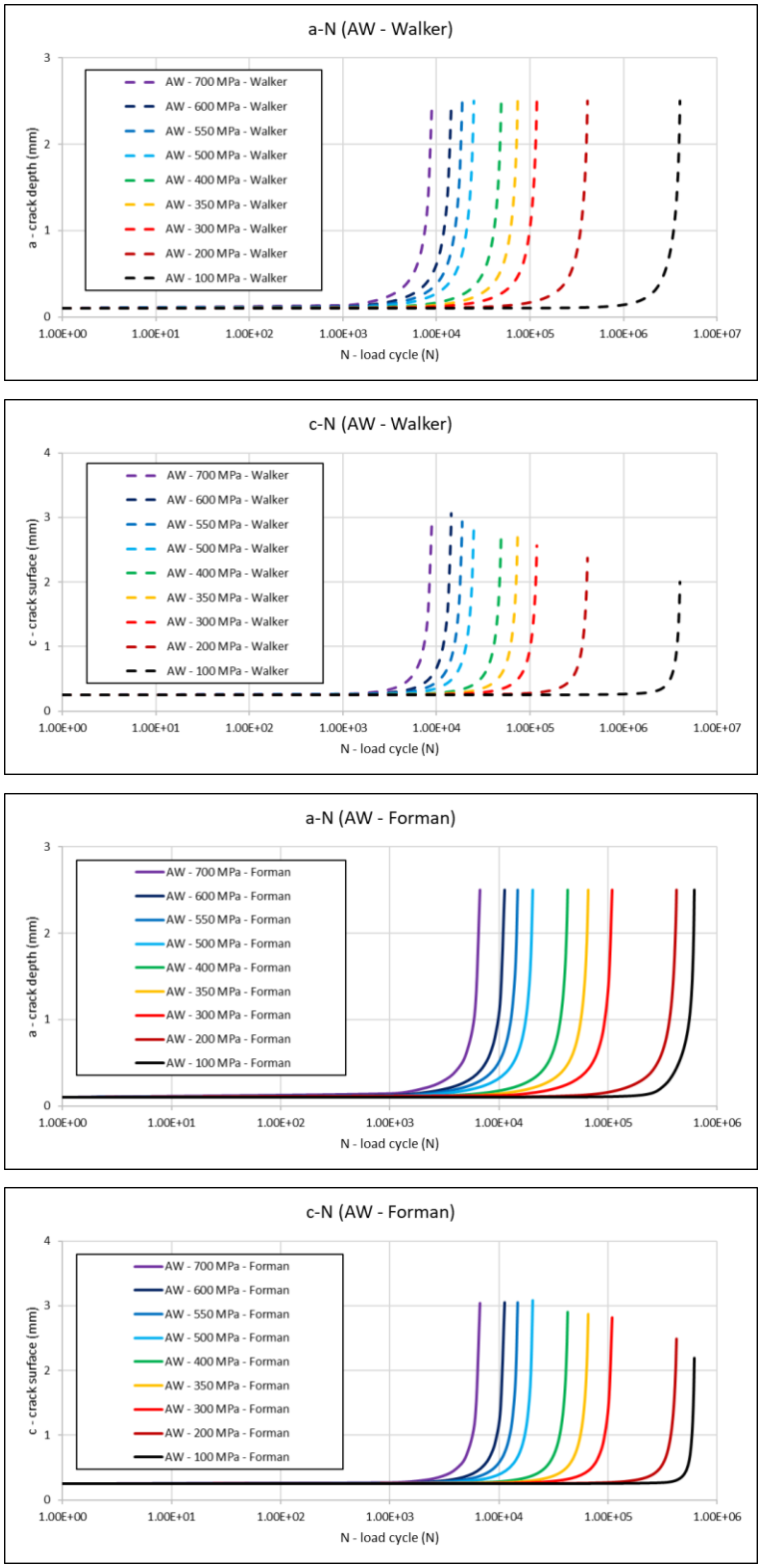

Figure 94: Fatigue crack growth analysis results of S960 under AW condition for Walker vs Forman, crack depth and crack surface against the number of cycles for the whole stress level ranges

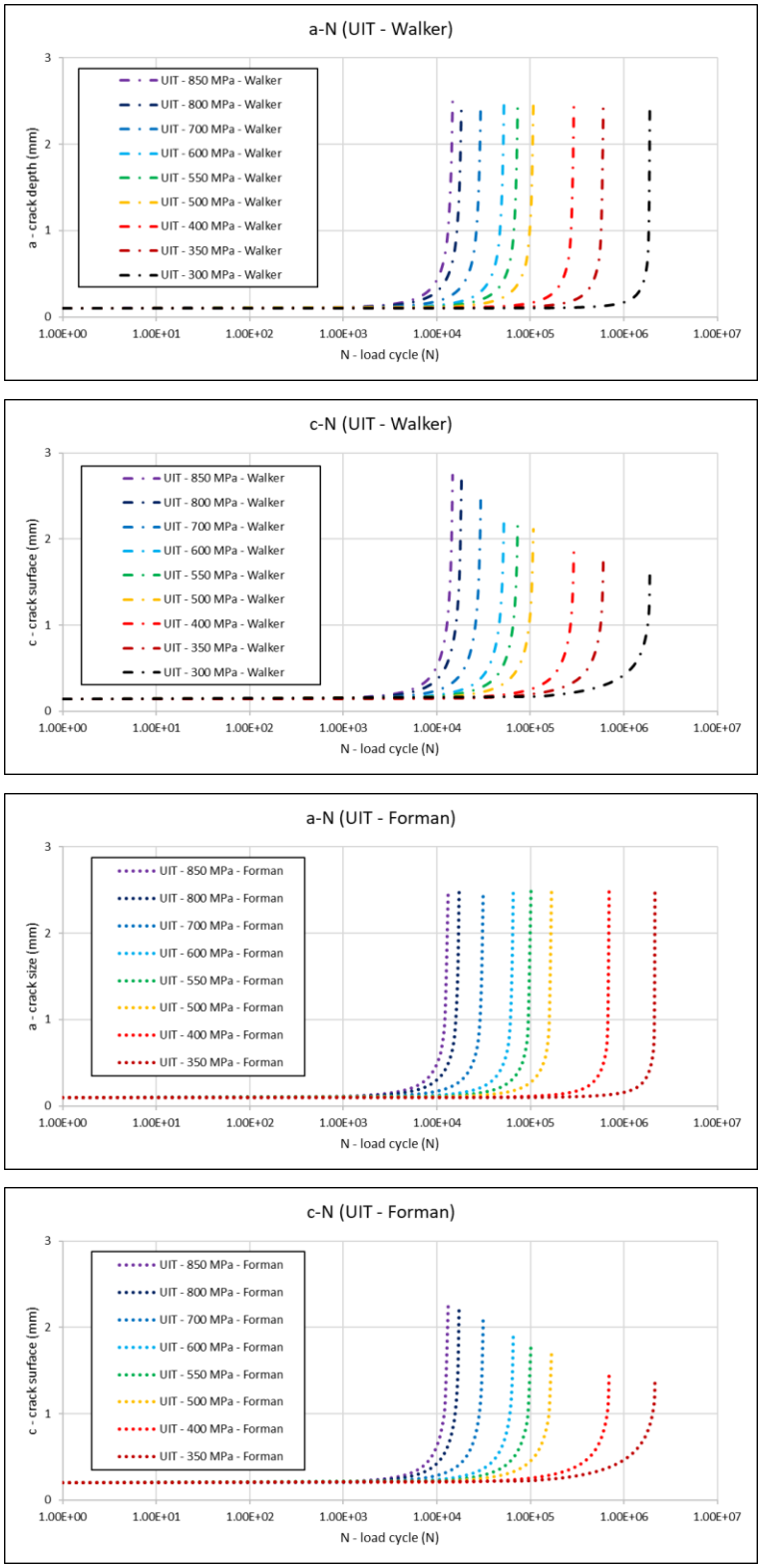

Figure 95: Fatigue crack growth analysis results of S960 under UIT condition for Walker vs Forman, crack depth and crack surface against the number of cycles for the whole stress level ranges

(B.7) 5083-H11 AL

Figure 96 and Figure 97 display diagrammatically fatigue crack growth analysis results of 5083-H11 AL under the AW and the UIT conditions for Walker and Forman models. Crack depth and crack surface versus the number of cycles are displayed in these figures.

Both models predicted crack propagation state quite well as it can be observed that the fatigue life has been shifted to the right and the surface of the crack has been either slightly or significantly diminished which means it has led to the successful UIT treatment.

As reflected in Figure 96, Forman performed an iota better forecasting of fatigue crack growth of the material in depth as well as on surface for the AW condition. From approximately $90\ MPa$ to $45\ MPa$ stress levels, Walker could not properly display the crack on the surface direction unlike Forman model due to the fact that the surface of the crack is somehow reduce even more than Forman.

As illustrated in Figure 97, both models anticipated the fatigue crack growth of the material in depth as well as on surface quite satisfactory under the UIT condition.

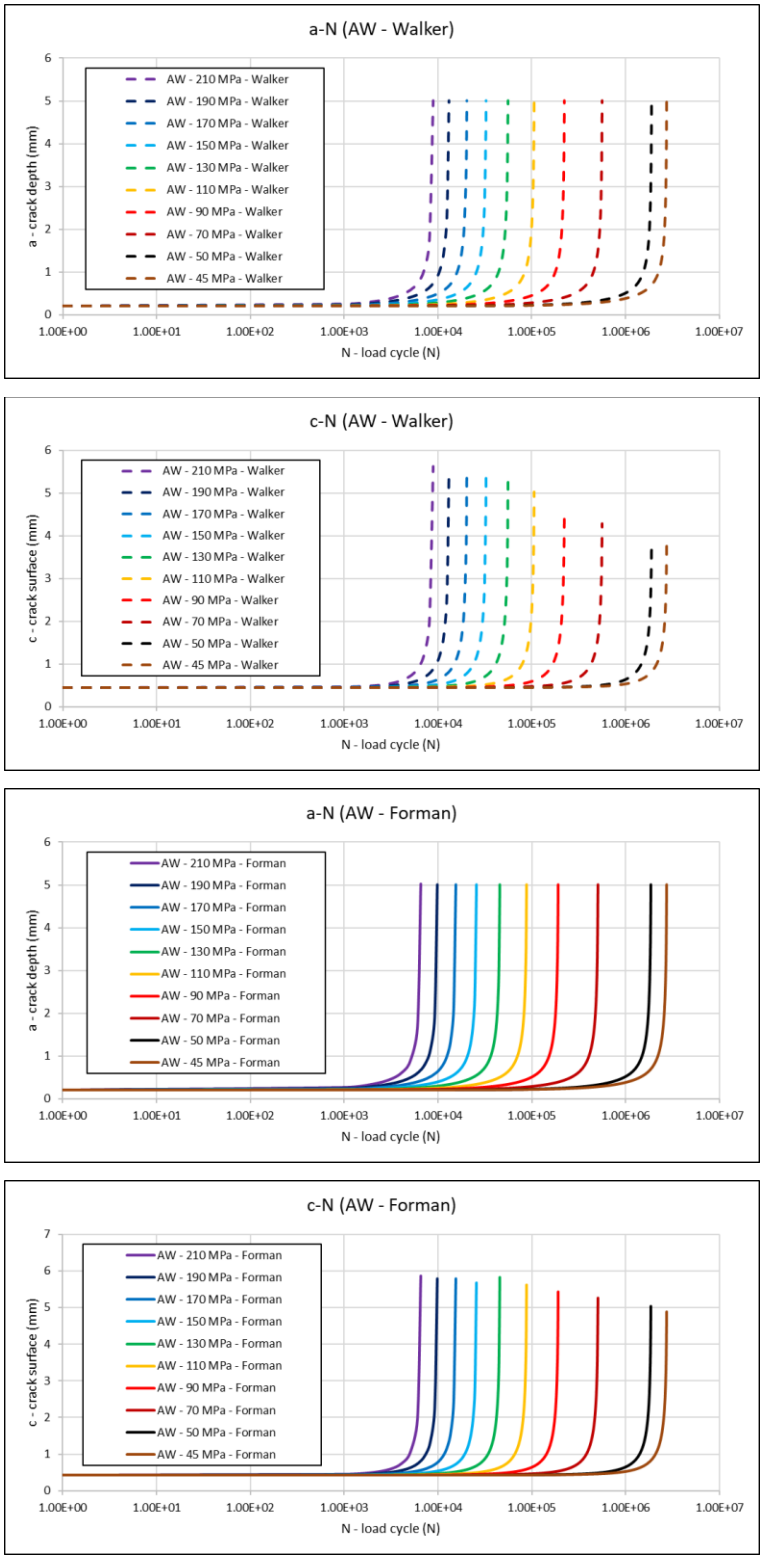

Figure 96: Fatigue crack growth analysis results of 5083-H11 AL under AW condition for Walker vs Forman, crack depth and crack surface against the number of cycles for the whole stress level ranges

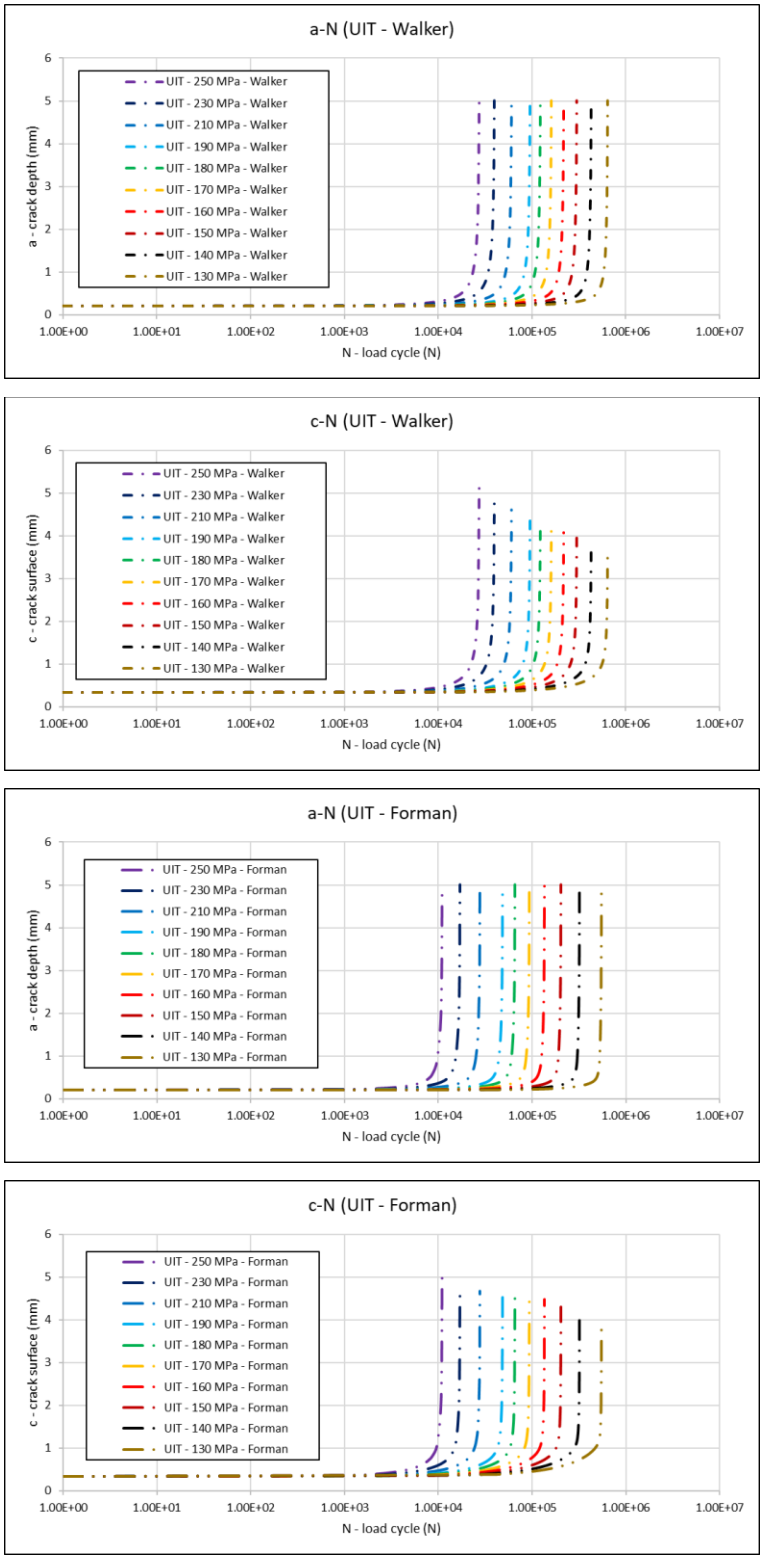

Figure 97: Fatigue crack growth analysis results of 5083-H11 AL under UIT condition for Walker vs Forman, crack depth and crack surface against the number of cycles for the whole stress level ranges

(B.8) 2024-T351 AL

Figure 98 and Figure 99 display diagrammatically fatigue crack growth analysis results of 2024-T351 AL under the AW and the UIT conditions for Walker and Forman models. Crack depth and crack surface versus the number of cycles are displayed in these figures.

It should be noted that 2024-T351 AL was a plate and the impact of the stress concentration has been avoided (Rodopoulos et al., 2007). In addition to that the fitting constants of the models as well as the undesirable residual stresses results could be also other contributing causes on the predictions of the fatigue crack growth. Yet, both models predicted crack propagation state quite well as it can be observed that rises in the fatigue life has led to the successful UIT treatment.

Further, both models evaluated the fatigue crack growth of the material still fairly satisfactory for both conditions considering the fact that it is a comparison among BR and UIT. As already stated, the weld imperfections play a pivotal role in diminishing fatigue strength and increasing fatigue crack growth rate of the material. Since it is BR versus UIT, it is difficult to make a good comparison between them considering the fact that Walker and Forman fatigue crack growth models were utilized for describing the behaviour of this material under these domains.

Apart from that, there were still some unknowns fatigue parameters for this material. Considered the fact that the weld defects generally cause severe damage to the welded structures like at the weld toe. Hence, these models can be employed to display such phenomena under the AW and the UIT conditions way better.

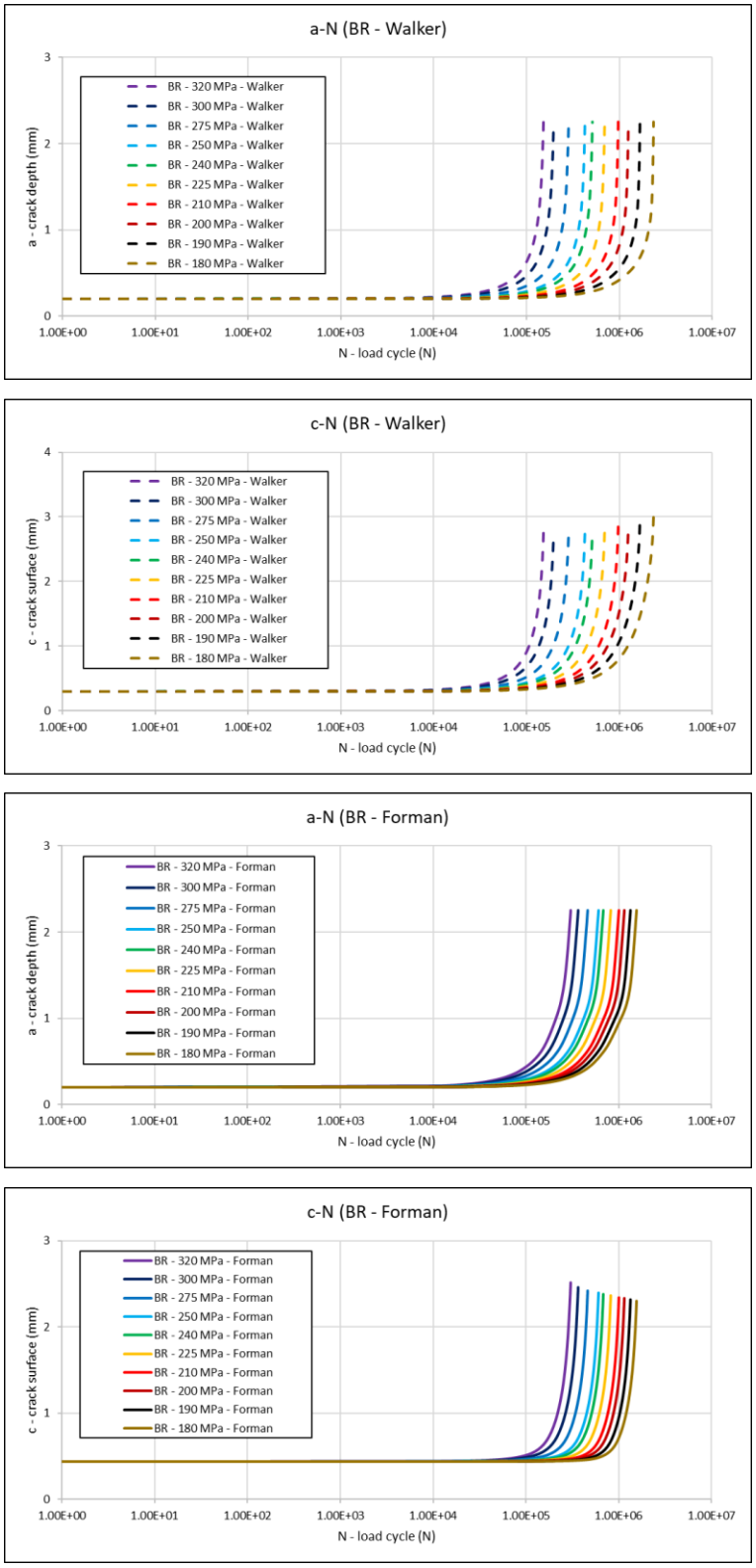

Figure 98: Fatigue crack growth analysis results of 2024-T351 AL for BR condition for Walker vs Forman, crack depth and crack surface against the number of cycles for the whole stress level ranges

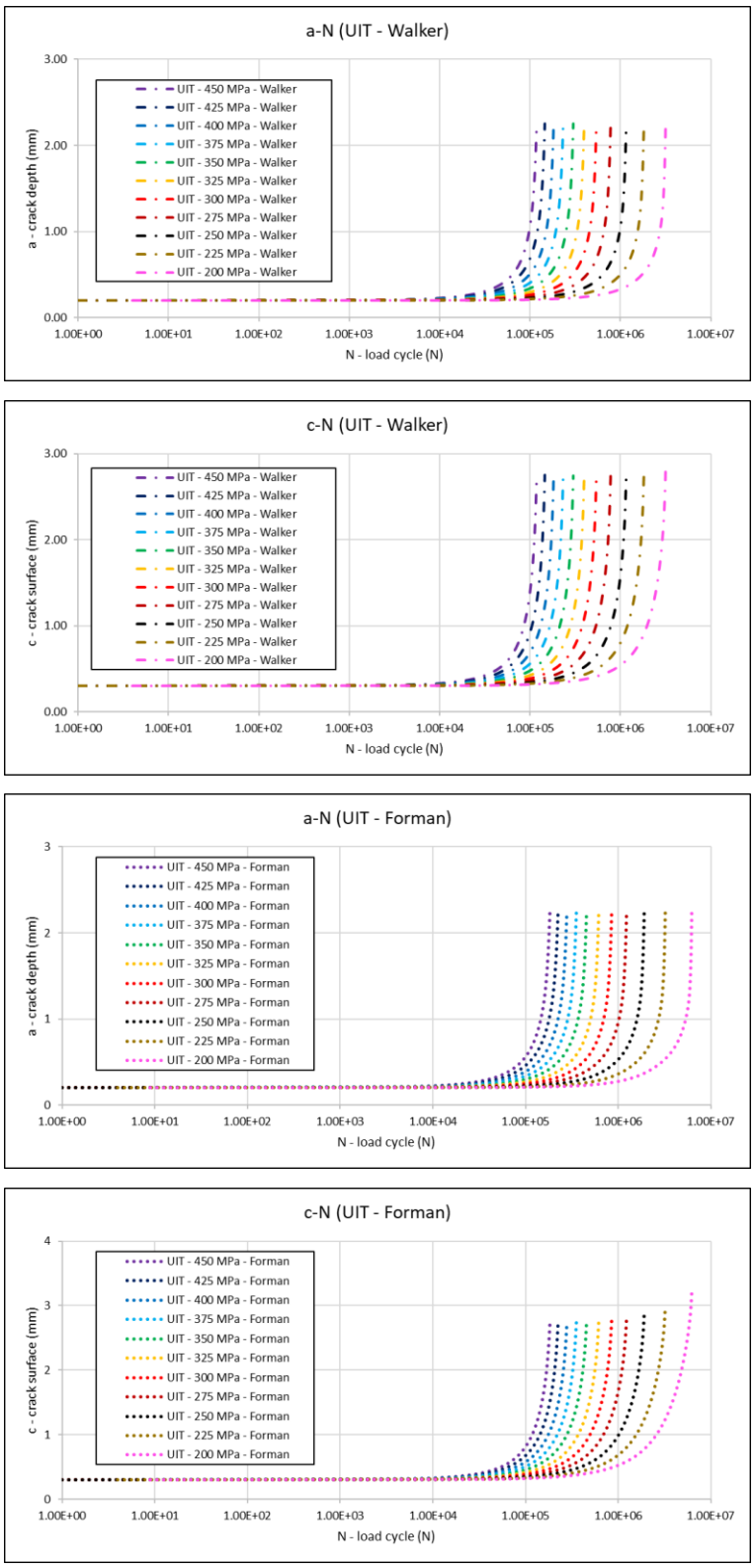

Figure 99: Fatigue crack growth analysis results of 2024-T351 AL under UIT condition for Walker vs Forman, crack depth and crack surface against the number of cycles for the whole stress level ranges

(C) Crack Shape Evolution Curves

(C.1) 5083-H311 AL

Figure 100 and Figure 101 and the figures here in Appendix (C.1) depict graphically crack shape evolution analysis results of 5083-H311 AL under the AW and the UIT conditions for Walker and Forman models as well as their comparisons under both conditions for that model. Crack depth versus crack surface is displayed in these figures.

From $AW-W-110$, $AW-W-90$ and $UIT-F-90$ which are the figures in Appendix (C.1), it should be pointed out that the last two curves are the way that Walker and Forman models tried to determine the final crack size for that condition.

For example, from $UIT-W-90$ and $UIT-F-90$ which are the figures in Appendix (C.1) versus that of the AW condition, it should be noted that UIT incredibly retarded crack initiation phase as well as remarkably slowed down crack propagation phase in depth and on surface so that the fatigue life was noticeably improved .

For instance, comparing $AWvsUIT-W-90$ and $AWvsUIT-F-90$ together, it demonstrates that Forman model predicted the crack growth and the crack shape evolution completely satisfactory. It is quite fascinating to note that the crack was at first advancing quicker into depth and on surface after reducing the stress it is a little bit slowed down for the AW condition. However, it is noteworthy that after achieving a certain depth, it still commenced expanding significantly for the AW condition. After impact treatment, the crack is extremely slowed down which indicates that UIT considerably enlarge the fatigue life.

From $AWvsUIT-F-90$, such phenomena can be comprehended as how effective UIT can close the surface of the crack to further delay crack initiation state as well as retarding crack propagation phase. On top of that, the crack behaviour and how fast the crack grows in depth and on surface can be properly comprehended.

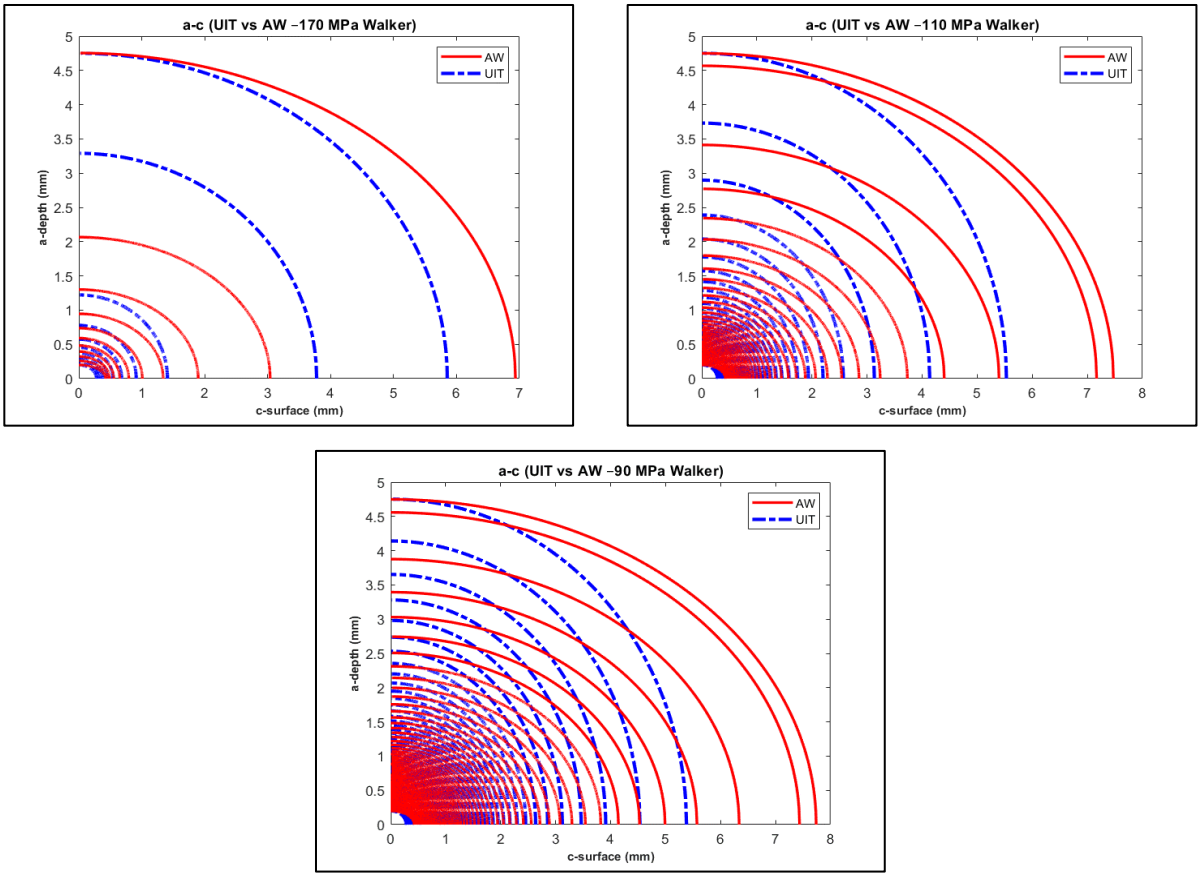

Figure 100: Crack shape evolution analysis results of 5083-H311 AL for AW vs UIT conditions for Walker, crack depth against crack surface for covering stress level ranges

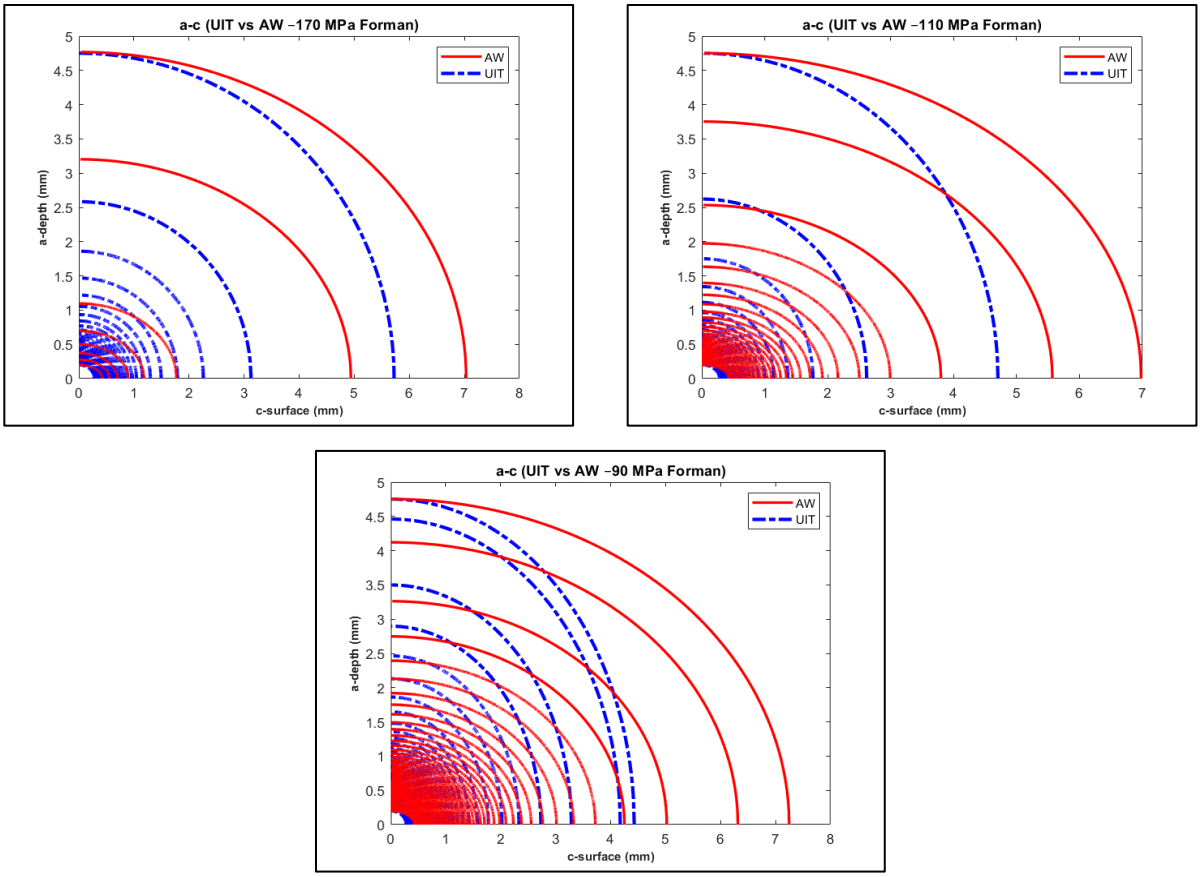

Figure 101: Crack shape evolution analysis results of 5083-H311 AL for AW vs UIT conditions for Forman, crack depth against crack surface for covering stress level ranges

The below figures are the crack shape evolution curves for 5083-H311 AL under the AW and the UIT conditions for Walker model.

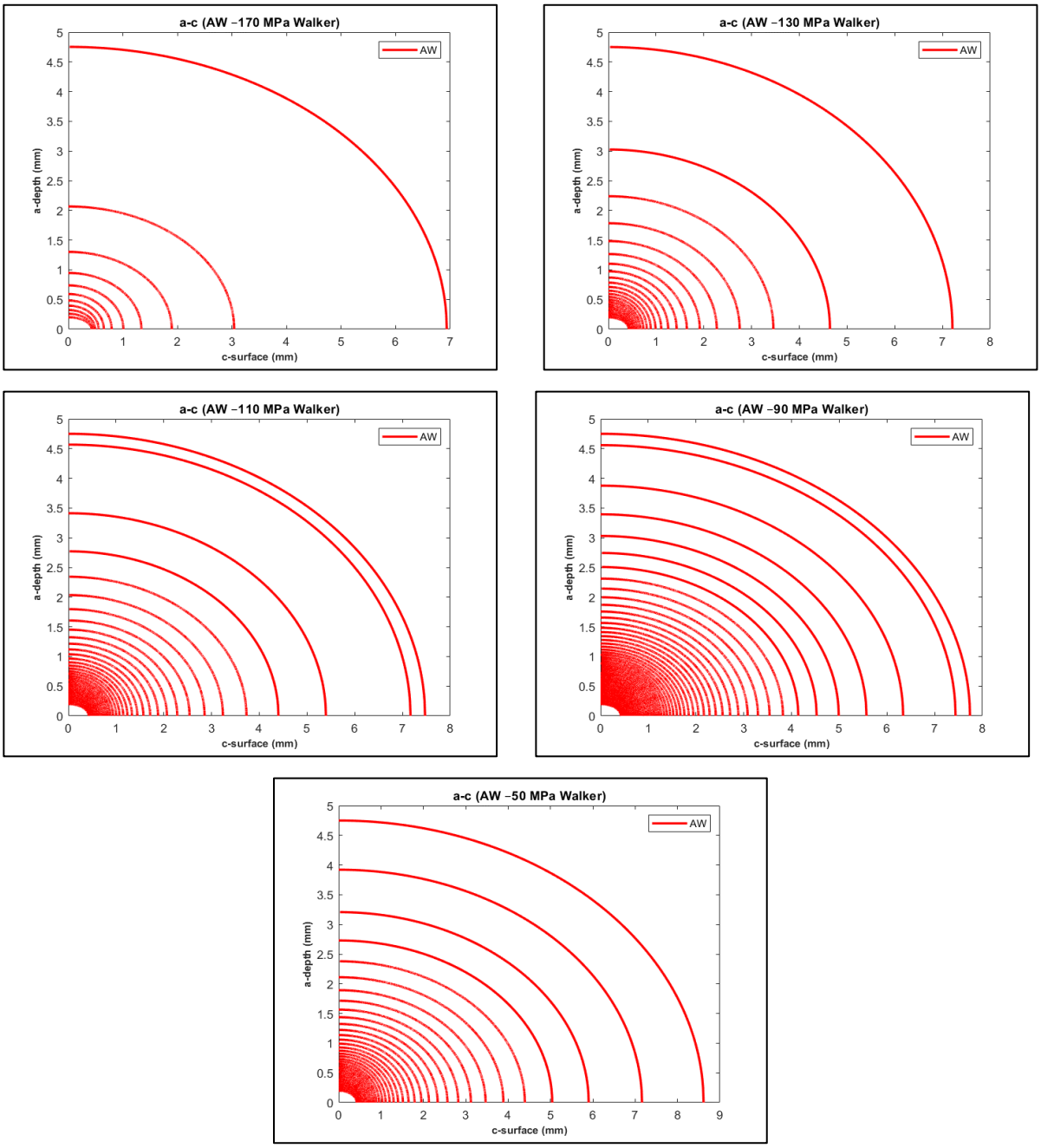

Figure 102: Crack shape evolution analysis results of 5083-H311 AL under AW condition for Walker, crack depth against crack surface for covering stress level ranges

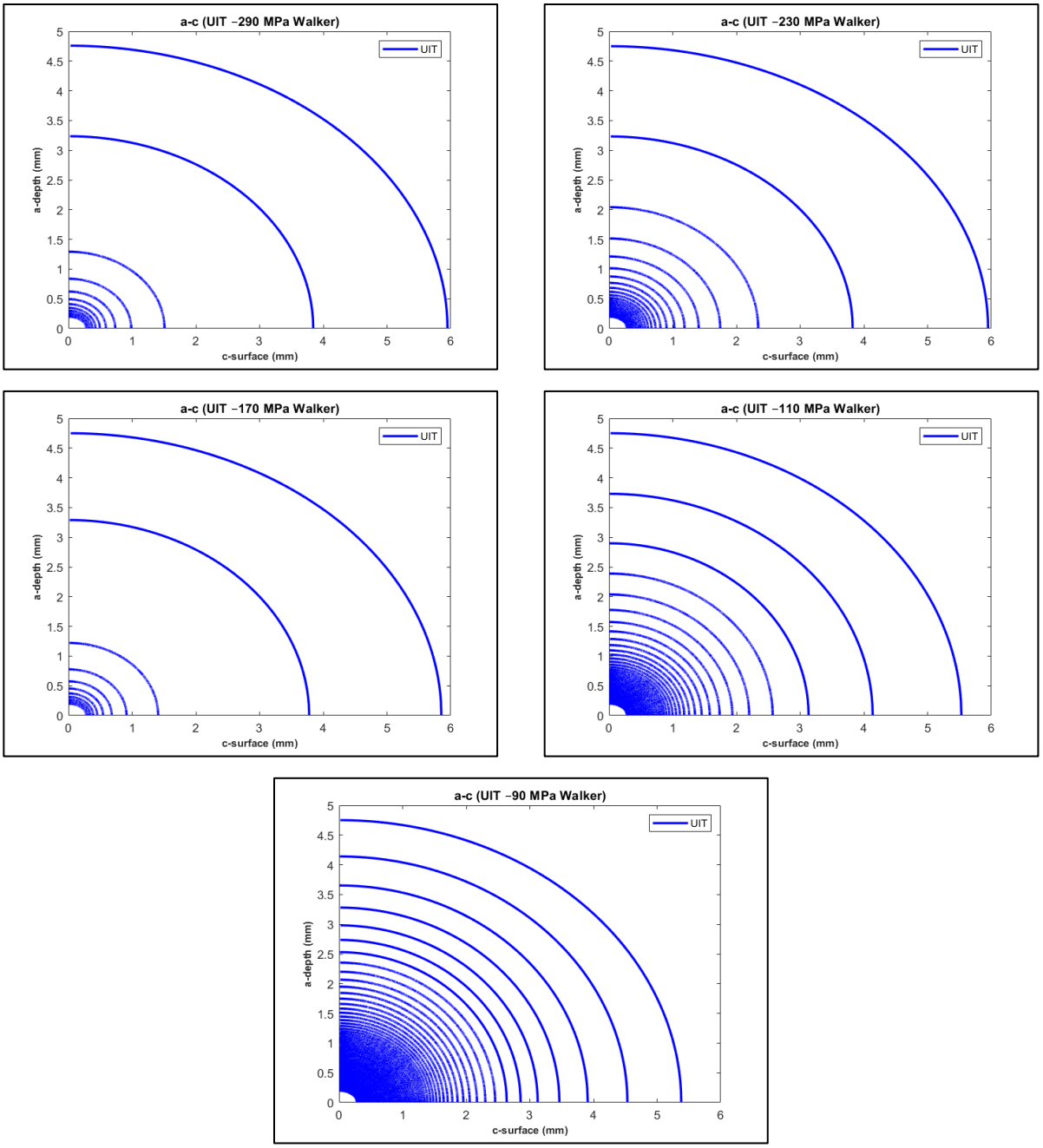

Figure 103: Crack shape evolution analysis results of 5083-H311 AL under UIT condition for Walker, crack depth against crack surface for covering stress level ranges

The below figures are the crack shape evolution curves for 5083-H311 AL under the AW and the UIT conditions for Forman model.

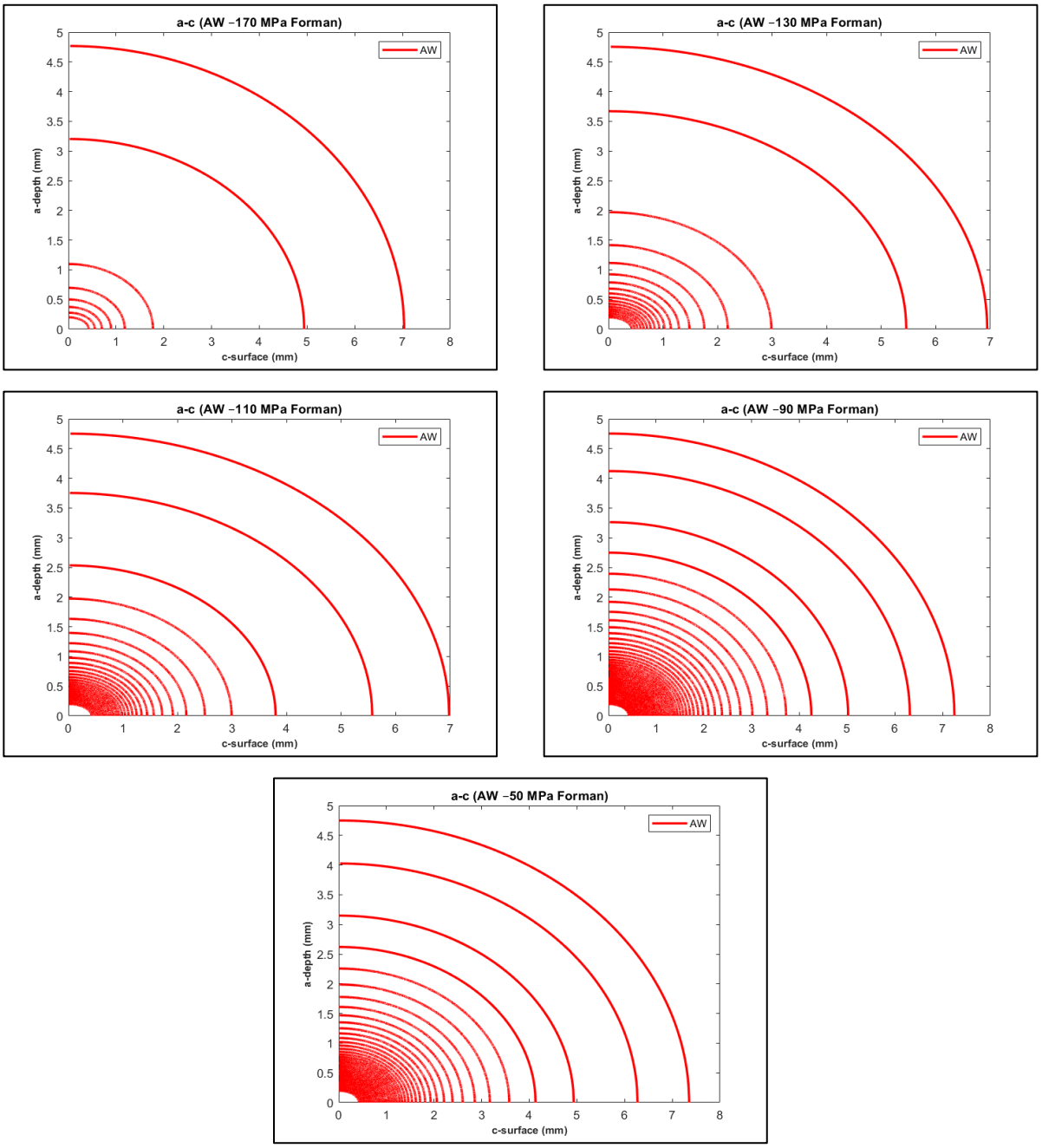

Figure 104: Crack shape evolution analysis results of 5083-H311 AL under AW condition for Forman, crack depth against crack surface for covering stress level ranges

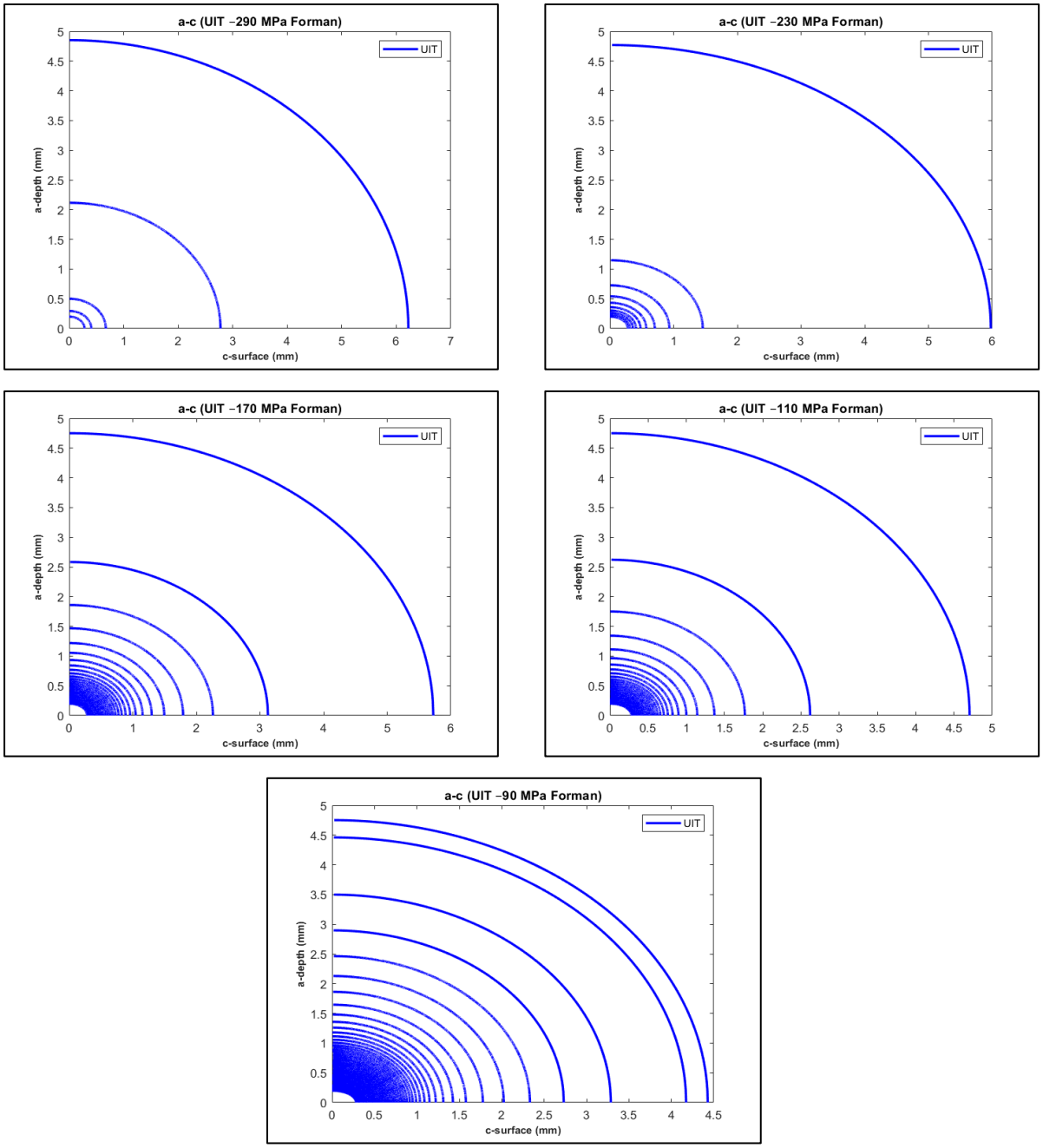

Figure 105: Crack shape evolution analysis results of 5083-H311 AL under AW condition for Forman, crack depth against crack surface for covering stress level ranges

(C.2) CSA 350W ST

Figure 106, Figure 107 and the figures here in Appendix (C.2) display diagrammatically crack shape evolution analysis results of CSA350W ST AL under the AW and the UIT conditions for Walker and Forman models as well as their comparisons under both conditions for that model. Crack depth versus crack surface is displayed in these figures.

As an example, from $UIT - W - 250$ and $UIT - F - 250$ which are the figures in Appendix (C.2) that of the AW condition, it should be pointed out that UIT incredibly retarded crack initiation phase as well as remarkably slowed down crack propagation phase in depth and on surface so that the fatigue life was noticeably improved .

For instance, comparing $AWvsUIT - W - 250$ and $AWvsUIT - F - 250$ together, it demonstrates that Forman model anticipated the crack growth and the crack shape evolution quite well. It is very interesting to note that the crack was at first advancing quicker into depth and on surface after reducing the stress it is a little bit slowed down for the AW condition. However, it is worth noting that after achieving a certain depth, it still commenced expanding significantly for the AW condition. After impact treatment, the crack is extremely slowed down which indicates that UIT considerably enlarge the fatigue life.

From $AWvsUIT - F - 250$, such phenomena can be seen as how effective UIT can close the surface of the crack to further delay crack initiation state as well as retarding crack propagation phase. Furthermore, the crack behaviour and how fast the crack grows in depth and on surface can be properly seen.

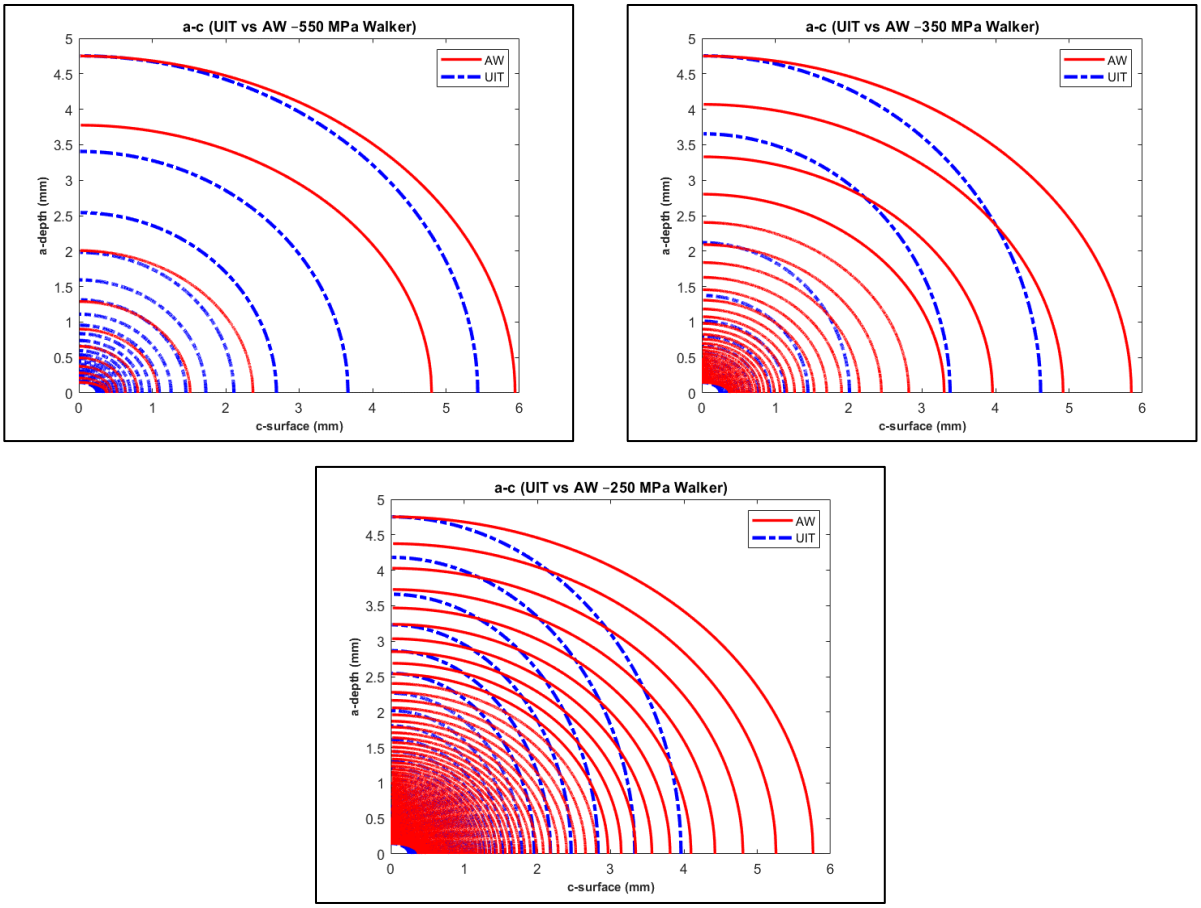

Figure 106: Crack shape evolution analysis results of CSA 350W ST for AW vs UIT conditions for Walker, crack depth against crack surface for covering stress level ranges

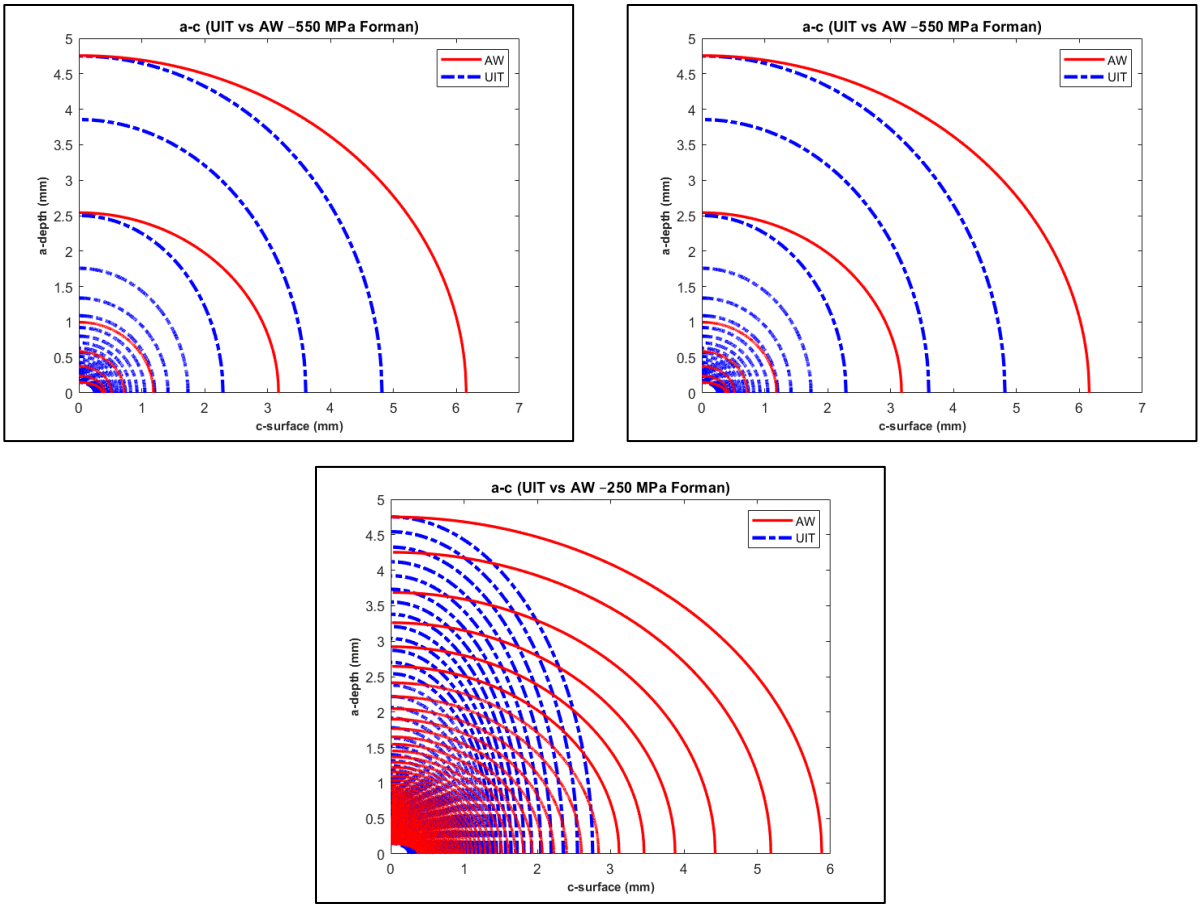

Figure 107: Crack shape evolution analysis results of CSA 350W ST for AW vs UIT conditions for Forman, crack depth against crack surface for covering stress level ranges

The below figures are the crack shape evolution curves for CSA 350W ST under the AW and the UIT conditions for Walker model.

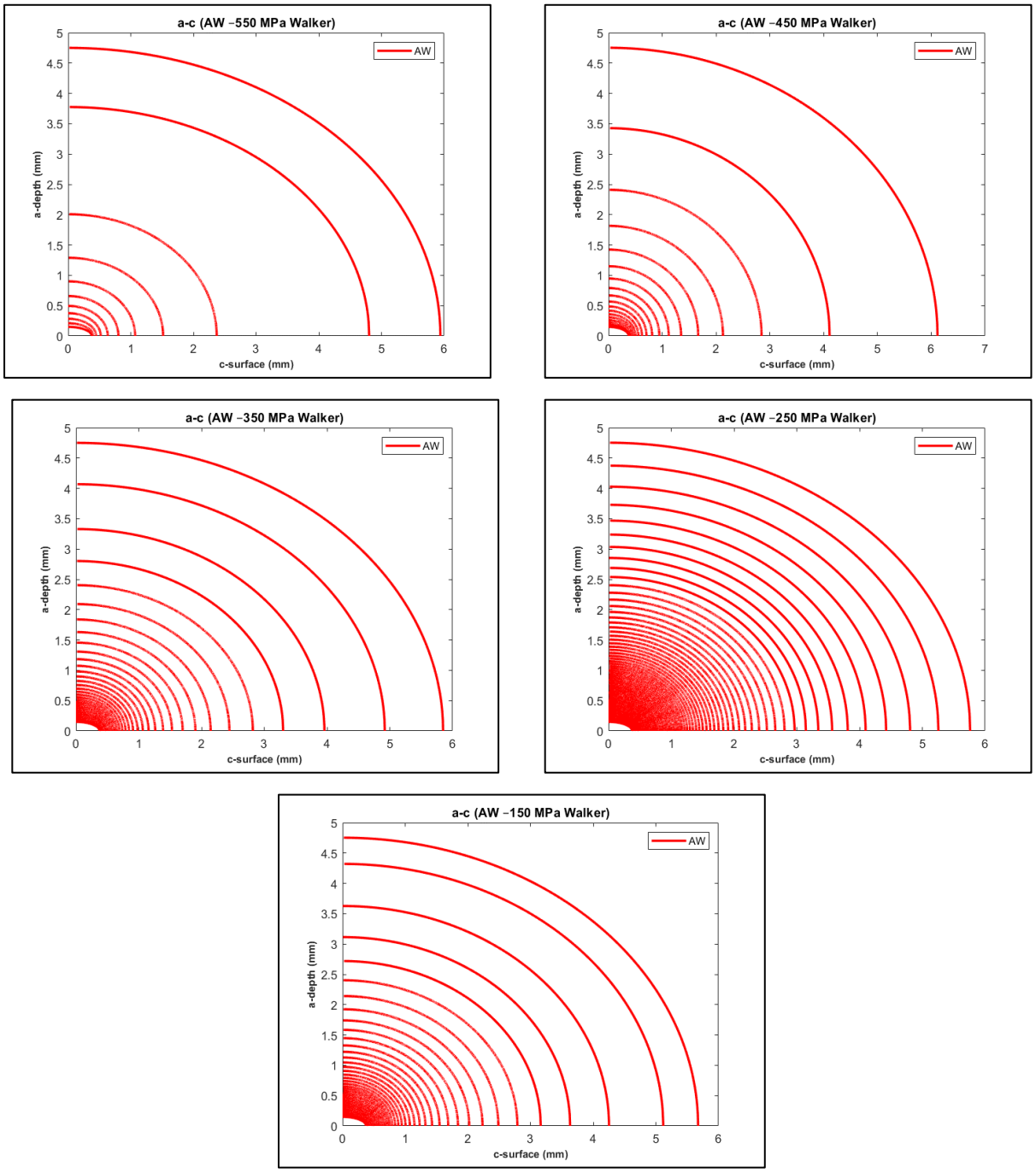

Figure 108: Crack shape evolution analysis results of CSA 350W ST under AW condition for Walker, crack depth against crack surface for covering stress level ranges

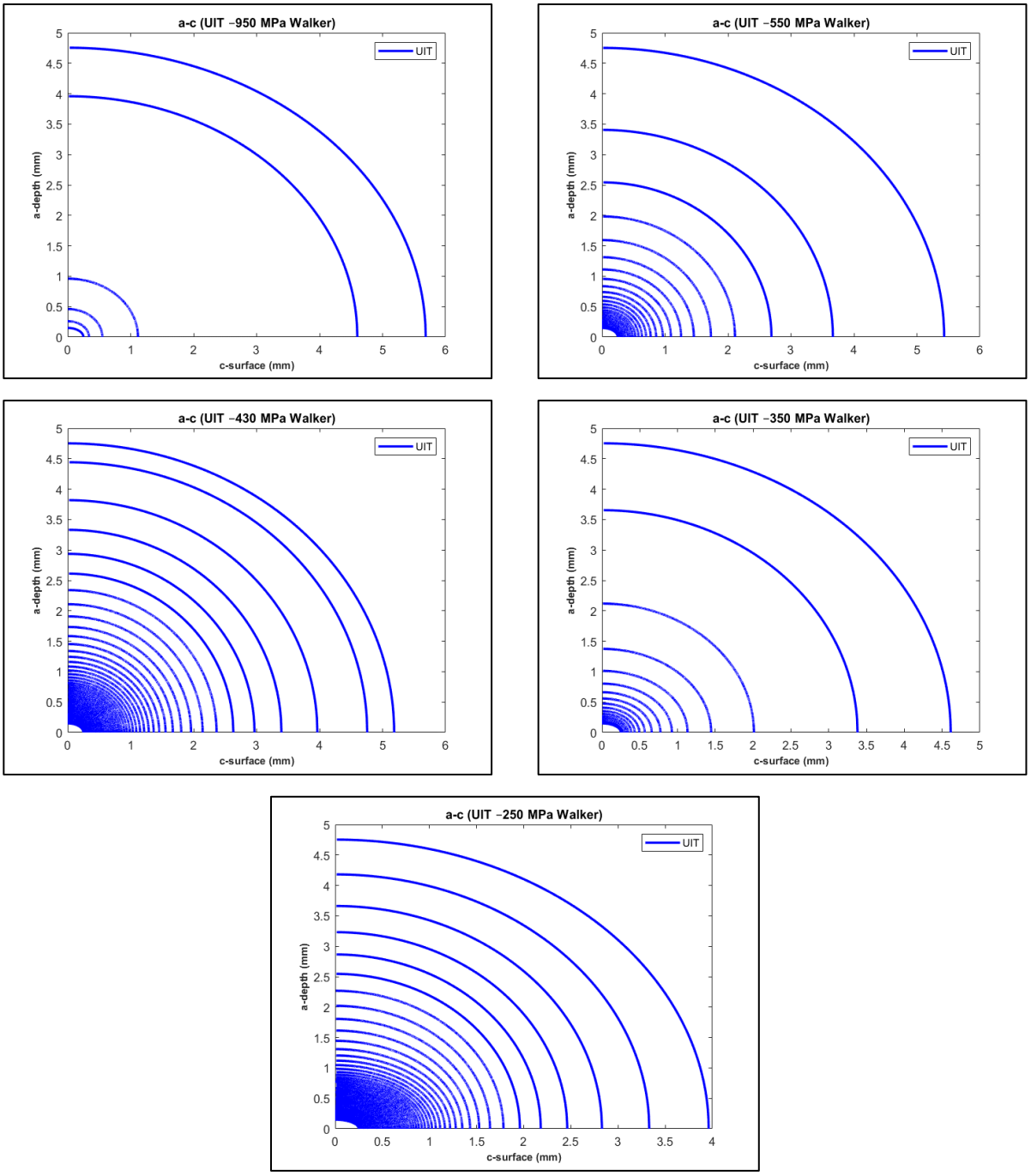

Figure 109: Crack shape evolution analysis results of CSA 350W ST under UIT condition for Walker, crack depth against crack surface for covering stress level ranges

The below figures are the crack shape evolution curves for CSA 350W ST under the AW and the UIT conditions for Forman model.

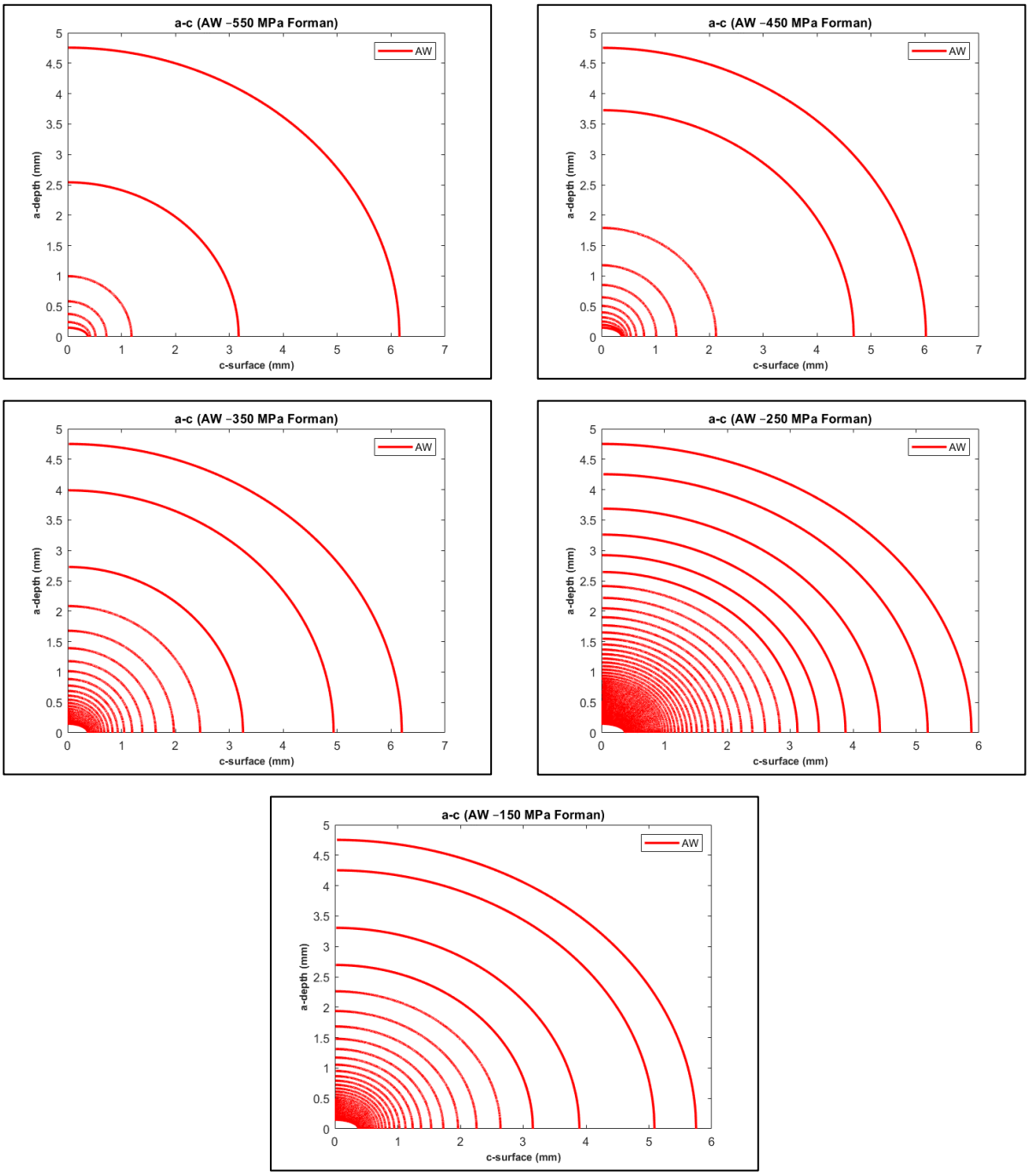

Figure 110: Crack shape evolution analysis results of CSA 350W ST under AW condition for Forman, crack depth against crack surface for covering stress level ranges

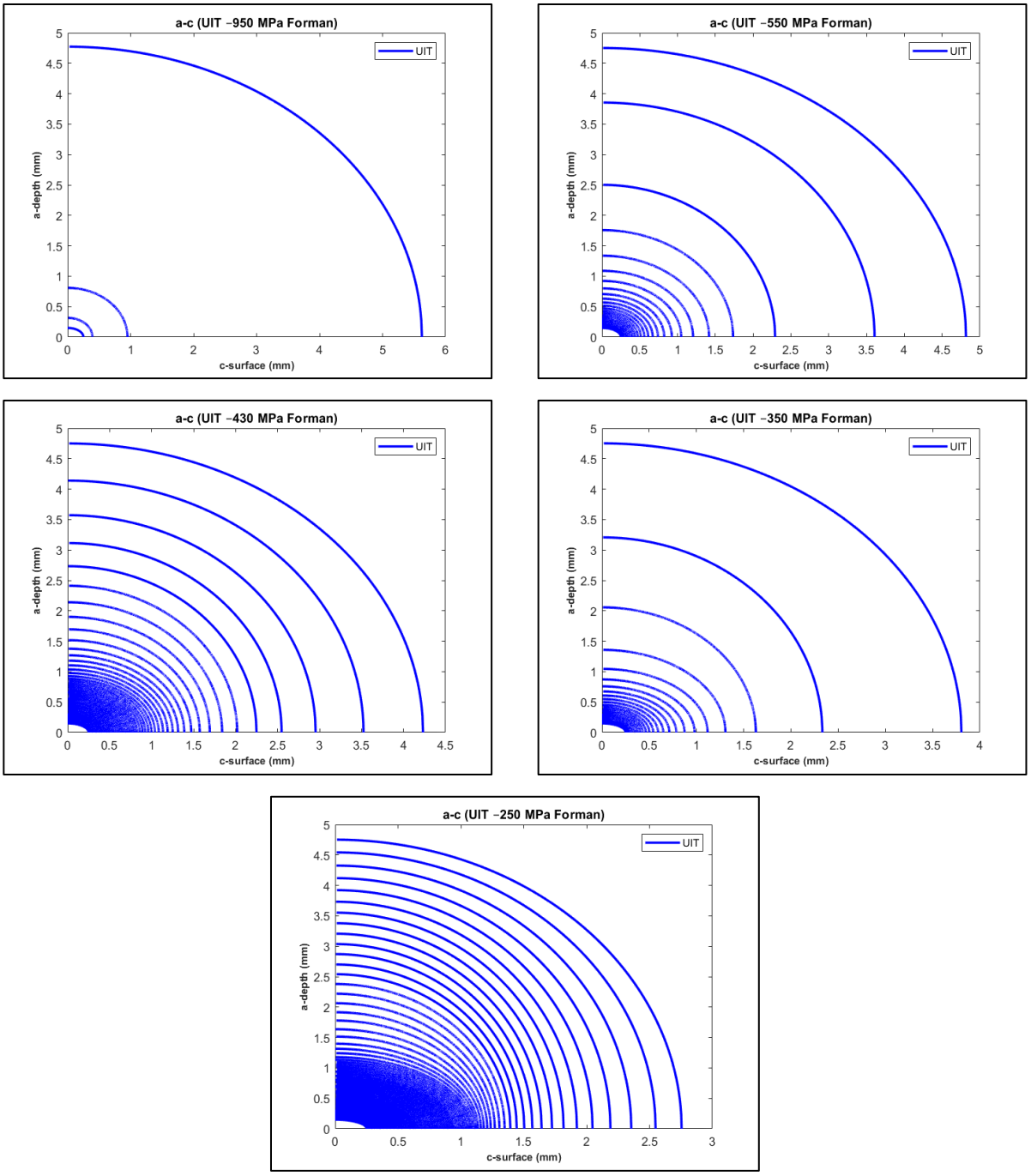

Figure 111: Crack shape evolution analysis results of CSA 350W ST under UIT condition for Forman, crack depth against crack surface for covering stress level ranges

(C.3) A514 ST

The below figures are the crack shape evolution curves for A514 ST under the AW and the UIT conditions for Walker model.

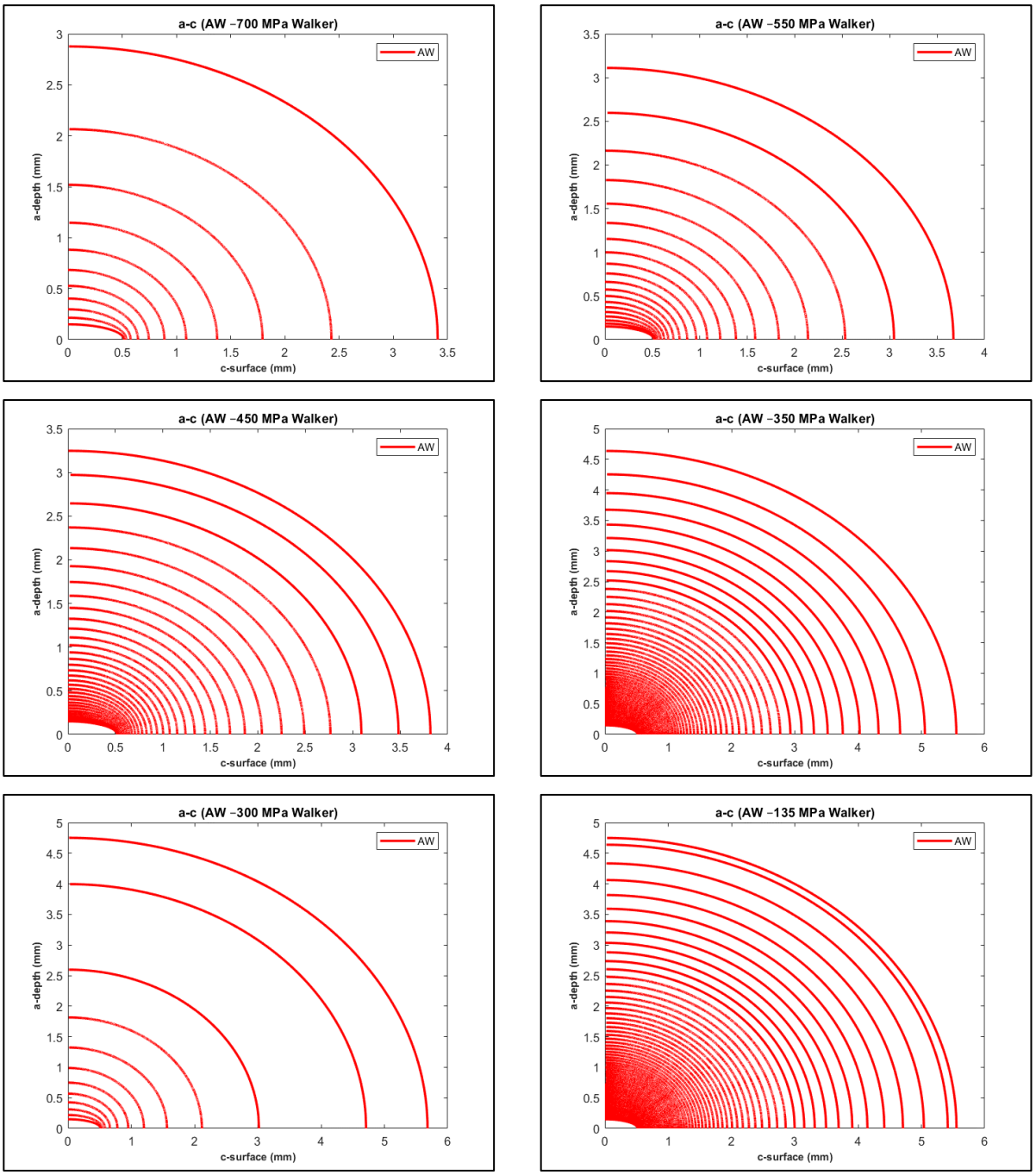

Figure 112: Crack shape evolution analysis results of A514 ST under AW condition for Walker, crack depth against crack surface for covering stress level ranges

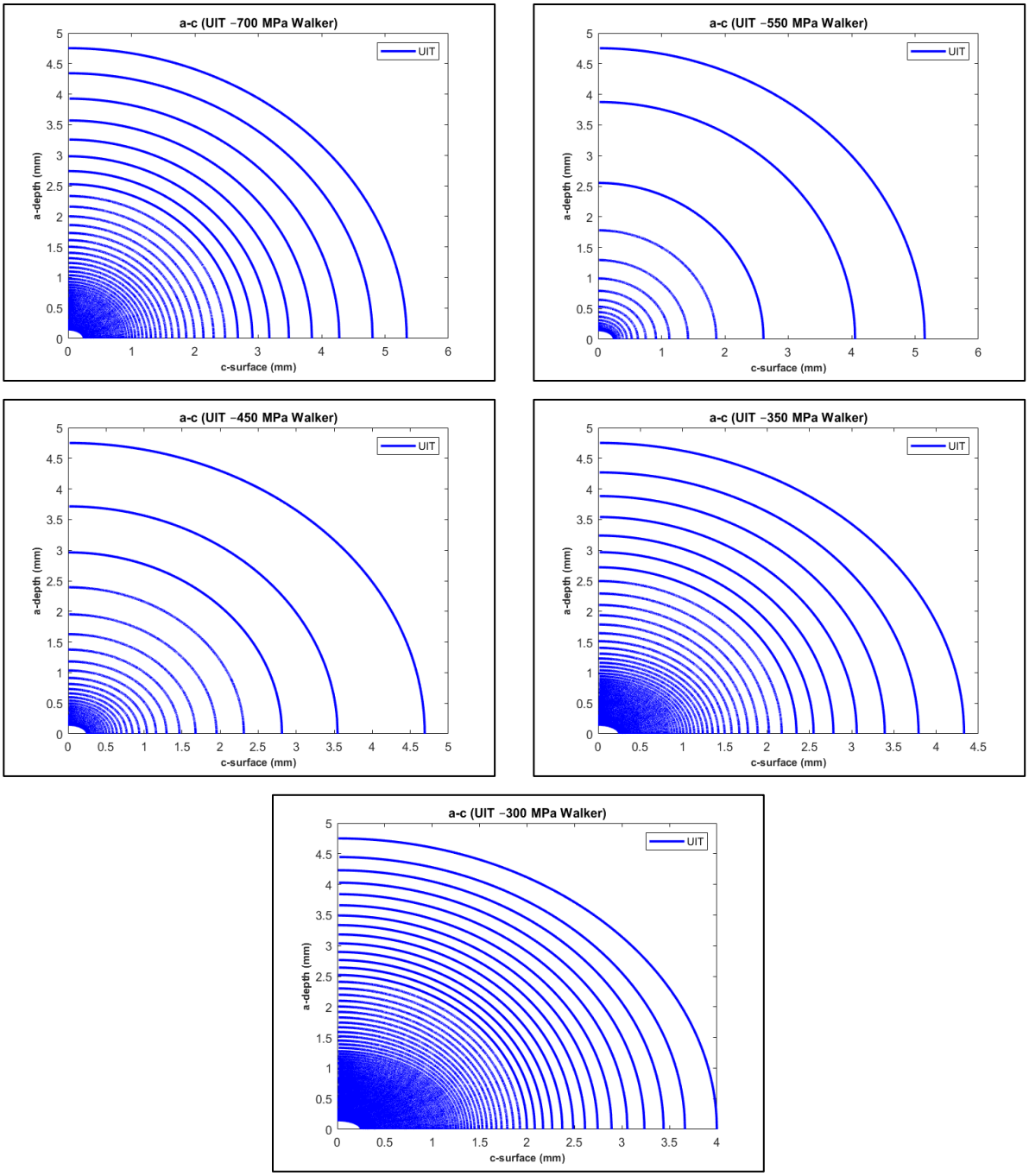

Figure 113: Crack shape evolution analysis results of A514 ST under UIT condition for Walker, crack depth against crack surface for covering stress level ranges

The below figures are the crack shape evolution curves for A514 ST under the AW and the UIT conditions for Forman model.

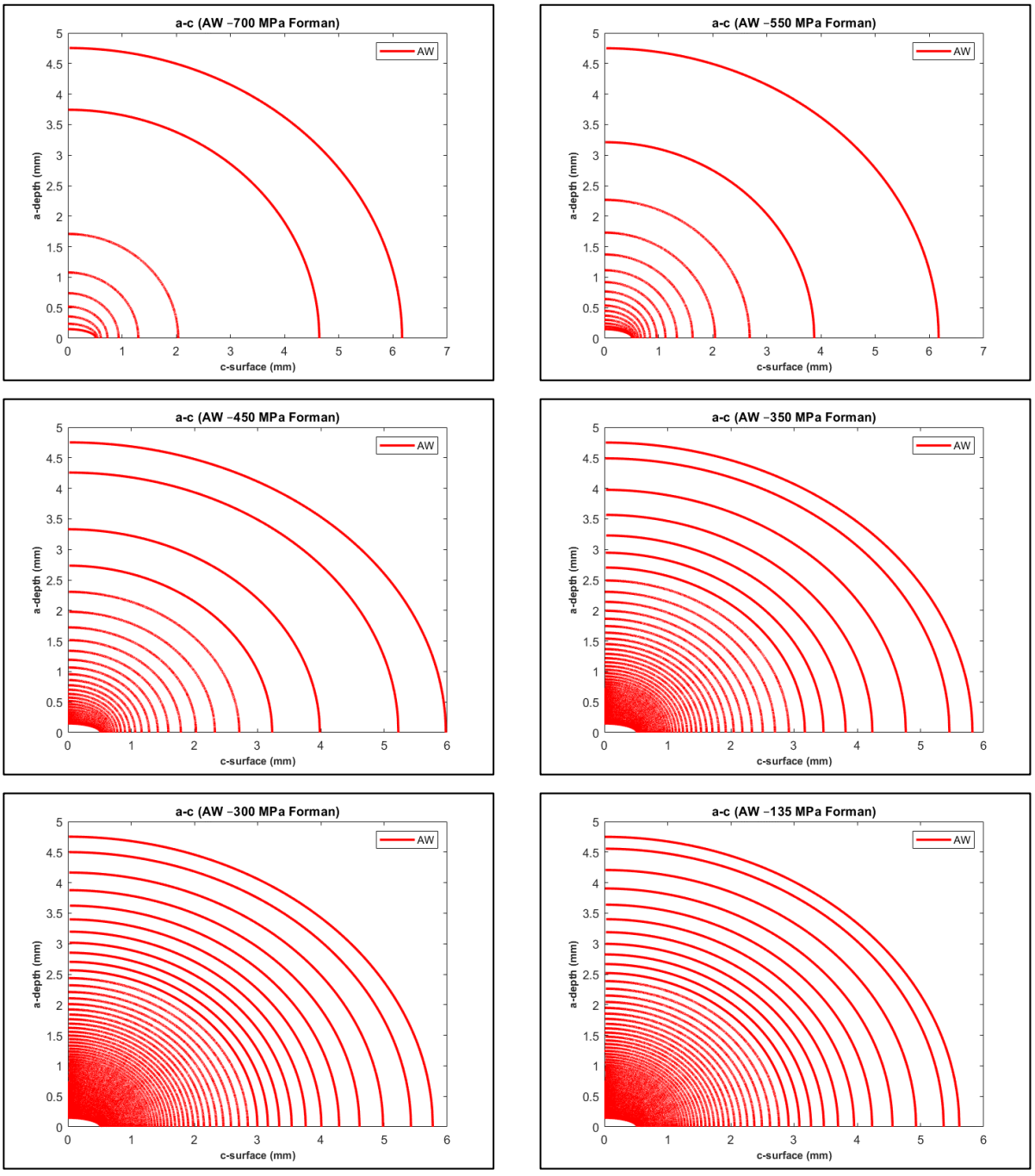

Figure 114: Crack shape evolution analysis results of A514 ST under AW condition for Forman, crack depth against crack surface for covering stress level ranges

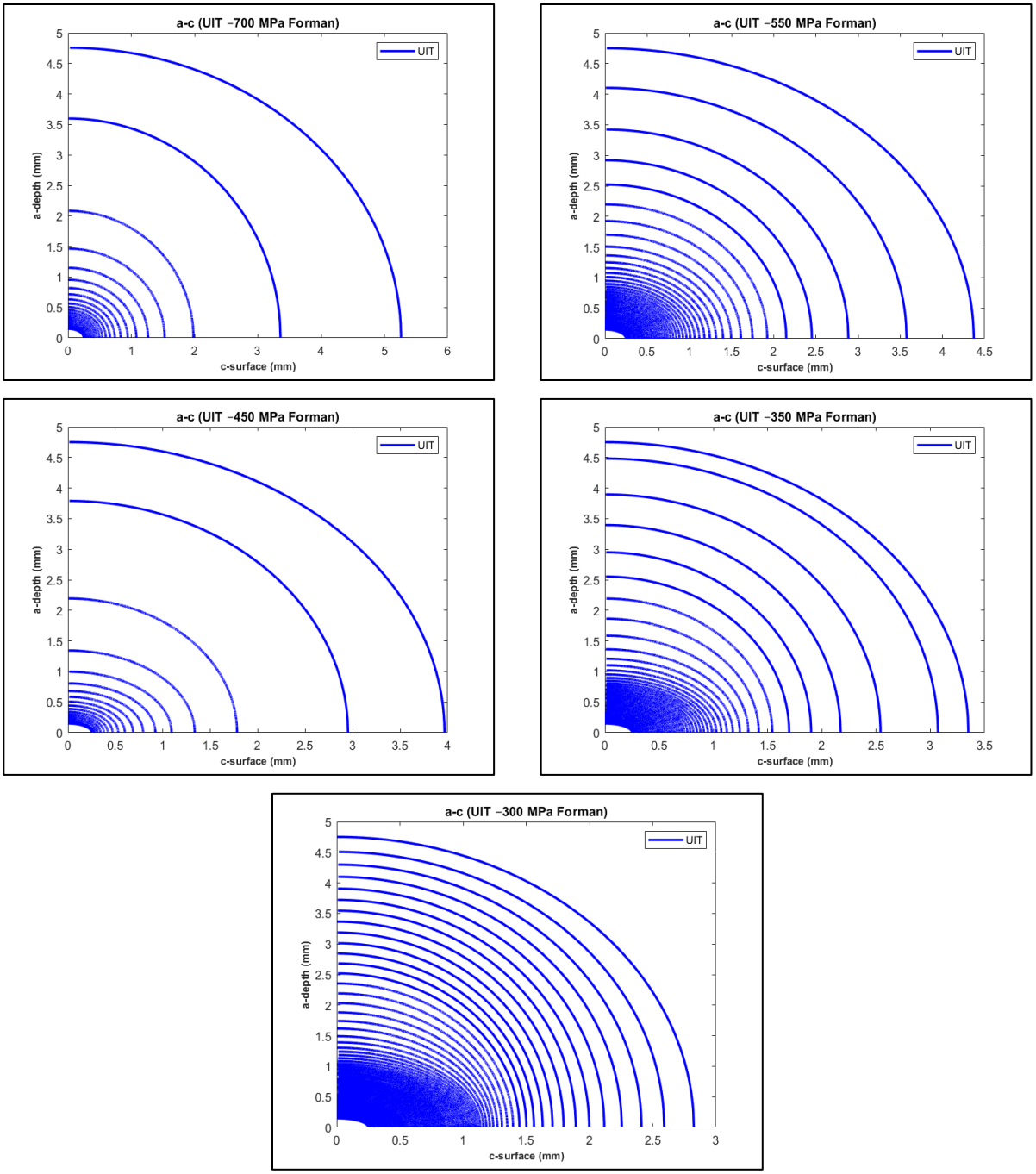

Figure 115: Crack shape evolution analysis results of A514 ST under UIT condition for Forman, crack depth against crack surface for covering stress level ranges

(C.4) S355

Figure 116, Figure 117and the figures here in Appendix (C.4) display diagrammatically crack shape evolution analysis results of S355 under the AW and the UIT conditions for Walker and Forman models as well as their comparisons under both conditions for that model. Crack depth versus crack surface is displayed in these figures.

From $AW-W-250$, $UIT-W-350$ and $UIT-W-200$ and $AW-F-200$ which are the figures in Appendix (C.4), it should be pointed out that the last two curves are the way that Walker and Forman models tried to determine the final crack size for that condition.

As an example, from $UIT-W-200$ and $UIT-F-200$ which are the figures in Appendix (C.4) that of the AW condition, it should be pointed out that UIT incredibly retarded crack initiation phase as well as remarkably slowed down crack propagation phase in depth and on surface so that the fatigue life was noticeably improved . It should be emphasized that the surface of the crack at $250\,MPa$ and $200\,MPa$ advanced in a really slow paced after impact treating the weld toe.

For instance, comparing $AWvsUIT-W-200$ and $AWvsUIT-F-200$ together, it demonstrates that Forman model anticipated the crack growth and the crack shape evolution quite well. It is very interesting to note that the crack was at first advancing quicker into depth and on surface after reducing the stress it is a little bit slowed down for the AW condition. However, it is worth noting that after achieving a certain depth, it still commenced expanding significantly for the AW condition. After impact treatment, the crack is extremely slowed down which indicates that UIT considerably enlarge the fatigue life. On top of that, it is essential to mention that Walker Model could not display properly the crack growth and the crack shape evolution for this material in comparison to Forman model.

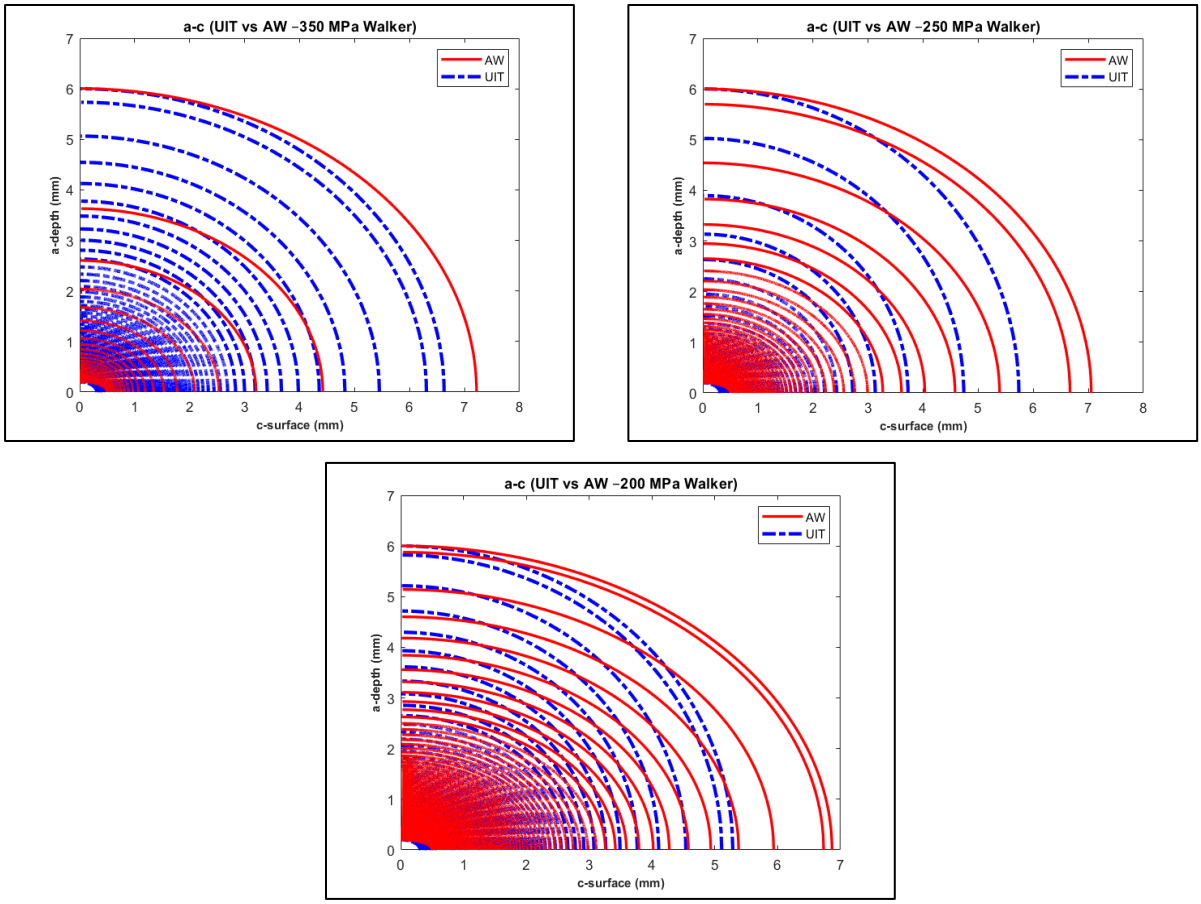

Figure 116: Crack shape evolution analysis results of S355 for AW vs UIT conditions for Walker, crack depth against crack surface for covering stress level ranges

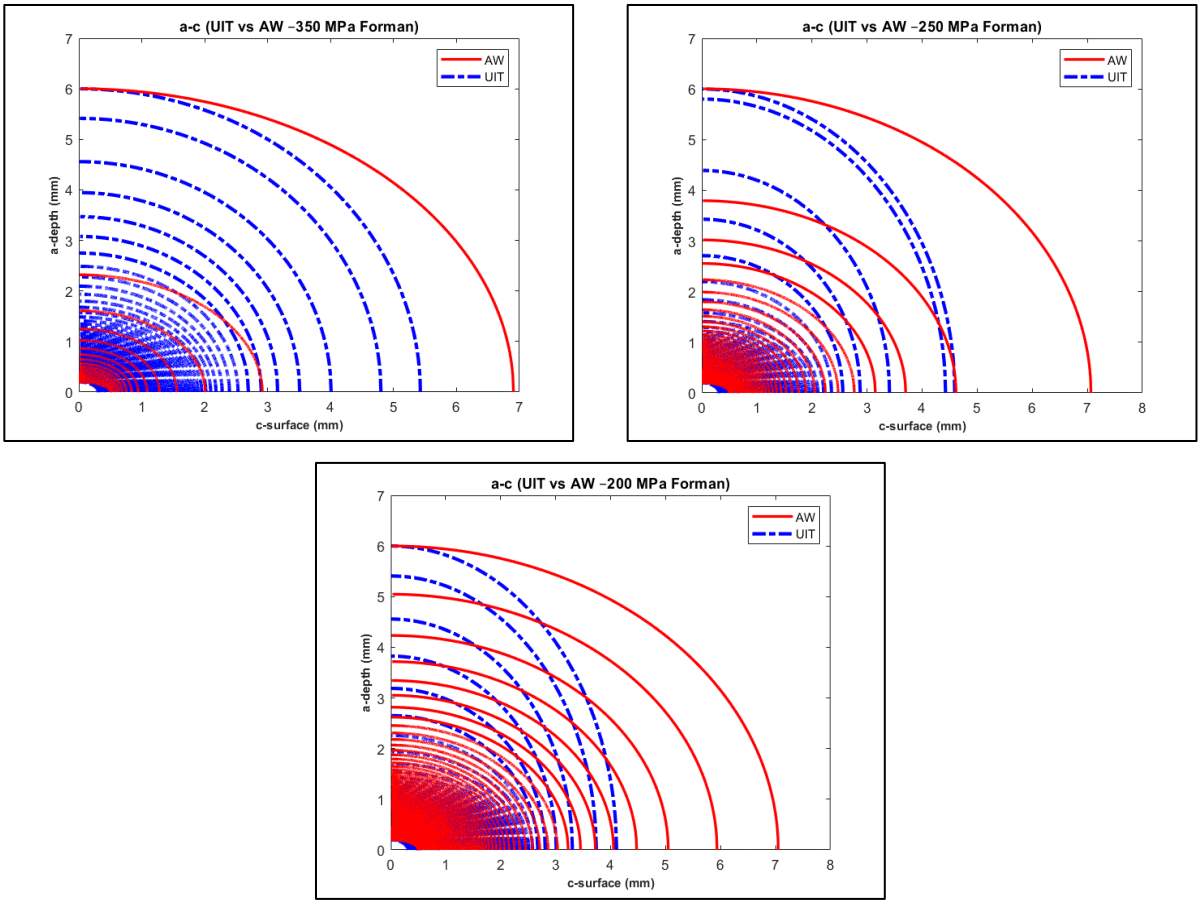

Figure 117: Crack shape evolution analysis results of S355 for AW vs UIT conditions for Forman, crack depth against crack surface for covering stress level ranges

The below figures are the crack shape evolution curves for CSA 350W ST under the AW and the UIT conditions for Walker model.

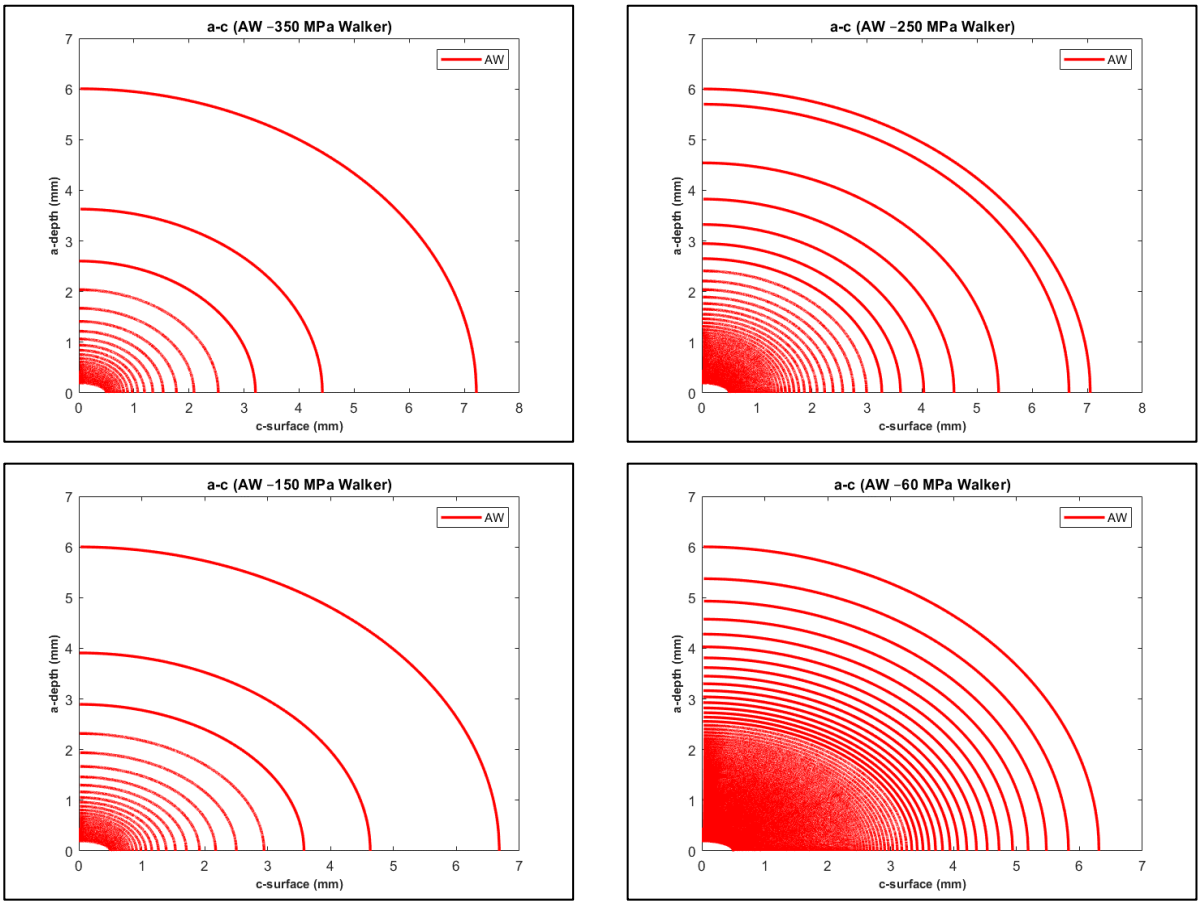

Figure 118: Crack shape evolution analysis results of S355 under AW condition for Walker, crack depth against crack surface for covering stress level ranges

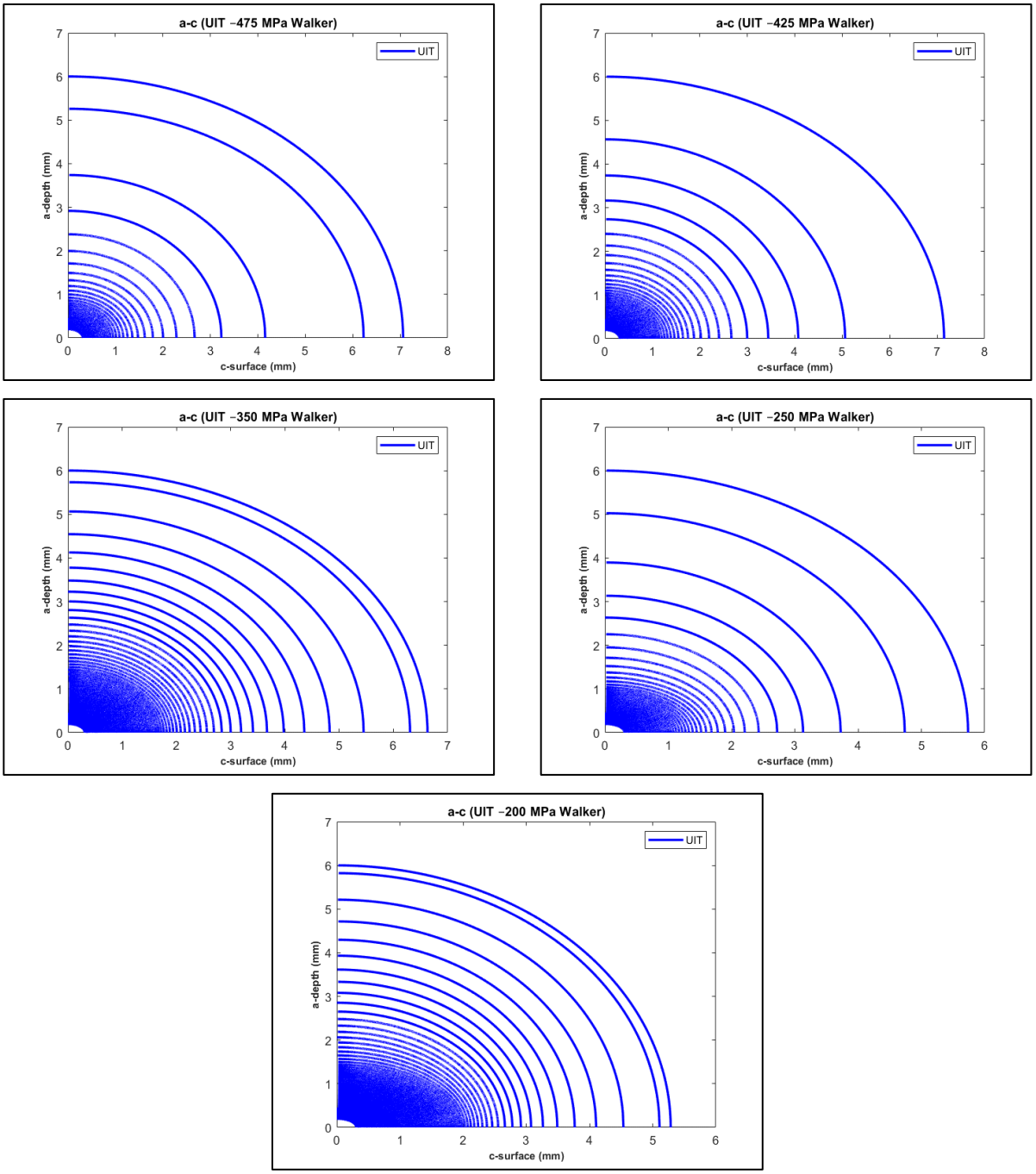

Figure 119: Crack shape evolution analysis results of S355 under UIT condition for Walker, crack depth against crack surface for covering stress level ranges

The below figures are the crack shape evolution curves for CSA 350W ST under the AW and the UIT conditions for Forman model.

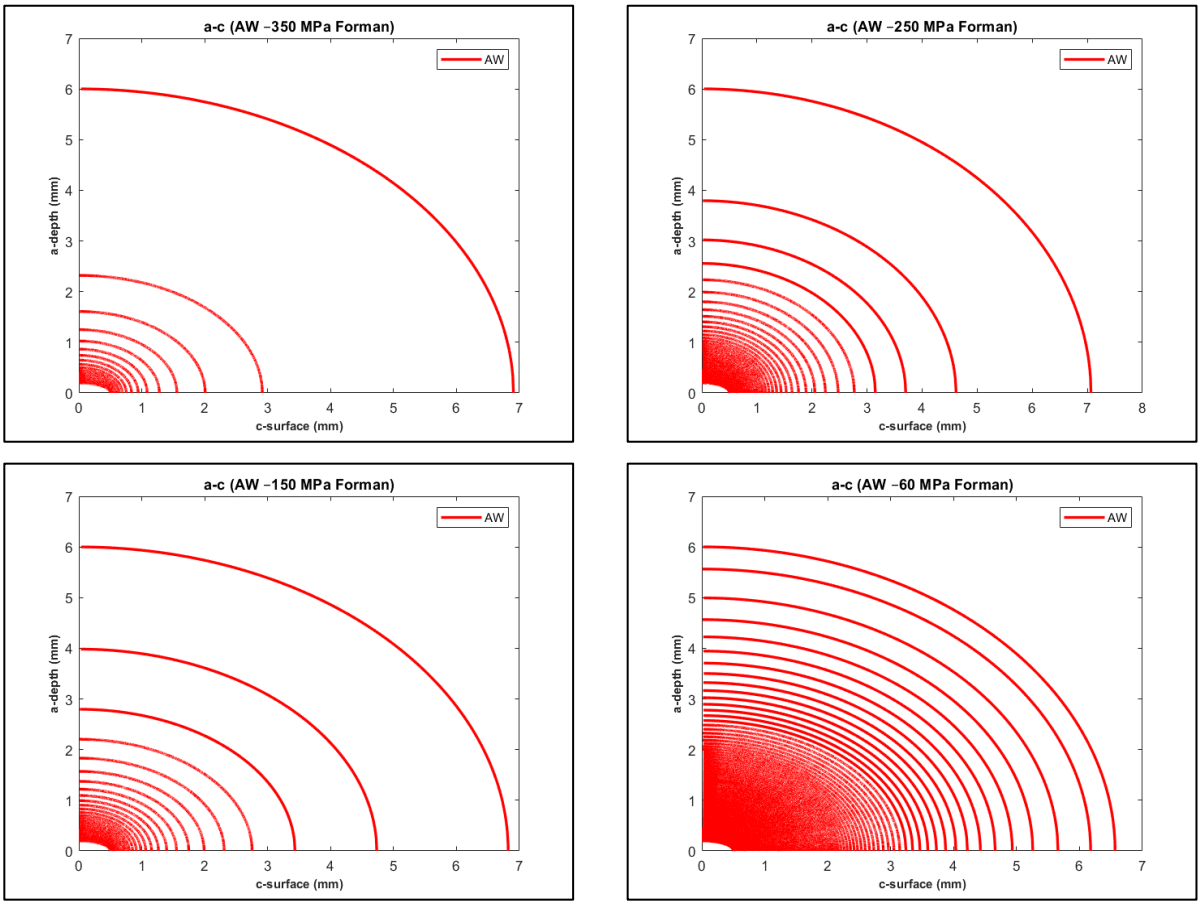

Figure 120: Crack shape evolution analysis results of S355 under AW condition for Forman, crack depth against crack surface for covering stress level ranges

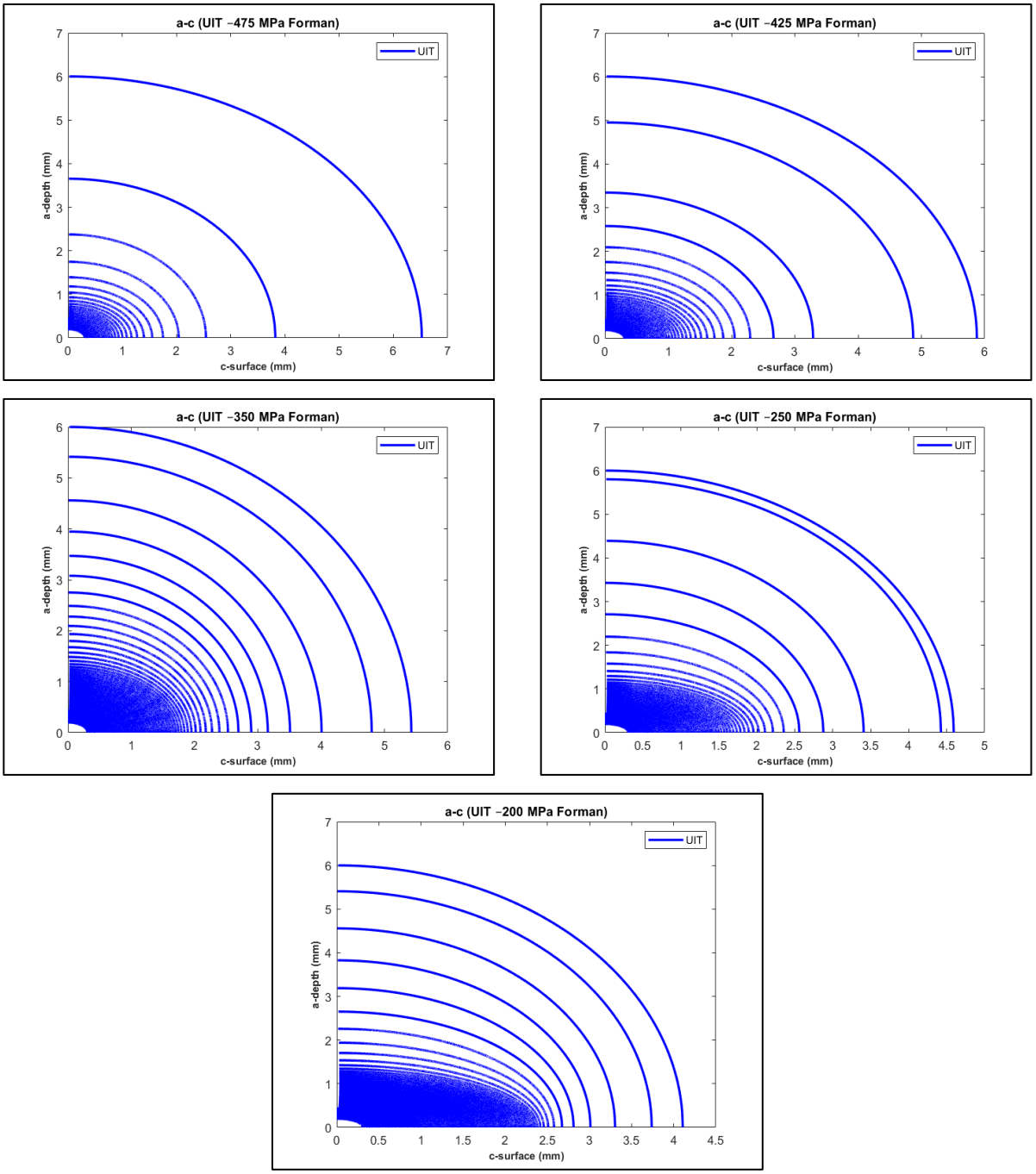

Figure 121: Crack shape evolution analysis results of S355 under UIT condition for Forman, crack depth against crack surface for covering stress level ranges

(C.5) S460

Figure 122, Figure 123 and the figures here in Appendix (C.5) depict graphically crack shape evolution analysis results of S460 under the AW and the UIT conditions for Walker and Forman models as well as their comparisons under both conditions for that model. Crack depth versus crack surface is displayed in these figures.

From $AW-W-350$, $AW-W-250$, $UIT-W-250$, $UIT-F-200$ and $UIT-W-200$ which are the figures in Appendix (C.5), it should be pointed out that the last two curves are the way that Walker and Forman models tried to determine the final crack size for that condition.

For example, from $UIT-W-200$ and $UIT-F-200$ which are the figures in Appendix (C.5) versus that of the AW condition, it should be noted that UIT incredibly retarded crack initiation phase as well as remarkably slowed down crack propagation phase in depth and on surface so that the fatigue life was noticeably improved .

For instance, comparing $AWvsUIT-W-200$ and $AWvsUIT-F-200$ together, it demonstrates that Forman model predicted the crack growth and the crack shape evolution completely satisfactory. It is quite fascinating to note that the crack was at first advancing quicker into depth and on surface after reducing the stress it is a little bit slowed down for the AW condition. However, it is noteworthy that after achieving a certain depth, it still commenced expanding significantly for the AW condition. After impact treatment, the crack is extremely slowed down which indicates that UIT considerably enlarge the fatigue life.

It should be mentioned here that from $AWvsUIT-W-250$ and $AWvsUIT-F-250$, it looks like that the crack grew really slow in depth and on surface. However, by looking at $AWvsUIT-W-200$, it can be perceived that in reality that is not the case. This is because of frequency increment of the number of cycles in HCF region which was set amount back at that time.

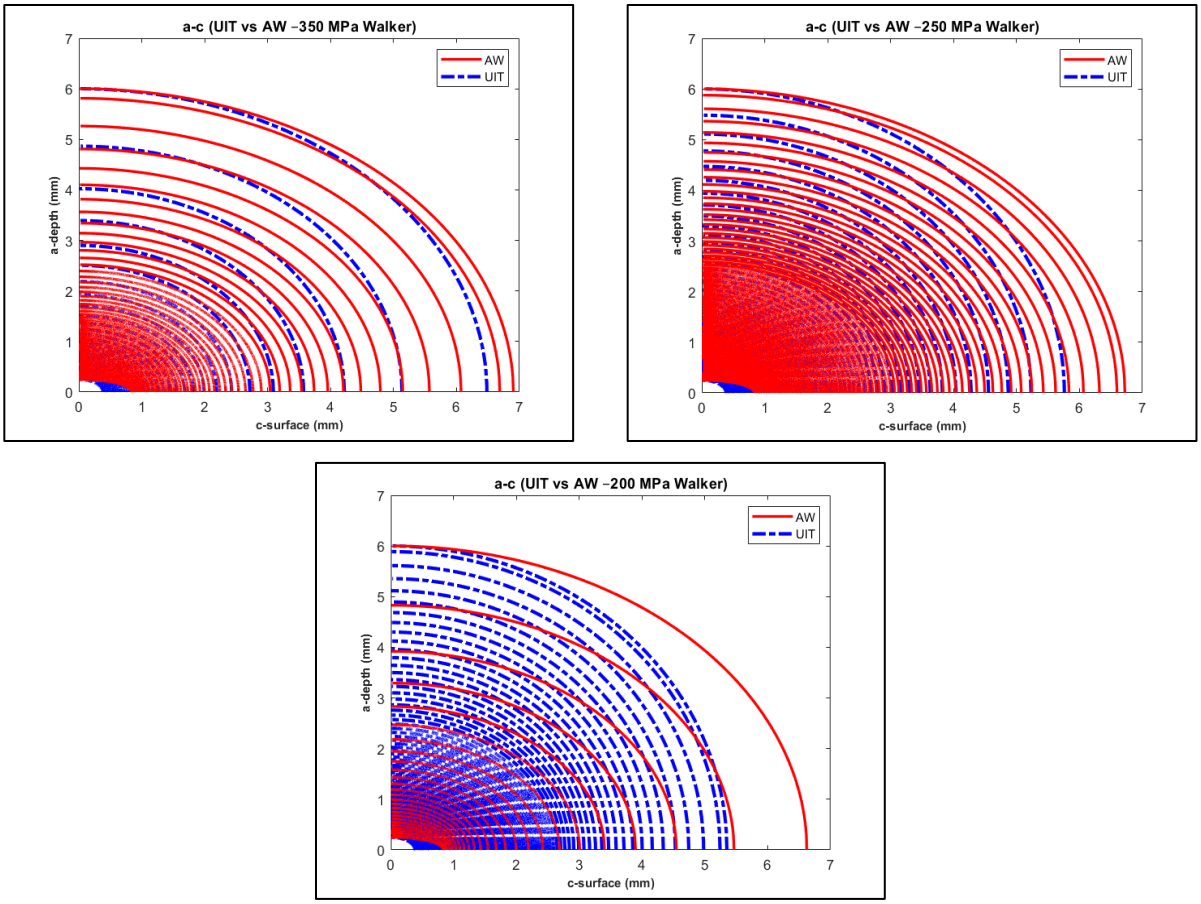

Figure 122: Crack shape evolution analysis results of S460 for AW vs UIT conditions for Walker, crack depth against crack surface for covering stress level ranges

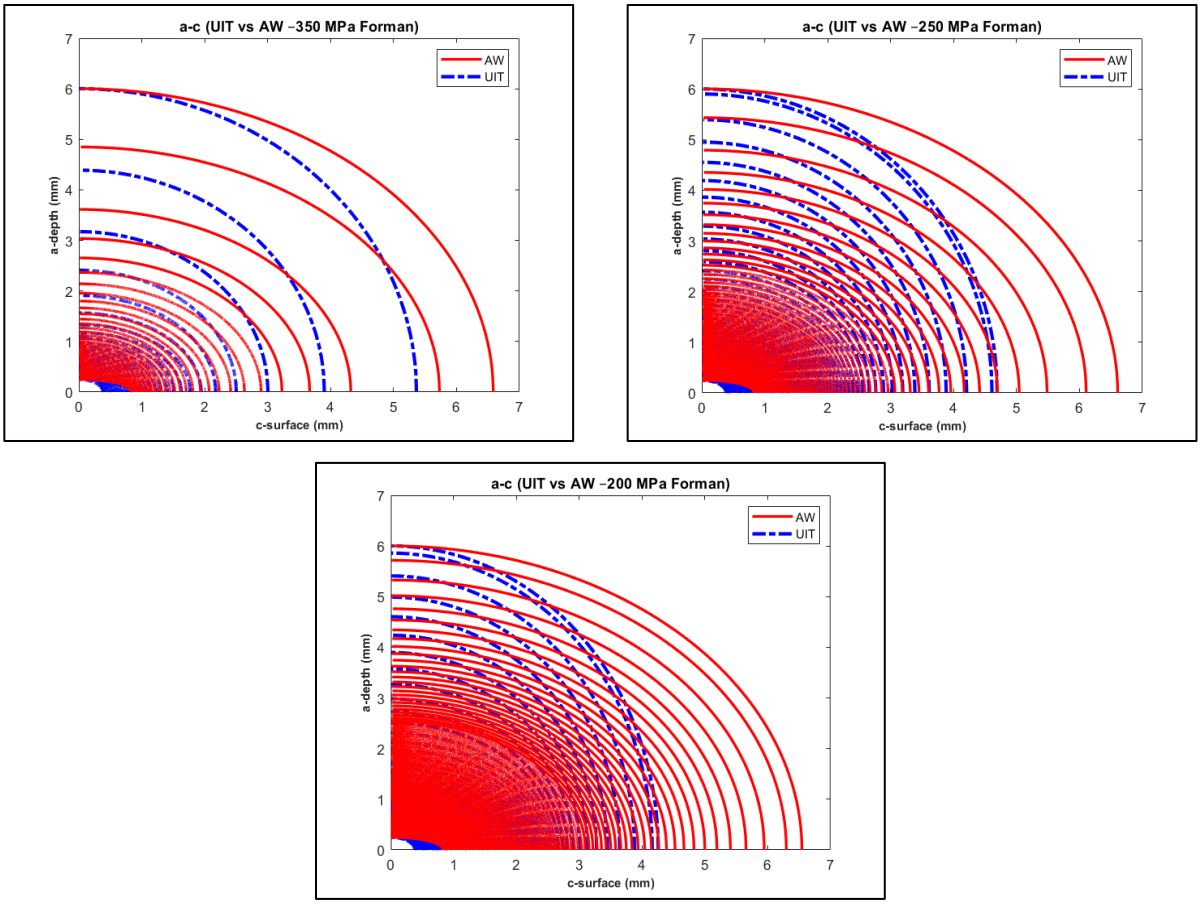

Figure 123: Crack shape evolution analysis results of S460 for AW and UIT conditions for Forman, crack depth against crack surface for covering stress level ranges

The below figures are the crack shape evolution curves for S460 under the AW and the UIT conditions for Walker model.

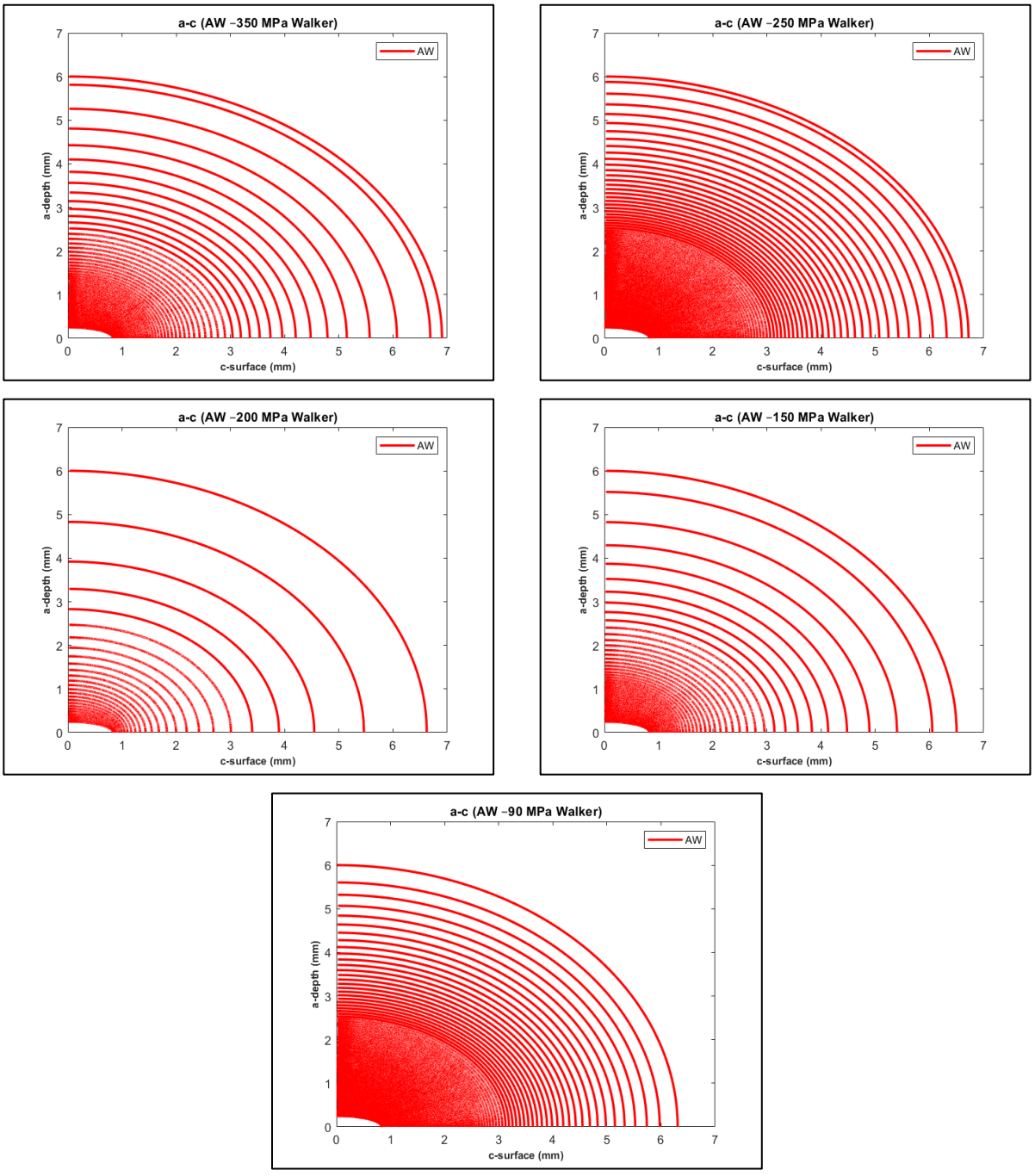

Figure 124: Crack shape evolution analysis results of S460 under AW condition for Walker, crack depth against crack surface for covering stress level ranges

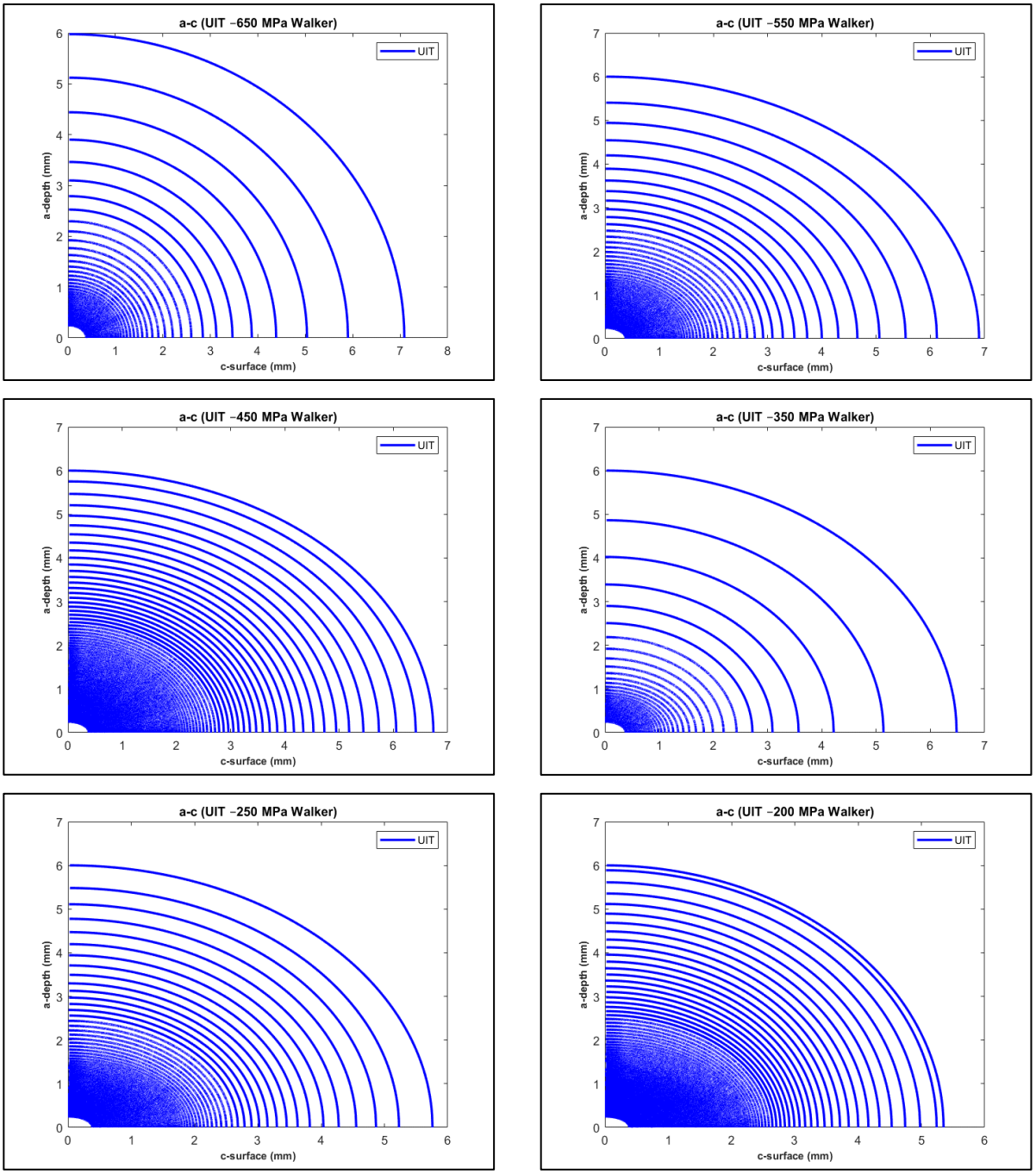

Figure 125: Crack shape evolution analysis results of S460 under UIT condition for Walker, crack depth against crack surface for covering stress level ranges

The below figures are the crack shape evolution curves for S460 under the AW and the UIT conditions for Forman model.

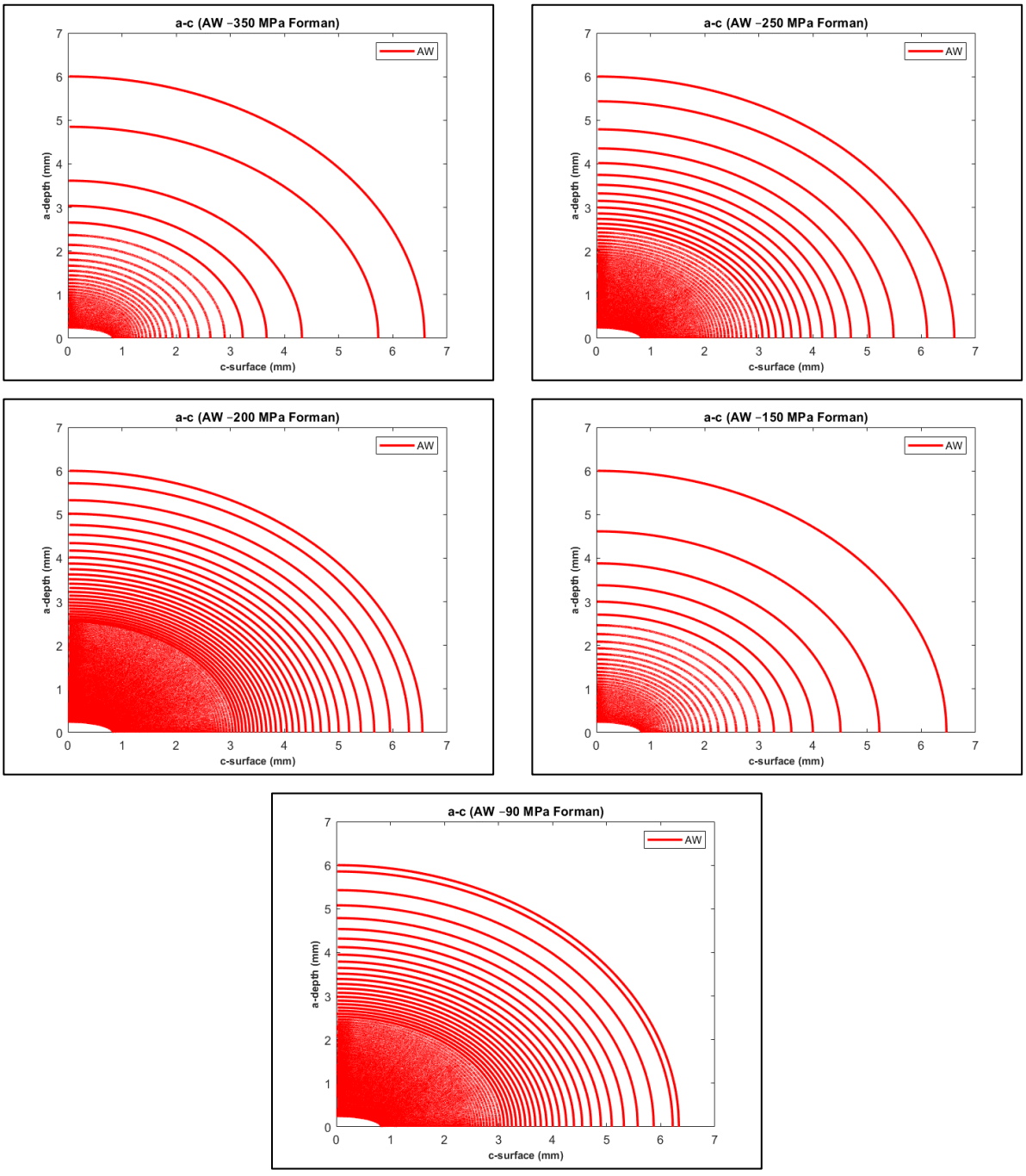

Figure 126: Crack shape evolution analysis results of S460 under AW condition for Forman, crack depth against crack surface for covering stress level ranges

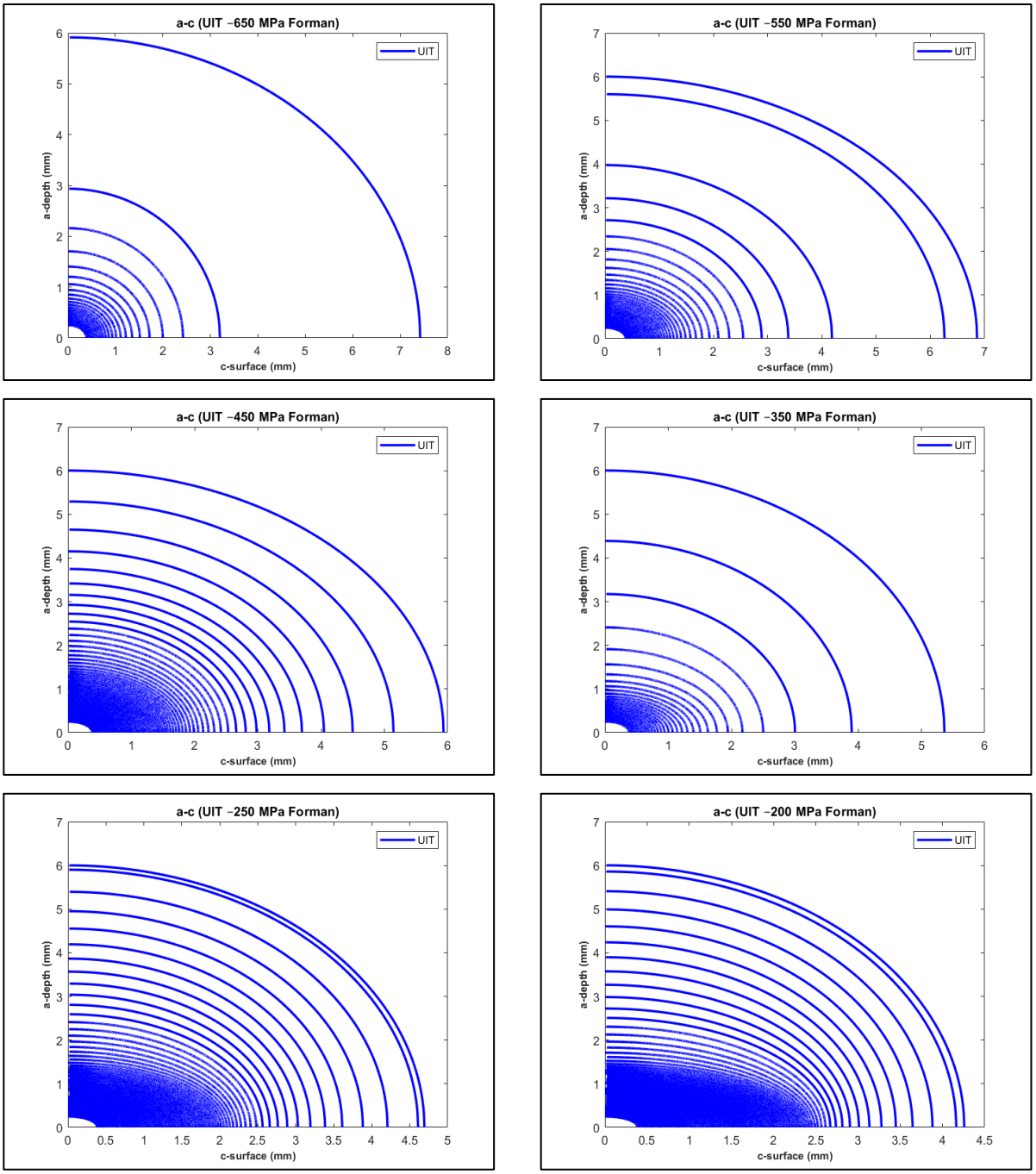

Figure 127: Crack shape evolution analysis results of S460 under UIT condition for Forman, crack depth against crack surface for covering stress level ranges

(C.6) S690

Figure 128, Figure 129 and the figures here in Appendix (C.6) display diagrammatically crack shape evolution analysis results of S690 under the AW and the UIT conditions for Walker and Forman models as well as their comparisons under both conditions for that model. Crack depth versus crack surface is displayed in these figures.

From $AW-F-250$, $AW-F-200$ and $UIT-W-300$ which are the figures in Appendix (C.6), it should be pointed out that the last two curves are the way that Walker and Forman models tried to determine the final crack size for that condition.

As an example, from $UIT-W-250$ and $UIT-F-250$ which are the figures in Appendix (C.6) that of the AW condition, it should be pointed out that UIT incredibly retarded crack initiation phase as well as remarkably slowed down crack propagation phase in depth and on surface so that the fatigue life was noticeably improved .

For instance, comparing $AWvsUIT-W-250$ and $AWvsUIT-F-250$ together, it demonstrates that Forman model anticipated the crack growth and the crack shape evolution quite well. It is very interesting to note that the crack was at first advancing quicker into depth and on surface after reducing the stress it is a little bit slowed down for the AW condition. However, it is worth noting that after achieving a certain depth, it still commenced expanding significantly for the AW condition. After impact treatment, the crack is extremely slowed down which indicates that UIT considerably enlarge the fatigue life.

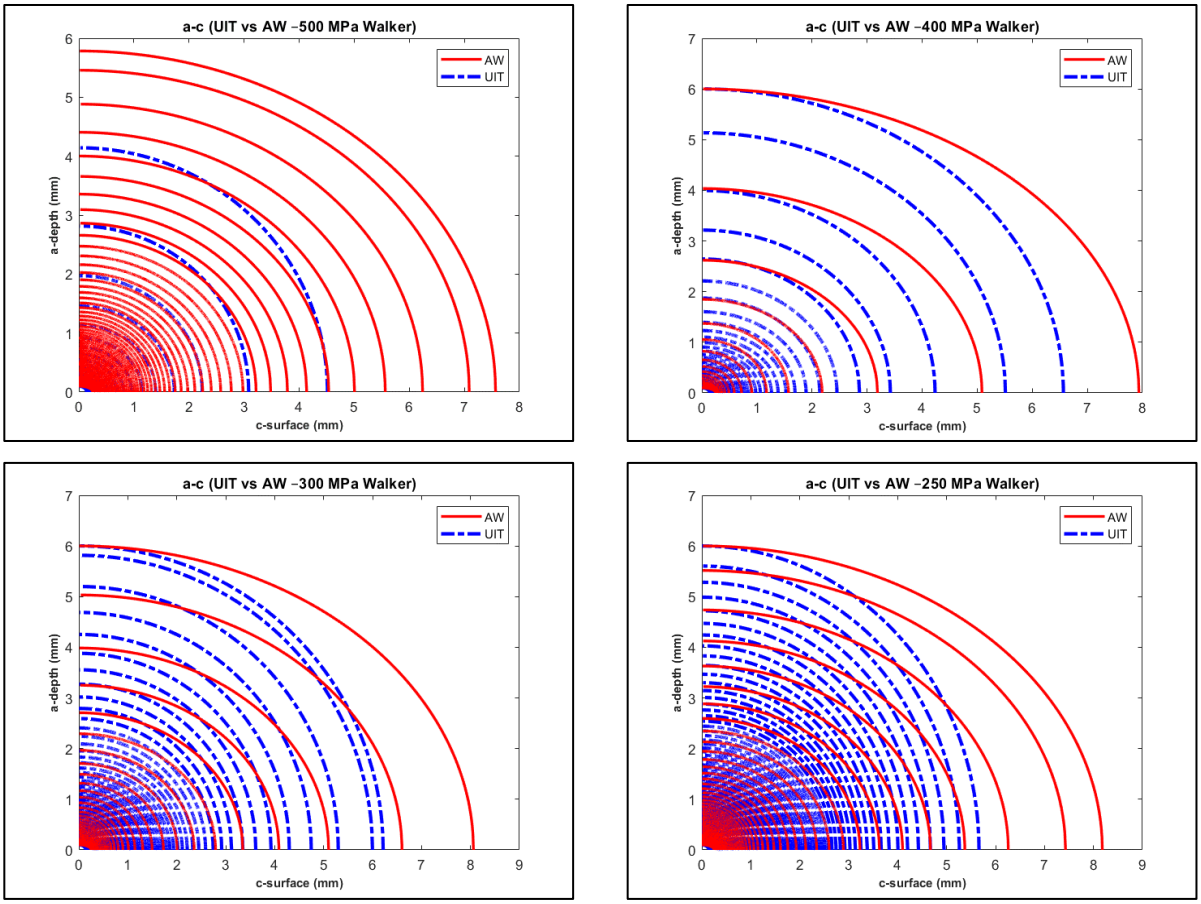

Figure 128: Crack shape evolution analysis results of S690 for AW vs UIT conditions for Walker, crack depth against crack surface for covering stress level ranges

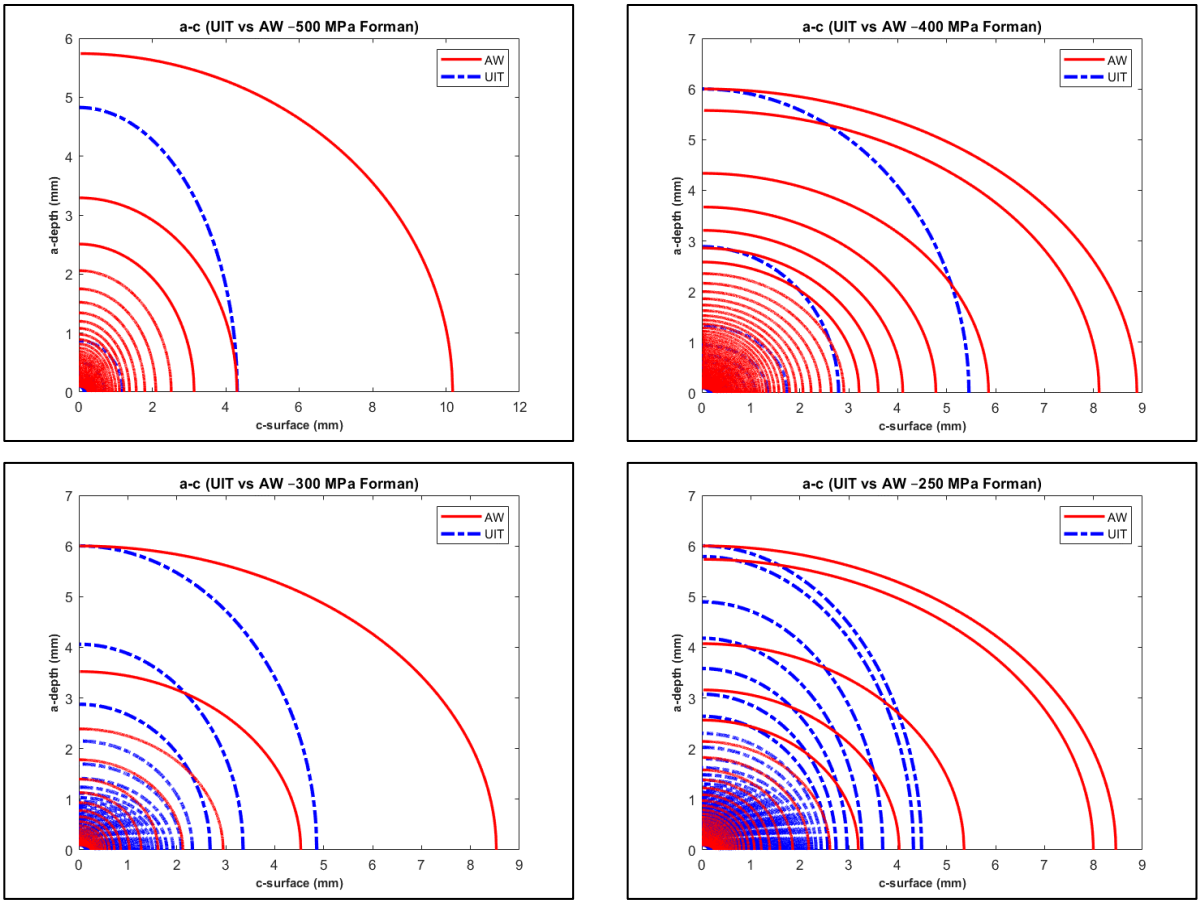

Figure 129: Crack shape evolution analysis results of S690 for AW vs UIT conditions for Forman, crack depth against crack surface for covering stress level ranges

The below figures are the crack shape evolution curves for S690 under the AW and the UIT conditions for Walker model.

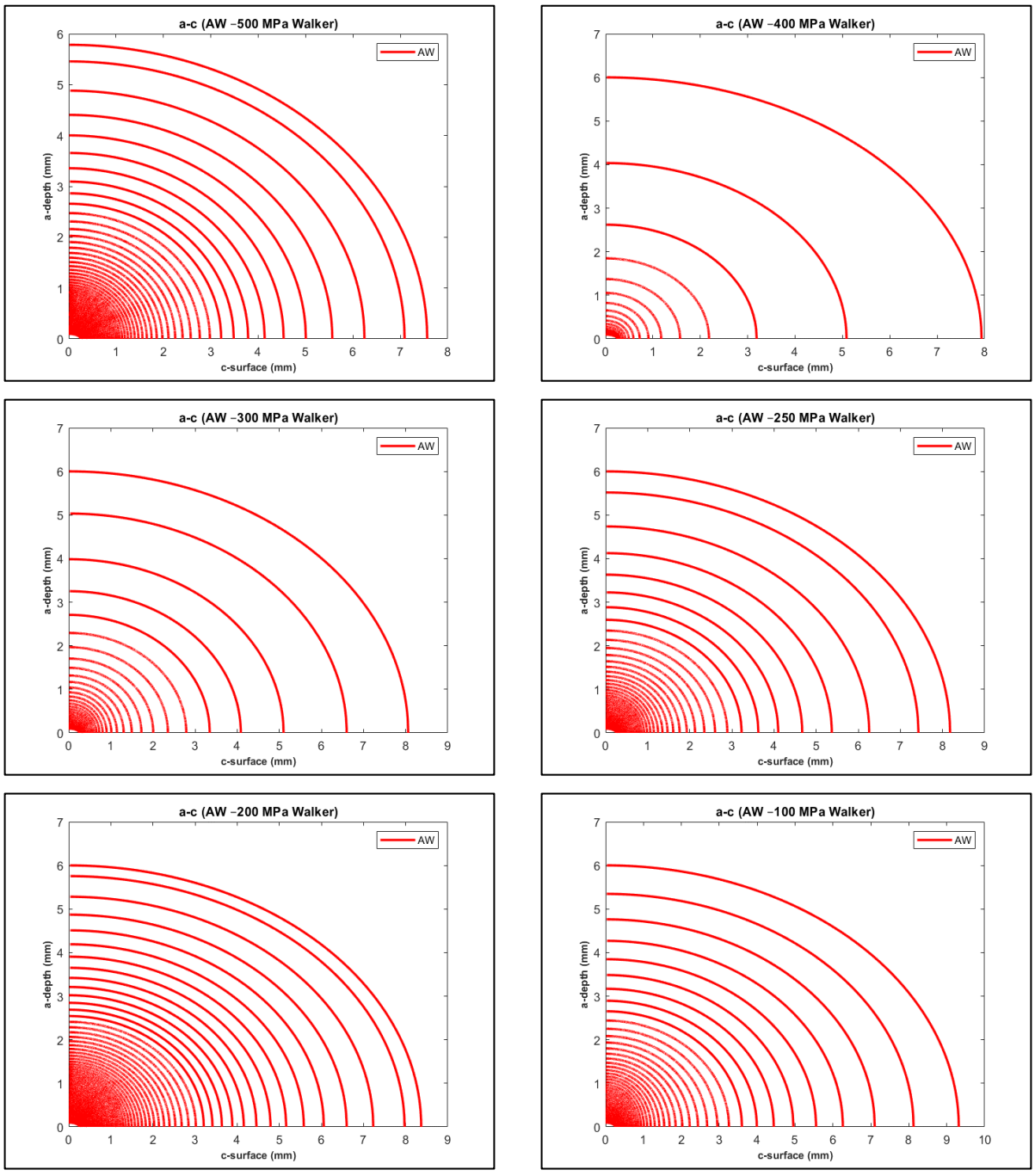

Figure 130: Crack shape evolution analysis results of S690 under AW condition for Walker, crack depth against crack surface for covering stress level ranges

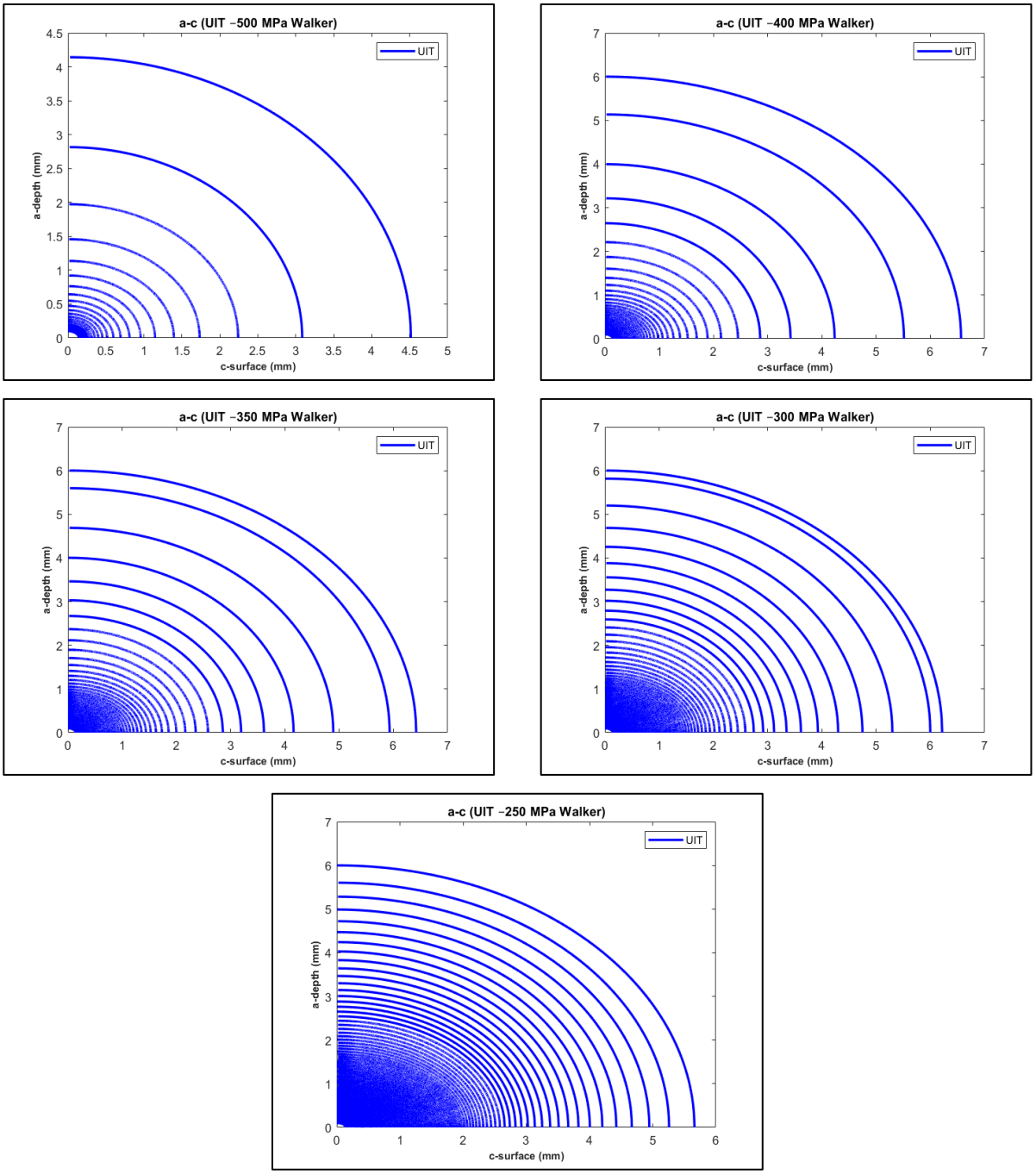

Figure 131: Crack shape evolution analysis results of S690 under UIT condition for Walker, crack depth against crack surface for covering stress level ranges

The below figures are the crack shape evolution curves for S690 under the AW and the UIT conditions for Forman model.

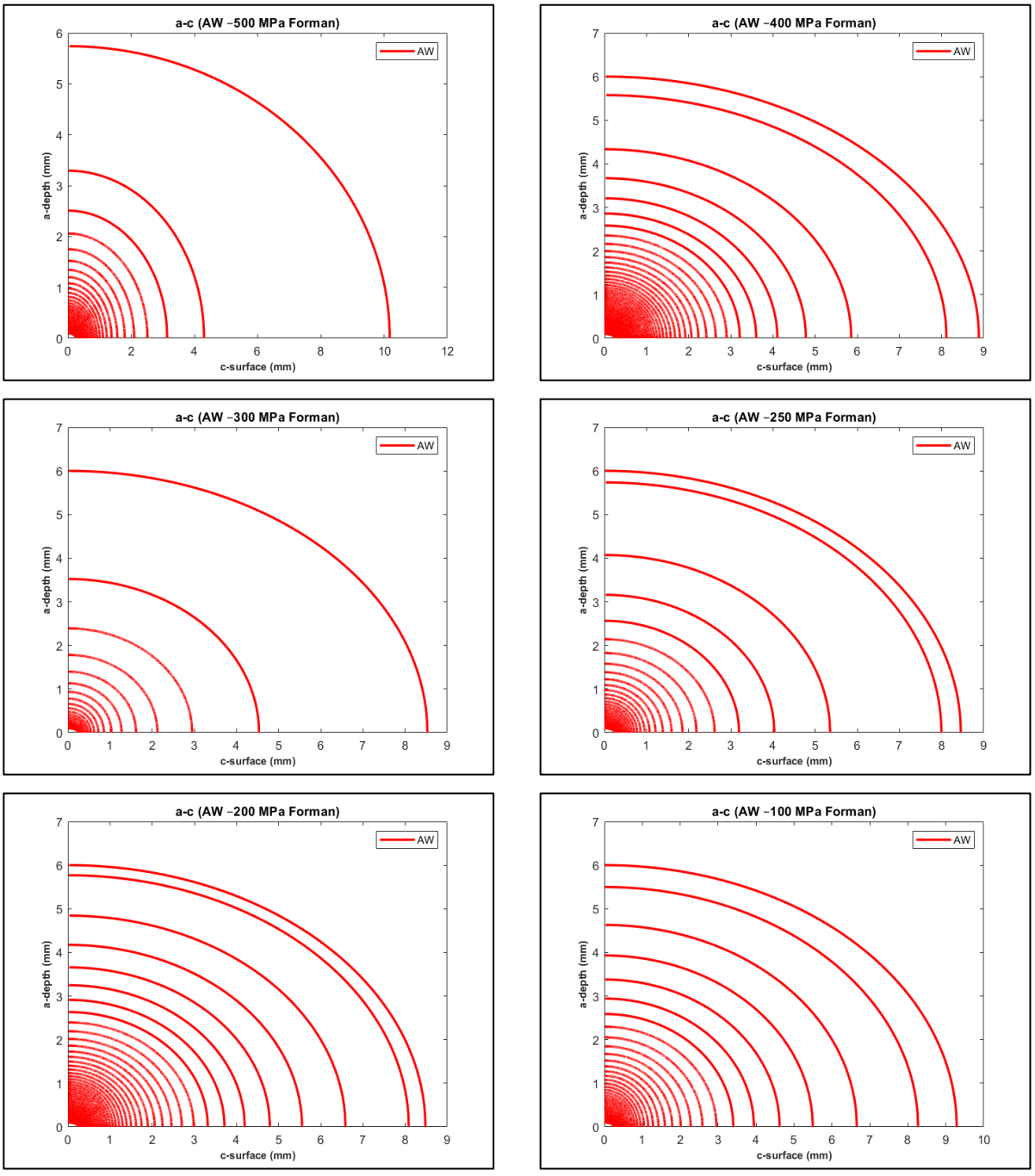

Figure 132: Crack shape evolution analysis results of S690 under AW condition for Forman, crack depth against crack surface for covering stress level ranges

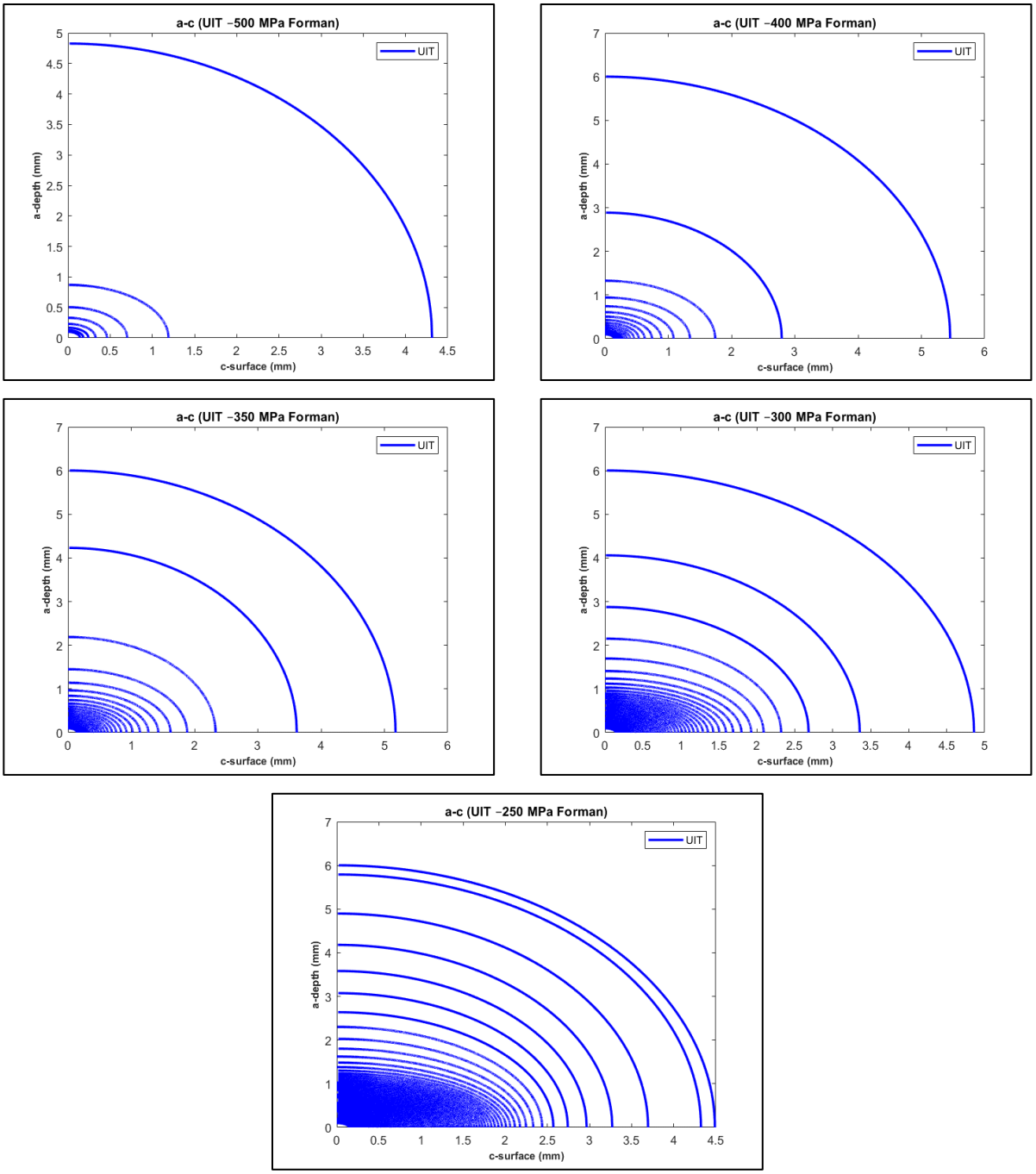

Figure 133: Crack shape evolution analysis results of S690 under UIT condition for Forman, crack depth against crack surface for covering stress level ranges

(C.7) S960

Figure 134, Figure 135 and the figures here in Appendix (C.7) depict graphically crack shape evolution analysis results of S960 under the AW and the UIT conditions for Walker and Forman models as well as their comparisons under both conditions for that model. Crack depth versus crack surface is displayed in these figures.

From $AW - F - 350$ and $UIT - F - 350$ which are the figures in Appendix (C.7), it should be pointed out that the last two curves are the way that Walker and Forman models tried to determine the final crack size for that condition.

For example, from $UIT - W - 350$ and $UIT - F - 350$ which are the figures in Appendix (C.7) versus that of the AW condition, it should be noted that UIT incredibly retarded crack initiation phase as well as remarkably slowed down crack propagation phase in depth and on surface so that the fatigue life was noticeably improved .

For instance, comparing $AWvsUIT - W - 350$ and $AWvsUIT - F - 350$ together, it demonstrates that Forman model predicted the crack growth and the crack shape evolution completely satisfactory. It is quite fascinating to note that the crack was at first advancing quicker into depth and on surface after reducing the stress it is a little bit slowed down for the AW condition. However, it is noteworthy that after achieving a certain depth, it still commenced expanding significantly for the AW condition. After impact treatment, the crack is extremely slowed down which indicates that UIT considerably enlarge the fatigue life.

It is important to note that $AW - W - 100$ which is in Appendix (C.7) indicates that the magnitude of the stress is not that much to accelerate the crack growth. In other words, it takes quite some time for the crack to reach its final crack size both in depth and on surface.

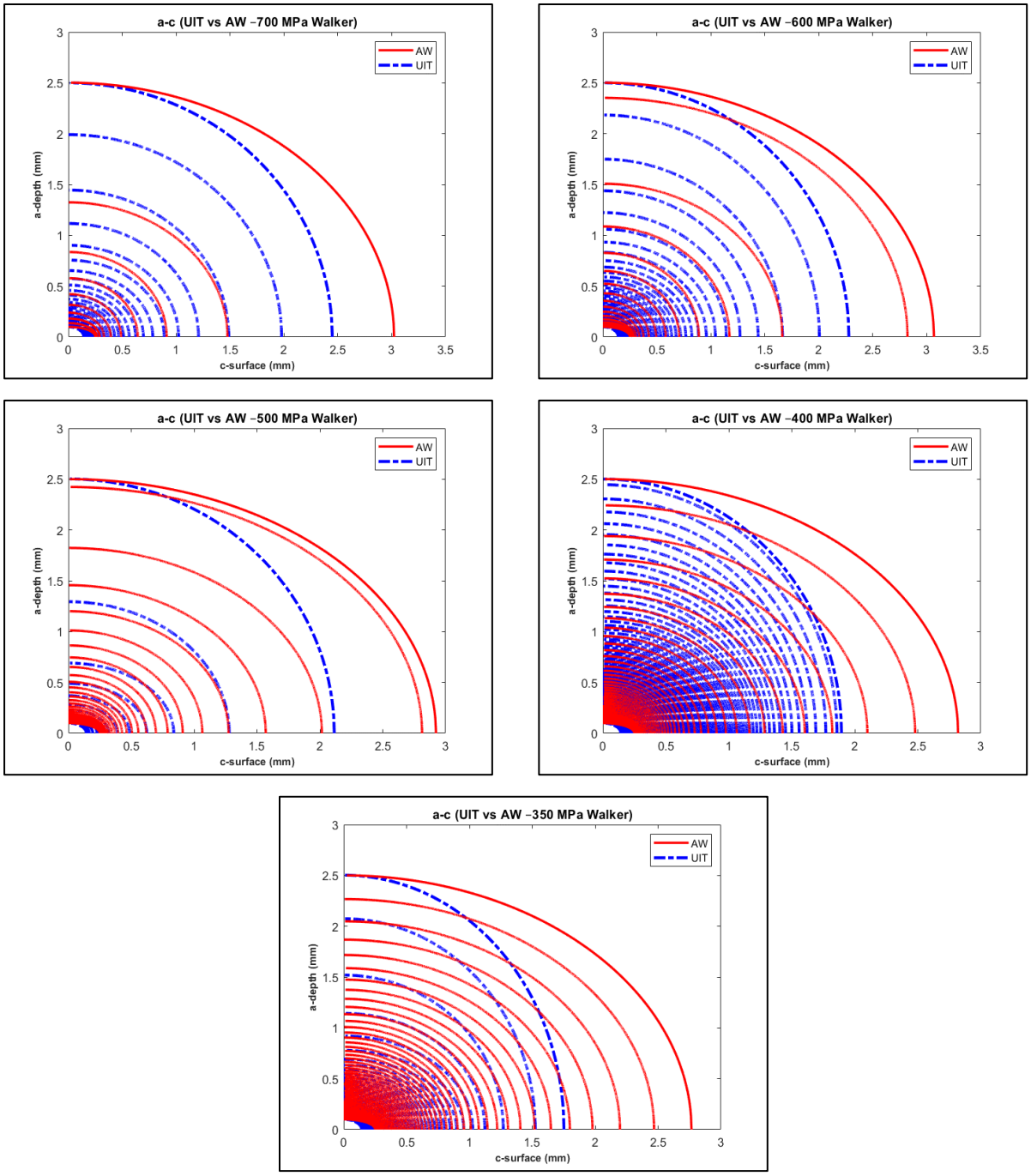

Figure 134: Crack shape evolution analysis results of S960 for AW vs UIT conditions for Walker, crack depth against crack surface for covering stress level ranges

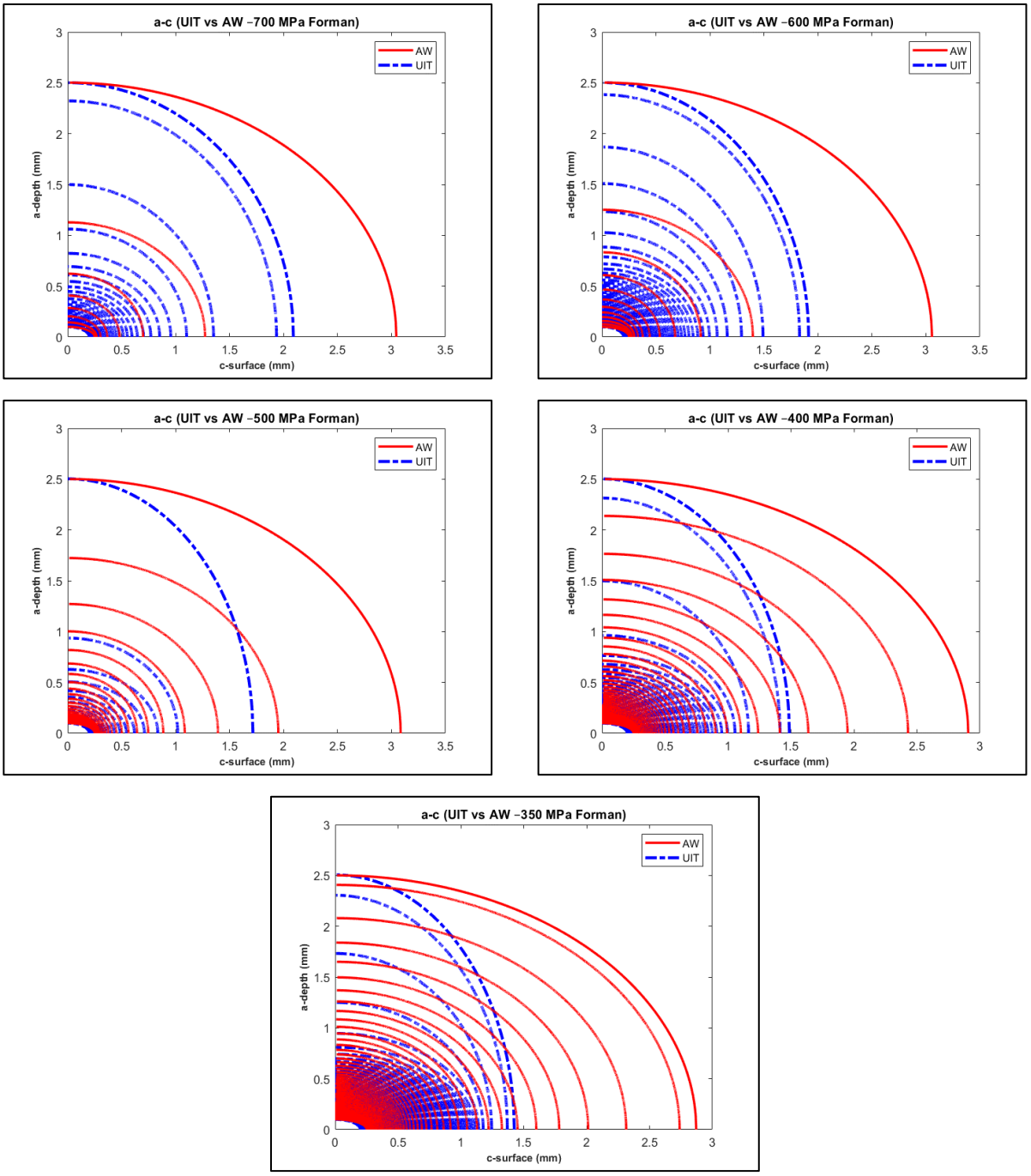

Figure 135: Crack shape evolution analysis results of S960 for AW vs UIT conditions for Forman, crack depth against crack surface for covering stress level ranges

The below figures are the crack shape evolution curves for S960 under the AW and the UIT conditions for Walker model.

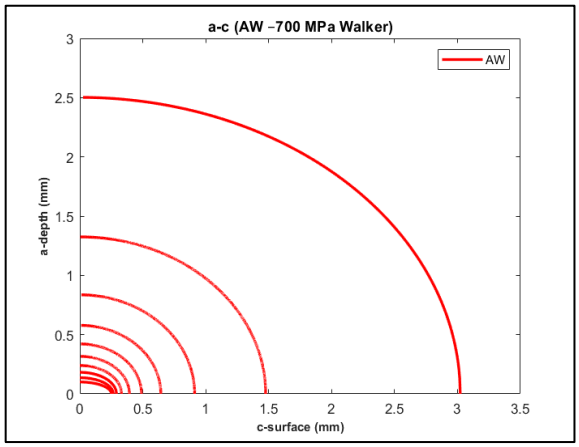

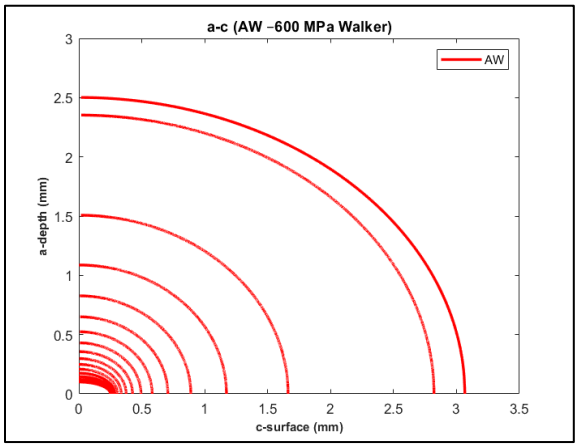

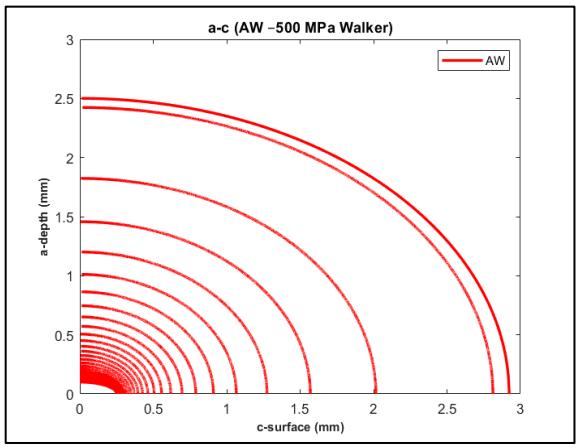

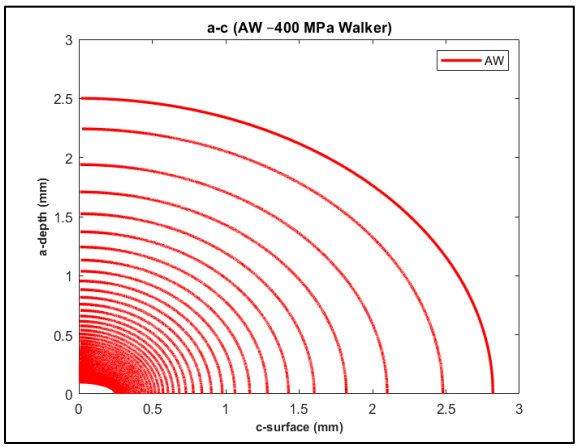

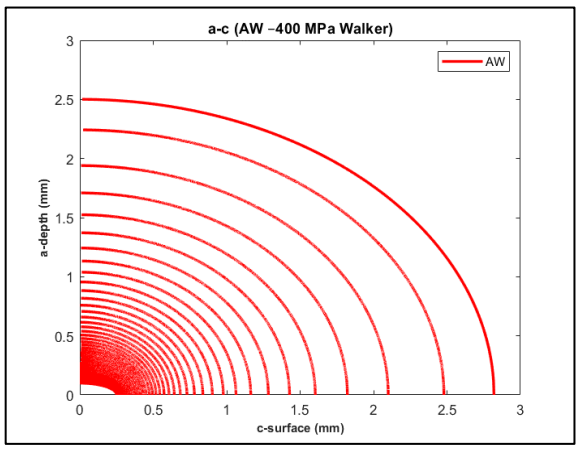

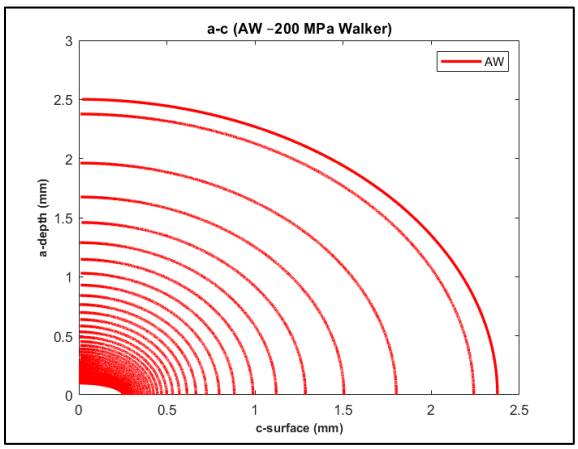

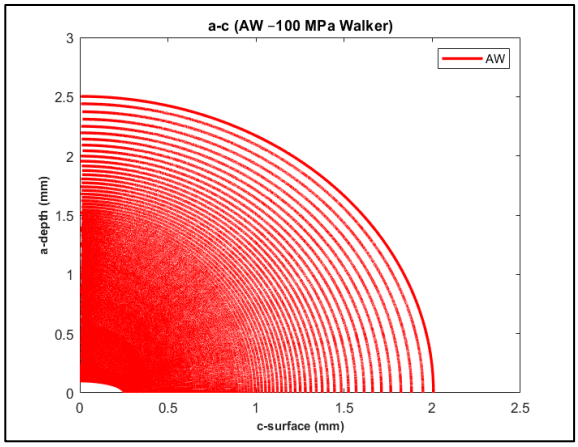

Figure 136: Crack shape evolution analysis results of S960 under AW condition for Walker, crack depth against crack surface for covering stress level ranges

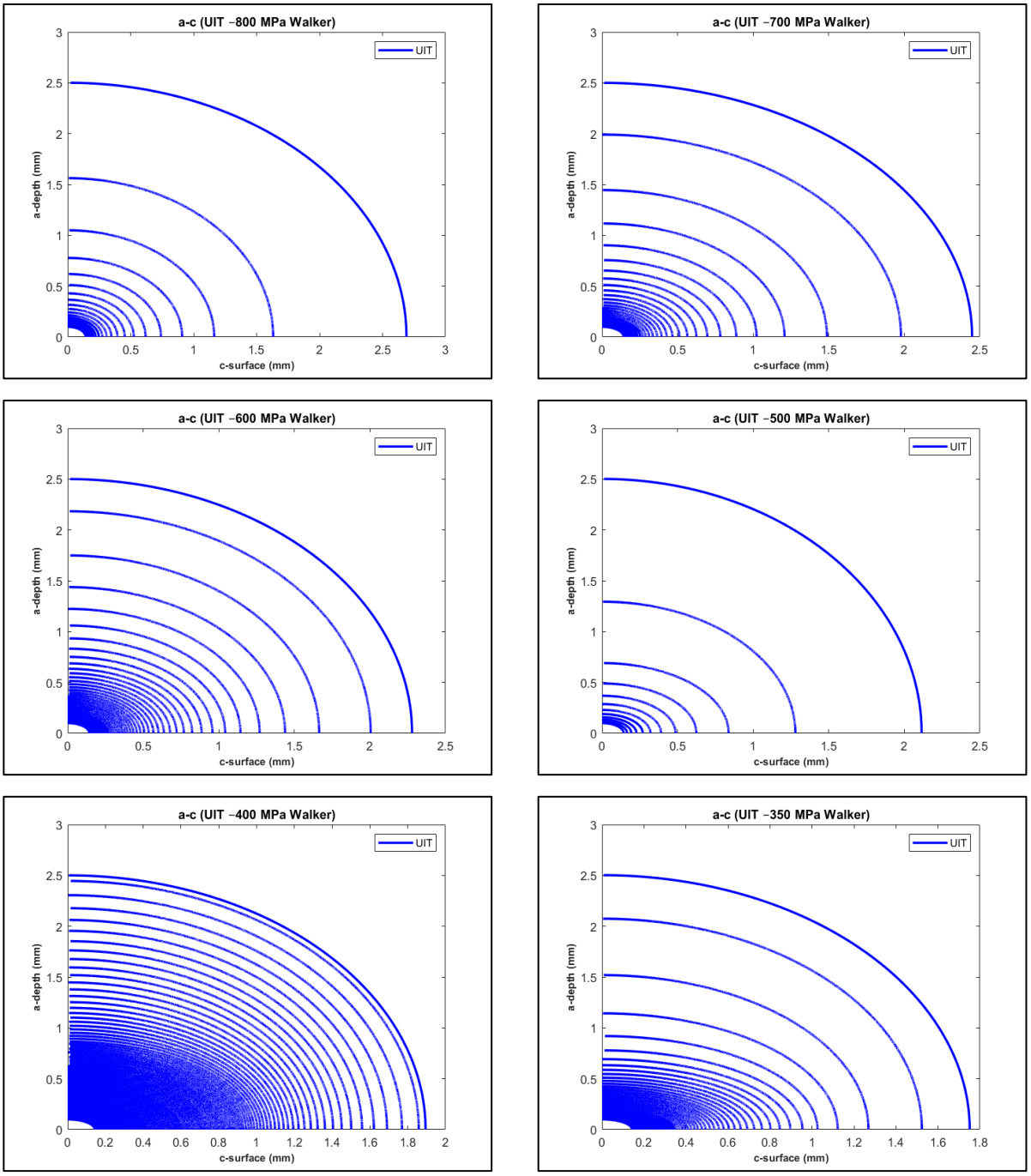

Figure 137: Crack shape evolution analysis results of S960 under UIT condition for Walker, crack depth against crack surface for covering stress level ranges

The below figures are the crack shape evolution curves for S960 under the AW and the UIT conditions for Forman model.

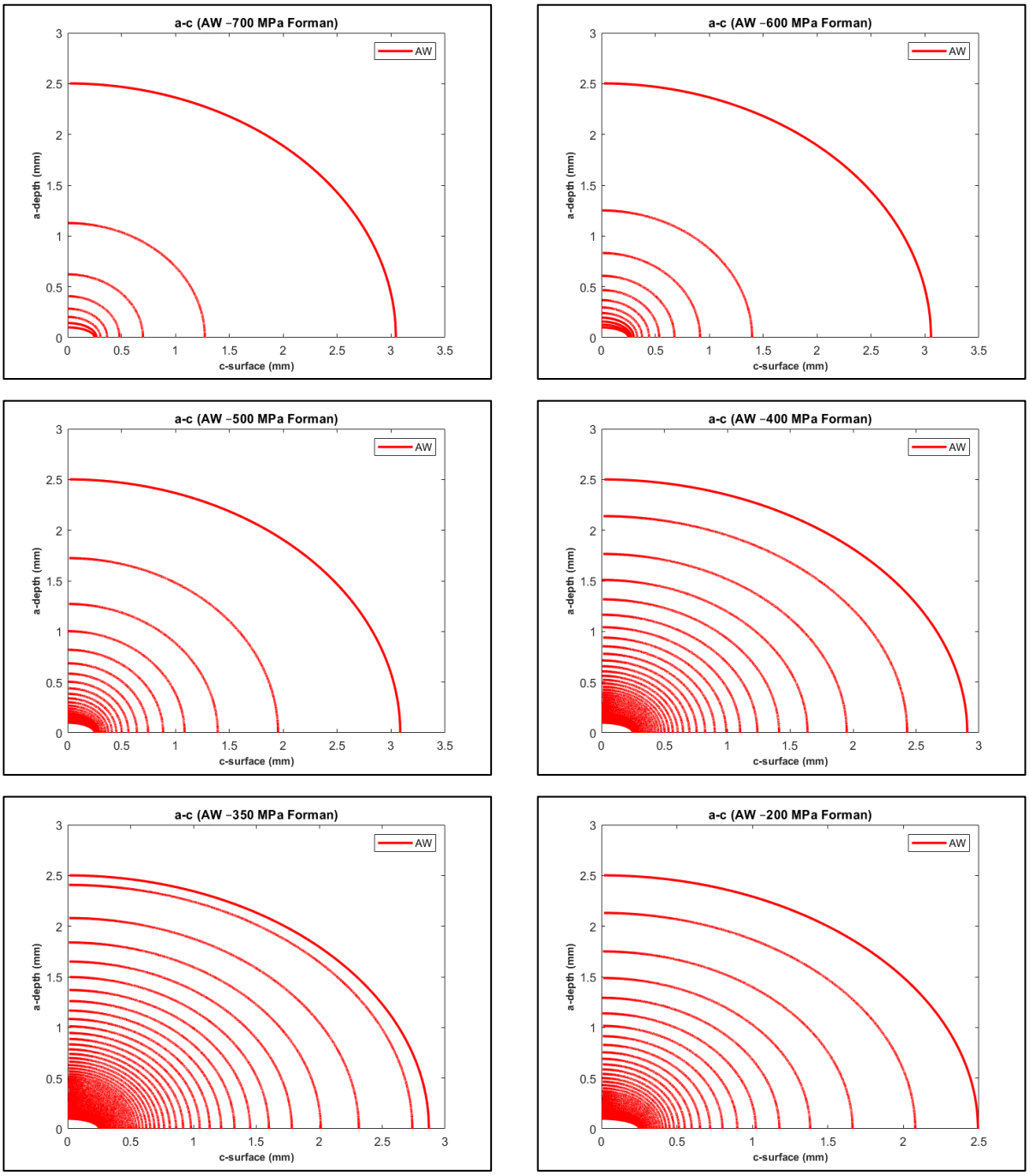

Figure 138: Crack shape evolution analysis results of S960 under AW condition for Forman, crack depth against crack surface for covering stress level ranges

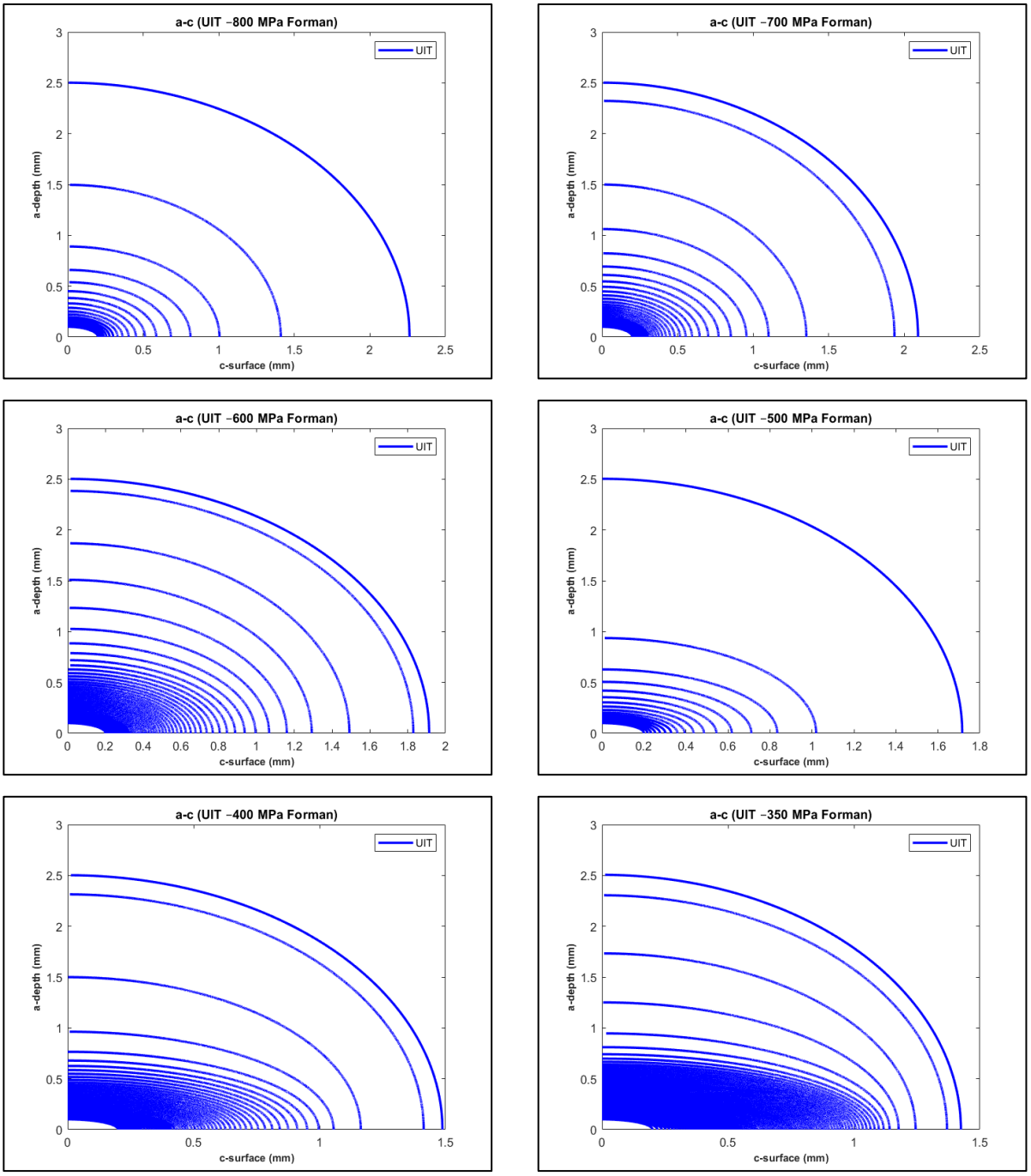

Figure 139: Crack shape evolution analysis results of S960 under UIT condition for Forman, crack depth against crack surface for covering stress level ranges

(C.8) 5083-H11 AL

Figure 140, Figure 141 and the figures here in Appendix (C.8) display diagrammatically crack shape evolution analysis results of 5083-H11 AL under the AW and the UIT conditions for Walker and Forman models as well as their comparisons under both conditions for that model. Crack depth versus crack surface is displayed in these figures.

From $AW-W-130$, $AW-W-110$ and $UIT-F-130$ which are the figures in Appendix (C.8), it should be pointed out that the last two curves are the way that Walker and Forman models tried to determine the final crack size for that condition.

As an example, from $UIT-W-140$ and $UIT-F-140$ which are the figures in Appendix (C.8) that of the AW condition, it should be pointed out that UIT incredibly retarded crack initiation phase as well as remarkably slowed down crack propagation phase in depth and on surface so that the fatigue life was noticeably improved .

For instance, comparing $AWvsUIT-W-140$ and $AWvsUIT-F-140$ together, it demonstrates that Forman model anticipated the crack growth and the crack shape evolution quite well. It is very interesting to note that the crack was at first advancing quicker into depth and on surface after reducing the stress it is a little bit slowed down for the AW condition. However, it is worth noting that after achieving a certain depth, it still commenced expanding significantly for the AW condition. After impact treatment, the crack is extremely slowed down which indicates that UIT considerably enlarge the fatigue life.

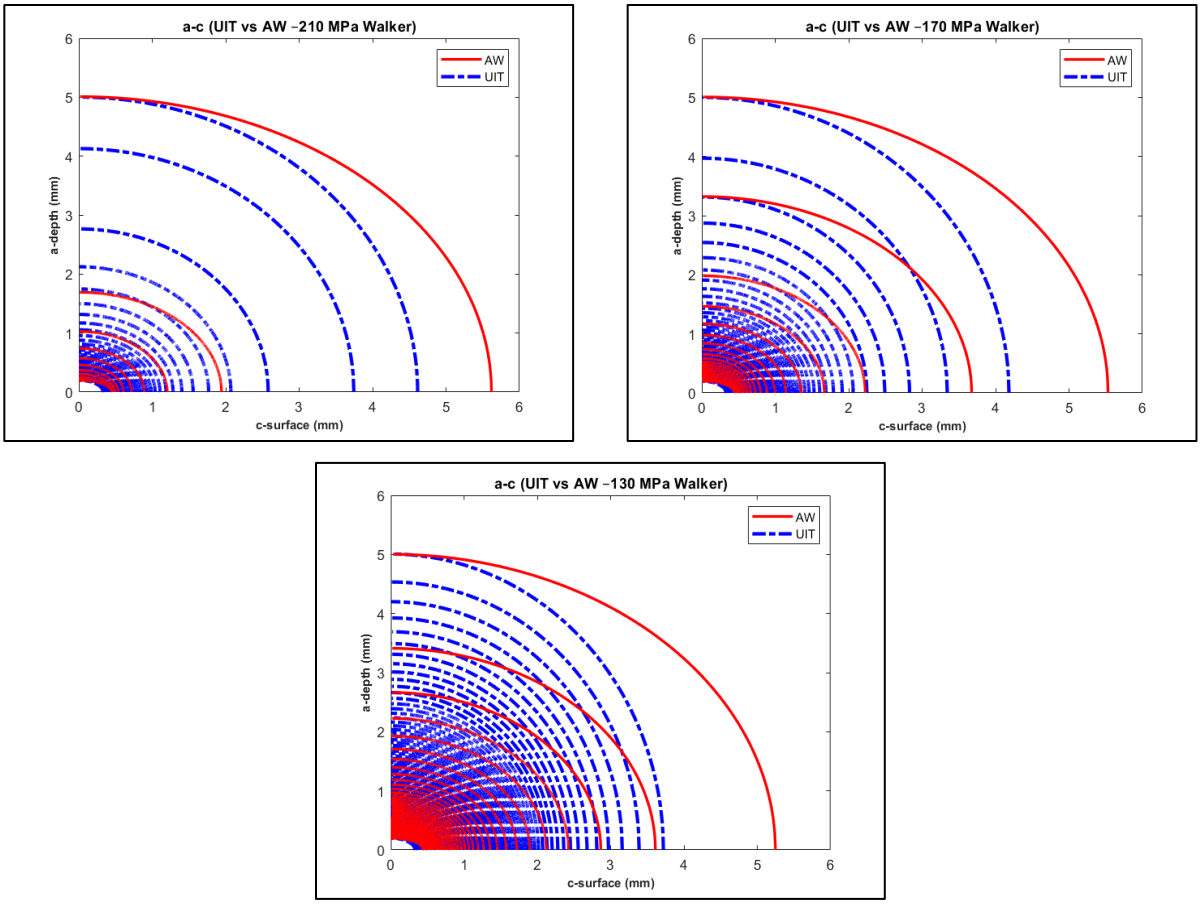

Figure 140: Crack shape evolution analysis results of 5083-H11 AL for AW and UIT conditions for Walker, crack depth against crack surface for covering stress level ranges

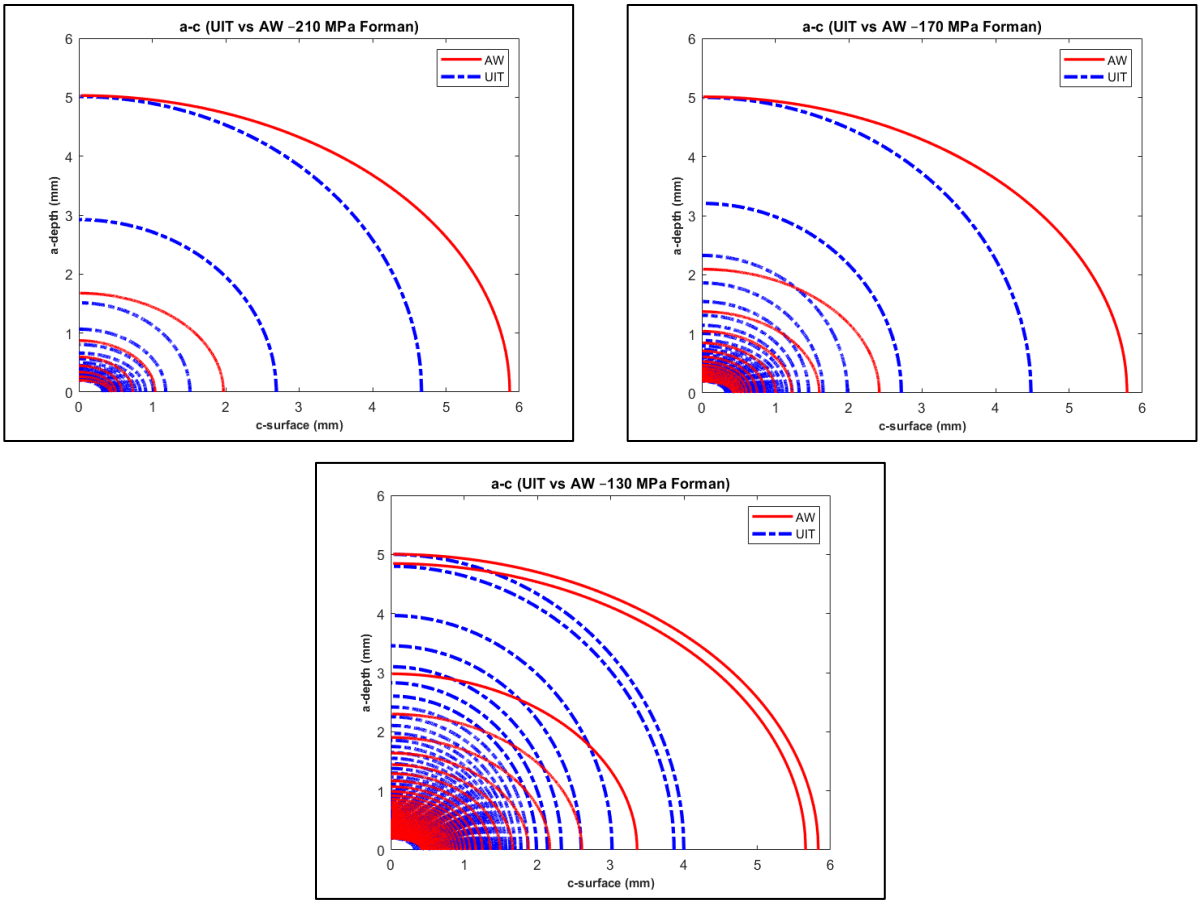

Figure 141: Crack shape evolution analysis results of 5083-H11 AL for AW and UIT conditions for Forman, crack depth against crack surface for covering stress level ranges

The below figures are the crack shape evolution curves for 5083-H11 AL under the AW and the UIT conditions for Walker model.

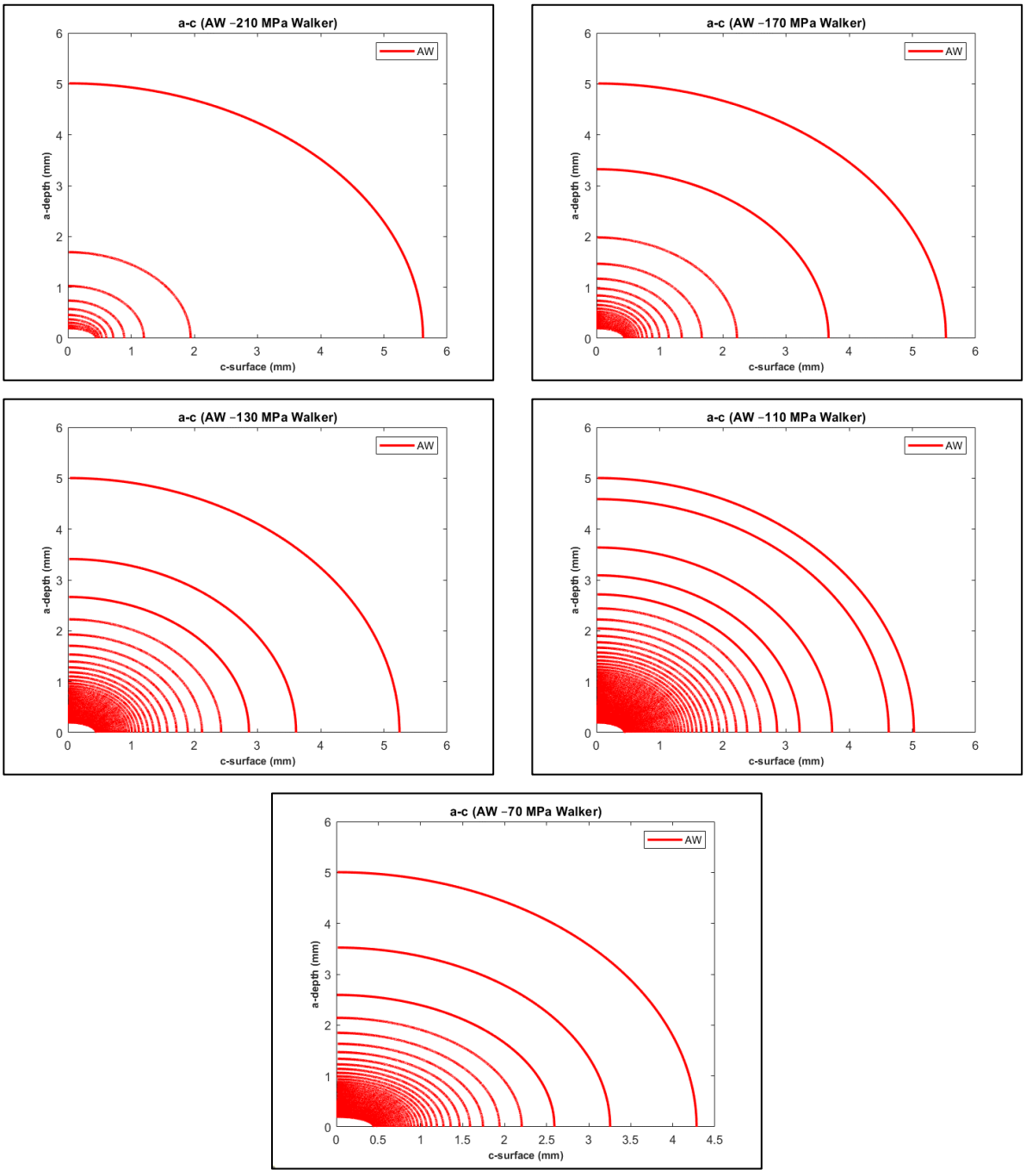

Figure 142: Crack shape evolution analysis results of 5083-H11 AL under AW condition for Walker, crack depth against crack surface for covering stress level ranges

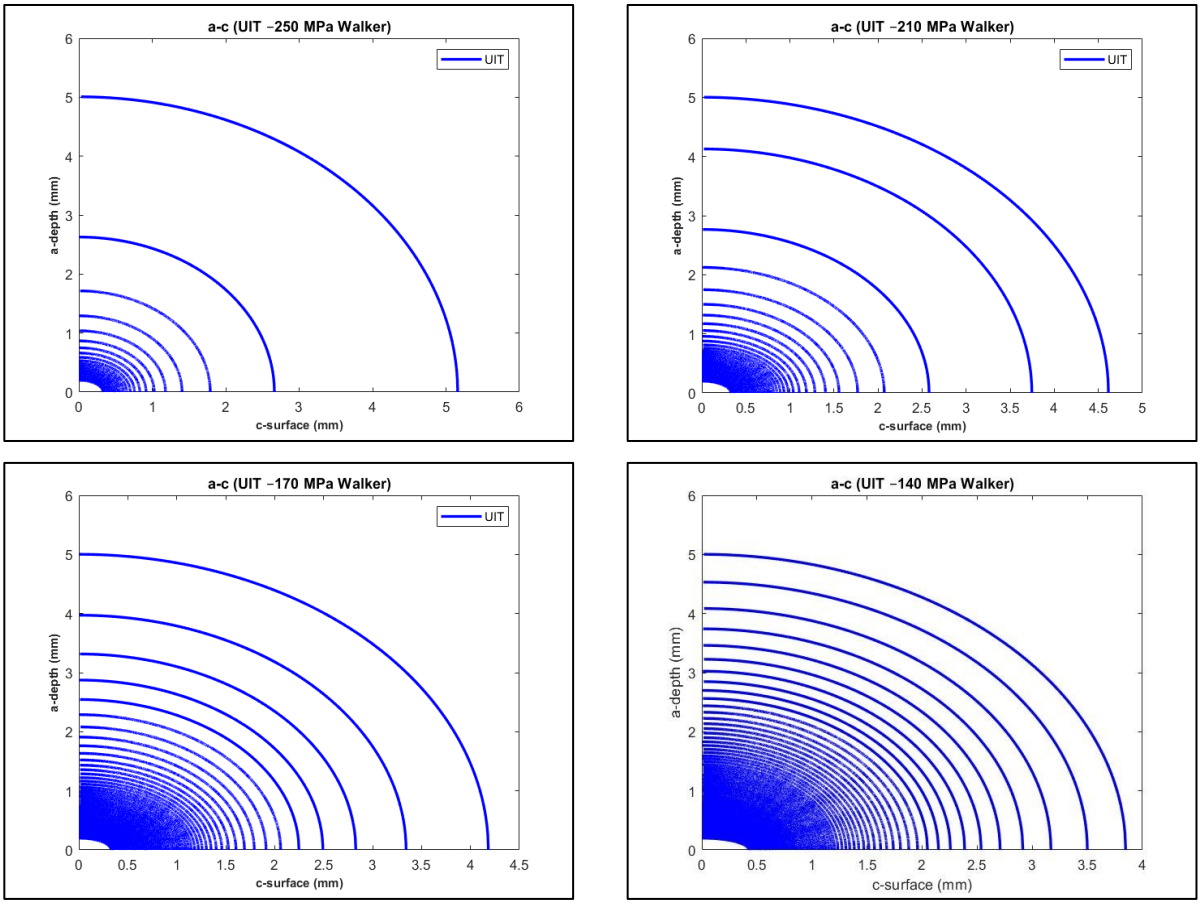

Figure 143: Crack shape evolution analysis results of 5083-H11 AL under UIT condition for Walker, crack depth against crack surface for covering stress level ranges

The below figures are the crack shape evolution curves for 5083-H11 AL under the AW and the UIT conditions for Forman model.

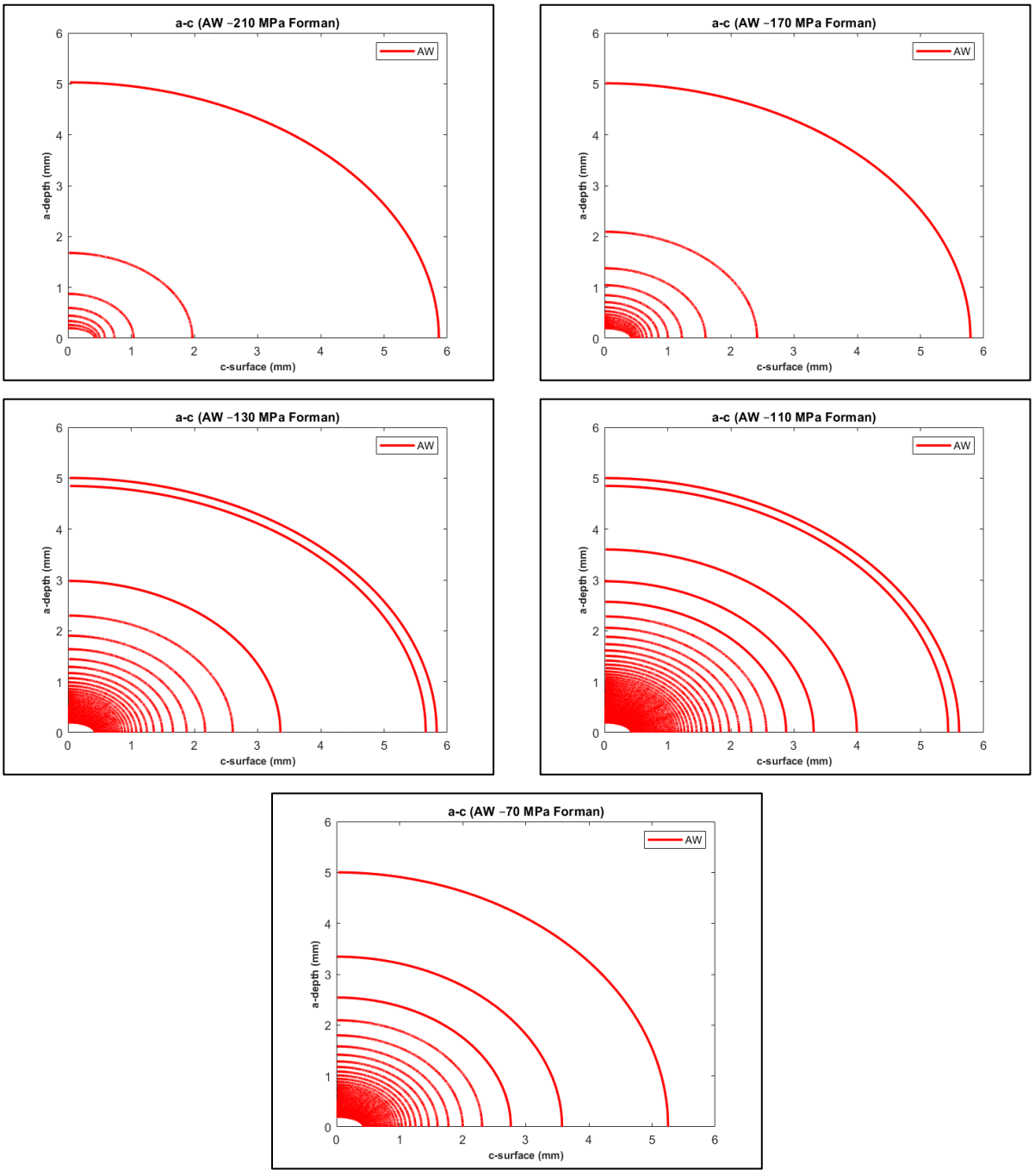

Figure 144: Crack shape evolution analysis results of 5083-H11 AL under AW condition for Forman, crack depth against crack surface for covering stress level ranges

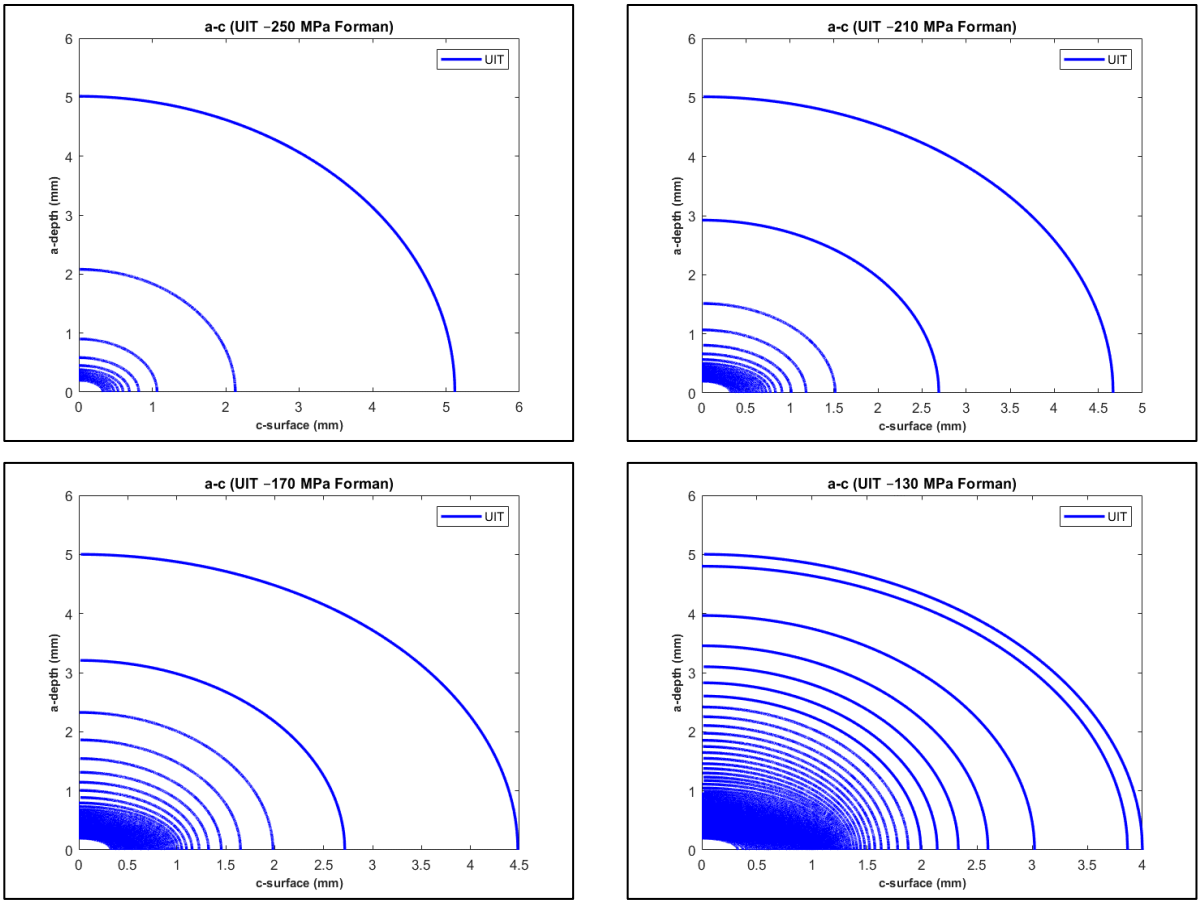

Figure 145: Crack shape evolution analysis results of 5083-H11 AL under UIT condition for Forman, crack depth against crack surface for covering stress level ranges

(C.9) 2024-T351 AL

Figure 146, Figure 147 and the figures here in Appendix (C.9) depicts graphically crack shape evolution analysis results of 5083-H311 AL under the BR and the UIT conditions for Walker and Forman models as well as their comparisons under both conditions for that model. Crack depth versus crack surface is displayed in these figures.

From $BR - W - 240$ and $UIT - W - 250$ which are the figures in Appendix (C.9), it should be pointed out that the last two curves are the way that Walker and Forman models tried to determine the final crack size for that condition.

As already mentioned, it should be noted that 2024-T351 AL was a plate and the impact of the stress concentration has been avoided. Yet, both models did not predict the crack growth and the crack shape evolution as good as they should. As already stated, the weld imperfections play a pivotal role in diminishing fatigue strength and increasing fatigue crack growth rate of the material. Since it is BR versus UIT, it is difficult to make a good comparison between them considering the fact that Walker and Forman fatigue crack growth models were utilized for describing the behaviour of this material under these domains. In addition to that the fitting constants of Forman model as well as the undesirable residual stresses result for the BR condition could be also other contributing causes on the prediction of the fatigue strength for the BR condition for Forman model.

Apart from that, there were still some unknowns fatigue parameters for this material. Considered the fact that the weld defects generally cause severe damage to the welded structures like at the weld toe. Hence, these models can be employed to display such phenomena under the AW and the UIT conditions unless defining boundary conditions and fatigue parameters, conducting experiments to capture image of the crack from initial size to final size etc. so that it can be experimentally verified.

Even from the figures below and in Appendix (C.9), it can be sensed that the crack grew really slow. In the end, it takes quite some time for the crack to reach its final crack size both in depth and on surface.

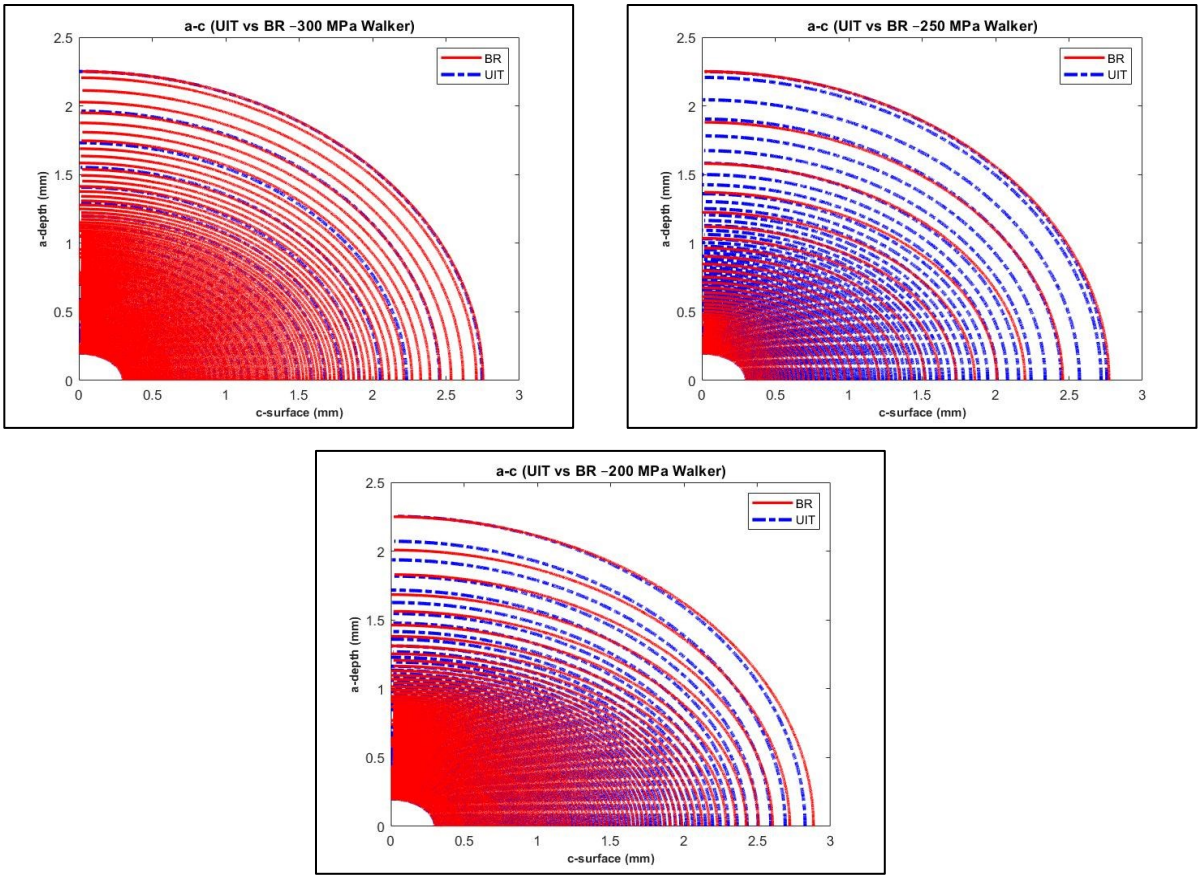

Figure 146: Crack shape evolution analysis results of 2024-T351 AL for BR and UIT conditions for Walker, crack depth against crack surface for covering stress level ranges

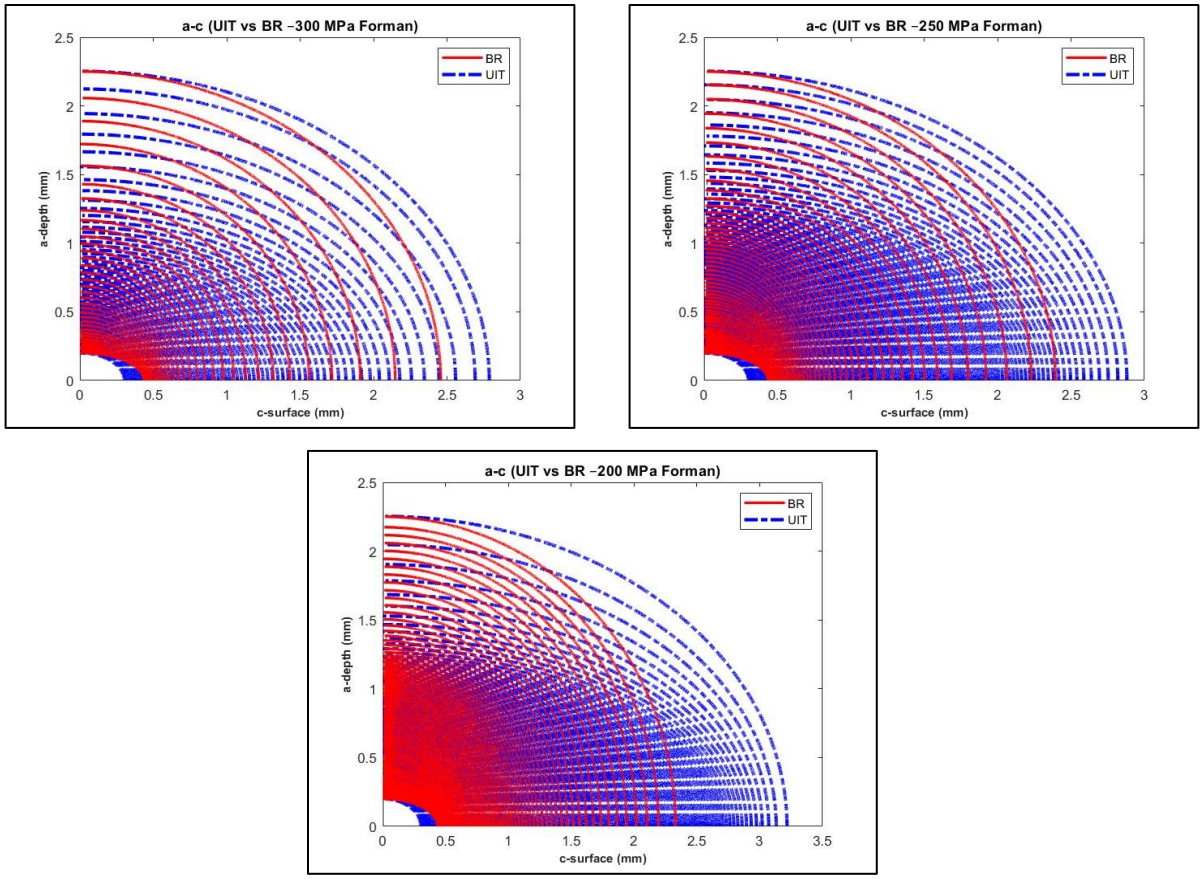

Figure 147: Crack shape evolution analysis results of 2024-T351 AL for BR vs UIT conditions for Forman, crack depth against crack surface for covering stress level ranges

The below figures are the crack shape evolution curves for 2024-T351 AL under the AW and the UIT conditions for Walker model.

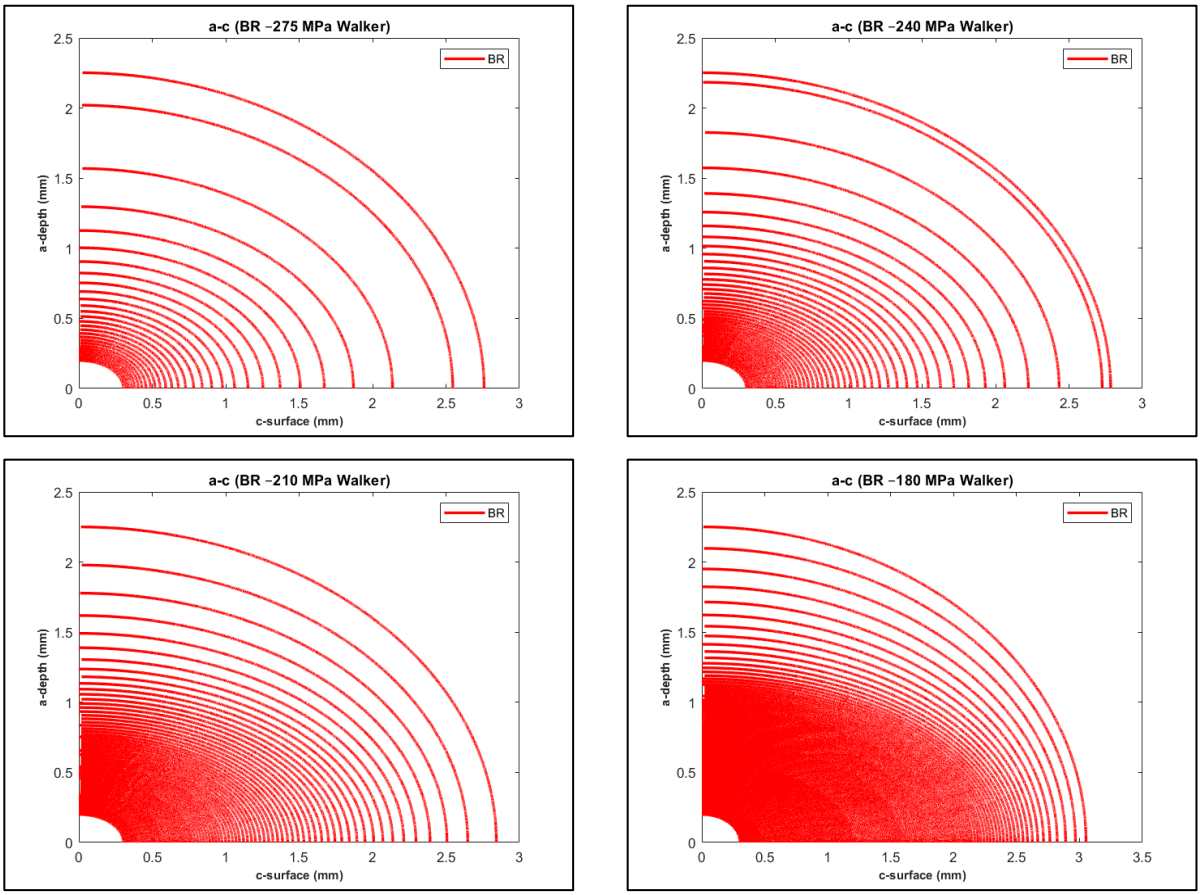

Figure 148: Crack shape evolution analysis results of 2024-T351 AL under BR condition for Walker, crack depth against crack surface for covering stress level ranges

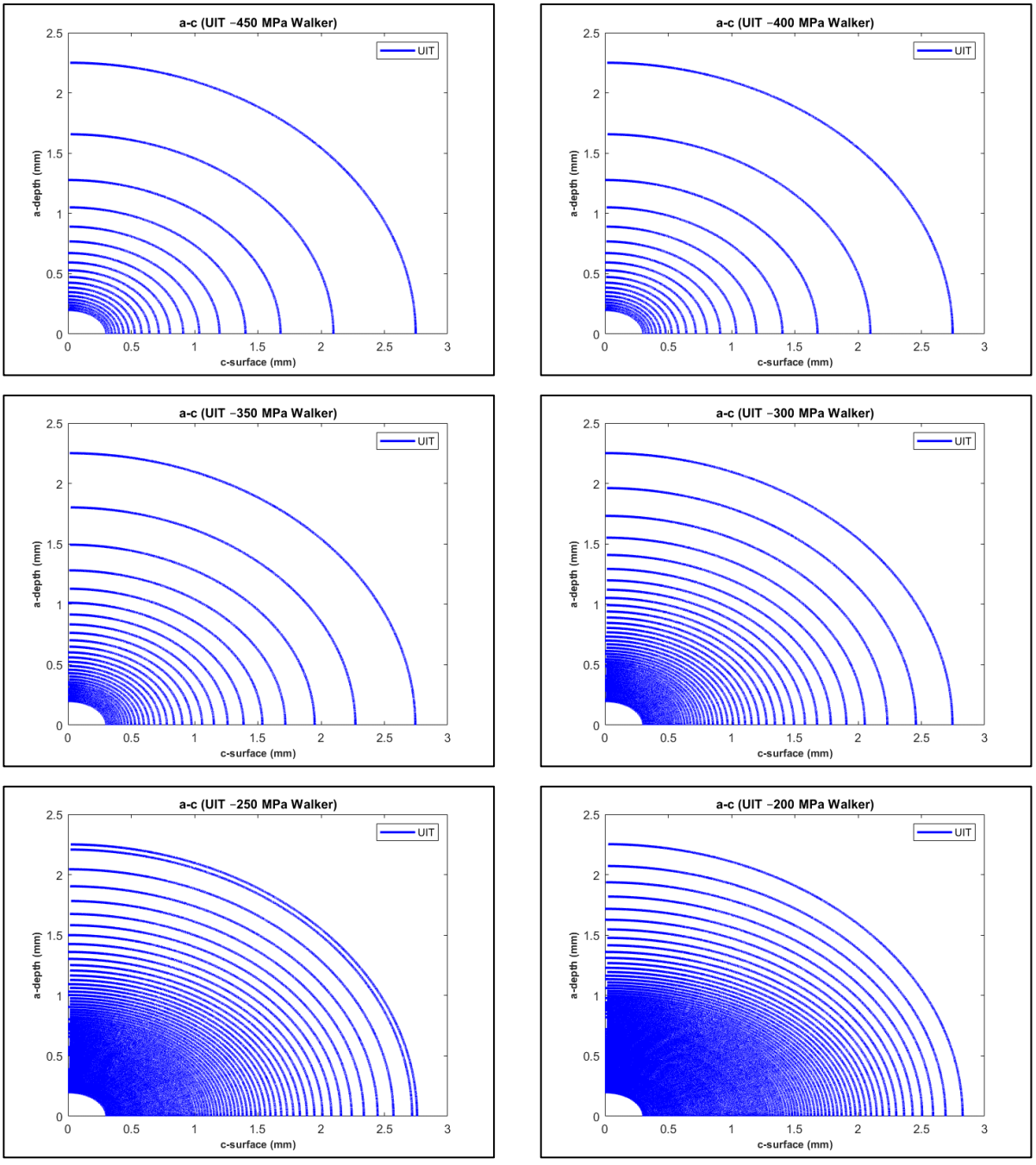

Figure 149: Crack shape evolution analysis results of 2024-T351 AL under UIT condition for Walker, crack depth against crack surface for covering stress level ranges

The below figures are the crack shape evolution curves for 2024-T351 under the AW and the UIT conditions for Forman model.

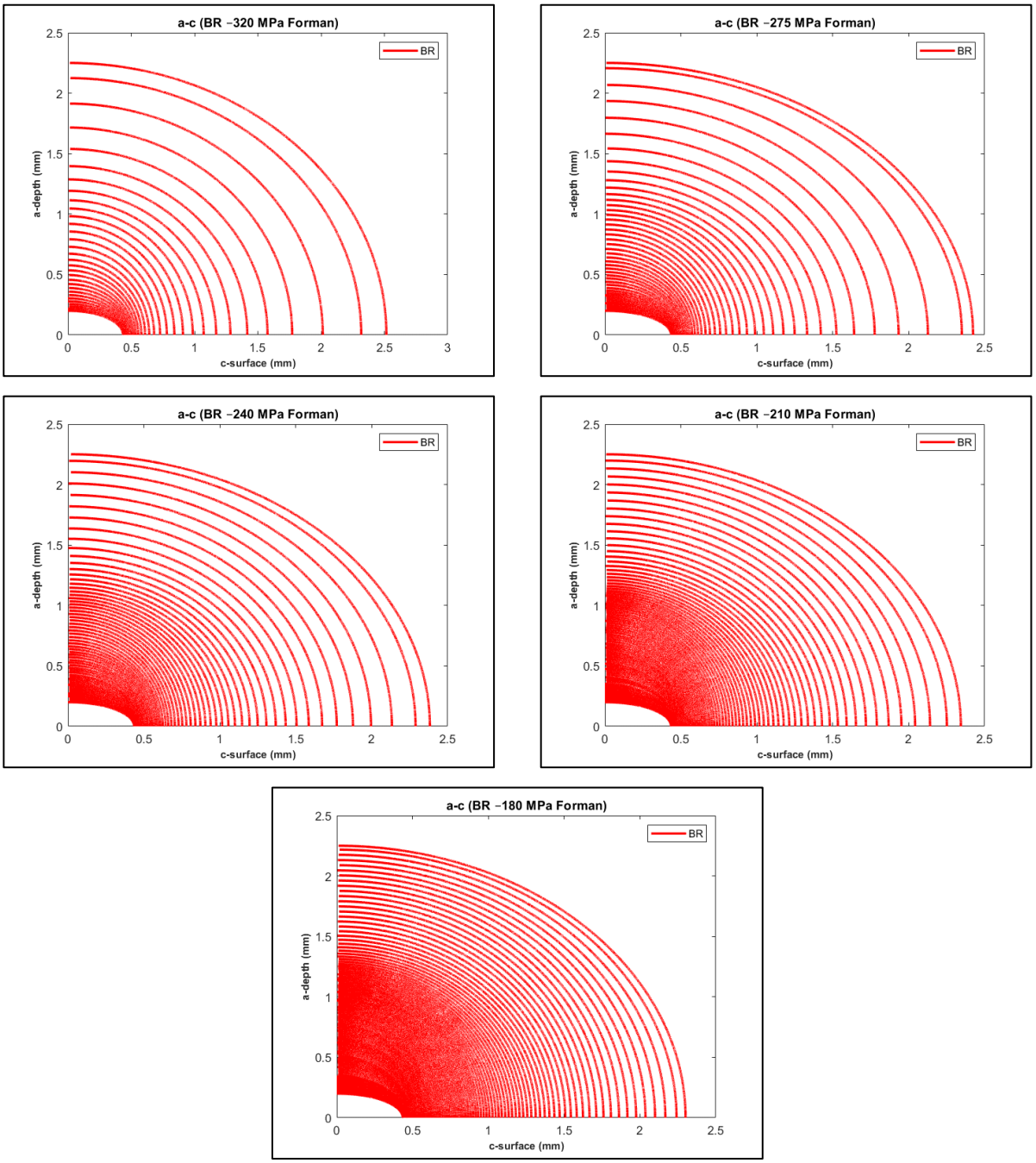

Figure 150: Crack shape evolution analysis results of 2024-T351 AL under BR condition for Forman, crack depth against crack surface for covering stress level ranges

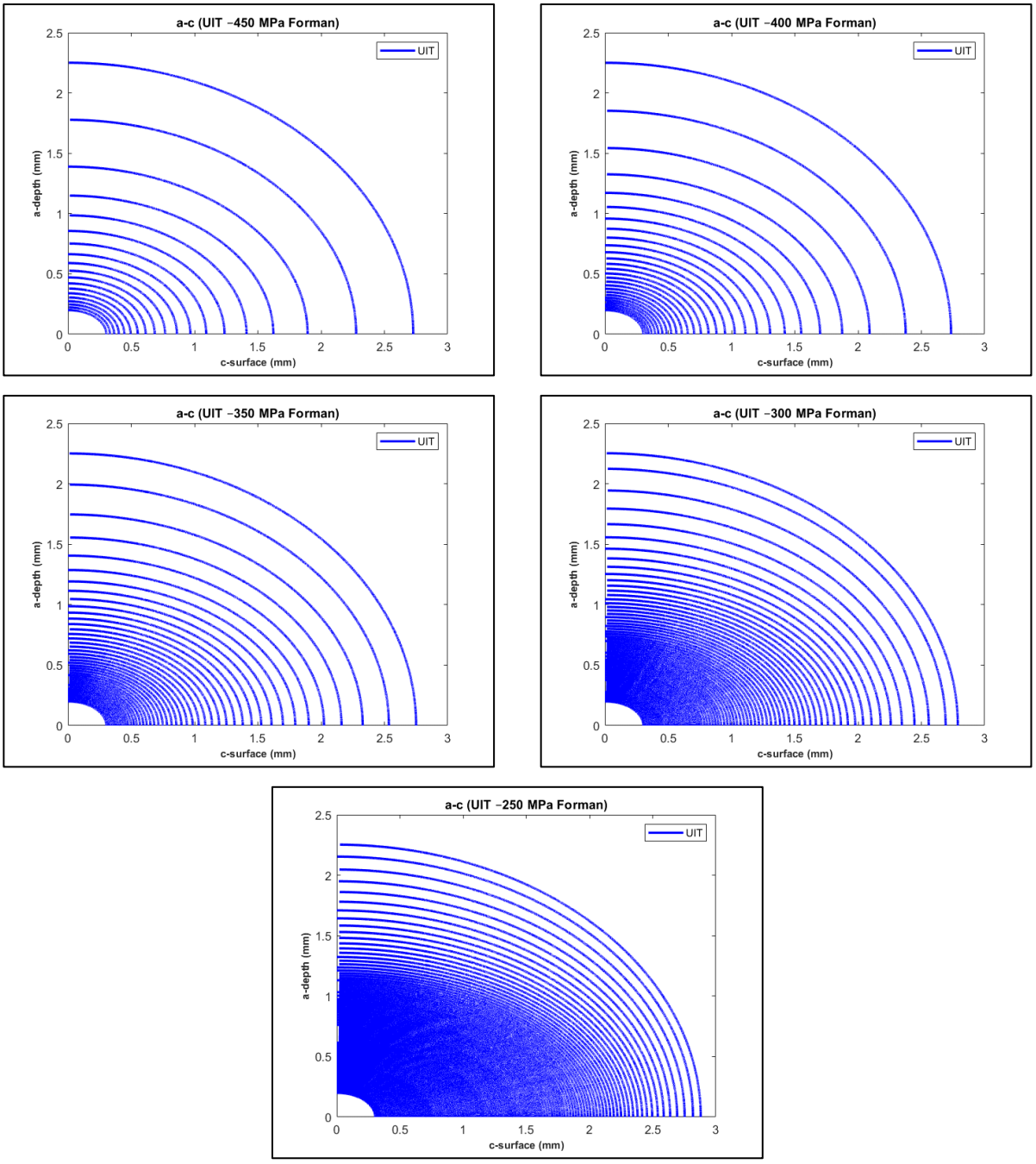

Figure 151: Crack shape evolution analysis results of 2024-T351 AL under UIT condition for Forman, crack depth against crack surface for covering stress level ranges

Fracture Mechanics Fatigue Life Assessment of Welded Joints Under Ultrasonic Impact Treatment

© MEHRDAD SARAFRAZI

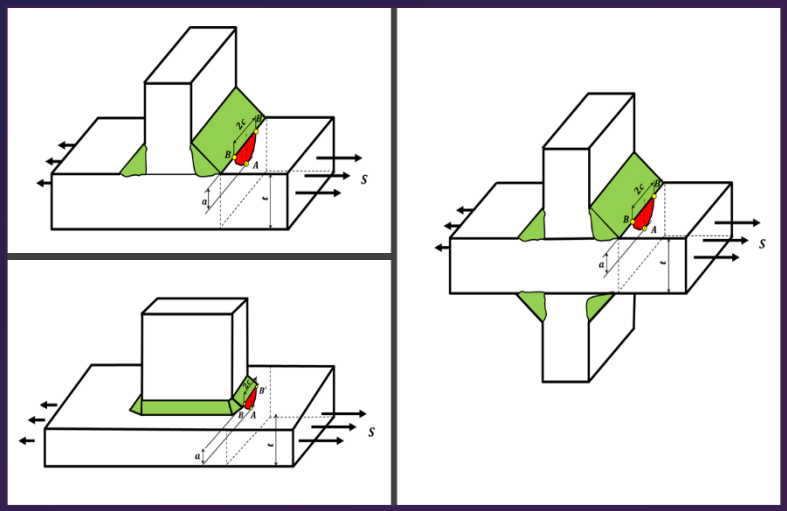

CONCORDIA UNIVERSITY

MASTER DISSERTATIONS

Automobile, aerospace and marine etc. industries are facing a growing demand for lighter structures. Presently, engineers are actively seeking for cost-effective solutions to reduce their products weight. Environmentally, greenhouse gas emissions can be dramatically reduced by weight reduction. Then, it will lead to rising payload and through this saving fuel consumption in the mentioned industries. Optimizing the weight can be safely accomplished by welding the joint components from high strength steels etc.

Welding joints are the most used joining method to fabricate engineering structures due to their low cost, structural strength, and geometric flexibility etc. Irregular geometries, micro cracks, defects, high stress concentration and tensile residual stresses are some of the results of a highly metallurgical process considered as welding.

Several engineering segments encounter fatigue loading throughout all or part of their lifetime. Thus, an important subject of growing concern in product design is to consider some of the critical factors caused from the weld process including high tensile residual stresses and stress concentrations to properly evaluate the fatigue life of the structures. Lightweight design of welded steel and aluminum structures in cyclic service requires the use of post-treatment approaches like Ultrasonic Impact Treatment (UIT).

There is a demand to discover efficiency of different models for predicting the fatigue life based on fatigue crack propagation of the welded joints under the as-welded (AW) and UIT conditions. Eventually, it leads to better understanding of the performance limitations of UIT which is required to develop a solid basis of fatigue recommendations.

Concordia University
School of Engineering and Computer Science
Department of Mechanical,
Industrial and Aerospace Engineering (MIAE)
www.concordia.ca